HAMMER

New Generation High-capacity Compact Mid Ranger

Final Report

Technische Universiteit Delft

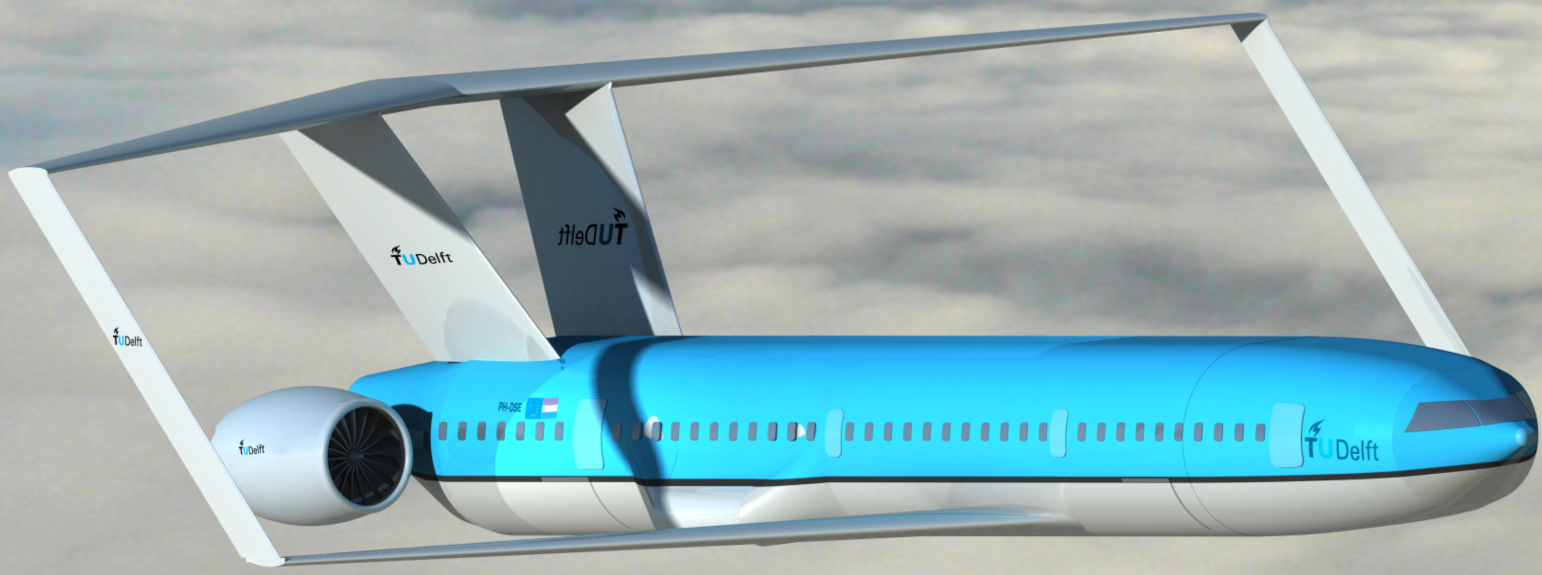

TU Delft

Page intentionally left blank

HAMMER

New Generation High-capacity Compact Mid Ranger

by

Group 18

Frederik Collot d'Escury	4668928
Gijs Frehe	4553683
Ivo Janssen	4660900
Wessel Kruin	4672771
Guy Maré	4670132
Paula Meseguer Berroy	4530934
Jimmy Phillips	4431553
Jim de Ridder	4669908
Sarah Vanleeuwen	4542320
Stan Verweij	4682653

at the Delft University of Technology

AE3200 - Design Synthesis Exercise

Version	Date	Chapters Affected	Brief Description of the Change
1	22/06/2020	All	New Document
2	27/06/2020	4 - 13, 17	Finalising work
3	30/06/2020	All	Implementing feedback from Coach, Tutors, TA and peers

June 30, 2020

Distributed to:	Dr. ir. G. La Rocca,	TU Delft, Tutor
	Dr. T. R. Mahon,	TU Delft, Coach
	Mr. B. R. Cheneka,	TU Delft, Coach
	Design Synthesis Exercise Coordination Committee Spring 2020	
	Design Synthesis Exercise Student Assistant Spring 2020	

Executive Summary

Problem[1]:
The ever increasing demand for passenger air transportation comes with a lot of challenges. Not only will emissions rise, but many airports are not able to expand any further and are struggling to keep up with the demand. Under constant pressure from communities and local governments they are forced to impose flight time restrictions and reduce the number of daily aircraft movements. The problem is most evident on medium-range and high frequency flights. Moving more passengers (pax) with less aircraft would require, in the current aircraft portfolio, to use wide-body aircraft designed for long range flights. This type of aircraft however, is either not cost-effective to operate on shorter flights or simply cannot land on medium size airports due size constraints. In short, the operational capacity of the medium haul aircraft segment cannot cope with the growth in demand for these flights. A solution explored is designing an aircraft that can carry more passengers (320 PAX) than the current narrow-body aircraft (130 - 200 PAX) while being more sustainable, cost-effective and fit within narrow body airport constraints (gate type C). The complete set of top level requirements imposed by [49] are the following:

- Payload = 250 - 320 pax (320 at full density) + typical luggage
- Harmonic range (max range at max payload) = 2200 Nautical Miles (NM)
- Minimum operative Mach at cruise = 0.78
- ICAO Aerodrome Ref. Code = 3/4C
  - 3 = 1200-1800m field length
  - 4 = $\geq$1800m field length
  - C = wing span $\leq$36m; outer main gear wheel span $\leq$9m
- Noise level = not higher than best aircraft in category 4D aircraft
- Wake turbulence category = M (not worse than current category ”medium”)
- Expected EIS (Entry into service): Year 2035

These top level requirements can be summarised in the mission need statement:
Provide a mid-range aircraft with 320 PAX, but with the airport compatibility of A320 and comparable ground turn-around time.
To achieve this, an innovative aircraft concept must be selected that is able to meet requirements on both the payload and dimensions. Furthermore, it shall be more sustainable and environmentally friendly than current generation aircraft, increase the economical profitability and have an expected entry into service by the year 2035. The project objective statement thus reads:
Evaluate the design feasibility of and assess the socio-economic benefit of a compact, high-capacity, mid-range aircraft that has a short ground turn-around time, with 10 students in 10 weeks.
For this new generation High cApacity coMpact Mid rangE aiRcraft, or HAMMER in this report, a first design is worked out and is displayed in Figure 1.

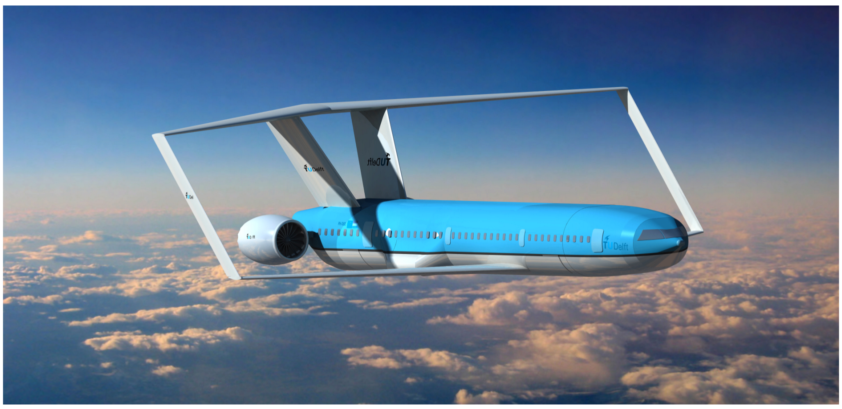

Figure 1: Rendered CAD drawing of HAMMER.

[1]This section matches the DOI ’jury summary DSE 18’

Financial Analysis
Economical viability and potential benefit for the HAMMER concept aircraft are investigated for three main stakeholders in the project. These stakeholders are the aircraft manufacturers, operators and the airport on which the aircraft will operate. Following the trend of passenger movements growth, the market analysis shows that the commercial passenger fleet is expected to nearly double from now until 2038[2]. Furthermore, 44% of the new aircraft deliveries will be replacing the current fleet. Operators and airports are looking for aircraft that are more sustainable and cost effective while decreasing the required number of aircraft movements. The medium haul market segment is expected to grow the fastest accounting for 75% of the total market by 2038. This trend can be identified in (see Figure 2).

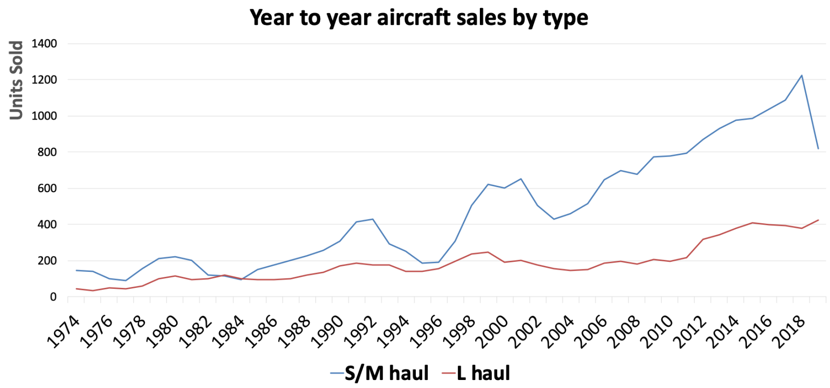

Figure 2: Aircraft sales by type.

Boeing commercial outlook predicts a total 44000 expected aircraft deliveries from 2018 until 2038. Of those deliveries, 33000 deliveries are forecasted to be in the medium haul market with an expected total value of $4.5 trillion. At an estimated research and development cost of $23.5 billion and a unit price of $220 million, with a margin of 12.35%, the manufacturers are expected to have their investment returned after 870 units. For the operators, the break even point is expected to drop by approximately 10% to 18.6 years. Furthermore the operational profitability of the HAMMER aircraft is calculated to be 112% higher than that of the current Large Narrow Body Jets (LNBJ, 150-200 PAX). This indicates the business opportunity the development of the HAMMER aircraft poses. With increased sustainability, profitability and demand created by operators and airports, the HAMMER concept aircraft is expected to outperform any current competing aircraft. To give a complete overview of the business facets of the HAMMER project, a SWOT analysis is carried out, displayed in Table 1 (EASA = European Union Aviation Safety Agency).

Table 1: SWOT analysis of HAMMER.

Strength	Weaknesses	Opportunities	Threats
Better profitability than current medium range aircraft	Higher capital investment required by operators and manufacturers	Disrupting the current aircraft market, increasing its market potential	Not enough incentive for manufactures to move from their current portfolio
Higher Return on Investment for operators	High research and development cost and effort required	Increased demand for aircraft originates from (congested) airports and operators	Might be difficult to be approved by governing aircraft agencies (i.e. EASA)
More sustainable, due to lower fuel consumption per seat mile	Unproven concept	Environmental friendly aircraft can have lower landing fees (Lower environmental tax)	Development of other sustainable aircraft could jeopardise the value of HAMMER

[2]Not adjusted for COVID-19

Conceptual Design
To find the aircraft concept that fits the top-level requirements best, four concepts: Box wing, blended wing body, conventional fixed wing and folding wing where traded off. This was done by means of five key performance parameters: Ground operations, structures and airframe performance, aerodynamic performance, flight performance and sustainability. It was found that the box wing aircraft performed best overall and was therefore selected to enter the final design phase. In the conceptual design phase, it was also decided to go with a conventional turbofan propulsion system and a double bubble fuselage.

Aerodynamics
The box wing design has major aerodynamic advantages over a conventional fixed wing. The two wings are designed to be 'slender' or have a high aspect ratio and thus higher lift to drag ratio. The lift to drag ratio is one of the most important in wing design and should therefore be optimised. Furthermore, the control surface and high lift device design could be implemented. An Athena Vortice Lattice model was used for verification and validation. From both the manual computational methods and the AVL model, values for drag and roll- and pitch performance where outputted that can be used for the optimisation of flight performance and stability and control. The key aerodynamic performance characteristics are shown in Table 2

Table 2: Key aerodynamic performance characteristics of HAMMER

Parameter	Symbol	Value	Unit
Cruise lift coefficient	$C_{L_{cruise}}$	0.51	[−]
Zero lift drag coefficient	C_{D_0}	0.0181	[−]
Wing surface area	S	238	[m^2]
Height to span ratio	h/b	0.294	[−]
Lift to drag ratio	L/D_{max}	17.3	[−]
Oswald efficiency factor	e	1.27	[−]
Airfoil		DFVLR-R4 transsonic	

Propulsion and Power Systems
For HAMMER's thrust provision, a twin-spool turbofan engine was designed. This turbofan has a bypass ratio (BPR) of 8 and an overall pressure ratio (OPR) of 50. These high values for OPR and BPR were adopted to aim for a more sustainable engine. It has a take-off and cruise thrust of 201 and 87 [kN] respectively. Furthermore, its thrust specific fuel consumption in the cruise phase is 0.05348 [$kg/N/h$], an over 20% decrease with respect to the CFM56 engine family, commonly used by the A320 and 737. For power provision of on-board systems, it was chosen to implement a no-bleed system, dropping the conventional pneumatic system. This system uses shaft driven generators instead of bleed air from the engines for energy provision of a large portion of the aircraft. With this system, HAMMER can lower fuel consumption in cruise phase by more than 2%. Also, implementation of an electric taxiing system was done successfully. HAMMER can thus completely autonomously perform all ground operations, lowering both turnaround time and emissions during this phase and working towards a new generation of hybrid electric aircrafts.

Fuselage and Payload
To accommodate 320 passengers within the 45 [m] fuselage length constraint , it was chosen to go for a double aisle fuselage interior design. To reduce the frontal area for aerodynamic reasons, a more oval, double bubble fuselage cross section was selected. This allowed for eight abreast seating with aisles twice as wide as the current standard aisle width. This decreases boarding and deplaning time which is beneficial for the ground turnaround time and aircraft profitability. Furthermore, there is also the capacity to carry 24 "LD-3" cargo containers together in the cargo hold behind the front wing, which is beneficial for loading and unloading. The cabin layout and cross section are displayed in Figure 3 and Figure 4 respectively.

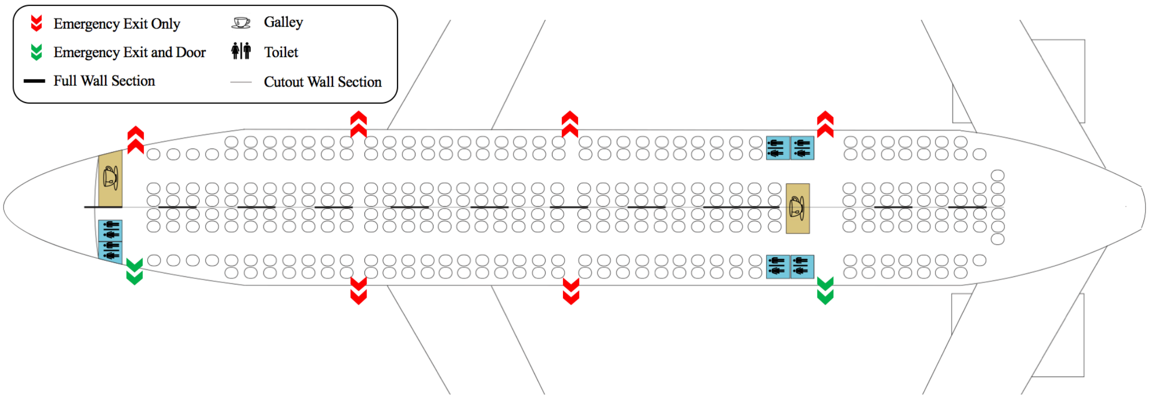

Figure 3: Cabin floor map showing seating configuration, emergency exits and location of toilets and galleys.

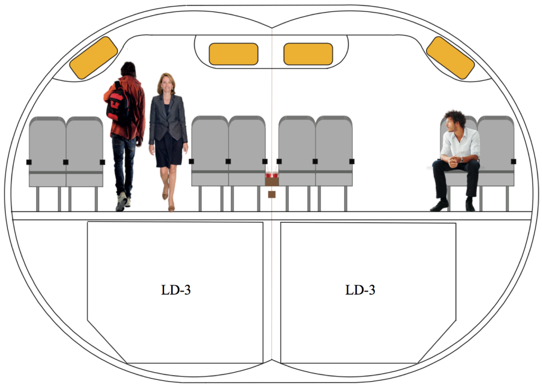

Figure 4: Fuselage cross-section of HAMMER.

Stability and Controllability

The two wings and the landing gear were positioned such that the HAMMER would be statically stable. This resulted in a longitudinal position of the leading edge of the root chord of 13.5 [m] for the first wing and 39.75 [m] for the second wing. The nose landing gear is positioned at 4 [m] from the nose and the main gear at 29 [m]. Furthermore, the two tracks of the main landing gear or 5.6 [m] apart. Both gears retract forward into the fuselage. The nose gear is fully positioned in the fuselage and the main gear is partly podded. In addition the vertical tail was sized and positioned. The two parts of the v-tail are 5.6 [m] apart and are 15°inclined. The height is 6.07 [m] and the mean aerodynamic chord 4.68 [m], which results in a surface area of 28.42 [m^2]. The root chord of the vertical tail starts at a longitudinal position of 34.1 [m] and the tail has a sweep angle of 38.3°. Lastly, the dynamic stability was also analysed and it was found that the aircraft has a good pitch damping, as expected for a box wing design.

Structures and Materials

The structures and materials department has prioritised the large components of the fuselage and wing system that contribute significantly to the weight. The general analysis sought a way to minimise the weight for better performance. However, considerations were made towards the impacts of the subsystem to the environment and passenger safety. For safety, load factors were applied to ensure the aircraft maintains structural integrity at the edge of the flight envelope.

Table 3: Summary overview of component weights.

Component	**Material**	**Weight [kg]**	**Savings**
Wing system	CFRP	11653	48%
Fuselage skin	CFRP	4334	36%
Cabin support wall	CFRP	963	54%
Stringers	Al 2024-T3	3511	-
Floor	Al 2024-T3	5560	-
Total		**26021**	**34%**

The materials have been optimised for the particular loads they are expected to encounter during operations. Lastly, the manufacturing cost and carbon footprint influenced the material choice such that the preferred material is aluminium 2024-T3 (Al 2024-T3). Carbon Fiber Reinforced Polymer (CFRP) was used only when significant weight savings could be made with respect to to Al2024-T3. Components that contribute significantly to the operational empty weight (OEW) have been sized for the HAMMER with their weight savings compared to Al2024-T3 as shown in Table 3 and the skin thicknesses of fuselage and wing material in Table 4.

Table 4: Summary of component thicknesses.

Fuselage [*mm*]		**Wing [*mm*]**	
Top skin	4.1	Spar	35
Mid skin	2.0		
Bottom skin	6.2	Skin	25
Cabin wall	3.7		

Flight Performance

HAMMER was designed to have a harmonic range of 2200 $[NM]$. The tanks are not filled at the harmonic range and thus a higher range is achievable. Additionally, the specific range and payload range efficiency of HAMMER were computed and compared to similar aircraft. A payload range efficiency of 6237 $[\frac{kg \cdot km}{kg}]$ was found for the harmonic range of HAMMER. Furthermore, a take-off and landing field length of 1266 and 1437 [*m*] was found respectively. HAMMER therefore belongs to aerodrome reference code 3C. However, it should be noted that no failure and ideal conditions at sea level were considered. The climb performance of HAMMER was computed and a service altitude of 11.000 [*m*] and a maximum Rate of Climb (RoC) of 22.5 [*m/s*] was found. Lastly, HAMMER falls in the International Civil Aviation Organisation (ICAO) wake category M and Wake Turbulence RE-CATegorisation (RECAT) category C.

Ground Operations

One of the key requirements states that the HAMMER aircraft should have comparable turnaround time to that of current type C aircraft. As normally, the critical phases in the turnaround time are the boarding and deplaning of passengers, wider aisles had to be fitted to cope with the 113% passenger increase. The optimised ground turnaround time for the HAMMER aircraft can be found in Figure 5. A turnaround time of 48.5 minutes was found, only 10% higher than the A320 and 18% lower than the A330.

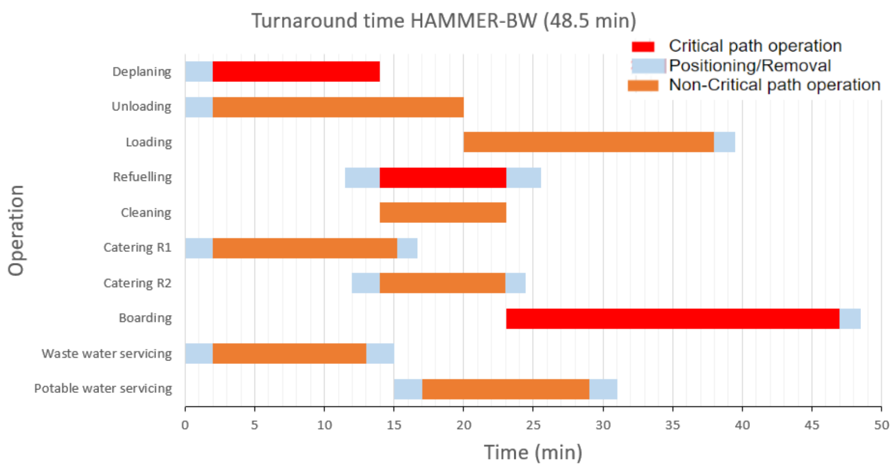

Figure 5: Gantt chart of the optimised turnaround time of HAMMER.

Sustainability

A lot of effort has gone in the sustainable design of the HAMMER aircraft. Not only should the aircraft be more fuel efficient in operation, also it should be low on noise production and have a sustainable end of life solution. The fuel efficiency per passenger is achieved by the efficient aerodynamic design of the aircraft and the efficient engines. Furthermore with the use of part bio fuels, cradle-to-cradle emissions are even further reduced. It was also found that the aircraft design adheres to the noise requirements set by governments and aviation authorities. By making use of recyclable and sustainable materials, the End Of Life (EOL) pollution was decreased and the EOL value of the aircraft increased, contributing to the sustainable footprint of the aircraft concept. It is expected that the HAMMER consumes 44% less fuel per passenger per kilometer than the A320, for example, contributing to the reduction of greenhouse gas emissions.

Conclusion and Recommendations

All in all, a more sustainable, cost-efficient, high capacity compact mid range aircraft was designed. The box wing design is an efficient solution to keep the wingspan of the aircraft below the required 36 [m], while being able to transport 1.5 times the amount of passengers of the current single aisle aircraft using airport gates of same dimensions (ICAO type C) Furthermore HAMMER was successfully designed to be operational by the year 2035. Following this report, a few recommendations are made:

- Improving the aerodynamics and flight dynamics model: One problem area of this project is the aerodynamic model used for analysis. Improving the accuracy of the gathered values has a lot of consequences for the aircraft. Many gains can be made for the departments of stability and controllability, structural and materials, and aerodynamics. This is mainly due to the uncertainty of the distributed forces of the wing. In a conventional wing configuration the lift is introduced in a single point. While lift distribution is still important, a change in distribution wont shift the application point much. In a box wing however the lift application points are separated by a large distance which greatly affect the stability and structural design. Improving the used tools will therefore greatly assist to advance the project. Especially a more accurate AVL model and a model that is standard for a box wing aircraft instead of a conventional aircraft.
- Improving the weight estimate: Due to the unconventional design, the weight distribution is different from conventional aircraft. For example, the vertical supports required for the double bubble design add weight that is not present in most aircraft. Furthermore, the initial weight estimation that was done uses a statistical relation based on reference aircraft that have a conventional configuration. This does not include the contribution of the extra central wing box required for the aft wing or the existence of the lateral connectors and vertical tail structural reinforcements. Lastly, a large number of LD-3 containers were added but these also greatly increase weight. Improving the weight estimation will yield a better estimate of the aircraft balance which improves the stability and controllability aspects. Additionally, a better estimate of the overall weight increases the accuracy of the flight performance analyses.
- Improving the structural model: Many structural components are sized using preliminary, conservative sizing estimates. The accuracy of these models is rather low, leading to a high uncertainty in structural parameters. On top of that, several failure modes of the structures are not covered. These include but are not limited to torsional loads, vibrational loads like flutter, as well as buckling. Including these failure modes into the analysis and adopting more complete (finite element) models will allow for a more efficient structural design, with a higher accuracy, leading to an overall safer and lighter structure.
- Further optimising the double bubble configuration: As stated in Chapter 8, the aircraft could benefit from optimising the double bubble configuration to minimise the cross section. This would not only reduce the structural weight, but it would also contribute to lower drag, which results in improvements such as lower fuel consumption.
- Further research in the double bubble cabin: The double bubble fuselage is a way of creating a wide fuselage without this fuselage being unnecessary high. However, a middle wall (closed or with holes) is needed for pressurisation, which limits freedom in the use of HAMMER volume. It is thus recommended to research efficient ways to deal with the pressurised double-bubble and the efficiency of other configurations that allow for a wide body.
- Further development of the electric taxi system and APU: The electric taxi system proved to be a promising system for the HAMMER project. However, such a system does increase the power consumption and requires extra batteries. To add to that, an off the shelf APU is used. To improve the sustainability, and improve future expandability, new types of APU system should be researched.

Preface

This report presents the product of ten weeks of distant, but close cooperation between ten aerospace students. An aircraft was designed that, we can proudly say, allows for further growth of the giant air transportation business by staying compact in itself.

We would like to express our gratitude to our tutor Dr. Ir. G. La Rocca and coaches Dr. T.R. Mahon and B.R. Cheneka for their valuable advice and readiness to answer our questions during this project.

Without the help of A. Altena, M. Seoane Alvarez, Ir. P. Roling, Dr. F. Oliviero, P. Proesmans, Ir. R.J.M. Elmendorp, A.E. Alves Vieira, C. Varriale, Prof.dr. D.G. Simons, Dr.ir. R.C. Alderliesten and Dr. C.D. Rans the HAMMER could not have been realised. We thank them for their feedback and suggestions.

The realisation of the HAMMER is experienced as a challenging but rewarding process. Hard work has lead to a result we are very proud to deliver.

Group 18
Delft, June 2020

Nomenclature

Acronyms

ADSEE	Aerospace Design & Systems Engineering Elements course
Al	Aluminium
ANOPP	Aircraft Noise Prediction Program
APU	Auxiliary Power Unit
ASK	Available Seat Kilometre
avg	Average
AVL	Athena Vortex Lattice
bat	Battery
BEP	Break Even Point
BET	Break Even Time
BPR	Bypass Ratio
c.g.	Centre of Gravity
CASM	Cost per Available Seat Mile
CFD	Computational Fluid Dynamics
CFRP	Carbon Fibre Reinforced Polymer
CO	Carbon Monoxide
CO_2	Carbon dioxide
Comb	Combustor
cr	cruise
CS	Certification Specification
DFVLR	Deutsche Forschungs- und Versuchsanstalt fur Luft- und Raumfahrt
DSHC	Direct Sugars to Hydrocarbons
EASA	European Union Aviation Safety Agency
EGTS	Electric Green Taxiing System
EIS	Entry Into Service
eng	Engine
EPNdB	Effective Perceived Noise in Decibels
ETS	Electric Taxiing System
FBS	Functional Breakdown Structure
FFD	Functional Flow Diagram
FML	Fibre Metal Laminate
FSTE	Full Size Trolley Equivalents
FT	Fischer-Tropsch
fwd	Forward
GDP	Gross Domestic Product
GLARE	Glass Laminate Aluminium Reinforced Epoxy
GO	Ground Operations
GSP	Gas turbine Simulation Program
HAMMER	High cApacity coMpact Mid rangER
HC	Hydrocarbons
HEFA	Hydroprocessed Esters and Fatty Acids
HLD	High Lift Devices
HPC	High Pressure Compressor
HPT	High Pressure Turbine
ICAO	International Civil Aviation Organisation
ISA	International Standard Atmosphere
LD	Loading Device
LNBJ	Large Narrow Body Jet
LPC	Low Pressure Compressor
LPT	Low Pressure Turbine
MAC	Mean Aerodynamic Chord
max	maximum
MDT	Mean Down Time
MLG	Main Landing Gear
MTBM	Mean Time Between Maintenance
MTOW	Maximum Take-Off Weight
MTTM	Mean Time To Maintain
MTTR	Mean Time To Repair
n.p.	Nacelle and pylon
nac	nacelle
NASA	National Aeronautics and Space Administration
nc	Nose Cone
NLF	Natural Laminar Flow
NLG	Nose Landing Gear
NO_x	Nitrogen oxides
NPSS	Numerical Propulsion System Simulation
OEW	Operational Empty Weight
OPR	Overall Pressure Ratio
PAX	Passenger
PNL	Perceived Noise Level
PRD	Payload Range Diagram
PRE	Payload Range Efficiency
R&D	Research and Development
RAMS	Reliability, Availability, Maintainability, Safety
RASM	Revenue per Available Seat Mile
RECAT	Wake Turbulence Re-categorisation
req	Required
ROI	Return On Investment
S.T.	Single Tire
SO_x	Sulfur Oxide
SR	Specific range
tc	Tail Cone
TO	Take-off
TSFC	Thrust Specific Fuel Consumption
UD	Uni-Directional
ULD	Unit Loading Device
VLM	Vortex Lattice Method
vt	Vertical Tail

Symbols

α	Angle of attack	[°]
α	Translation angle coordinate system	[*rad*]
α_f	Alpha factor	[min^{-1}]
$\bar{c}$	Chord length	[*m*]
$\bar{y}$	Y-location of the centroid	[*m*]
$\bar{z}$	Z-location of the centroid	[*m*]
β	Prandtl glauert correction factor	[-]
β_i	Plate angle w.r.t. the horizontal	[°]

δp	Infinite small pressure difference	[N]
Δ	Difference	[-]
δ_x	Mobile surface deflection	[°]
$\varnothing$	Diameter	[-]
$\dot{m}$	Mass flow	[kg/s]
$\dot{v}$	Fuel volume flow	[L/min]
ϵ	Downwash	[m/s]
η	Efficiency factor	[-]
Γ	Dihedral angle	[°]
γ_a	Approach flight angle	[°]
γ_{TO}	Take-off flight angle	[°]
Λ	Sweep angle	[°]
λ	Taper ratio	[-]
$\Lambda_{0.25c}$	Sweep angle at quarter-chord	[°]
μ	Fluid viscosity	[Pa·s]
μ_{br}	Breaking friction coefficient	[-]
μ_r	Rolling friction coefficient	[-]
Φ	Wing twist	[°]
ϕ	Integration angle	[rad]
ϕ	Pitch angle	[°]
ϕ	Sound angle in azimuth	[°]
ϕ	Wing twist angle	[°]
π	Pressure ratio	[-]
ρ	Density	[kg/m^3]
ρ_0	Density at zero altitude	[kg/m^3]
ρ_∞	Upstream air density	[kg/m^3]
σ	Stress	[Pa]
τ	Shear stress	[Pa]
τ	Torsion	[Pa]
θ	Angle	[°]
θ	Double bubble layout angle	[rad]
θ	Polar sound angle	[°]
ϕ	Ground effect factor	[-]
A	Area	[m^2]
a	Acceleration	[m/s^2]
a	Noise constant	[-]
a_2	Lift curve slope of the aft wing	[1/°]
A_f	Flap area	[m^2]
A_m	Enclosed area	[m^2]
A_w	Wing area	[m^2]
A_y	Vertical reaction force fwd wing root	[N]
b	Wing span	[m]
b_f	Flap span	[m]
b_w	Wing span	[m]
B_y	Internal shear force fwd wing tip	[N]
C	Integration constant	[-]
c	Chord length	[m]
c	Speed of sound	[m/s]
$C_{1/2}$	MAC length of the fwd/aft wing	[m]
C_{D_0}	Zero lift drag coefficient	[-]
C_D	Drag coefficient	[-]
C_L	Lift coefficient	[-]
C_m	Moment coefficient	[-]
c_r	Root chord length	[m]
C_{slope}	Chord reduction per unit span	[-]
c_t	Tip chord length	[m]
C_y	Internal shear force aft wing tip	[N]
D	Drag	[N]
d	Diameter	[m]
$D(\theta, \phi)$	Directivity function	[-]
D_y	Vertical reaction force aft wing root	[m]
E	Energy	[Wh]
E	Young's modulus	[Pa]
e	Oswald span efficiency factor	[-]
F	Force	[N]
F	Pure tone correction factor	[dB]
f	Frequency	[Hz]
$F(S)$	Spectral function	[-]
$F/\dot{m}$	Specific thrust	[Ns/kg]
F_p	Pressure force	[N]
F_r	Resultant force	[N]
F_{tr}	Traction force	[N]
G	Shear modulus	[Pa]
G	Sound geometry function	[-]
g	Gravitational acceleration	[m/s^2]
$h \cdot C_1$	Distance from leading edge to c.g.	[m]
H	Altitude	[m]
h	Height	[m]
h_0	Distance fraction	[-]
h_{scr}	Screen height	[m]
h_W	Wing height	[m]
I	Moment of inertia	[m^4]
I_{xx}	Area moment of inertia	[m^4]
J	Torsional constant	[m^4]
K	Noise constant	[-]
$k_{n.p.}$	Fraction n.p. weight of engine weight	[-]
K_t	Stress concentration factor	[-]
k_T	Thrust correction factor	[-]
k_x	Correction factor	[-]
L	Lift	[N]
L	Noise length scale characteristic	[-]
l	Length	[m]
l_b	Quarter chord length fwd wing	[m]
l_c	Distance between l_b and l_t	[m]
l_t	Quarter chord length aft wing	[m]
M	Bending moment	[Nm]
M	Mach number	[-]
m	Distributed moment along span	[Nm/m]
m	Mass	[kg]
M_a	Reaction moment fwd wing root	[Nm]
M_b	Bending moment fwd wing tip	[Nm]
M_{cr}	Cruise mach number	[-]
M_c	Bending moment aft wing tip	[Nm]
M_{dd}	Drag divergence number	[-]
M_d	Reaction moment aft wing root	[Nm]
N	Number of Cycles	[-]

n	Load Factor	[-]
n_1	Limit load factor	[-]
n_2	Proof load factor	[-]
n_3	Ultimate load factor	[-]
n_t	Number of tires	[-]
P	Power	[W]
P	Roll performance	[$°/s$]
P	Sound power function	[-]
p	Pressure	[Pa]
p_0^2	Reference sound pressure	[N/m^2]
p_e^2	Effective sound pressure	[N/m^2]
q	Shear	[Pa]
q	Shear flow	[N/m]
R	Range	[m]
r	Radius	[m]
$R(\phi)$	Distance to differential element	[m]
Re	Reynolds number	[-]
S	Strength	[MPa]
S	Strouhal number	[-]
S	Surface area	[m^2]
s	Length along circumference	[m]
s	Length along the fuselage	[m]
S_1	Trapezoidal area at the wing root	[m^2]
S_2	Trapezoidal area the wing tip	[m^2]
S_e	Fatigue strength at 10^6 cycle	[MPa]
S_m	Fatigue strength at 10^3 cycles	[MPa]
S_u	Ultimate strength	[MPa]
S_{wet}	Wetted surface area	[m^2]
T	Temperature	[K]
T	Thrust	[N]
T	Torque	[Nm]
T	Twist	[°]
t	Thickness	[m]
t	Time	[s]
T_1	Torsion of the fwd wing	[Nm]
T_2	Torsion of the aft wing	[Nm]
t_{10}	Duration noise level within ±10dB	[s]
T_a	Torsional moment fwd wing root	[Nm]
T_b	Torsional moment fwd wing tip	[Nm]
T_{cr}	Cruise thrust	[N]
T_c	Torsional moment aft wing tip	[Nm]
T_d	Torsional moment aft wing root	[Nm]
t_f	Refuelling time	[min]
T_{rev}	Thrust reversal	[N]
T_{stat}	Static thrust	[N]
T_{t4}	Combustor exit temperature	[$Kelvin$]
T_{TO}	Take-off thrust	[N]
V	Velocity	[m/s]
V	Volume	[L]
v	Velocity	[m/s]
V'	Adjusted tail volume	[-]
v_a	Approach velocity	[m/s]
V_f	Fuel refill volume	[L]
v_{LOF}	Lift-off velocity	[m/s]
v_{stall}	Stall velocity	[m/s]
V_{tank}	Volume of the fuel tank	[m^3]
v_{TAS}	True air speed	[m/s]
W	Weight	[N]
w	Width	[m]
W_{cr}	Cruise weight	[N]
W_{eng}	Weight of the engines	[N]
W_{TO}	Take-off weight	[N]
x	Spanwise location	[m]
$x_{\mathrm{ABC,TO}}$	ABC phase take-off distance	[m]
x_{ABC}	ABC phase landing distance	[m]

Contents

1 Project Objective

The worldwide aviation market has been growing in the past and will keep on growing in the future. Therefore, there is also a need for a growth in air traffic capacity. This results in rising emissions, increasing noise around airports and most importantly, airports need to expand, but are often not able to. The challenge is then to design an aircraft that fits in the current airport infrastructure and can transport more passengers than current single aisle aircraft, while staying as climate friendly as possible. Medium capacity, medium-range aircraft like the Airbus A320 or the Boeing 737 currently have the biggest contribution to air traffic, that is why these aircraft will serve as reference in this project. The top level requirements manifest themselves as follows:

- Payload = 250 - 320 pax (320 at full density) + typical luggage
- Harmonic range (max range at max payload) = 2200 Nautical Miles (NM)
- Minimum operative Mach at cruise = 0.78
- ICAO Aerodrome Ref. Code = 3/4C
  - 3 = 1200-1800m field length
  - 4 = $\geq$1800m field length
  - C = wing span $\leq$36m; outer main gear wheel span $\leq$9m
- Noise level = not higher than best aircraft in category 4D aircraft
- Wake turbulence category = M (not worse than current category "medium")
- Expected EIS (Entry into service): Year 2035

The aircraft designed here will thus have overall dimensions to makes sure it fits in the gate type C, on which the A320 and the B737 aircraft operate. The desired range is also similar to the reference aircraft. The most important change, however, is the amount of passengers the aircraft can carry. The aircraft that will be designed in this report is expected to be able to carry 320 passengers, while the A320 and the B737 aircraft only have a capacity of 150-200 passengers. In addition, effort should be made to have a turnaround time similar to the reference aircraft, despite the higher amount of passengers. In this project, a concept will be selected and studied to meet these demands. Besides the technical feasibility of such a design, its social and economical benefits will be assessed.

The mission need statement is then as follows: *Provide a mid-range aircraft with an A330 capacity, but with the airport compatibility of an A320 and similar ground turn-around time.*
And the project objective statement reads: *Evaluate the design feasibility and socio-economical accessibility of a compact, high-capacity, mid-range aircraft that has a short ground turn-around time, with 10 students in 10 weeks.*

The structure of the report is as follows: in Chapter 2 the possible market for the aircraft is investigated. In Chapter 3 the previous design phases are summarised after which the aircraft is designed in more detail from Chapter 4 until Chapter 10. These technical design chapters all have a specific structure: The first section(s) will describe the technical design(s), after which the verification and validation, the sustainability and the risk of that design are given. Each chapter concludes with the requirements that are already met and some recommendations for future phases.
A sensitivity analysis on the complete design is done in Chapter 11 and a budget breakdown is described in Chapter 12. In Chapter 13 and Chapter 14, a sustainability analysis and a risk analysis are performed respectively. A requirement compliance matrix is given in Chapter 15. The report ends with a description of the functions of the aircraft, the phases that come after this project and the general conclusion and recommendations in Chapter 16 and Chapter 17. In Appendix D, drawings of the designed parts, as well as logic diagrams can be found.

2 Financial Analysis

This chapter assesses the economical viability and the business opportunities of the potential aircraft. The chapter identifies the main stakeholders for HAMMER and explores the market in which HAMMER lands. This is followed by an evaluation of the operational financial performance of the aircraft and its return of investments. A breakdown of the development costs is presented, after which HAMMER is compared to competitive aircraft and the strengths, weaknesses, opportunities and threats for the aircraft are listed.

2.1. Stakeholder Identification

In the research of the economical viability of the HAMMER aircraft concept, three main stakeholders were identified. Of course, there are many more parties with a potential economical stake in the development and operation of the aircraft concept, but for these three the introduction of the aircraft will influence their core business. Therefore, to assess the economical impact of the HAMMER aircraft on the aviation industry, the focus was put on the aircraft manufacturers, aircraft operators and the airports.

Aircraft Operators

The drivers of the demand for the HAMMER aircraft are expected to be the customers and operators of the aircraft. They are in the first place running into their operational capacity limit on medium range flights. Furthermore, they are constricted from further growth in aircraft movements due to the maximum airport capacity and flight time restrictions. To further enlarge their capacity and thus revenues on short to medium haul flights (on domestic airports), a new type of aircraft is needed. Provided that it offers similar- or greater financial performance, the HAMMER aircraft could be an interesting solution. Especially budget airlines which usually rely on high-volume-low-margin business models, an increase in operational capacity is very valuable.

Aircraft Manufacturers

The second important stakeholder in the development of the HAMMER aircraft are the aircraft manufacturing companies. They carry the largest risk and are required to put in the largest capital investment into an unproven aircraft design. Over the past decades, these companies have merged into large corporations that are able to produce aircraft on a highly efficient production line. Investments made into the optimisation of the production process are and have been huge. On the other hand, even very large corporations like Boeing and Airbus are continuously looking for ways to innovate in the aircraft industry in order to gain a competitive edge over the competition. If the HAMMER aircraft has promising business potential, with the possibility of exclusive production by a single manufacturer, could provide the necessary incentive to develop and produce it.

On a side note, for the financial analysis of the HAMMER aircraft concept for the aircraft manufacturers, only products and the potential of Boeing and Airbus are considered. These two companies are the largest in the commercial aviation industry and are therefore most affected by the introduction of a new aircraft concept, but also have the most potential to endeavour on the development of a new aircraft.

Airports

Under constant pressure from local communities, municipalities and governments, airports are looking desperately for a way to reduce and decongest air-traffic without loosing their revenues. Flight time restrictions are imposed on airports out of environmental- and noise constraints. This results in an ever increasing amount of aircraft movements per hour and airports increasing struggle with the demand and congestion during the operational hours. On the other hand, as airports charge operators not only per passenger but also by the amount of aircraft movements and time spent at the gate (on average 35%)[1], it is for them important to have as many aircraft coming and going as possible. The introduction of the HAMMER aircraft would therefore, on first sight, only solve half of the problem.

An interesting solution could be a change in the business model of an airport. When operators are charged per transported kilogram instead of aircraft movement, the introduction of the HAMMER aircraft will

[1] http://www.aeroportal.org/AIOct07.htm [Cited 28 June 2020]

only have positive consequences for airports. While the aircraft movements decrease, aiding in decongestion and the reduction of environmental impact, the transported passengers/cargo (thus kilograms) will remain the same with room for future growth. Furthermore, income from shopping passengers, leases to restaurants and other service companies also contribute to the airport's income. Therefore, more passengers moving through the airport would mean an increase in the latter revenue stream.

2.2. Market Analysis

To assess the demand and opportunities of the HAMMER concept aircraft, it is important to first look at the market for commercial aircraft. The need and purchases of commercial aircraft follow directly from the number of passengers or cargo that needs to be transported. To illustrate the growing demand for air transportation, two parameters have been used. First of all, it is interesting to look at the historic passenger growth as displayed in Figure 2.2. From this figure, it can be seen that the amount of passengers transported each year experiences a near exponential growth. More importantly however, it shows that the amount of passengers transported per year is fairly resilient to financial and geopolitical crises. With respect to the current COVID-19 crisis, this is an important factor to look at. It must be noted however that for example a virus outbreak where governments impose travel restrictions can cause a (temporary) massive decline in passenger (pax) volume.

The second parameter used to indicate the market growth is the average global Gross Domestic Product (GDP) divided by the average available seat kilometres (ASK). ASK is computed by multiplying each flying seat (irrespective whether it is full or empty), by the kilometres it has travelled. This gives an indication of the rising available air transport with the rising global GDP. This metric is plotted and forecasted in Figure 2.1. If the GDP keeps on rising as it has been since 1990, it is expected that the ASK and thus air travel continues to rise with it. To realise the increase in ASK, it is required that the global commercial fleet size also increases, indicating the demand for new aircraft.

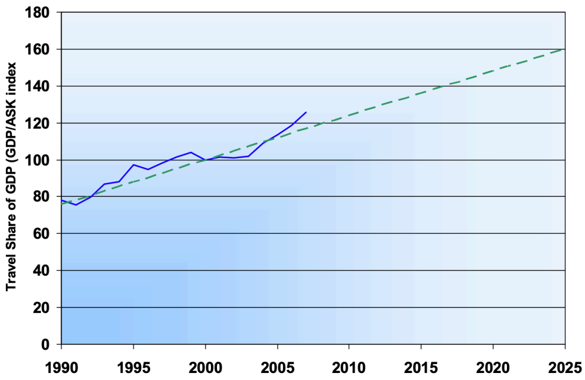

Figure 2.1: GPD vs ASK trend analysis [16].

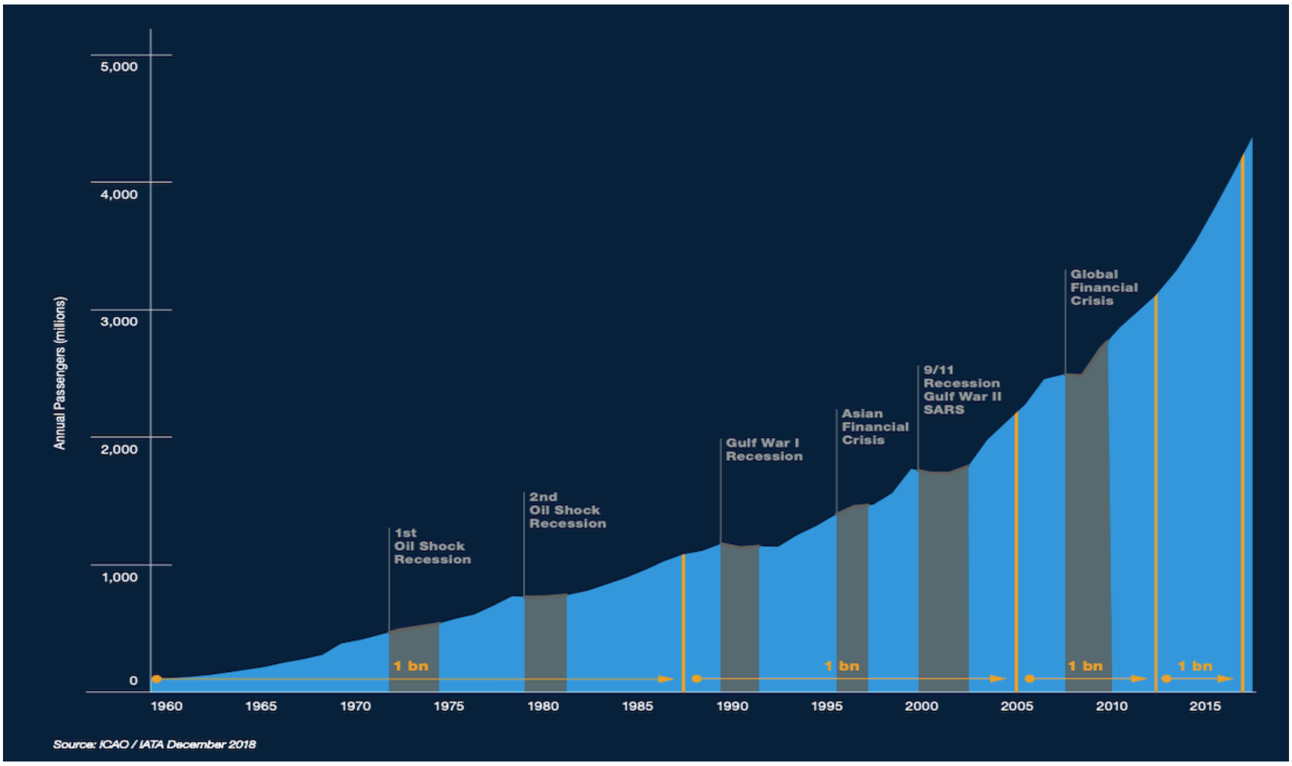

Figure 2.2: Historic passenger growth [13].

2.2.1. Market Segmentation

To see where the HAMMER aircraft will fit in the market, the market segmentation is analysed. When dividing the market into different aircraft types, 3 main categories can be found. These are:

1. short haul- or regional jets (< 36 $[m]$ wingspan, < 90 seats)
2. medium haul- (domestic)[2] or narrow body jets (< 36 $[m]$ wingspan, 90-220 seats)
3. long haul- or wide body jets (> 36 $[m]$ wingspan, > 220 seats)

With the clear requirement to be able to land at short-to-medium range airports (or domestic airports), but with the passenger capacity between the medium and long haul aircraft, the market segment for the HAMMER aircraft is considered to be the medium-haul aircraft. The two best selling aircraft in the world, the Airbus A320 and Boeing 737, will therefore be its direct competitors.

2.2.2. Medium-range Aircraft Market

With the primary market segment for the HAMMER aircraft now established, it is important to assess it's performance with respect to the rest of the commercial aircraft market. Again it is best to start by analysing the passenger movements. Comparing the medium-haul (domestic) to the long haul (intercontinental) travel data will illustrate the decisions operators make for their fleet composition and aircraft purchases/leases. The first parameter to assess this is passenger movements through an example airport (Schiphol International Aiport) where all type of aircraft can land and thus all types of passengers use. Furthermore, a forecast for the weekly flight frequency vs aircraft size will be used.

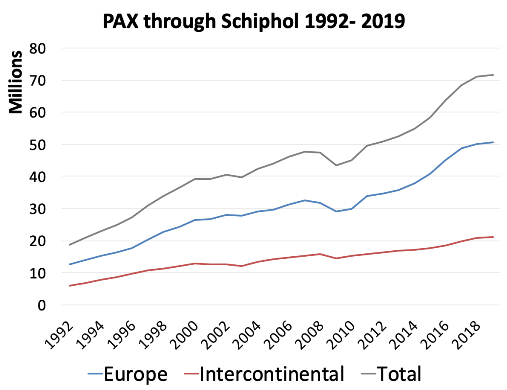

(a) Pax through Schiphol.

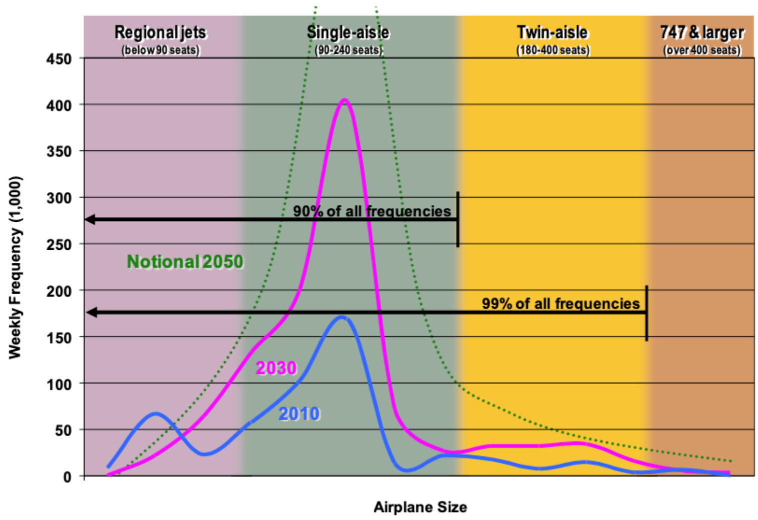

(b) Weekly frequency vs Aircraft size [16].

Figure 2.3: Market segment growth and forecast parameters.

In Figure 2.3a the intercontinental-, domestic- and total passenger movements are analysed. It can be deduced that the yearly growth of medium haul (or domestic) passengers is higher than the growth of the total passenger movements at an average rate of +5.39% vs +5.20%. Where in 1992, only 67% of the passengers travelled domestically, this increased to 71% in 2019. This is in line with the results and forecast as displayed in Figure 2.3b. This model, from the SUGAR [3] phase I design report [16], predicts that the narrow body aircraft flight frequency will increase the most until 2030. This illustrates the demand for an aircraft with a higher passenger capacity on medium range flights as it can relieve the required increase in flight frequency. It is important to note that the demand for medium range flights originates from both an increase in demand on current routes, and demand for new medium haul routes. The increase in new routes is driven by customer demand for point to point (direct flights) transportation between airports instead of the more traditional hub and spoke (connecting flights) model. On new, low volume routes, it is likely that HAMMER will not be operated as operators are likely not able to fill the aircraft. On the other hand, the demand for passenger capacity on high volume, high frequency routes also increases. This is where the HAMMER aircraft will be very effective. For example: On average, there are 21 flights per

[2]Although domestic flights literally mean flights within one country, in market analyses it is often used for medium haul flights. This is due to the American market where the average domestic flight distance (between costs) is a medium range flight

[3]Subsonic Ultra Green Aircraft Research

day between Amsterdam Schiphol and London Heathrow[4]. This number can be decreased to 12 when operating the HAMMER aircraft. It is therefore likely that the HAMMER aircraft will be purchased and operated on the routes with high passenger demand.

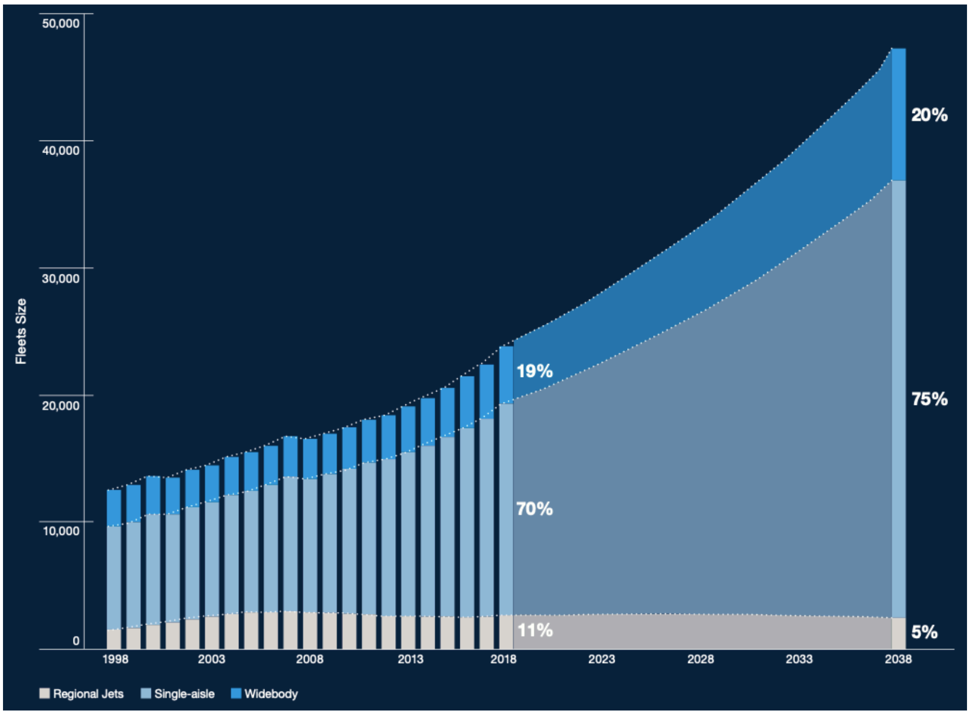

Figure 2.4: Fleet composition from 1998 to 2038 [13].

For the aircraft operators, manufacturers and airports it is relevant to adjust their fleet to the predicted passenger capacity demand. A first indication can be obtained by looking at the global fleet composition historic data and forecast as laid out by the Boeing Commercial Outlook 2019-2038[5] [13]. A graphic representation of the fleet composition can be found in Figure 2.4. It can easily be seen that the medium haul (or narrow body) aircraft not only has had the largest share in the fleet historically, but is also forecasted to grow the fastest. The share of narrow-body aircraft is expected to increase by +5%, against a +1% increase for wide-body jets and a 6% decrease for regional aircraft. This forecast can be supported by looking at the sales data for the different aircraft types.

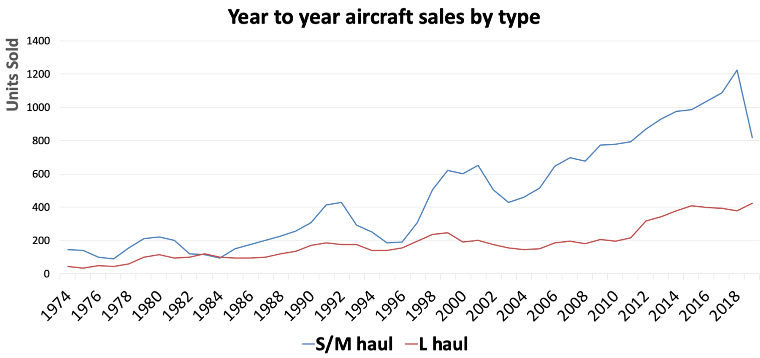

Figure 2.5: Aircraft sales by type.

From the sales data as in Figure 2.5 two relevant conclusions about sales and market performance can be drawn. First of all, medium haul aircraft have been continuously outselling the long haul aircraft type. Furthermore, the difference is sales has only been increasing in favour of the medium haul aircraft category. The second conclusion that can be drawn is that, although total passenger movements are fairly resilient to crises Figure 2.2, the sales of medium haul aircraft reacts much more. The long-haul aircraft sales perform more steady and the impact of market demand, fluctuations and external influences

[4]https://www.skyscanner.net/routes/lhr/ams/london-heathrow-to-amsterdam.html#: :text=As%20of%20June%2C%20there%20are,from%20L 28 June 2020]

[5]It is important to note that in this report, the effects of the COVID-19 crises are not incorporated.

has less effect. It can be explained by the fact that medium haul aircraft are often the only aircraft type operated by budget airlines for which it is disastrous if they temporarily experience a decrease in customers. Furthermore, due to the low price of domestic flight tickets, a large share of the passengers is travelling for leisure. Something that is easily put on hold during financially difficult times. As passengers on long haul flights are largely travelling for business, they are less likely to stop travelling. This is a risk to be considered upon entering the medium haul aircraft market with the HAMMER aircraft concept. On a final note, the drop in sales of the medium haul aircraft in 2019 can be explained by the issues Boeing currently experiences with the Boeing 737-MAX. This causes an approximate 80% drop in sales of the Boeing 737. This however does not affect the global market for medium haul aircraft.

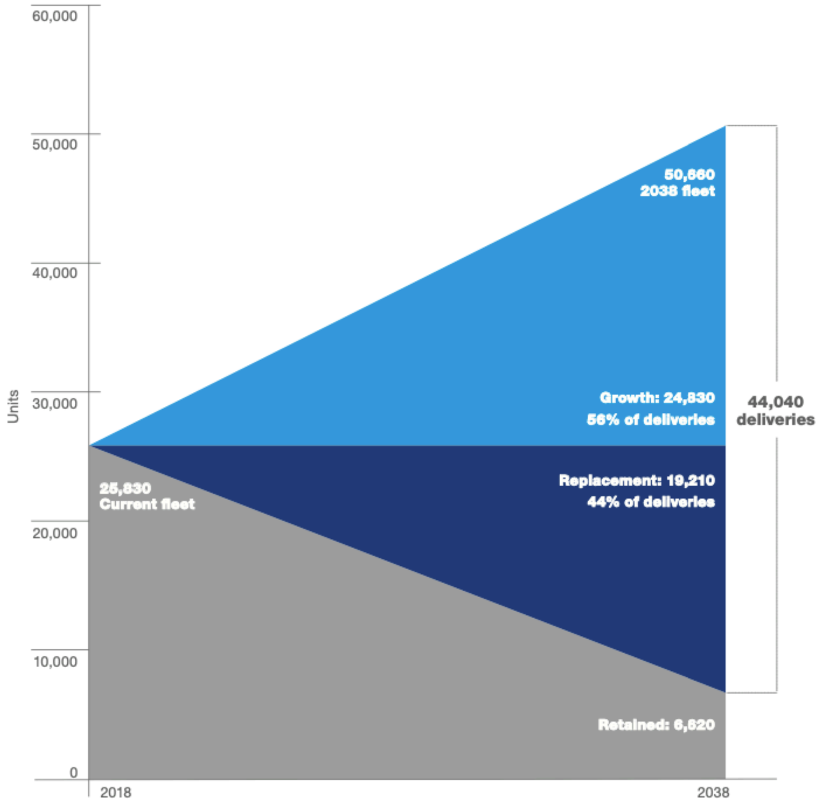

Figure 2.6: Forecast for the delivery of new aircraft 2019 - 2038 [13].

The Boeing commercial outlook [13] also forecasts the number of new aircraft deliveries from 2019 until 2038. Although the HAMMER aircraft will have an expected entry into service (EIS) by the year 2035, it is still relevant to know what the market outlook will be by that time. Furthermore, as aircraft operators or lease corporations try to spread their aircraft purchases and deliveries over multiple years (to have a near continuous in- and outflow of inventory/aircraft) it is likely that the principle of the forecast still holds by the time HAMMER is introduced. The forecast, as shown in Figure 2.6, predicts approximately 44,000 new aircraft deliveries until 2038 globally across all market segments. From these aircraft, approximately 44% will replace the current fleet and 56% will be an addition to the fleet. The total value of these aircraft is estimated to be $6 trillion. This means that the medium range aircraft market has a potential of $4.5 trillion the HAMMER concept could capitalise on.

2.3. Financial Analysis in Operation

For a market to exist for the HAMMER aircraft concept, it is essential to assess its cost effectiveness and operational financial performance against the current standard. As stated before, it is the operators of the aircraft that drive the demand for a new aircraft type first and foremost. To assess this, three main parameters are compared, which are:

1. Block hour cost
2. Revenue and cost per available seat mile
3. Return On Investment (ROI)

As a side note on this section, some of the estimations done in this section are based on the technical design of the aircraft, performed in the rest of this report. For clarity and ease of reading reasons, it was decided to display the results of the economical performance in this chapter.

2.3.1. Block Hour Cost

Block hour cost is a financial parameter in the aviation industry that averages the total operational cost of an aircraft, during regular operation, over the time it does not spend at a gate. For the HAMMER aircraft concept, this is expected to increase. The number of block hours is expected to remain approximately similar to the current medium haul aircraft, while the increased aircraft size will lead to an increase in fuel consumption and cost. Furthermore, it is expected that the maintenance cost, and insurance cost of this more complex and expensive aircraft will increase in absolute sense.

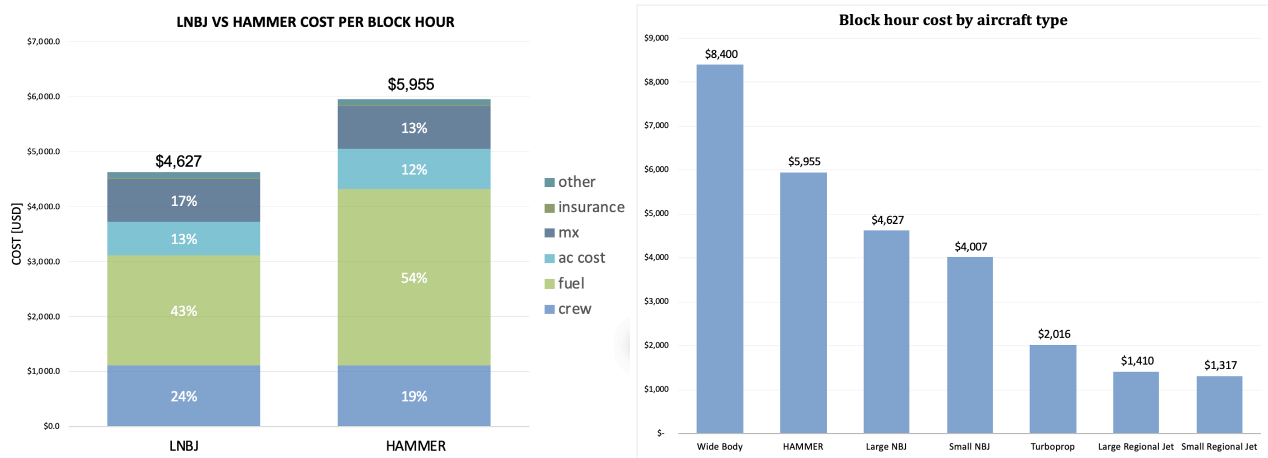

(a) Large Narrow Body Jet vs HAMMER. (b) HAMMER vs rest of market segments.

Figure 2.7: Block Hour cost breakdown.

To put this into perspective, the block hour cost of the HAMMER aircraft concept has been analysed and compared to that of an average large narrow body jet (LNBJ, 170 - 220 pax)[6][7]. From Figure 2.7a it can be seen that the block hour cost of the HAMMER aircraft indeed increases by approximately $1300. The largest increase comes from the fuel consumption (approx. projected as 1.5 times that of a LNBJ). Furthermore, when compared to other aircraft categories in Figure 2.7b, one can see that the HAMMER fits between the LNBJ and the wide body aircraft. The conclusion from these statistics is that the operational capital investment in a HAMMER aircraft is bigger than that into a LNBJ. This is a disadvantage as operators try to keep their investment into inventory and operation as low as possible.

2.3.2. Revenue- and Cost per Available Seat Mile

When looking at the Revenue- and Cost per Available Seat Mile (RASM and CASM respectively) however, the HAMMER aircraft outperforms its current competitors. These financial performance parameters are worked out for both the HAMMER aircraft and the current market standard large narrow body jet (LNBJ)[8] and are displayed in Table 2.1. The cost model from planestats[9], an aircraft database by respected manamagment consultancy firm Oliver Wyman Group, and Oliver Wyman Group annual reports [68] is used.

[6]https://www.statista.com/statistics/599262/us-airlines-cost-per-block-hour-by-aircraft/ [cited 22 June 2020]
[7]https://www.planestats.com/bhsn_2018dec [cited 22 June 2020]
[8]http://web.mit.edu/airlinedata/www/default.html [cited 28 June 2020]
[9]https://www.planestats.com/bhsn_2018dec [cited 28 June 2020]

Table 2.1: RASM and CASM comparison between LNBJ and HAMMER.

		LNBJ		HAMMER		
	Parameter	**Value**	**%**	**Value**	**%**	Δ
CASM	Crew	1.53	14.71%	1.53	15.11%	
	Fuel	2.76	26.49%	2.56	25.77%	
	Aircraft cost	0.85	8.12%	0.57	5.78%	
	Mx	1.11	10.68%	1.11	11.18%	
	Insurance	0.01	0.08%	0.02	0.20%	
	Other	0.15	1.46%	0.15	1.52%	
	Overhead	4.0	38.46%	4.0	40.21%	
	Total	**10.4**	**100%**	**9.95**	**100%**	**-4.37%**
RASM	**Total**	**14.64**	**100%**	**14.64**	**100%**	**0%**
Daily Performance	ASM	790958 seat km		1361800 seat km		+72%
	RPM	665949 seat km		1146572 seat km		+72%
	Load Factor	84%		84%		
	Cost	$82271		$135461		+64%
	Revenue	$97495		$167858		+72%
	Profit	**$15224**		**$32397**		**+112%**
	Margin ASM	**29%**		**32%**		**+3.1%**

A couple of things are important to note with Table 2.1:

- All CASM and RASM costs are in USD cents ($0,xx)
- Crew, overhead, Mx and other costs are assumed to be the same per ASM for both aircraft types
- Revenue per paying customer (RPM) is assumed to be the same due to expected similar ticket pricing
- Load factor is assumed to be the same
- Fuel cost is increased as in Subsection 2.3.1 (160%), due to the increased ASM however, the fuel CASM decreased
- Aircraft cost is increased as in Subsection 2.3.1 (120%), due to the increased ASM however, the fuel CASM decreased
- Insurance cost on a entirely new aircraft type is assumed to double

When all is summed, the daily profit is expected to increase by +112% from the current LNBJ. Furthermore, the profit margin per available seat mile increases by +3%. For the operators, along with the added benefit of decreasing the aircraft movements, this is very beneficial.

2.4. Return on Investment

To further illustrate the financial advantage the HAMMER aircraft could bring, the return on investment is analysed. For both the aircraft manufacturers and the aircraft operators, this direct financial performance parameter is often the decisive factor in the development/operation of a certain aircraft type.

2.4.1. Aircraft Manufacturers

As the aircraft manufacturers establish the unit price for the aircraft, it is important to analyse the manufacturers return on investment (ROI) first. To do this, quantitative data is taken from the commercial aircraft division of Boeing and Airbus. Most aircraft models have been developed over many years, so that it is difficult to estimate total development costs. The program cost for HAMMER is therefore based on two completely newly developed aircraft types, the Boeing 787 ($32 Billion) and Airbus A350 ($15 Billion). This was considered accurate enough because the nature of the development of the 787 and A350 is approximately the same as the HAMMER aircraft. All are completely new (from the ground up) designs, making use of new composite materials and introducing the latest aircraft innovations. As it is currently unclear (company sensitive data) why the development cost of the similar B787 and A350 are so far apart, it was chosen to simply average them for a first estimation of the HAMMER development cost. This results to a total estimated development cost for the HAMMER aircraft of $23.5 billion. The development cost is very rudimentary determined and a more detailed estimation should be made before advancing with the development of HAMMER.

To come up with a unit price for the HAMMER aircraft, again the direct competition is analysed. The large narrow body jet (A320, B737) unit prices[10][11] were divided by their number of seats. This unit-price/seat was then multiplied by the number of seats in the concept aircraft to come up with the initial estimate of the aircraft unit price. As the exact breakdown of profit per aircraft model is usually a trade secret, estimations on the margin Airbus[12] and Boeing[13] make on their aircraft are based on the yearly revenue and earnings before income and taxes of the commercial aircraft division. The margins for Boeing (13.1%) and Airbus (11.6%) are averaged to find the potential margin for the HAMMER aircraft (12.35%).

This results in a computed ROI for the manufacturers of 965 aircraft units. This is higher than the competition as can be seen from Table 2.2. However, due to the innovative nature of the HAMMER aircraft, it is likely that the aircraft can be sold at a premium. At an approximate 10% price increase to $220 million, the aircraft is still competitively priced (looking at price/seat) between the medium haul and long haul aircraft. The break even point (BEP) for manufacturers drops to 865 units which is comparable to the other models in the aircraft range. Furthermore, with a potential of 44,000 aircraft sales to capitulate on (see Figure 2.4), there is sufficient market capacity to make the HAMMER profitable.

2.4.2. Aircraft Operators

To underline the market potential of the HAMMER aircraft, it is also relevant to analyse the ROI for the operators of the HAMMER concept. For this metric it is also most relevant to look at the aircraft the HAMMER will compete with (A320, B737). With the costs and as explained in Subsection 2.3.2 (Depreciation and inflation accounted for), it was found that both aircraft have a break even point of approximately 21 years. The HAMMER concept with the adjusted, premium price was found to have an predicted break even time (BET) of 18.5 years. This 10% decrease in break even time is very attractive for operators, driving the demand for HAMMER box wing even further. This also indicates the increase in return on investment for operators of HAMMER w.r.t. current LNBJ aircraft.

All values used in the computation for BEP for the manufacturers and operators are summarised and displayed in Table 2.2. In Table 2.2 the data for the HAMMER concept aircraft with the adjusted premium price is displayed as **HAMMER adj.**. In this table, R&D stands for research and development.

Table 2.2: Unit cost and ROI for HAMMER.

				Manufacturers			Operators
Aircraft	**Unit price ($M)**	**# Seats**	**Price/Seat**	**R&D Cost ($B)**	**Margin**	**BEP (Units)**	**BET (y)**
Boeing 737	114.75	185	620270	-	-	-	20.7
Airbus A320	114.85	185	620811	-	-	-	20.7
Boeing 787	264.75	350	756429	32	13.1%	834	-
Airbus A330	293.01	350	837343	15	11.6%	489	-
HAMMER init.	197.33	320	620541	23.5	12.4%	965	16.7
HAMMER adj.	**220.00**	**320**	**691824**	**23.5**	**12.4%**	**865**	**18.6**

2.5. Cost Breakdown Structure

Usually, the aircraft development cost and unit price are based on statistics and models that can be found in for example Roskam's [52]. The disadvantage, however, is that these models are more than 30 years old and therefore difficult to apply on a project with an expected entry into service of 2035 (by the time the models are 45 years old). Therefore, as explained in Section 2.4, the total project cost for the developers and the unit cost are estimated based on the market outlook and the most recent aircraft developments.

[10] https://www.statista.com/statistics/273962/prices-of-airbus-aircraft-by-type/ [cited 22 June 2020]
[11] https://www.statista.com/statistics/273941/prices-of-boeing-aircraft-by-type/ [cited 22 June 2020]
[12] https://www.airbus.com/newsroom/press-releases/en/2020/02/airbus-reports-full-year-2019-results.html [cited 22 June 2020]
[13] https://investors.boeing.com/investors/investor-news/press-release-details/2019/Boeing-Reports-Record-2018-Results-and-Provides-2019-Guidance/default.aspx [cited 22 June 2020]

To summarise, the HAMMER aircraft is expected to have a project cost of $23.5 billion and a unit price of $220 million.

From Roskam's book on aircraft cost estimation [52], the breakdown model of the aircraft development cost was taken. Although the methods are old, it is assumed that the proportions of the different development activities remain the same. This breakdown of cost is summarised along with values relevant for HAMMER in Table 2.3 with all values in $ billion.

Table 2.3: HAMMER development cost breakdown as by [52].

	HAMMER Development Cost		
	$23.5		
	Engineering	**Tooling**	**Other**
Percentage	42%	35%	25%
Cost	$9.87	$8.23	$5.88

These are all non recurring cost in order to initiate the production of the HAMMER aircraft. The activities that fall under the non-recurring cost are:

- Engineering: Airframe design/analysis, control and configuration, systems engineering
- Tooling: tool and fixture design and fabrication, build of production line
- Other: development support, certification, flight testing

If put in production, an analysis of the recurring cost (labour, material, support) should be analysed.

2.6. Competition

To complete the market analysis of the HAMMER aircraft, the (potential) competition is analysed. In the metrics and financial parameters used up until now, HAMMER was only compared to the existing competition of large narrow body aircraft. With an expected entry into service of 2035, it is also relevant to analyse the expected market outlook by that time. There are two ways in which aircraft manufacturers will create competition for the HAMMER aircraft. First of all, the development of LNBJ aircraft will continue and following the historic trend will increase their capacity. However, due to their conventional design, this capacity will have a limit. At the moment, the largest single class LNBJ has the capacity to carry 220 passengers. It is expected that this is reaching the limit of the efficiency of the conventional aircraft design. The risk that conventional aircraft are developed to a point where flying two of them is more efficient than flying one HAMMER aircraft is considered very low. The profitability of the HAMMER aircraft is expected to be more than twice as high of that of a normal aircraft and with only one aircraft flying instead of two, there is much less operational risks and cost involved.

Secondly, different experimental aircraft concepts are worked out that focus on solving the same set of top level requirements. R&D-teams of different universities and aircraft manufactures are working on more efficient aircraft design and operation on all facets, while decreasing the number of aircraft movements. It is likely that a strong competitor for the HAMMER aircraft will emerge. Furthermore, there is a risk that an aircraft concept which is smaller, but much more efficient than HAMMER is developed. This would mean that, although not alleviating congestion at airports, for operators is could become more cost efficient to operate multiple smaller aircraft instead of HAMMER. The possibility of this should be kept track of during the development of HAMMER.

Finally, the HAMMER aircraft will experience competitions from other forms of innovative passenger transportation. A good example of this would be the development of a Hyperloop infrastructure[14]. It is not expected, with regards to the financial aspect, that current alternative transporation methods (train and car) will be able to compete with HAMMER. Like with innovative aircraft development, it is difficult to assess the potential competition of innovative passenger transportation means and should therefore be kept track of during HAMMER development.

2.7. SWOT

To conclude the financial analysis of the HAMMER aircraft, a SWOT analysis is performed. This summarises the Strengths, Weaknesses, Opportunities and Threats discussed in this chapter and introduces some more. These are on a very high level but still specific to HAMMER. The analysis captures the business outlook of the concept aircraft.

[14][accessed 28/06/20] https://delfthyperloop.nl/en/

Table 2.4: SWOT analysis HAMMER aircraft concept.

Strength	Weaknesses	Opportunities	Threats
Better profitability than current medium range aircraft	Higher capital investment required by operators and manufacturers	Disrupting the current aircraft market, increasing its market potential	Not enough incentive to motivate manufactures to move from their current portfolio
Higher Return on Investment for operators	High research and development cost and effort required	Increased demand for aircraft originates from (congested) airports and operators	Might be difficult to be approved by governing aircraft agencies (i.e. EASA)
More sustainable, due to lower fuel consumption per seat mile	Unproven concept	Environmental friendly aircraft can have lower landing fees (cheaper pax tickets)	Development of other sustainable aircraft could jeopardise the value of HAMMER

2.8. Conclusion

In short, the market analysis forecasts that in the coming 20 years 44,000 new aircraft will be deliverd with a market value of \$6 trillion, of which 75% is the medium haul market in which the HAMMER concept aircraft will fall. This market segment is therefore the fastest growing with the most potential. The capital investment in the purchase and operation of HAMMER will be higher than the current LNBJ's. The profitability of HAMMER for operators will increase by 112% compared to the LNBJ and the break even point will decrease by 10% to 18.5 years. For manufacturers, the return on investment will be similar to current aircraft in their portfolio and for operators the ROI will increase. This, combined with its increased sustainability, innovative design and alleviation of airport congestion makes for a powerful combination of demand by customers and incentive for manufacturers. From a financial standpoint, the HAMMER aircraft is predicted to outperform current aircraft. Before advancing with HAMMER detailed development, there are some parameters to be worked out into further detail:

- Calculate exact values for the return of investment for HAMMER aircraft w.r.t. LNBJ (detailed, sensitive company data needed), both for operators and manufacturers
- A more detailed analysis of the aircraft development cost will need to be made (detailed, sensitive company data needed).
- A sensitivity analysis of the aircraft development cost on ROI, BEP and profitability for manufacturers should be performed.
- A sensitivity analysis of the aircraft unit price on ROI, BEP and profitability for aircraft operators should be performed.

3 Conceptual Trade-off & Initial Sizing

This chapter presents a summary of the requirements the design needs to meet, and how the different concepts to meet these requirements, came to be. In addition, the trade-off procedure to choose a concept is explained and the conceptual design, on which this report builds, is described. Lastly, the functions of the aircraft are layed out.

3.1. Top-Level Requirements

In order to be more specific on how the design will meet the demands presented in Chapter 1, some top level requirements were given. They are listed below:

- The aircraft shall have a capacity of 250 to 320 passengers including accompanying cargo
- The aircraft shall have a harmonic range (max range at max payload) of 2200 [NM]
- The cruise Mach number shall be no lower than 0.78
- The aircraft shall follow the International Civil Aviation Organisation (ICAO) Aerodrome ref code= 3/4C
  - The aircraft has a wingspan smaller than 36 [m], according to the C designation
  - The outer main wheel gear span is smaller than 9 [m], according to the C designation
  - The aircraft height shall be no more than 13.5 [m], according to the C designation
  - The aircraft balanced field length shall be ICAO Category 3, between 1200 [m] and 1800 [m], for any configuration not in high density
  - The aircraft balanced field length shall be a maximum ICAO Category 4, 1800 [m] and above, for a high density configuration, if ICAO Category 3 can not be fulfilled in high density configuration
- The aircraft shall comply with ICAO Stage 5 noise certification
- The aircraft shall fall in the wake turbulence category C 'Lower Heavy' of the RECAT EU system

In addition to these requirements, there are some other aspects the design needs to take into account:

- The design shall be a 'wing lifting' design, meaning that it should have a fixed wing.
- The year the aircraft is expected to entry into service is 2035. This means only off the shelf products can be used, or new technologies that are proven to be much more sustainable and are expected to be ready by 2035.
- The aircraft must comply with the Certification Specification (CS) - 25 airworthiness regulations and the air traffic management safety.
- The design will not require significant changes to current airport infrastructure and servicing gear.

These top-level requirements result in many smaller subsystem requirements. They are provided in the baseline report and can be found in this report in the different compliance tables [20].
Lastly, the primary design objective for this project was summarised as: Maximise the aircraft's Payload Range Efficiency (PRE) parameter, while minimising time required for ground operations (passengers/luggage boarding and disembarking, servicing, etc.).

3.2. Concept Selection

As the aircraft will be a fixed wing aircraft, it will need a fuselage that is relatively large compared to the span, in order to fit the requirements. Therefore, a rather disruptive configuration will be needed. For the preliminary analysis, four concepts were analysed. They can be found in Table 3.1 [21].

Table 3.1: Description of the selected HAMMER-concepts.

Concept	Description	Sketch
HAMMER-BW (Box Wing)	• Enclosed wing • Aft wing connected to fuselage with v-tail • No horizontal tail • Single deck • Double-bubble fuselage • Two turbofans and Electric fan in between	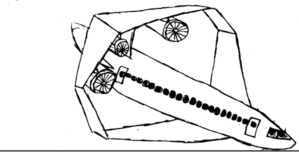
HAMMER-BWB (Blended Wing Body)	• Integration of fuselage and wing • Body contributes to lift • Wing more aft than conventional • Has winglet rudders • Single deck • Multi-bubble fuselage • Hydrogen propulsion system	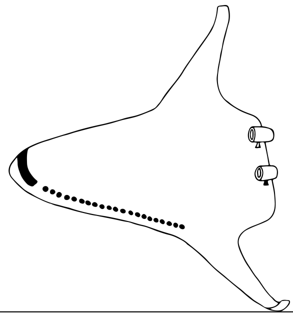
HAMMER-CFW (Conventional Fixed Wing)	• Conventional swept wings with winglets • Conventional horizontal and vertical tail • Single deck • Double-bubble fuselage • Two turbofans under the wing	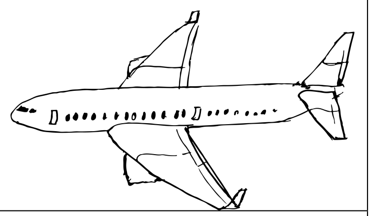
HAMMER-FW (Foldable Wing)	• Wings foldable over the span • Conventional horizontal and vertical tail • Single deck • Double-bubble fuselage • Two turbofans under the wing	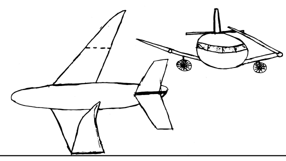

3.3. Trade-Off

In order to choose the best concept a trade-off was performed based on an initial analysis on a number of criteria. The performance of each concept in the areas of ground operations, structures, aerodynamics, flight performance and sustainability and resources was taken into account. Other areas were deemed to be independent from the selected concept or not important enough for the trade-off. The subjects analysed for each criteria are listed below:

- Ground Operations:
  - Accessibility
  - (De)Boarding Time
  - Fuel Time
  - Possible Autonomy
  - Extra Cabin Luggage
- Structures and Airframe:
  - Subsytem Integration Efficiency
  - Weight
  - Fuel Tank Space
  - Landing Gear Bay
  - Flutter
- Sustainability Analysis:
  - Fuel Savings with respect to an A320
  - Noise Performance
  - Development Readiness and Economic Sustainability
- Aerodynamics:
  - Lift-over-Drag Ratio
  - Cruise Performance
  - High-Lift Devices Complexity

- Flight Performance:
  - Payload-Range Efficiency
  - Stability and Control
  - Specific Range
  - Specific Endurance

Table 3.2: Final trade-off table.

Parameter	Weight	BW	BWB	CFW	FW
Ground Operations	30%	4.5	4.2	4.0	4.6
Structures and Airframe	15%	3.0	4.6	4.1	3.8
Aerodynamics	15%	5.0	3.2	2.9	4.1
Flight Performance	15%	4.7	3.2	4.1	4.2
Sustainability	25%	4.4	3.7	4.1	4.2
Final Grade	**/5**	**4.3**	**3.8**	**3.9**	**4.2**

Finally all these grades are combined in a trade-off table, which can be seen in Table 3.2, to choose the best concept. The trade-off clearly led to the selection of the box wing concept. This trade-off was also accompanied by a risks assessment and a sensitivity analysis, which confirmed the box wing as the winning concept.

3.4. Initial Sizing

The mission profile was first analysed to obtain data for the rest of the weight sizing methods. The mission profile can be seen in Figure 3.1. Initial weight estimation and sizing was performed using Class I & II iteration weight estimation methods. The starting point for this iterative process were the passenger and range requirements. Combined with reference data on fuel use, an initial estimation for the maximum take off weight (MTOW) and fuel weight was gathered which allowed for the construction of a thrust to weight-wing loading diagram that can be seen in Figure 3.2.

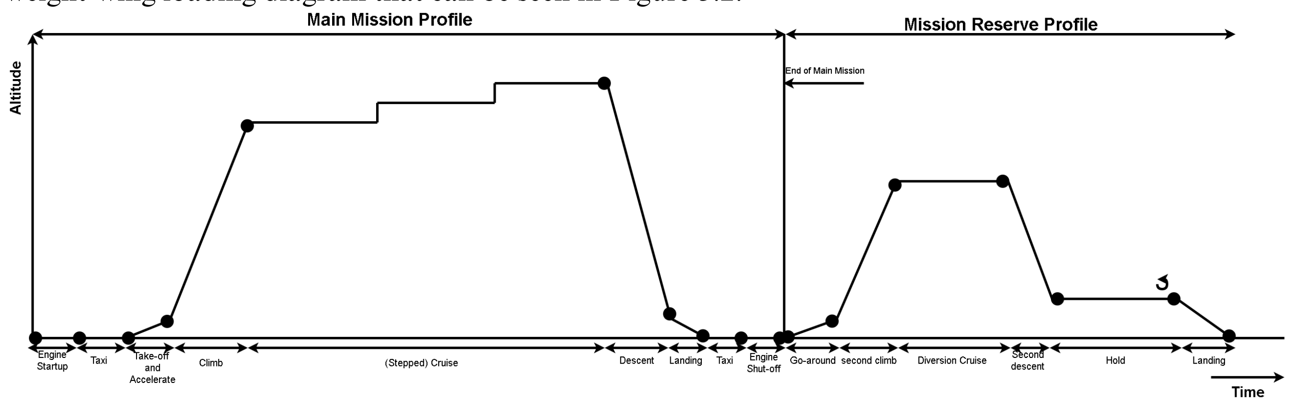

Figure 3.1: The projected HAMMER mission profile

Using Figure 3.2, the design point for this project was chosen. This is indicated by the red dot in the graph. Using the acquired values, a Class II weight estimation was performed. Structural components were estimated using the Raymer method for initial aircraft sizing. The engines were sized based on a similar project which also used advanced turbofan engines [17]. The results of the Class I & II and initial aerodynamic sizing as well as flight performance analysis findings can be found in Table 3.6.

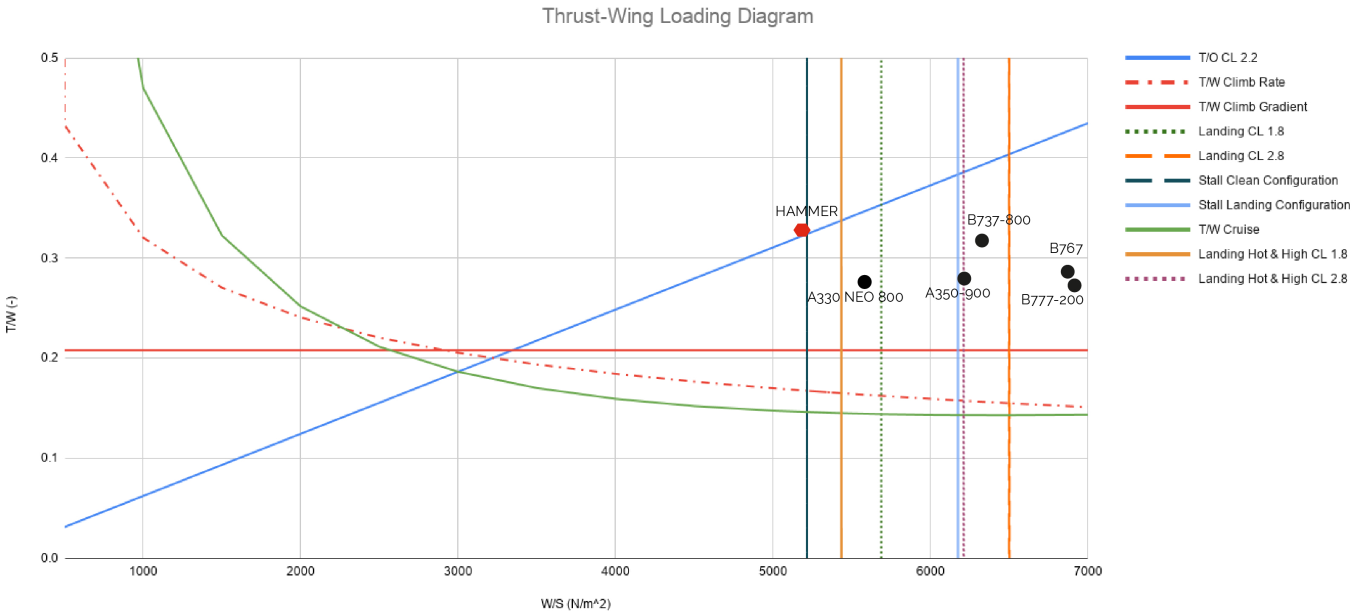

Figure 3.2: Thrust to weight-wing loading diagram for initial sizing of HAMMER. The red dot represents the design point. Clean stall lift coefficient (C_L) was assumed to be 1.8, and the aspect ratio 5.5.

3.5. Manoeuvre Diagram

To size for the maximum load case, an initial manoeuvre diagram was setup using methods from the Aerospace Design & Systems Engineering Elements (ADSEE) I course [70]. This diagram can be seen in Figure 3.3 and is constructed using calculated load factors for each phase of the flight, using Equation 3.1.

$$n = \frac{L}{W} = \frac{\frac{1}{2}\rho V^2 S C_L}{W} \tag{3.1}$$

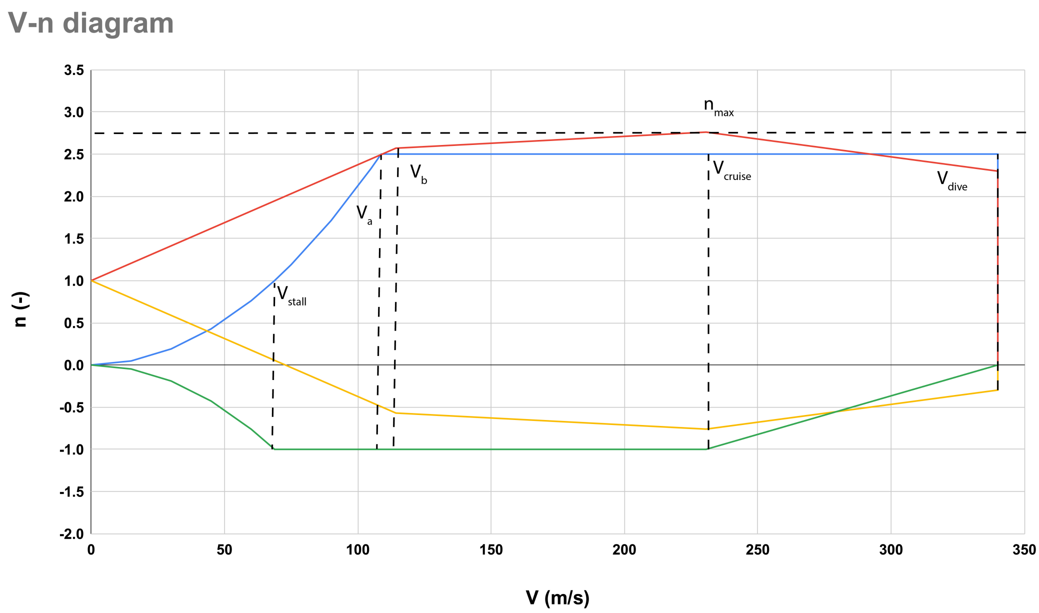

Figure 3.3: The manoeuvre diagram.

Gust manoeuvring is also incorporated. They are represented by the yellow and red lines. Gusts can significantly increase the loading and indeed, for the HAMMER the gust loading is the highest load factor possible.

The first speed shown is the stall speed V_{stall}, the minimum speed at which the aircraft can fly, calculated using Equation 3.2. Below this speed the aircraft does not generate enough lift to fly. The next speed is V_a, which is the minimum speed at which the maximum load factor defined by aviation authorities for normal steady flight is reached, which for the HAMMER is $n = 2.5$ and $n = -1$. It is calculated using Equation 3.3. Then, the cruise speed V_{cruise} is the speed at which the aircraft flies during cruise. Finally, V_{dive} is is defined as $V_{dive} = 1.5 \cdot V_{cruise}$ [70]. This is a bit peculiar, as this results in a supersonic speed. However this is defined by aviation authorities and as such the dive speed is quite high.

$$V_{stall} = \sqrt{\frac{2W}{\rho C_{L_{Max}} S}} \tag{3.2}$$

$$V_a = \sqrt{\frac{2n_{max}W}{\rho C_{L_{Max}} S}} \tag{3.3}$$

For the gusts, maximum gusts speeds were identified to size the aircraft for. An additional speed, V_b, is defined as the bad weather speed. The gust speeds are usually given in feet per second, as seen in Table 3.3. The calculated speeds for the diagram are shown in Table 3.4.

Table 3.3: The gust speeds.

Velocity	Gust Speed [$\frac{ft}{s}$]
V_b	66
V_{cruise}	50
V_{dive}	25

Table 3.4: The calculated speeds.

Velocity Type	Speed [$\frac{m}{s}$]
V_{stall}	68.8
V_a	108.7
V_b	114.3
V_{cruise}	230.6
V_{dive}	340.0

Knowing all these speeds and gust speeds, the diagram can be constructed. It is seen that the gust is the main determining factor, with a load factor of $n = 2.75$. The ultimate load factor is then defined as $n_{ultimate} = 1.5 \cdot n_{max}$. Thus $n_{ultimate} = 4.13$, which shall be used for further calculations in the report.

Load factors were applied to ensure safety during the most critical manoeuvres an aircraft can make during its lifetime. The load factors that were used are summarised in Table 3.5.

Table 3.5: Load factors derived from the V-n diagram [37].

Load factor	n_i	**magnitude**
Limit load	n_1	2.75
Proof load	$n_2 = 1.25n_1$	3.44
Ultimate load	$n_3 = 1.5n_2$	4.13

3.6. Conceptual Design

The analyses and trade-off presented in the previous sections led to the conceptual design of the box wing, on which this report will build. An overview of some of the characteristics of the preliminary design can be found in Table 3.6.These values were built upon for the final design, with most of them iterated to provide an optimal configuration. Additionally, a double bubble design was chosen for the cross-section and gas turbofans were chosen as propulsion method over electrical propulsion and hydrogen. The material composition of the aircraft was also looked into, and aluminium, Carbon Fibre Reinforced Polymers (CFRP) and Glass Laminate Aluminium Reinforced Epoxy (GLARE) were chosen as the main materials. More detail on how this design came to be and more values can be found in [21].

Table 3.6: The initial sizing parameters for the aircraft.

Parameter	Value	Parameter	Value
MTOW [*kg*]	126517	$C_{L_{Max_{clean}}}$ in clean configuration [-]	1.8
Fuel Mass [*kg*]	26821	$C_{L_{Max_{takeoff}}}$ [-]	2.2
Operative Empty Weight (OEW) [*kg*]	55703	$C_{L_{Max_{landing}}}$ [-]	2.8
Wing Loading [$\frac{N}{m^2}$]	5215	Climb gradient [-]	0.15
Thrust to weight [-]	0.33	Climb speed [$\frac{m}{s}$]	15
Span [*m*]	36	Cruise Height [*ft*]	36000
Wing Area [m^2]	237.9	Cruise Mach Number M_{cruise} [-]	0.78

3.7. Internal Communication

For a smooth design process, it is important to know how information is shared between the different department. Also if certain requirements or design choices change, knowing which department is affected allows for better handling of the subsequent problems. To show this dynamic between departments, the communication diagram in Figure 3.4 is made. On the diagonal each engineering department is shown. On the horizontal the output of that department is given, whereas the vertical is the input for each department.

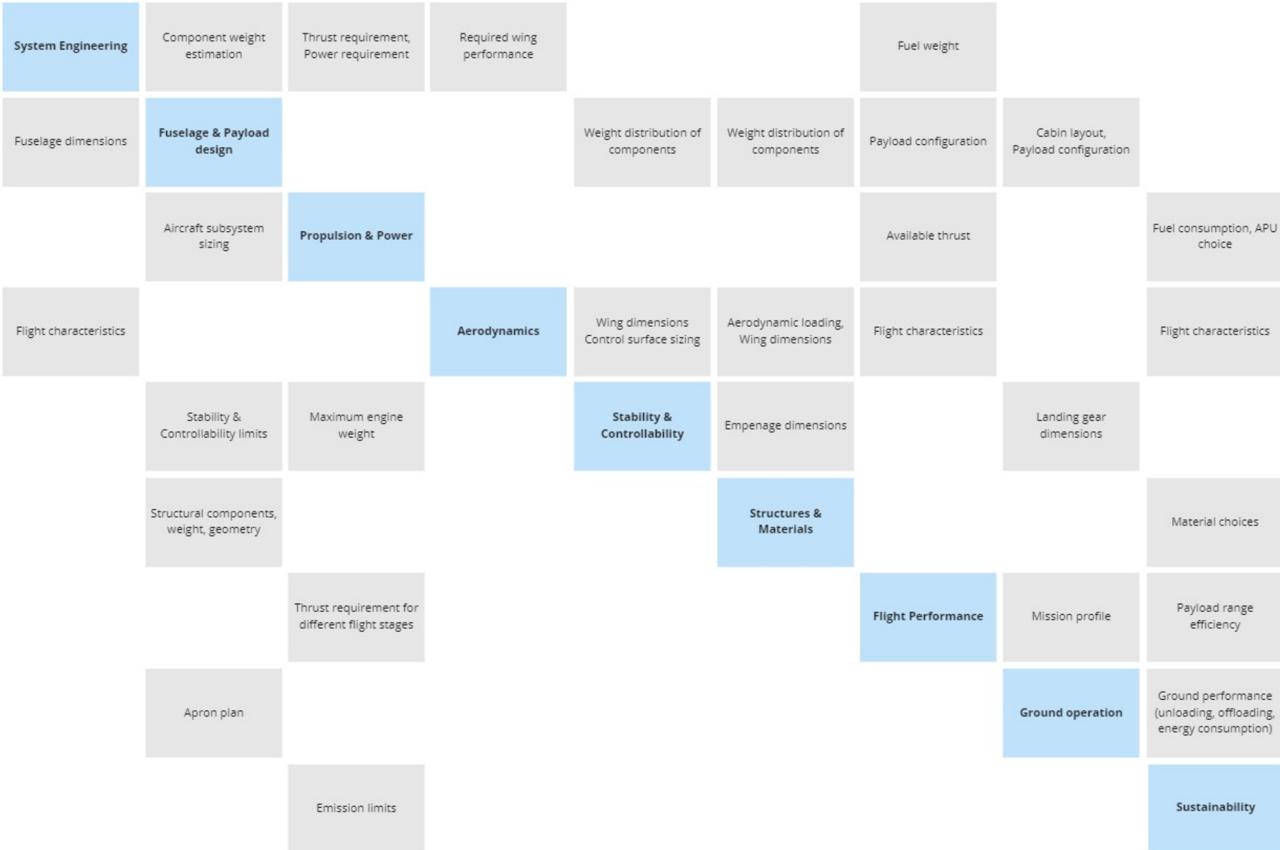

Figure 3.4: Communication diagram showing how the different departments are interrelated.

3.8. Functional Analysis

3.8.1. Functional Breakdown Structure

The Functional Breakdown Structure (FBS) represents hierarchically the functions that the product or system must perform in the form of an AND tree. As the team focused on ensuring that HAMMER is designed in a way in which it can be operated, most of the detail went into the operational part. However, a brief description on how the production, distribution and disposal phases should be carried out are present in the diagram. Each top level occupies one branch of the tree. The blocks represent the different functions the system must be capable of doing. As the operations part of HAMMER has many different functions, five additional branches were added below the operations sector, each referring to a different flight phase going from pre-flight to post-flight. The numbering was attributed following the hierarchy of the tree, which can be seen in Appendix D.

3.8.2. Functional Flow Diagram

The Functional Flow Diagram (FFD) shows the logical order of function the system must perform. It was developed from the FBS and the function blocks are linked by arrows, which indicate the order in which these functions must be performed. AND loops show activities that can be done simultaneously and OR loops show that activities are mutually excluded. A map can be found on the top part of the FFD, stating the order of the blocks in the top level. Five top level functions were identified in the FFD and each of these functions is developed in a more detailed way on the sublevels of the diagram. The FFD can be found in Appendix D. The numbering is consistent with the Functional Breakdown Structure.

4 Aerodynamics

The excellent aerodynamic characteristics of the box wing are one of the HAMMER's greatest benefits. This section details the aerodynamic design and performance of the box wing aircraft. The chapters structure adheres to the structure explained in Chapter 1, starting with the technical design.

4.1. Technical Design

4.1.1. Aerodynamic Theory of Box Wings

The main advantage introduced by the inherent design of a box wing is the dramatic reduction in induced drag due to the connection of the two wings. Ludwig Prandtl, in a famous paper, described this as the "Best Wing System" [47]. The Oswald span efficiency factor can be greater than unity in such a configuration, which is very beneficial with regards to induced drag. This is due to multiple reasons, but one of the factors is the reduced effect of wingtip vortices, which are reduced due to the vertical connection between the wings. One can think of the connection as a massive winglet, which are currently in use in most modern day aircraft to also reduce induced drag. The vertical connector must also have a specific lift distribution to optimize the lift distribution, as shown in Figure 4.1. In any case the box wing is aerodynamically an optimal configuration due to its large reduction in induced drag.

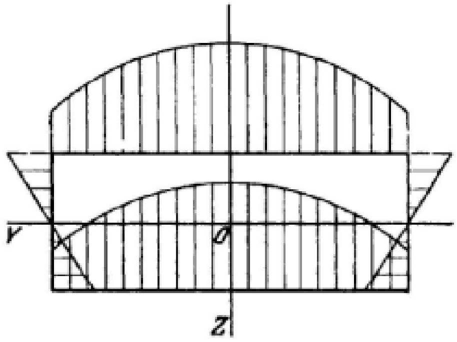

Figure 4.1: The optimal lift distribution for a box wing type aircraft [60].

Box wings also offer the advantage of increasing the aspect ratio of each wing, thereby also increasing aerodynamic efficiency for each wing in terms of induced drag. The two wings do influence each other, with the forward wing having downwash on the aft wing and the aft wing producing upwash for the forward wing, which is quite a complex interaction.

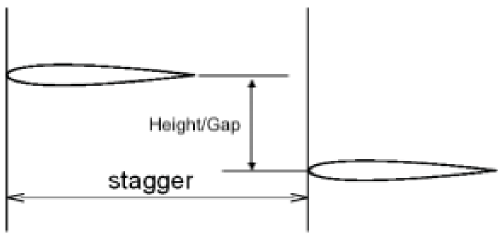

Figure 4.2: Stagger and Height/Gap parameters in box wing design [60].

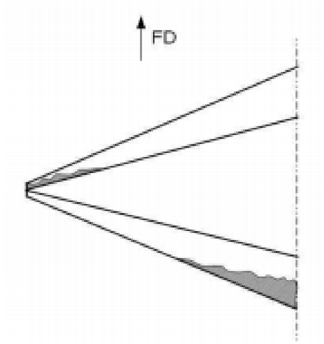

Figure 4.3: The initial stall location for box wing type aircraft [60].

In the design of a box wing aircraft, there are two major design parameters that are not as prominently present in conventional aircraft design. These are the height/gap parameter: The vertical distance between the two wings, and the stagger: The horizontal distance between the two wings. These parameters are visualised in Figure 4.2 and should be optimised in the wing system design. In terms of stall performance, box wings also offer advantages, with the forward wing stalling earlier than the aft wing. This helps with regards to reducing the pitch up moment, and indeed make the aircraft safer to use. The stall characteristics can be seen in Figure 4.3.

4.1.2. Initial Design Point

To calculate the design lift coefficient, Equation 4.1 was used [70]. The mass fractions for cruise are taken from the Class I iteration performed previously. In Equation 4.1, $C_{L_{des}}$ is the design lift coefficient for cruise flight conditions, ρ the air density, W is the aircraft weight in Newton and S is the wing surface area. To calculate the design Reynolds numbers (Re), Equation 4.2 can be used, where l is the length of the object to be evaluated, in this case the chord line of the airfoil to be examined, and μ is the dynamic viscosity of the fluid under examination.

$$C_{L_{des}} = 1.1 \cdot \frac{1}{\frac{1}{2}\rho V^2}\left(\frac{1}{2}\left[\frac{W}{S}_{startcruise} + \frac{W}{S}_{endcruise}\right]\right) \quad (4.1)$$

$$Re = \frac{\rho V l}{\mu} \quad (4.2)$$

From this the initial design point can be calculated, as seen in Table 4.1. Furthermore, with the short take-off and landing distance requirements (1800 $[m]$), it is estimated by methods from [70] that the $C_{L_{max}}$ in clean configuration should be 1.8. Clean configuration indicates that no high lift devices are used.

Table 4.1: The initial design point used to which the aircraft should be sized.

Parameter	Value [−]
$C_{L_{des}}$	0.51
$Re_{takeoff+landing}$	$17.4 \cdot 10^6$
Re_{cruise}	$32.8 \cdot 10^6$
$C_{L_{max}clean}$	1.8

4.1.3. Airfoil Selection

An important initial part of the aerodynamic design is choosing an airfoil. An optimal solution would be the design of a new airfoil specifically for the box wing, but as airfoil design is a very complex process it is considered out of the scope of this project. Therefore several already designed airfoils are looked into. Some different requirements can be set for the airfoils of the HAMMER:

- They should be able to reach the desired max clean lift coefficient of $C_L = 1.8$, as set in the initial sizing.
- They should provide for space for systems and fuel tanks to be installed. As wings on a box wing configuration tend to be slender (high aspect ratio) to obtain their effective aerodynamic design, there is not much room in chord direction. Thus, to provide the required volume, the thickness to chord ratio $\frac{t}{c}$ must be larger than 0.11. [60].
- They should not cause wave drag due to the high-speed conditions at cruise.
- They should not cause unwanted stall behaviour (e.g. sudden flow separation at low angles of attack)
- They should be designed for the design point of $Re = 32.8 \cdot 10^6$ and $C_L = 0.51$, or come sufficiently close to be considered a valid choice (see Subsection 4.1.2).

For this, several options were looked into, namely supercritical, transonic, and natural laminar flow (NLF) airfoils. Supercritical and transonic airfoils are designed for the rather high-speed regime that the HAMMER will fly in ($M = 0.78$). They help delay the effect of drag divergence on the wing. NLF airfoils are designed to have sustained laminar flow over the length of the airfoil and delay transition into turbulent flow. This helps reduce the drag on the wing. Laminar flow airfoils are difficult to operate however, as they require a very smooth surface and thus manufacturing and maintenance play a crucial role in making sure that they produce the desired laminar flow.

For the airfoils, four were selected as promising, as presented in Table 4.2.

Table 4.2: The four selected airfoils to be researched.

Airfoil	Type
DFVLR-R4	Transsonic
KC-135 Winglet	Supercritical
Grumman K-1	Supercritical
NASA/Langley NLF(1)-0215F	Natural Laminar Flow

The airfoils are modeled with XFLR5. This program uses essentially the same code as XFOIL. XFOIL utilizes a so called panel method to solve the La Place equation in Equation 4.3. For this program, the following assumptions are made. The flow field is described by the gradient of the flow potential (ϕ). The flow is analysed as a number of basic linear contributions of either sources or sinks, with vortices representing the sinks.

- Steady conditions
- Subsonic & incompressible flow
- Uniform flow, with constant ρ
- Inviscid flow, so friction is neglected
- Irrotational flow ($\nabla \cdot V = 0$)

$$\nabla^2\phi = (\frac{\delta^2}{\delta x^2}\phi + \frac{\delta^2}{\delta y^2}\phi + \frac{\delta^2}{\delta x^2}\phi) = 0 \quad (4.3)$$

Figure 4.4: The method used by panelmethods to calculate the flow. The outgoing and ingoing lines represent a source and sink, respectively [42].

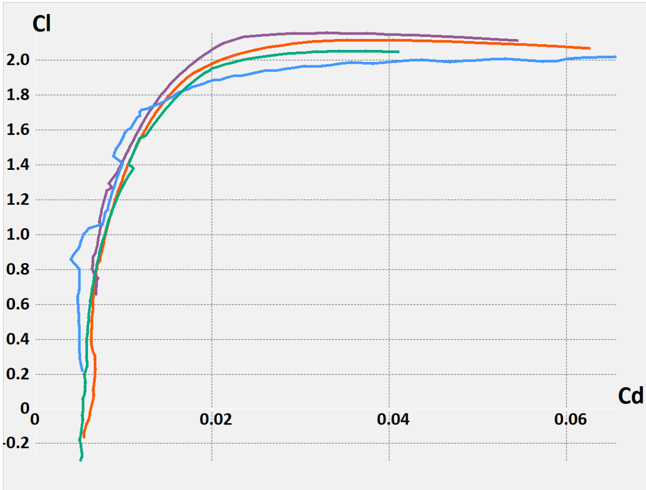

Figure 4.5: The $\frac{C_l}{C_d}$ ratio of the airfoils at $Re = 17.4 \cdot 10^6$ and $M = 0.2$

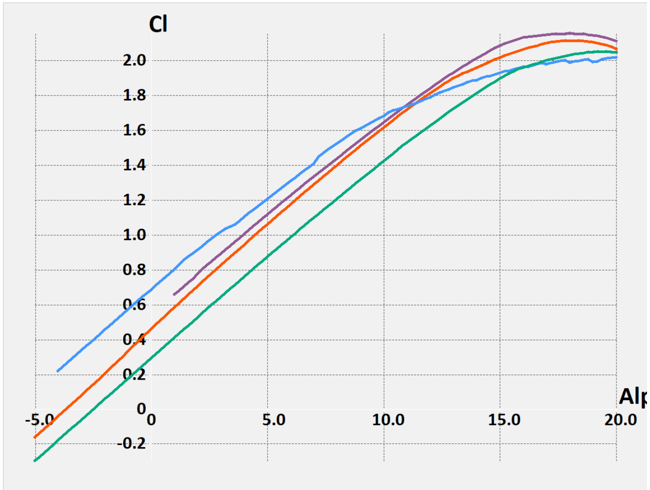

Figure 4.6: The lift curve slope of the airfoils at $Re = 17.4 \cdot 10^6$ and $M = 0.2$

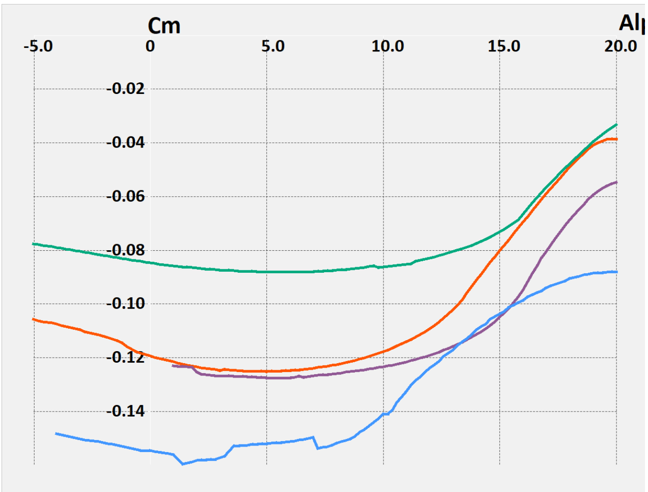

Figure 4.7: The moment coefficient data w.r.t. different angles of attack at $Re = 17.4 \cdot 10^6$ and $M = 0.2$

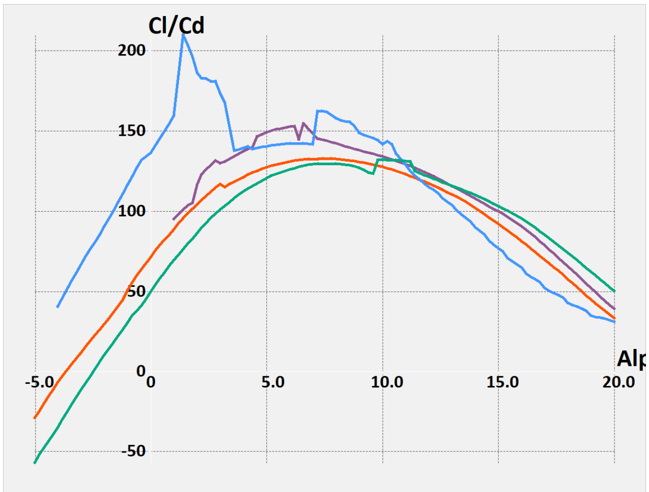

Figure 4.8: The $\frac{C_l}{C_d}$ ratio of the airfoils compared to the angle of attack at $Re = 17.4 \cdot 10^6$ and $M = 0.2$

Table 4.3: The four airfoil curves and associated lines.

Airfoil	Type
DFVLR-R4	Orange
KC-135 Winglet	Purple
Grumman K-1	Green
NASA/Langley NLF(1)-0215F	Blue

As can be seen in Figure 4.5, Figure 4.6,Figure 4.7, and Figure 4.8, with the lines shown coloured as in Table 4.3, the KC135 (purple line) beat the other airfoils in terms of overall performance, with for the most lift coefficients a higher $\frac{C_l}{C_d}$ ratio, and the highest $C_{L_{Max}}$. However, as stated before, the thickness limitation was critical and thus it was decided to go for the second best option, the DFVLR-R4 [1] airfoil. Although the NLF airfoil also showed promise, its maximum lift coefficient was too low, and it showed significant performance drops at higher angles of attack. Using the XFLR5 programme, the moment coefficient (C_m) could also be plotted against the angle of attack.

The DFVLR-R4, as seen in Figure 4.9, was identified as a good choice for high-speed subsonic transport aircraft by the DFVLR, a German aerospace research institution. Furthermore, it was designed for the Airbus A310, an aircraft with similar size in terms of MTOW and wing area. The airfoil was designed for a similar lift coefficient and Reynolds number according to a paper [33] presented by the DFVLR. It also has a thickness to chord ratio of 13.4%, which is sufficiently high to provide enough volume for the fuel tanks and subsystems in the wings. An additional peculiarity is that usually thicker airfoils actually result in a lighter wing structure, due to the moment of inertia being higher. This is an added benefit of a thicker airfoil.

As an airfoil applied to a finite wing under performs w.r.t. the theoretical (infinite) airfoil (see Figure 4.9), the effect of sweep (Λ in degrees) needs to be taken into account. This is done using Equation 4.4. A statistical relation was also used, as seen in Equation 4.5, to check if this value is still correct. With the chosen sweep of 30°the $C_{L_{Max}}$ is just able to reach 1.8. The statistical relation in Equation 4.5 was used as well to check, and it produced max $C_{L_{Max}}$ of 1.84, showing that the airfoil can provide the wing with the required lift coefficient as specified in the initial concept sizing.

$$C_{L_{Max}} = 0.9C_{l_{Max}} cos(\Lambda_{0.25c}) \qquad (4.4)$$

$$C_{L_{Max}} = \frac{C_{L_{Max}}}{C_{l_{Max}}} C_{l_{Max}} \qquad (4.5)$$

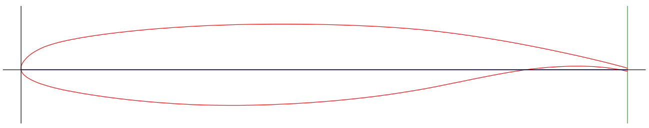

Figure 4.9: Side view of the DFVLR-R4 transsonic airfoil

Table 4.4: Some important characteristics of the DFVLR-R4 airfoil

Parameter	Value
$C_{l_{max}}$	2.3
α_{stall}	$-3.8°$
C_{l_α}	0.12/°
$\frac{C_l}{C_d}_{max}$	124
$\frac{t}{c}_{max}$	0.139
$c_{m_{cruise}}$	-0.14

4.1.4. Wing System Design

The wing comprises the most important part of the aerodynamic analysis of the design. The preliminary wing design was sized using the thrust-wing loading diagram and the methods from the ADSEE I course [70]. This was then iterated to provide an optimal design. The planform parameters can be seen in Table 4.5. To calculate the Mean Aerodynamic Chord (MAC), which is an important metric in aerodynamic design, Equation 4.10 and Equation 4.11.S_i is the surface area under examination, $c(y)$ is the chord at spanwise location y. $\lambda_{0.25c}$ is the quarter-chord sweep angle, $M*$ is the airfoil technology factor, equal to 0.935 [70], b is the span, λ is the taper ratio, c_r is the root chord, c_t is the tip chord, A is the aspect ratio, and Γ is the dihedral angle.

$$cos(\Lambda_{0.25c}) = 0.75\frac{M^*}{M_{dd}} \qquad (4.6)$$

$$\lambda = 0.2(2 - \Lambda_{0.25c}\frac{\pi}{180}) \qquad (4.7)$$

$$c_r = \frac{2S}{(1+\lambda)b} \qquad (4.8)$$

$$c_t = \lambda c_r \qquad (4.9)$$

$$MAC = \frac{2}{S_i}\int_0^{b/2} c^2(y)dy \qquad (4.10)$$

$$MAC_{total} = s_1 MAC_1 + s_2 MAC_2 \qquad (4.11)$$

$$A = \frac{b^2}{S} \qquad (4.12)$$

$$\Gamma = 3 - \frac{\Lambda_{0.25c}}{10} + 2 \qquad (4.13)$$

[1] Deutsche Forschungs- und Versuch-sanstalt fur Luft- und Raumfahrt

Geometry Considerations In this stage of the wing system design, it was decided to divide the total wing area equally over the two wings. Furthermore it was chosen to let the front- and aft wing have the same geometry. However, the front wing is swept backward, while the aft wing is swept forward. This is done to reduce the stagger between the wing tips, which will help to reduce the sweep angle of the vertical connector. The larger the sweep of the vertical connector, the more difficult it will be to make it structurally sound. In future phases of the design, box-wings with different area's and geometry for the front- and aft wing should be researched to find an optimum division of the total wing area. The vertical connector also has to provide a certain lift distribution to counter the vortices generated by the wings. For now, the symmetrical NACA0012[2] airfoil was chosen due to its relatively large thickness to chord ratio (t/c) of 12%. A high t/c airfoil shape will be more easy to produce and therefore likely to be lighter.

Lift Distribution The front and aft wing should both provide an elliptical lift distribution for optimal induced drag reduction. This can be achieved by varying a variety of factors such as sweep, taper ratio, twist, camber, airfoils, etc. To maintain proper stability & control the front wing needs to provide a larger portion of the lift than the aft wing. This is somewhat naturally achieved by the lower angle of attack the aft wing experiences already, as well as the downwash from the forward wing. For stable and controlled flight, the front wing must stall before the aft wing. Introducing wing twist at the aft wing will make sure that this will happen for every angle of attack the aircraft flies at. The lift distribution between the forward- and aft wing where computed to be 60% for the front wing and 40% for the aft wing. A twist angle Φ was introduced to make sure that this occurs.

Sweep A sweep angle of 30° was computed using Equation 4.6. It is the optimal angle to counter the drag divergence encountered during trans-sonic flight. For this computation, estimations from ADSEE [70] for the drag divergence mach (M_{dd}) where used. This resulted in an M_{dd} of 0.81.

Dihedral A dihedral angle (Γ) of 2°is calculated using Equation 4.13 for lateral stability for the front wing. For the aft wing, no dihedral angle is chosen, because decreasing the height gap negatively impacts the aerodynamic performance of the wing.

Height As mentioned in Subsection 4.1.1, the vertical distance or height between the wings is an important aerodynamic design parameter. The effect of the height, usually expressed in height to span ratio (h/b), can be summarised as: The larger the height between the two wings, the lower the induced drag. This can be seen from Figure 4.10 in which D_b is the induced drag from a box wing, D_m is the induced drag of a reference wing and h/d the height to span ratio. It can indeed be seen that the induced drag of a box wing reduces with increasing span.

With the height restrictions for a ICAO type C aircraft, and the landing gear length from Section 7.2 in mind, it was chosen to have the height as large as possible. This will result in the lowest induced drag as can be seen from Figure 4.10. However, the drag of the four vertical surfaces (connectors and the two vertical tails), will increase with increasing h/b. In a future design stage, a trade-off between the reduction of induced drag and increase in drag of the vertical surfaces should be made. In this design stage, a h/b of 0.29 was chosen.

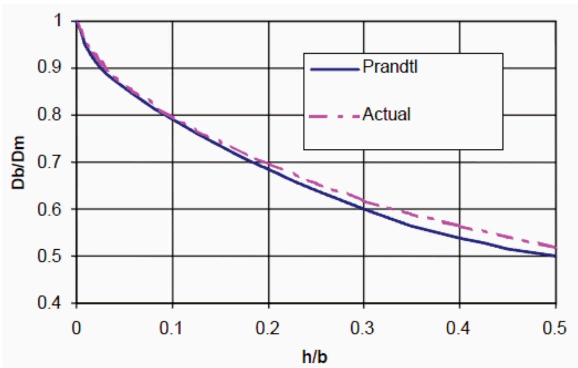

Figure 4.10: $\frac{D_b}{D_m}$ set out against the h/b ratio [60].

Resulting Wing Geometry The resulting wing geometry data and planform drawings can be found in Table 4.5 and Figure 4.12 respectively. A render of the planform of the top view can be seen in Figure 4.11.

[2]National Advisory Committee for Aeronautics

Table 4.5: Planform parameters of the wing

Parameter	Forward Wing	Aft Wing
$S[m^2]$	119.0	119.0
$A[-]$	10.9	10.9
$b[m]$	36.0	36.0
$c_r[m]$	5.10	5.10
$c_t[m]$	1.51	1.51
$MAC[m]$	3.63	3.63
$\Lambda_{0.25c}[^\circ]$	30.0	-30.0
$\lambda[-]$	0.295	0.295
$\Gamma[^\circ]$	2.0	0
$\Phi[^\circ]$	-3.0	-5.0
$\frac{h}{b}[-]$	0.294	0.294

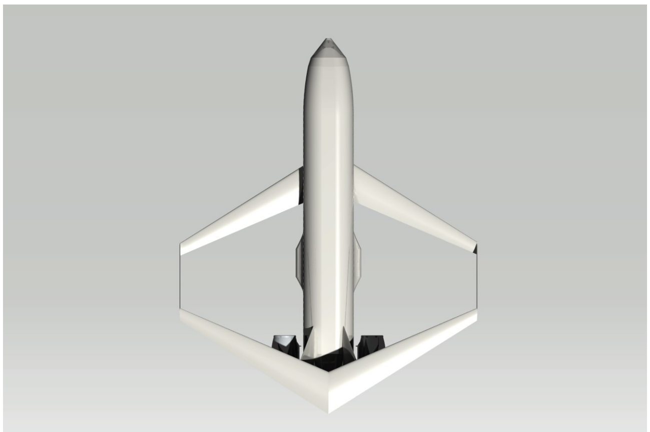

Figure 4.11: A render of the wing planform.

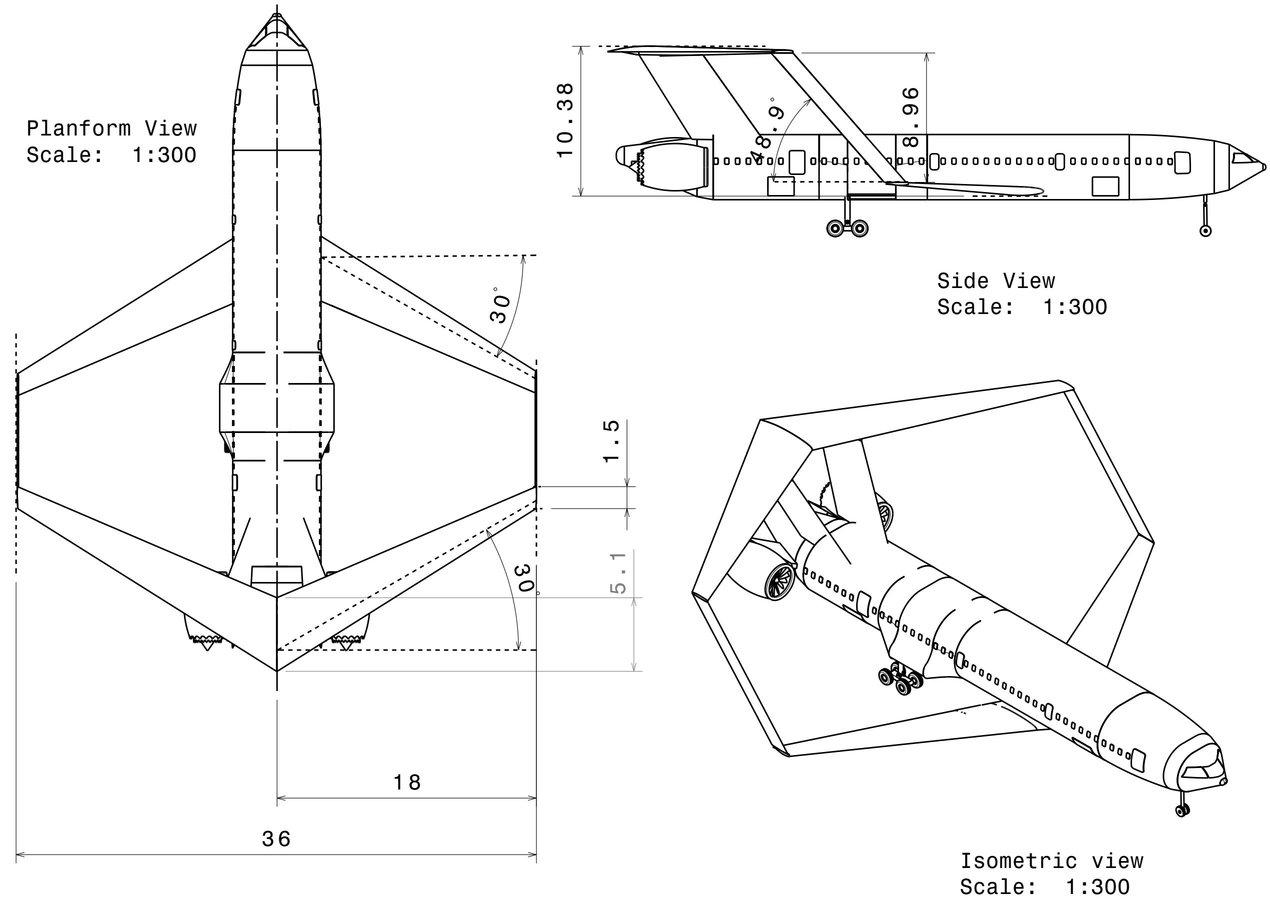

Figure 4.12: A drawing of the aircraft showing the wing system.

4.1.5. Aerodynamic Performance

To get an initial aerodynamic performance analysis of the wing, a preliminary aerodynamic model was set up.

Oswald span efficiency factor To calculate the Oswald span efficiency factor the relation in Equation 4.14 was used. The e_{ref} was taken as 0.85. This number represents the reference span efficiency factor taken from a conventional aircraft. In this case 0.85 was determined as a realistic value [60]. As can be seen from Equation 4.14, the efficiency only depends on the height gap between the two wings. Similar to the induced drag, increasing the h/c ratio has a positive effect on the span efficiency factor. It was shown that this effect only lasts until $\frac{h}{b} = 0.5$, after which a maximum is reached [60]. Thus for aerodynamic performance it is vital to increase this number, until the maximum possible value is reached with regards to geometry constraints and other factors such as structural integrity. It was therefore decided to place the forward wings as low as possible, in the lowest part of the fuselage. The aft wings were mounted on top of the vertical stabilizers to maximize this effect. The height constraint for C type aircraft was also taken into account, which is equal to a maximum height of 13.5 [m].

$$e_{box} = e_{ref} \frac{0.44 + 2.219\frac{h}{b}}{0.44 + 0.9594\frac{h}{b}} \tag{4.14}$$

Zero-lift drag coefficient To calculate the zero-lift drag coefficient, a method from the ADSEE course was used [42], where each component's contribution the drag was taken into account, instead of the more general method presented previously in the midterm report. Equation 4.15 shows the calculation method.It should be noted this method is to be used for the clean configuration, thus the effects of deployed flaps are not taken into account for example. This method takes into account the zero-lift drag from the entire aircraft. For the wetted area due to the landing gear fairings, an estimated extra wetted area of 45 [m^2] was taken into account with the help of CATIA drawings. For the vertical connector an additional 52 [m^2] was added after the CATIA drawings were made to account for them. The wetted surface area is calculated for each component according to Equation 4.16, Equation 4.17, and Equation 4.18. In Figure 4.13 a schematic drawing is seen to visualise the way the fuselage drag contribution is taken into account [42]. The fact that there are two wings and two vertical tail surfaces is also taken into account, of course. S_{ref} is the reference wing area, C_{D_c} is the component part drag, S_{wet_c} is the component part wetted surface area and $C_{D_{misc}}$ is the miscellaneous drag, usually about 10% of total drag. S_{exp} is the exposed surface area of each component modelled.

$$C_{D_0} = \frac{1}{S_{ref}} \Sigma C_{D_c} S_{wet_c} + C_{D_{misc}} \tag{4.15}$$

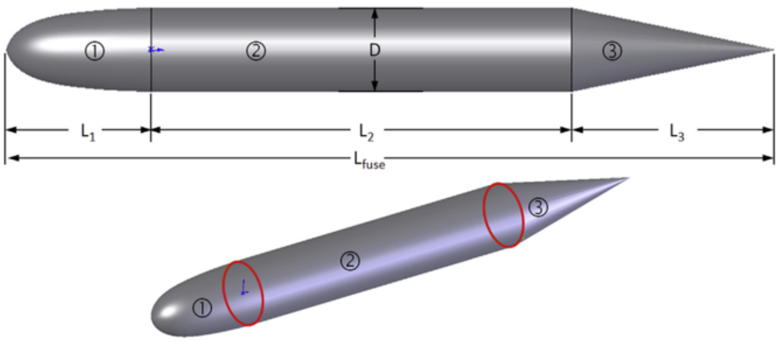

Figure 4.13: The preliminary model used to calculate the wetted fuselage surface area [42].

$$S_{wet_W} = 1.07 \cdot S_{exp_W} \cdot 2 \cdot 2 \tag{4.16}$$

$$S_{wet_{VT}} = 1.05 \cdot S_{exp_{VT}} \cdot 2 \cdot 2 \tag{4.17}$$

$$S_{wet_{fuselage}} = \frac{\pi D}{4}\left(\frac{1}{3L_1^2}\left[(4L_1^2 + \frac{D^2}{4})^{1.5} - \frac{D^3}{8}\right] - D + 4L_2 + 2\sqrt{L_3^2 + \frac{D^2}{f}}\right) \tag{4.18}$$

The drag divergence Mach number is calculated for values for the wing design and to check if the cruise Mach number is lower than this number. If this would not be the case, then additional wave drag must be taken into account, which can be quite large. $\frac{t}{c}_{streamwise}$ is the streamwise thickness over chord ratio, k_a is an airfoil factor, and Λ is the sweep angle at the leading edge.

$$M_{dd} = \frac{k_a}{cos(\Lambda)} - \frac{\frac{t}{c}_{streamwise}}{cos^2(\Lambda)} - \frac{C_L}{10cos^3(\Lambda)} \tag{4.19}$$

To give an estimate for drag polars, Equation 4.20 can be used. The drag polars are shown in Figure 4.14. The extra drag and other aerodynamic effects due to flap deployment can also be calculated for use in the drag polar quantification using Equation 4.21 and Equation 4.22, where δ_f is the flap deflection, F_{flap} is a constant value of 0.0074 for slotted flaps and c_f is the flap chord.

$$C_D = C_{D_0} + \frac{C_L^2}{\pi A e} \tag{4.20}$$

$$\Delta C_{D_{flap}} = F_{flap}(\frac{c_f}{c})(\frac{S_{flap}}{S_{ref}})(\delta_{flap} - 10) \tag{4.21}$$

$$\Delta e = 0.0046\delta_f \tag{4.22}$$

To calculate the lift curves, Equation 4.23 can be used. The final lift curve slope of the box wing can then be found by using Equation 4.24. This accounts for the effect of downwash from the forward wing on the aft wing [60]. s_1 and s_2 represent the areas of the two main wings. If treated as individual wings the lift curve slope would be the same for both in this theory. The downwash gradient ($\frac{d\epsilon}{d\alpha}$) is estimated using Equation 4.25 [60]. β is the Prandtl-Glauert correction factor equal to $\beta = \frac{1}{\sqrt{1-M^2}}$, with M as the Mach number. η is an airfoil efficiency factor. $cos(\phi_{25.1}$ is simply equal to a cosine of 25°[60]. $C_{L_{\alpha 1,M=0}}$ and $C_{L_{\alpha 1,M}}$ are equal to the lift curve slope at $M = 0$ and the lift curve slope at the Mach number under consideration.

$$C_{L_\alpha} = \frac{2\pi A}{2 + \sqrt{4 + (\frac{A\beta}{\eta})^2 (1 + \frac{tan(\Lambda_{0.5c})}{\beta^2})}} \quad (4.23) \qquad C_{L_{\alpha_{box}}} = C_{L_{\alpha_{fw}}} s_1 + C_{L_{\alpha_{aft}}} s_2 (1 - \frac{d\epsilon}{d\alpha}) \quad (4.24)$$

$$\frac{d\epsilon}{d\alpha} = 4.44(k_{A,1} \cdot K_{\lambda,1} \cdot K_H \cdot \sqrt{cos(\phi_{25.1})})^{1.19} \cdot \frac{C_{L_{\alpha 1,M}}}{C_{L_{\alpha 1,M=0}}} \quad (4.25)$$

As can be seen in Equation 4.25, a large number of factors influence the downwash gradient. These are calculated with Equation 4.26, Equation 4.27, Equation 4.28, and a number of other factors. The k factors are all constants defined with the following variables. A_1 represents the wing area of the front wing, λ_1 represents the quarter chord sweep of the front wing, $\frac{z}{b_1}$ is the ratio of the vertical distance between the front and aft chords and the front wing span, and l' is the longitudinal distance between the aerodynamic centres of the two wings.

$$k_{A,1} = \frac{1}{A_1} - \frac{1}{1 + A_1^{1.7}} \quad (4.26) \qquad k_{\lambda,1} = \frac{10 - 3\lambda_1}{7} \quad (4.27) \qquad k_H = \frac{1 - |\frac{z}{b_1}|}{\sqrt[3]{\frac{2l'}{b_1}}} \quad (4.28)$$

To get the lift curve slopes, the lift curve as estimated can be used. For the landing and takeoff situation slight adjustments have to be made. The stall angle is estimated using Equation 4.29, with $\Delta\alpha_{C_{L_{Max}}}$ accounting for the difference in the lift curve slope at stall conditions.

$$\alpha_s = \frac{C_{L_{Max}}}{C_{L_\alpha}} + \alpha_{0L} + \Delta\alpha_{C_{L_{Max}}} \quad (4.29) \qquad \frac{L}{D}_{max} = \frac{1}{2}\sqrt{\frac{\pi A e}{C_{D_0}}} \quad (4.30)$$

This can evaluated for the landing and takeoff angles as well, which will be elaborated on further in Subsection 4.1.6.
The maximum lift to drag ratio is computed using Equation 4.30, where A is the aspect ratio of the wing, e is the Oswald efficiency factor, and C_{D_0} is the zero-lift drag coefficient. The computed lift to drag ratio incorporates the drag induced by both the fuselage and the wing. This is the theoretical maximum ratio possible with the given configuration. This gives a solid indication of the aerodynamic efficiency of the aircraft.
In Table 4.6 the value for each important aerodynamic parameter previously described is presented.

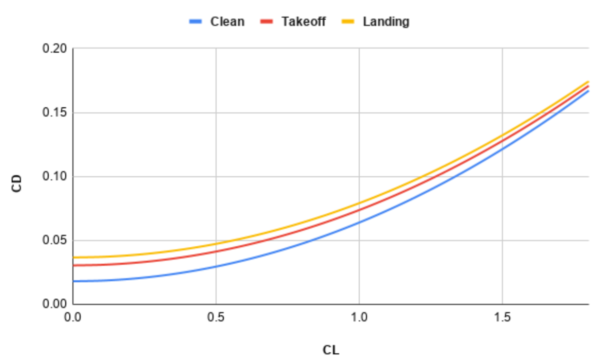

Figure 4.14: The drag polars for clean, take-off and landing configuration.

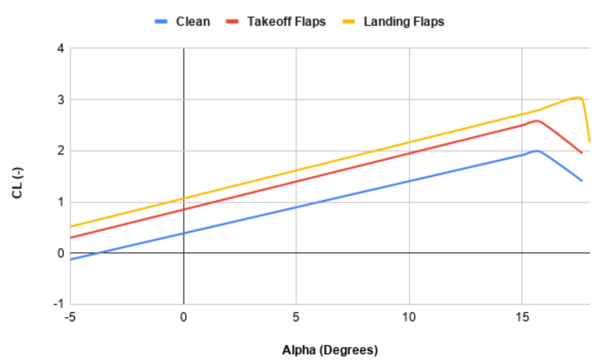

Figure 4.15: The lift curve slopes for clean, take-off and landing configuration.

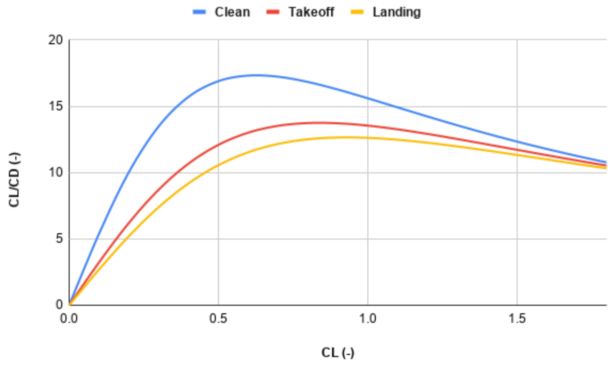

Figure 4.16: Calculated maximum lift coefficient over drag coefficient values, offset against the lift coefficient.

Table 4.6: The important aerodynamic characteristics for the wing system

Parameter	Value	Parameter	Value
$C_{D_0}[-]$	0.0181	$M_{dd}[-]$	0.84
$e[-]$	1.27	$\frac{L}{D}_{Max}[-]$	17.3
$\frac{h}{b}[-]$	0.29	$\alpha_{Stall}[^\circ]$	15.75
$\frac{d\epsilon}{d\alpha}[-]$	0.1296	$\alpha_{Stall_{takeoff}}[^\circ]$	15.08
$\alpha_{0_L}[^\circ]$	-3.8	$\alpha_{Stall_{landing}}[^\circ]$	17.67
$C_{L_\alpha}[\frac{1}{^\circ}]$	0.102	$C_{L_{Max_{clean}}}[-]$	1.8

4.1.6. Mobile Surface Design

High Lift Devices (HLD) are used to increase lift during takeoff and landing when additional lift needs to be generated. Trailing edge (TE) high lift devices, or flaps, work due four major principals [42]:

- They increase the total wing camber
- They increase the effective angle of attack
- They increase the surface area of the wing
- They control and energise the boundary layer over the wing.

Leading edge high lift devices work well in combination with TE devices. They work by moving the nose of the wing more towards the flow, lowering the angle of attack and can energise the boundary layer flowing over the wing. For the box wing, there is a fairly large amount of surface area where flaps can be used.

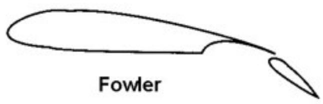

(a) A drawing of a Fowler flap [42].

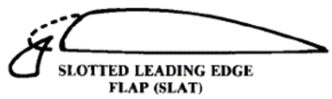

(b) A drawing of a leading edge slat [42].

Figure 4.17: High lift devices selected for HAMMER.

The high-lift devices chosen to use were Fowler flaps and slats, which can be seen in Figure 4.17a and Figure 4.17b respectively. A design trade of was performed in the conceptual design phase [21], where the additional lift of different HLDs is put against their complexity (and thus cost). Fowler flaps and slats are relatively simple, easy and cheap to produce, maintain and operate while providing the necessary additional lift. Both devices extend during deployment, which helps increase the efficiency with regards to lift generation. The trailing edge Fowler flap mostly helps with increasing the max lift coefficient, while the leading edge slat helps with delaying the onset of stall. With the design of the spars in mind detailed later in Chapter 8, the slats were chosen to extend into 10% of the chord and the flaps 30%. The calculations were done using Equation 4.31, Equation 4.32, Equation 4.33, and inputs from Table 4.7. $\Delta C_{L_{max}}$ is equal to the maximum difference in lift coefficient, $C_{l_{max}}$ is the max airfoil lift coefficient, S_{wf} is the flapped surface area, $\lambda_{hingeline}$ is the sweep angle at the hinge line of the flaps, $\Delta\alpha_{0_L}$ is the difference in zero lift angle for the aircraft and $\Delta\alpha_{0_l}$ is the difference in zero lift angle for the airfoil. S' is the wing surface area with the extra flapped surface area added due to flap extension.

$$\Delta C_{L_{max}} = 0.9\Delta C_{l_{max}} \frac{S_{wf}}{S} cos(\lambda_{hingeline}) \quad (4.31)$$

$$\Delta\alpha_{0_L} = \Delta\alpha_{0_l} \frac{S_{wf}}{S} cos(\lambda_{hingeline}) \quad (4.32)$$

$$C_{L_{\alpha_{flapped}}} = \frac{S'}{S} C_{L_{\alpha_{clean}}} \quad (4.33)$$

However, after consulting Carmine Varriale, Ph.D., it was discovered that having an equal flapped area on the aft wing makes it almost impossible to take off due to the large moment generated by the aft wing due to the extra lift. This makes flipping the aft wing impractical, but imposes some heavy constraints on the front wing, as all the flapped area needs to be there in the most optimal scenario. This might also cause structural issues, as the wing structure of the front wing would need to be reinforced more than the aft wing. As this is still very new research, it is difficult to fully quantify this effect. It is therefore decided to have 66% of the flapped area on the front wing, and 33% on the aft wing, as the calculated flapped area is too large to only have the front wing flapped, keeping in mind the fact that other control surfaces occupy the wing surface area as well. This is the most optimal solution that could be found to account for this effect.It is a recommendation that more research is done in this area. One effect of this is an uneven lift distribution for both of the wings, with the forward wing contributing much more to the total lift than the aft wing during takeoff and landing. The specifications of the flap system can be seen in Table 4.8.

Table 4.7: The changes in max lift coefficient that can be achieved with the HLD types [42].

HLD Type	$\Delta C_{l_{max}}$
Fowler flap	$1.3\frac{c'}{c}$
Slat	$0.4\frac{c'}{c}$

Table 4.8: Flap system characteristics.

Parameter	**Value**	**Parameter**	**Value**
$S_{wf}[m^2]$	110	$C_{L_{\alpha_{flapped}}}[^\circ]$	0.109
$\frac{S_f}{S}[-]$	0.47	$\alpha_{takeoff}[^\circ]$	10.2
$\frac{c_{fTE}}{c}[-]$	0.3	$\alpha_{landing}[^\circ]$	12.1
$\frac{c_{fLE}}{c}[-]$	0.1	$\delta_{f_{takeoff}}[^\circ]$	25
$\Delta C_{L_{Max}}[-]$	1.0	$\delta_{f_{landing}}[^\circ]$	40

Aileron Design Ailerons are control surfaces that provide roll control to the aircraft. As the box wing configuration has multiple options for aileron placement, several were considered. To size the ailerons, first the requirements for rolling must be identified. The aircraft falls in the Class II Category [70]. Therefore the aircraft needs to be able to roll 45°in 1.4 [s], as seen in Table 4.9, in addition to any CS-25 requirements.

Table 4.9: Required roll performance for the aircraft classes.

Class	**Required Roll Performance**
I	60°in 1.3 [s]
II	45°in 1.4 [s]
III	30°in 1.5 [s]
IVA	90°in 1.3 [s]
IVB	90°in 1.0 [s]
IVC	90°in 1.7 [s]

To find the required roll rate, first the aileron control derivatives $C_{l_{\delta\alpha}}$ and C_{l_p} must be found using Equation 4.34 and Equation 4.35. Then the roll rate can be calculate using Equation 4.36. If this is not met an iteration can be performed until the requirement is met. τ is the aileron effectiveness, a function of the aileron chord to total airfoil chord [42]. The chosen ratio for this is 0.3, to comply with spar requirements. τ is then equal to about 0.52. c_{d_0} is the airfoils drag coefficient, and $c_{l\alpha}$ the airfoils lift curve slope, both at specific flight conditions as specified at section y. δ_a is the deflection of the ailerons.

$$C_{l_{\delta\alpha}} = \frac{2c_{l\alpha}\tau}{S_{ref}b}\int_{b_1}^{b_2} c(y)ydy \quad (4.34) \qquad C_{l_p} = \frac{-4(c_{l\alpha}+c_{d_0})}{S_{ref}b^2}\int_0^{b/2} y^2c(y)dy \quad (4.35)$$

$$P = \frac{-C_{l_{\delta\alpha}}}{C_{l_p}}\delta_a\left(\frac{2V}{b}\right) \quad (4.36)$$

In the end, it was found the most effective solution is for 4 ailerons placed at the tips of each of the wings, for maximum roll control and optimal sizing [69]. If positioned at this end, the aileron has a longer moment arm, increasing its effectiveness. The fact that it is possible to place 4 instead of 2 ailerons at the tips allows for a decrease in individual aileron size. The aircraft falls in the Class II Category [70]. Therefore the aircraft needs to be able to roll 45°in 1.4s, as seen in Table 4.9. Data regarding an initial size was used from a research paper by Carmine Varriale [69], which generated results for a generic box wing layout. It is seen in Table 4.10, that the aircraft handily meets the roll requirements. This also means that the ailerons are slightly overdesigned, but this is recommended as a possible optimisation. In any case, the box wing layout shows good roll performance.

Table 4.10: The aileron performance characteristics and sizing.

Parameter	**Value**
Position [$\cdot c$]	$0.85-0.95$
$\frac{c_{aileron}}{c}[-]$	0.3
$C_{l_{\delta\alpha}}[^\circ]$	0.000178
$C_{l_p}[\frac{1}{\circ}]$	0.0082
$\delta_a[^\circ]$	25
$P[\frac{\circ}{s}]$	69.44

Elevator Design Elevators are critical for trimming the aircraft and creating enough force during takeoff and landing for maneuvering. Due to the box wing layout, elevators can be placed on the forward and aft wing, increasing effectiveness [69]. If the elevators are deflected in an opposite manner, (so forward up and aft down for example), the elevators can be very effective due to the coupled moment generated. As mentioned in Subsection 4.1.6, the elevators need to account for the increased lift that the aft wing should provide during takeoff and landing. As currently, no conceptual theoretical elevator sizing methods exist for box wing configurations, initial sizing was again based on the paper from C. Varriale [69]. For optimisation of the elevator design in a future design phase, the elevator size will need to be iterated in AVL until appropriate trim conditions and landing and takeoff performance can be achieved.

Table 4.11: The elevator sizing and locations.

Parameter	Value
Forward Elevator Location	$0.2-0.3c$
Aft Elevator Location	$0.0-0.3c$
$\frac{c_{elevator}}{c}$	0.3

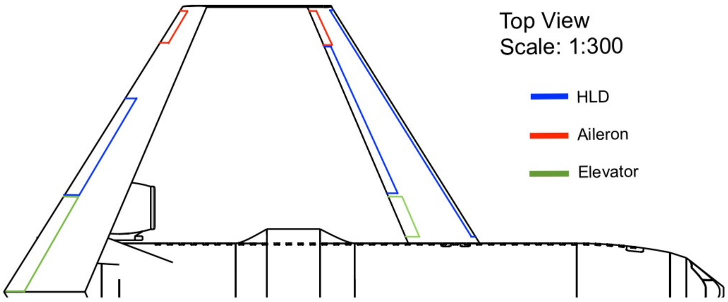

Figure 4.18: A general layout of the mobile surfaces on the wing.

4.2. Verification and Validation

For verification numerous methods were developed. First of all, extensively verified computer programs in the form of XFLR5 and AVL were used to quantify the performance of the airfoil and planform, respectively. Secondly, for all calculated values were compared with conventional, existing aircraft to check if the developed programs and methods produce values that are in line with validated numbers. Also, data obtained for HAMMER was compared with comparable box wing research such as [60] [61] [44]. Besides this, sanity checks were performed, for example for the flaps. These were checked to ensure that they provide adequate extra lift to provide a takeoff and landing angle that would not cause a tail strike.

Athena Vortex Lattice (AVL) After the preliminary modeling was done, a 3D computer-generated model was made using AVL to verify the results obtained in Section 4.1. AVL employs the vortice-lattice method (VLM)[3] to calculate the aerodynamic properties of a given input configuration. VLM employs the lifting line theory and horseshoe vortices, whereby the wing system is modeled as many infinitely thin horseshoe vortices. The vortice-lattice model utilizes some of the same assumptions as the panel method, and can be seen as somewhat of an extension of this method into the 3D space. The airfoil is taken into account by modelling the camber. AVL also works best at small angles of attack and for thin surfaces. Fuselage modeling is therefore difficult to do accurately and can be left out, as the results would not be accurate anyway. VLM disregards the effects of viscosity. This means that effects such as stall are poorly modelled, and turbulence and boundary layers in general are not taken into account. To model that accurately, computational fluid dynamics (CFD) software should be used. However, as CFD is complex and computationally expensive, it is not used in this stage of the project, where it would not provide any more accurate results than using a program such as AVL for example. A picture of the lift distribution can be seen in Figure 4.19. The AVL values are compared with the theoretical values in Table 4.12 for validation.

Table 4.12: The important aerodynamic characteristics for the wing system as calculated in theory and in AVL.

Parameter	Computed Value	AVL Value	Δ
$M_{cruise}[-]$	0.78	0.78	
$C_L[-]$	0.51	0.51	0
$\alpha_{trim[^\circ]}$	1.20	0.29	-76%
$C_D[-]$	0.030	0.0105	- 65%
$e[-]$	1.27	1.46	+15%

[3][accessed 27/06/20] http://www.aerodynamics4students.com/subsonic-aerofoil-and-wing-theory/3d-vortex-lattice-method.php

From Table 4.12, it can be seen that the computed values for trim angle of attack (α_{trim}), lift coefficient, drag coefficient and oswald efficiency factor where in the right order of magnitude. It is expected that the values differ due to the different level of detail in the computational technique. A 76% decrease in trim angle of attack is however a very large deviation. Both methods are relatively basic and it is therefore not possible to tell what value gives a better indication of reality. It does make sense that with the decrease in trim angle, the drag coefficient also decreases and the oswald efficiency increases. For further design optimisation and validation, it is suggested that computational fluid dynamics (CFD) software and wind-tunnel tests are used.

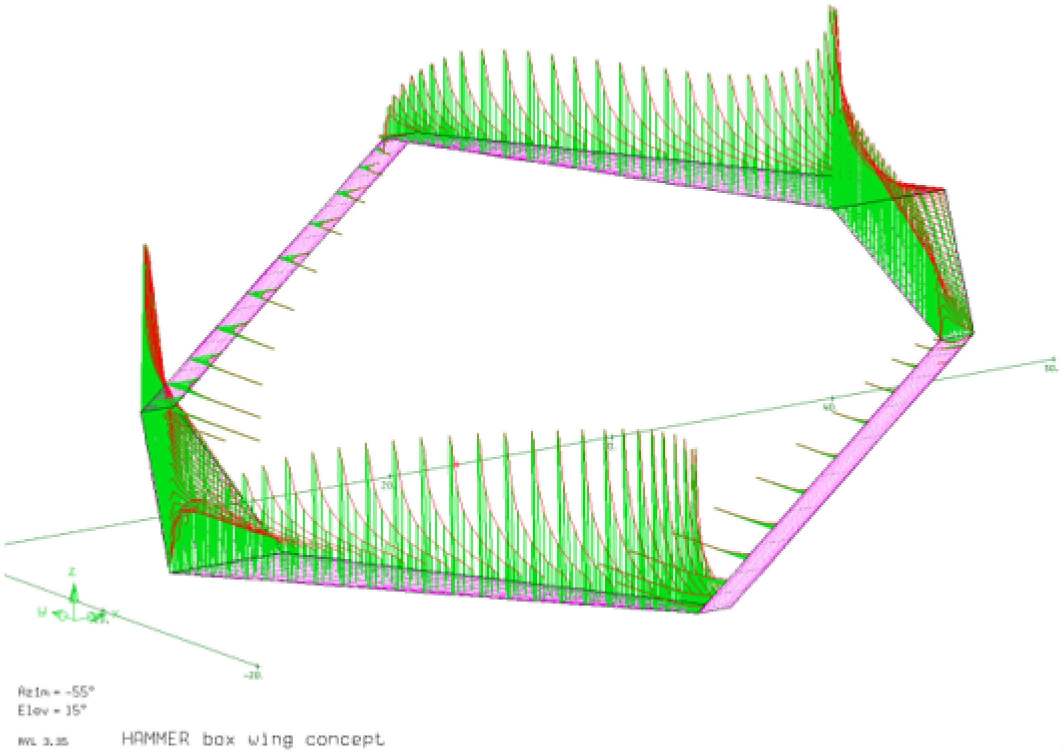

Figure 4.19: The lift distribution for cruise conditions.

The AVL model can also be used to verify the wing loading distribution over the wing. From Figure 4.19 it can be seen that both the front and aft wing have a positive wing loading at the trimmed angle of attack for cruise of $0.29°$. Also, it can be noted that the vertical connectors have a lift distribution as expected by Section 4.1 and Figure 4.1. Due to the 60% - 40% lift division between the front- and aft wing respectively, the point where the wing loading crosses the vertical connectors is shifted upwards. This can be clearly identified in Figure 4.19.

From the AVL model, it was discovered that the airfoil and wing lift curves differed quite significantly from the expectations. An induced angle of attack of $-3°$ was introduced for both the front- and aft wing to account for the offset. This resulted in a more suitable cruise angle of attack and to ensure that the angle of attack required for takeoff and landing would not cause a tail strike. The effect of wing twist is that it moves the lift curve slope more to the left in the graph. This means that the aircraft also stalls at a lower angle of attack. As the airfoil stalls around $20°$, the $3°$ of twist would not cause the stall angle to become too low, especially as the aircraft experiences a tail strike around $15°$ anyway.

High lift devices To verify if the design of the high-lift devices is correct, a drawing is made to ensure that they do not overlap with the other mobile surfaces (see Figure 4.18). Also, the takeoff and landing angles are checked, to see if the aircraft does not have a tail strike with the ground. Indeed the takeoff angles are within the tail strike limit of $15°$ and thus the takeoff and landing angles are within limits.

4.3. Sustainability Analysis

With aerodynamics, any improvement is usually good for sustainability as well, by decreasing the amount of fuel needed to fly the aircraft. The box wing in itself is optimised to reduce drag by reducing the induced drag as mentioned previously, which reduces fuel burn.

As HLDs produce a fair amount of noise, making sure that they are the minimum size is good for social as well as environmental sustainability. Relatively simple high lift devices were selected, although it is an area of future study if they can be made even simpler.

One interesting area of improvement would be morphing wings and boundary layer control. A morphing wing would allow a more optimal wing shape to be made during flight that adapts to the flight conditions, which can help improve the aerodynamics of the aircraft. Boundary layer control would help with replacing high lift devices and the noise that they generate. Boundary layer control works by placing small nozzles along the wing that can shoot jets of air, energizing the airflow.

4.4. Risk Assessment

With regards to aerodynamics a number of risks can be identified. The main risk is the lack of overall development with regards to box wing aerodynamics, as no box wings exist that can fly as of this moment. This means that validation of the results can prove quite difficult. A risk is that the lift distribution is less than optimal, which can decrease the overall aerodynamic efficiency of the aircraft. Another risk is that the airfoil performs poorly in practice. It would be the most beneficial to design a special box wing airfoil, but as this is out of the scope of the project, normal monoplane airfoils are used. Lastly, a big risk that is identified is the trimming of the aircraft at takeoff and landing. As previously stated, the flaps could cause issues with the trimming, especially flaps on the aft wing. During takeoff and landing the elevators must trim the aircraft for quite high angles of attack which requires a large amount of force. It is however hoped that with the use of 4 coupled elevators this can be avoided.

4.5. Requirements Compliance

After this first analysis the requirements concerning aerodynamics are all met. These can be found in the table below. Some other requirements concerning aerodynamics are user requirements, for which the compliance is described in Chapter 15.

Table 4.13: Compliance with the aerodynamic requirements.

	Requirement
✓	**CMR-SR-AC-CR-2** - The aircraft shall have adequate manoeuvrability at cruise.
✓	CMR-SR-AC-CR-2.1 - The aircraft shall be able to roll from an initial, steady 30°bank angle over 60°in order to reverse directions, in no more than 7 seconds, under specified conditions.
✓	HAMMER-AERO-01 - The aircraft shall be able to roll 45°in no more than 1.4 seconds.

4.6. Conclusion

To conclude, the wing system has been sized and analysed using a theoretical model and verified with AVL software. It was found that the box wing has good aerodynamic performance and that the airfoil and planform are a good combination. The mobile surfaces have also been sized. A number of recommendations can be made for the future development with regards to the aerodynamics of the HAMMER:

- Improve the aerodynamic model with regards to drag calculation and accurate assessment of the stalling performance, which for the box wing is quite complex and difficult to fully assess in the current conceptual stage.
- Investigate if the trimming issues can be solved by decreasing the amount of flaps or researching if the HAMMER can land using lower lift coefficients.
- Investigate if a custom built airfoil can be incorporated in the design.
- Thorougly investigate the requirements for the vertical connectors between the wings and see what airfoil would be the most beneficial.
- Compute the lift and drag polars for more Reynolds numbers (during different flight conditions)
- Optimise the reduction of induced drag due to the increased h/b ratio versus the increased drag of the larger area of the vertical surfaces.
- Investigate and optimise different wing area divisions and explore the possibilities of having different wing geometries between the two wings.
- Investigate the effect of the aerodynamic drag produced by the landing gear pods and see if there is a more efficient way to incorporate the landing gear.

5 Propulsion and Power Systems

This chapter discusses all power providing systems of the aircraft. First, the process of designing the engines for HAMMER is completely discussed. Secondly, the system powering the on-board systems is explained, highlighting some specific components that were changed with respect to conventional aircraft.

5.1. Turbofan Engines

In this section, the complete design process that was followed during the engine design is described. In earlier design phases it was determined that two turbofans would be used for the thrust provision of HAMMER. They were placed at the back of the aircraft, mounted to the fuselage. First, an overview of the design and its rationale are discussed in Subsection 5.1.1. The complete process, with results, is described in Subsection 5.1.2. It finishes off with an overview of the design in Subsection 5.1.3.

5.1.1. General Characteristics & Approach

For engine design of commercial jets, it is usual to optimise the engine for cruise as it is the longest flight phase. An engine with the best fuel consumption characteristics in this phase would thus consume less fuel overall than if its design was focused on best take-off performance. After the engine's optimal functioning during the cruise phase is verified, compliance with other phases such as take-off and top of climb can be calculated and confirmed.

To be able to size the engine, first, the required thrust was calculated. This was done with the thrust to weight vs. wing loading diagram shown in Figure 3.2, in combination with the fuel fraction method, to be able to adjust the weight for the various flight stages. This resulted in the following thrust levels for the two phases that were investigated:

$$T_{TO} = T/W_{TO} \cdot MTOW \tag{5.1}$$

$$T_{TO} = 402.09\ [kN] \quad and \quad T_{TO_{eng}} = 201.05\ [kN] \tag{5.2}$$

$$T_{cr} = T/W_{cr} \cdot W_{cr} \tag{5.3}$$

$$T_{cr} = 173.06\ [kN] \quad and \quad T_{cr_{eng}} = \frac{T_{cr}}{2} = 86.53\ [kN] \tag{5.4}$$

In the formulas above, T_{cr} and T_{TO} are the required thrust during cruise and take-off respectively, in Newtons. W_{cr} and W_{TO} are the weights of HAMMER at the start of these phases, in Newtons as well. T/W_{TO} and T/W_{cr} are the corresponding thrust to weight fractions of the take-off and cruise flight phase from Figure 3.2.

The next step in the design was to simulate the engine using Gas turbine Simulation Program (GSP). GSP is an object-orientated program and allows one to build and simulate gas turbine engines. It is mostly used because of its ability to predict both on-design as off-design performance. An engine can be created by linking components from GSP's library and it is based on 0-dimensional modelling. GSP runs every component after one another, this means that the exit conditions of one component are the inlet conditions of the next. Component maps are required but could not be constructed at this design stage, thus the built-in map library was used. For every component, either a low- or high-speed map was available. The appropriate map was selected based on the component's location and pressure ratio.

The engine with the topology as described in the midterm report was built in this program [21]. An overview is found in Figure 5.1. It is a twin-spool turbofan, without an exhaust mixer or afterburner. An exhaust mixer mixes the hot and cold airflow. This system was not used since for high bypass ratio turbofans, the required weight increase of the nacelle to implement this does not add up to slight thrust gain the mixer provides. The afterburner was not used due to its great increase in fuel consumption and noise. The resulting engine works by air flowing through the inlet to the fan. Here the air goes either through the core, where it is subsequently compressed by the Low Pressure Compressor (LPC) and the High Pressure Compressor (HPC) or it flows past the core via the duct to the exhaust. The ratio between these flows is one of the main engine characteristics and is called the bypass ratio (BPR). After the HPC, the air flows through the combustor, where ignition takes place, to the High Pressure Turbine (HPT) and Low Pressure Turbine (LPT), both connected to a spool linked to the HPC or the fan and LPC respectively. After this the air exits via the duct and exhaust.

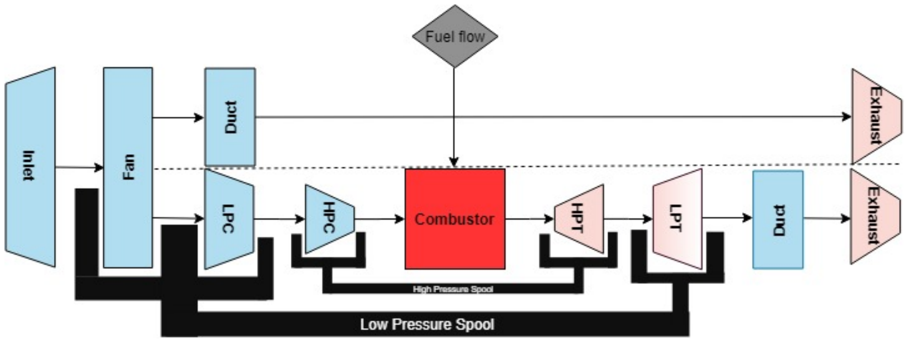

Figure 5.1: Topology of the engine in GSP.

The design process aimed to keep the Thrust Specific Fuel Consumption (TSFC) as low as possible and maximising the $F/\dot{m}$. TSFC is the fuel consumption of the engine, in kilograms per hour, divided by the thrust it can provide, in Newtons. This allows for a fair comparison of the fuel consumption of different engines. A low TSFC means better performance with respect to sustainability. $F/\dot{m}$ is the thrust, in Newtons, divided by the mass flow, in kilogram per second, also known as specific thrust. This also allows for comparing the thrust generated by different engines.

It was decided to investigate the engine's performance while varying the BPR and Overall Pressure Ratio (OPR). OPR is the product of the fan's, LPC's and HPC's pressure ratio, denoted with π_{fan}, π_{LPC} and π_{HPC} respectively. After consultation with P. Proesmans, the reasonable ranges and possibilities were determined, while keeping the 2035 EIS in mind[1]. They are listed in Table 5.1.

Table 5.1: Considered pressure and bypass ratio's for the design.

Variable [−]	**Considered range**
BPR	8-12
OPR	20-50
π_{fan}	1.3-1.7
π_{LPC}	1.3-1.6
π_{HPC}	19-25

It must be noted that an increase of BPR and OPR comes at the cost of a weight increase. For estimating the engine weight, W_{eng}, based on these characteristics, the following relation was used [48]:

$$W_{eng}[lbs] = a \cdot \left(\frac{\dot{m}[lb/s]}{100}\right)^{b} \cdot \left(\frac{OPR}{40}\right)^{c} \tag{5.5}$$

$$a = 18.09 \cdot BPR^2 + (4.769 \cdot 10^2) \cdot BPR + 701.3 \tag{5.6}$$

$$b = (1.077 \cdot 10^{-3}) \cdot BPR^2 - (3.716 \cdot 10^{-2}) \cdot BPR + 1.190 \tag{5.7}$$

$$c = (-1.058 \cdot 10^{-2}) \cdot BPR + 0.232 \tag{5.8}$$

The mass flow used in this equation could be retrieved from GSP, by sizing the engine to comply with the thrust requirements. This must thus be calculated for every combination of BPR and OPR. The relationship fits nicely in this case since it includes the effect of thrust and technology level on the engine mass.

[1]PhD Candidate Flight Performance, Delft University of Technology

The weight of the engine of an aircraft also has a certain maximum. Therefore, a weight constraint was added. The weight constraint followed from the stability and control department. Based on the limits of the c.g. range, an initial 12000 $[kg]$ was available for the engines, nacelles and pylons. This had to be reduced to bare engine weight to be able to link it to the relation mentioned above in Equation 5.5. Thus, a relation for nacelle & pylon weight based on engine weight described in Equation 5.9 by Mattingly [36] was used to reduce this 12000 $[kg]$ to only bare engine weight. A margin of 10% for weight increase caused by further optimisation of engine components was applied on this estimate, to allow fur enough optimisation cycles. This led to the fact that of the total 12000 $[kg]$ that was available for the engines, nacelles and pylons, 8200 $[kg]$ was available for the two bare engines, and thus 4100 $[kg]$ per engine. This is the maximum initial weight constraint.

Collecting the TSFC and $F/\dot{m}$ of the various OPR and BPR engine compositions considered together with the weight constraint, allowed for selecting the most optimal combination of BPR and OPR, which could then be further optimised.

5.1.2. Design and Optimisation

In this subsection, the process described above will be walked through, showing intermediate and final engine optimisation results.

Design Process

For various combinations of BPR and OPR, the TSFC and $F/\dot{m}$ were calculated and plotted. A plot like this is called a carpet plot. To ease the process and limit the computation time in GSP, it was determined to only vary the HPC's compression ratio for a change in the OPR. An overview of the inputs used for GSP (these are thus initial and not optimised yet) is found in Table 5.2. The efficiency factors, denoted by an η, were based on the GE90-94B engine [72]. Thus this means that no component development for the remaining time frame was considered at this stage. The combustor's exit temperature (T_{t4}) and efficiency were based on GSP's initial settings.

Little information was available for specific component's performance as engine manufacturers tend to not share this information due to the competitive advantage it creates. As a result, the GE90-94B engine was considered as a basis for this design. This particular engine was considered since it was the most representative engine found with all data online available. It is a 2000 EIS turbofan used by the Boeing 777-200ER and was the most powerful turbofan at that time. Since it was already certified in 2000, component development was estimated for the engine that is to be designed by extrapolating the GE90 values, but it was decided to do so in a future design stage.

With the component data of the GE90, the weight constraint for the different combinations of OPR & BPR was determined. The graph is shown in Figure 5.2. To calculate this, first, the cruise condition was simulated, after which the off-design take-off case was also investigated. This was necessary since the $\dot{m}_{TO}$ was required for engine weight determination. The resulting carpet plot, using the cruise case, is found in Figure 5.3.

Table 5.2: Initial inputs for GSP calculations.

Variable	Initial Value	Variable	Initial Value	Design Constraints	Value
$\pi_{fan}[-]$	1.6	$\eta_{fan}[-]$	0.9153	BPR $[-]$	8-12
$\pi_{LPC}[-]$	1.4	$\eta_{LPC}[-]$	0.9037	OPR $[-]$	20-50
$\pi_{HPC}[-]$	8.93-22.32	$\eta_{HPC}[-]$	0.9247	Alititude $[m]$	10000
$\eta_{HPT}[-]$	0.9121	$\eta_{LPT}[-]$	0.9228	$M_{cr}[-]$	0.78
T_{t4} $[K]$	1700	$\eta_{comb}[-]$	0.995	T_{cr} $[kN]$	86.53

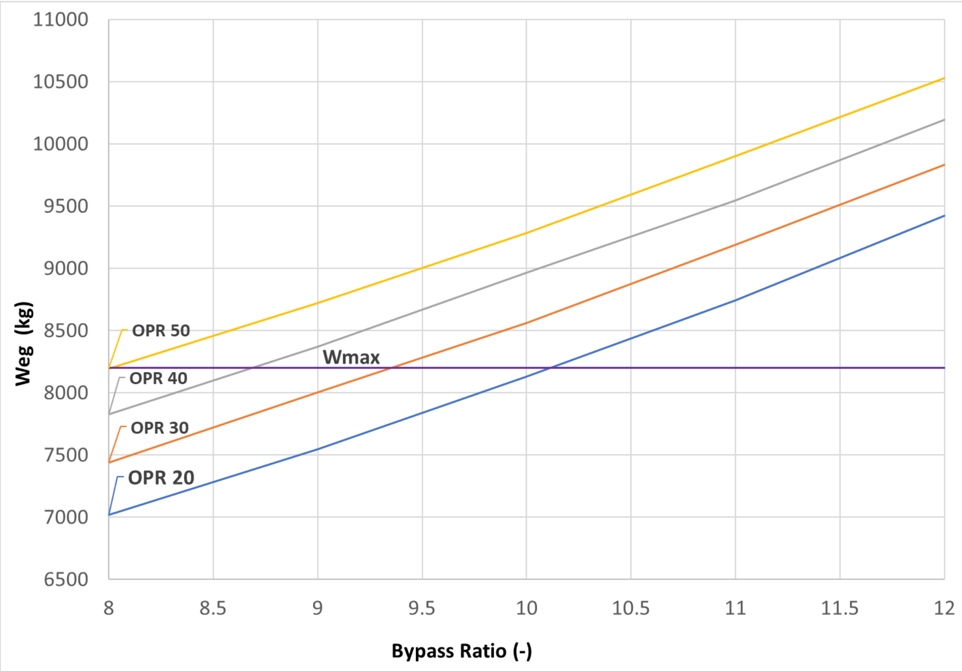

Figure 5.2: Bare engines weight for the various OPR's and BPR's considered, intersecting the maximum initial weight.

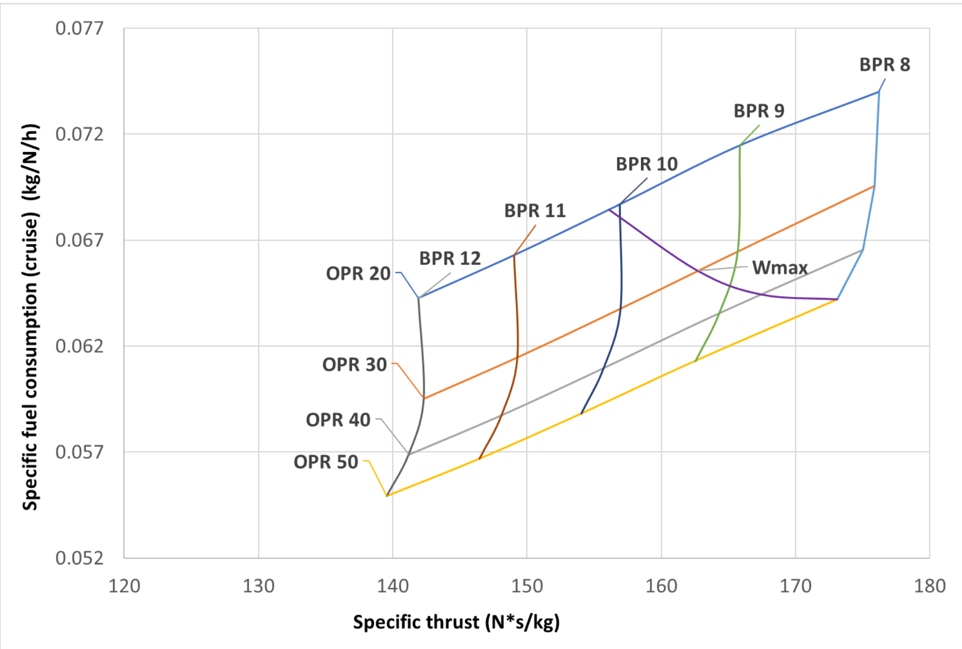

Figure 5.3: TSFC vs. Specific Thrust carpet plot, varying OPR and BPR.

The optimal design scenario following from Figure 5.3 is thus the lower right-hand corner. This has the lowest TSFC and highest $F/\dot{m}$ within the allowed range. An OPR of 50 and BPR of 8 was thus selected. It was noted at this stage that the TSFC was on the high side in comparison to other engines [36].

To lower the TSFC, amongst others, a lower T_{t4} was chosen, at the cost of $F/\dot{m}$. This was done to provide a more sustainable solution, as this was one of the main incentives in the engine design. Designing an engine with worse fuel consumption characteristics was deemed not allowed. Further reasons to do so are that lower fuel consumption leads to a lighter aircraft and lower operational costs as less fuel is needed. A result of this lower combustor exit temperature was a slight increase in engine weight since the engine diameter must increase for provision of similar thrust levels. The engine weight was always kept within the allowed limit. Furthermore, it was estimated that engine development could increase efficiencies for the components with another 10% with respect to the GE90 [72]. This was also based on the faster than expected development rates of turbofan components in the past, this can be seen when comparing the relations shown in Mattingly et al. with the GE90 data [36]. Only the combustor efficiency increase was estimated to develop slower with respect to the GE90 since this is already almost at its maximum.

After these final efficiency values were determined, the engine could be optimised within the allowed component pressure ratios. After this was completed, the off-design case, being take-off, was investigated and its compliance was verified. The take-off parameter was verified for a maximum take-off height of 500 [m], together with a temperature of 30 °Celsius. This allows HAMMER to comply with take-off requirements in hot and high conditions as well.

Nacelle and Pylon

Apart from the engine, the nacelle and pylon were also sized. The relation described in Mattingly et al. was used, this relation provides a fraction, $k_{n.p.}$, which estimates the nacelle and pylon weight, $W_{n.p.}$, based on engine weight [34]. For a bypass ratio of 8, the relation is as follows:

$$W_{n.p.} = k_{n.p.} \cdot W_{eng} \quad with \quad k_{n.p.} = 0.32 - 0.34 \tag{5.9}$$

For other bypass ratios, the value of k would be different. In this case, in the range of 0.32-0.34 for the BPR of 8, it was chosen to use 0.32 for k since aircraft material development tends to aim for lowering the weight of these components. Since the engines are mounted at the aft of the fuselage, the pylons were considered clamped beams.

It needs to be considered that when locating the nacelles at the aft fuselage using these pylons that clearance of the fuselage boundary layer and wing wake is necessary. From Kundu et al. [34], it was retrieved that the pylon's length needs to be almost the full engine length with a thickness over chord ratio of 0.08. The depth of the pylon can be estimated by half of the fan face diameter for the current design stage, but for further optimisation, this needs to be investigated using CFD analysis. An overview of the resultant pylon is shown in Figure 5.4a. The vertical position was based on minimising the pitch moment around the centre of gravity. The longitudinal position was decided to be 40 [m] from the nose, fuselage-mounted, as mentioned in the midterm report [21]. This was decided upon mainly due to the aerodynamic benefit this provides, but also since this keeps the engines thrust vector close to the centre of gravity and the ease of maintenance operations.

The sizing of the engine nacelle was a cumbersome process since it varies a lot based on engine layout, characteristics and design preferences. In general, it can be said that a higher OPR leads to significantly larger engines since more compressor stages need to be present. Also, a higher BPR leads to a larger engine diameter and thus nacelle diameter. Except for these base relationships, little information could be found and thus, no clear final values could be determined, but only estimates could be given. These estimates are based on the relations described in Jenkinson et al. [32]. These link BPR, OPR, fan diameter, max operating Mach number and mass flow to the nacelle sizes. The relations used are found in Appendix B.

5.1.3. Design Process Results

After the steps described were executed, the design of the engine, nacelle and pylon group was finished. The results of the design process of this high-bypass twin-spool turbofan engine are displayed in Table 5.4. The overall dimensions and weight of the engine, nacelle and pylon group are shown in Table 5.3. The final engine render can be seen in Figure 5.4.

Table 5.3: Engine components' weight and size.

Variable	**Value**	**Variable**	**Value**
$\varnothing_{eng_{face}}$ [m]	2.70	W_{eng} [kg]	4497
$\varnothing_{nacelle_{max}}$ [m]	3.27	$W_{n.p.}$ [kg]	1484
l_{cowl} [m]	4.63	W_{tot} [kg]	11962
$l_{afterbody}$ [m]	0.58	$l_{nac_{tot}}$ [m]	5.21

Table 5.4: Final Engine Characteristics.

Variable	Value	Variable	Value	Variable	Value
BPR $[-]$	8	$\pi_{fan}[-]$	1.7	$\eta_{fan}[-]$	0.9245
OPR $[-]$	50	$\pi_{LPC}[-]$	1.6	$\eta_{LPC}[-]$	0.9127
Altitude $[m]$	10000	$\pi_{HPC}[-]$	18.38	$\eta_{HPC}[-]$	0.9340
$M_{cr}[-]$	0.78	$\eta_{HPT}[-]$	0.9121	$\eta_{LPT}[-]$	0.9320
T_{cr} $[kn]$	86.55	T_{TO} $[kN]$	201.09	$\eta_{comb}[-]$	0.997
$TSFC_{cr}$ $[kg/N/h]$	0.05348	$TSFC_{TO}$ $[kg/N/h]$	0.02825	T_{t4} $[K]$	1500

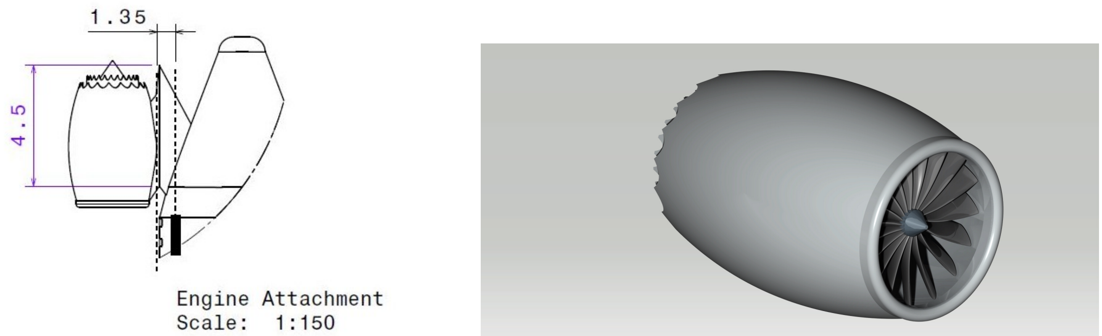

(a) Drawing of engine and attachment.

(b) The engine render.

Figure 5.4: Final engine design overview.

5.2. Power Systems

In this section, the power provision of the on-board aircraft systems and its working are discussed. The main focus is on systems that are changed with respect to conventional aircraft. The details of these systems and their interactions are explained using block-diagrams and descriptions.

5.2.1. No-Bleed Aircraft System Description

As a main driver for this project is sustainability, a no-bleed air system was adopted to work towards a greener, electrical powered, aircraft. Aircraft which have a higher degree of hybridisation include better mass and fuel consumption characteristics, but also tend to lower operating costs and maintenance costs. Technological development allowed to eliminate almost all of the pneumatic systems found in conventional aircraft, in favour for the use of electrical ones. This section discusses the impact this design choice has on the general aircraft systems.

Bleed air is mainly is used for pressurisation of the cabin, de-icing of specific aircraft parts and for supporting the hydraulic system used for flight control.

The use of bleed air originates from the reliability of such systems. The air is usually taken from the HPC, thus before fuel burning takes place. Since this air is always available when the engines are running, the system is quite reliable. Other advantages of this conventional system are the easy access and the high amount of power this source contains.

Using a no-bleed system uses electrical power for these operations. The pneumatic systems using bleed air are not necessary anymore and can thus be eliminated. The advantages include but are not limited to:

- Better fuel consumption performance. No air is taken from the engines and electrical energy works more efficiently.
- Weight reduction. The bleed-less Boeing 787 experienced weight reduction due to the elimination of all the valves and tubes used in a bleed-air system. [66]

- Less maintenance and higher reliability. Electrical systems provide improved reliability but can also easily isolate faulty systems, easing the reparation. A bleed-air system can not isolate in such a way but only indicates an entire circuit. Further improvements, such as monitoring the systems, could even lead to the opportunity to predict failure, lowering the indirect operating costs even further.
- Safety. No heated air is transported through the aircraft. A leak in such a system could cause damage to surrounding components.

The main drawbacks found for the no-bleed architecture are an increase in system cost and Boeing's patents that are hard to workaround. The last is assumed to be not of importance in this project. The cost is a drawback, but considering all the significant advantages, the system was adopted. Also, a portion can be earned back due to the lower operating costs. A schematic overview is shown in Figure 5.5 In this schematic overview, redundant/extra connections are not shown to keep the overview clear. Of course, in the final aircraft design, redundant systems and connections are in place. For example, only one Starter Generator is shown per engine, but two per engine would be implemented. Not only to have better start performance but also to be able to start if one fails. The starter generators start the engines and auxiliary power unit (APU) similarly as the Boeing 737 Next Gen. The process is controlled by start converters, which govern the required electrical power. The APU is started using the battery as a source, the APU generator is able to provide power for starting the two engines afterwards. Also, ground power sources can be used for this.

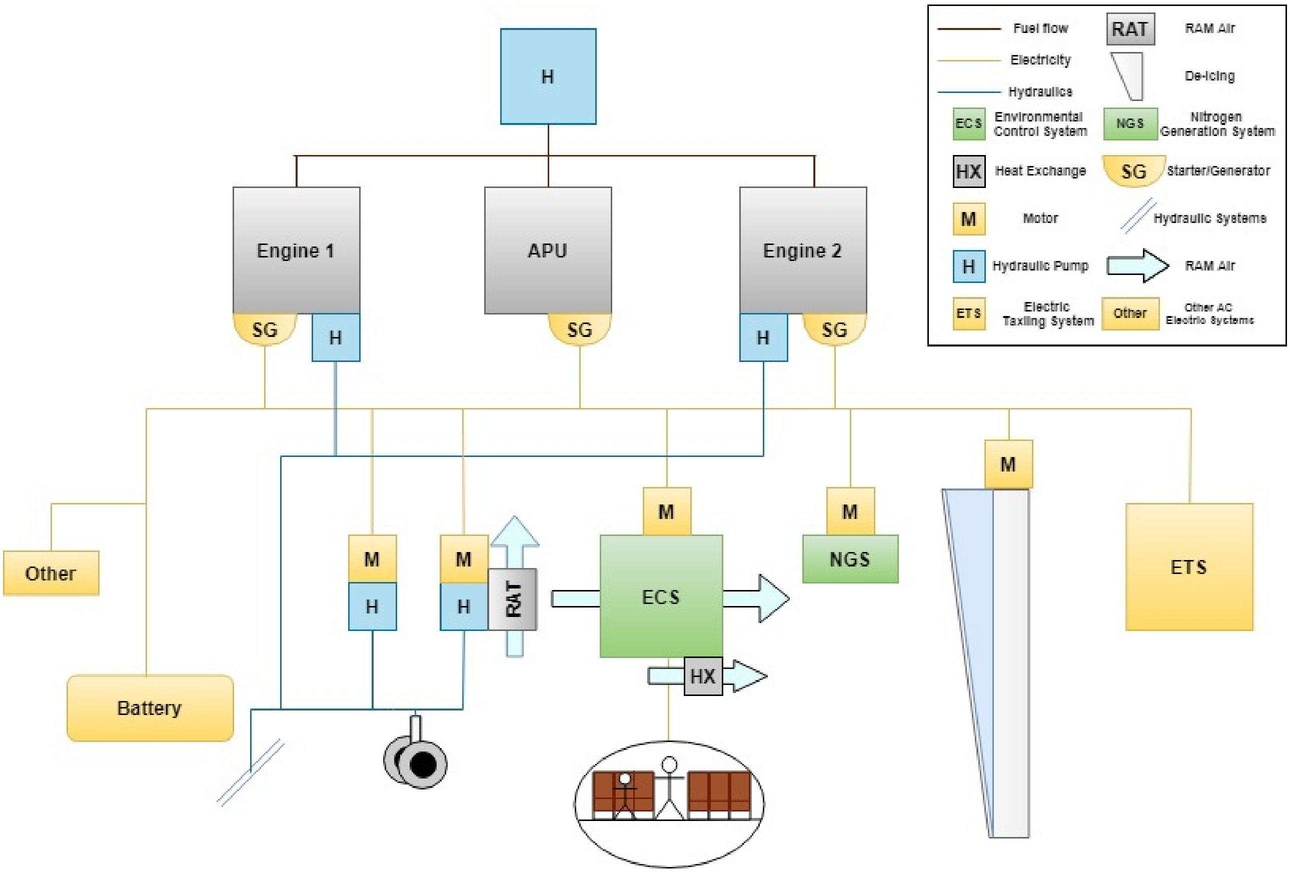

Figure 5.5: Schematic Overview of the interaction between the General Aircraft Systems.

5.2.2. System Components

Engine Electrical Power Generator

In conventional aircraft, pneumatic systems steal high-speed air from the engines, lowering the thrust and increasing its fuel consumption. Electrical power is more efficient than pneumatics, and will, therefore, decrease this effect. Also, pneumatic systems usually draw more power than needed since it is hard to continuously optimise the bleed. This energy is not useful and is thus simply dumped. The no-bleed system uses shaft-driven generators for providing electrical power, this more efficient method does not extract as much and lowers fuel consumption. It was shown that this improvement reduces fuel consumption with 1-2% in cruise [66]. Also, the no-bleed system does not need all the pneumatic valves, ducts and coolers, reducing the engine weight and simplifying the engine build.

Auxiliary Power Unit
HAMMER's APU only delivers electrical power. Its design is thus much simpler than conventional, adding to lower maintenance costs and higher reliability. It is located at the same position as conventional, being the tailcone. Also, this fully electric APU can work with variable speeds to further optimise the performance. For the APU's sizing, the 787's APU was used. This Pratt & Whitney APS500 is the only electric APU currently available on the market. It has both the lowest emissions of the industry and also produces the least noise in its class. An image of this APU is shown in Figure 5.6[2], it can be noted that all tubes and other equipment for a pneumatic system are cut.

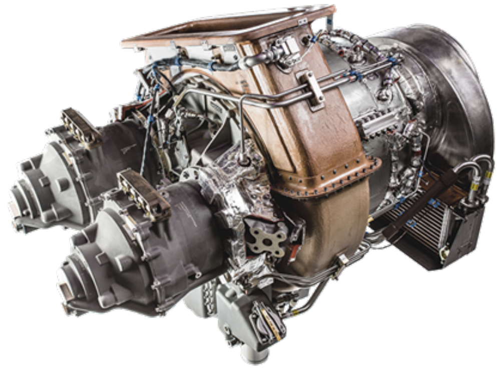

Figure 5.6: Pratt & Whitney's no-bleed APU: APS5000.

Hydraulics
With respect to conventional aircraft, the hydraulic system did not change a lot. The hydraulic system supports the actuators, landing gear and flaps, amongst others. The hydraulics are partly powered by the pumps located in the engine gearbox. Additional electrically driven pumps are also in place for extra power during the highest demanding operational points, as well as during ground operations. One of the key differences is that higher pressures can be achieved using the electric motor to power the hydraulic system, allowing for smaller components, when comparing to pneumatic one. In conventional configurations, the pumps are driven by a significantly larger turbine-powered hydraulic pumps during peak-demands, but this is not longer necessary.

Environmental Control System
Cabin pressurisation is thus also done electrically. In this no-bleed system, the pressure is provided by compressors and air from cabin air inlets. The variable setting of the electrical motors that are powering the pressurisation allows for optimal energy usage control. Also, the inlet flow of air can be varied according to the aircraft weight and number of passengers. This way, no excess energy is to be dumped and the system operates at almost ideal efficiency.

De-icing
The problem of ice forming on, for example, the leading edge of the wings, is tackled by the use of heating blankets, as successfully done by the Boeing 787. These blankets are powered electrically and can either work by removing ice or preventing ice-forming. Traditional systems need large amounts of valves with bleed air and a 'piccolo' duct to distribute heat over the concerning areas. Additionally, for slats, telescoping valves are needed, further complicating this approach. As a result, the electrical version uses approximately half the power for protection, when comparing to the pneumatic version [66]. It also reduces noise and drag since no exhaust holes are present.

Electric Taxiing System
It was chosen to include an electric taxiing system (ETS), making HAMMER able to taxi completely carbon neutral. This is a very innovative system that requires some further development but has a promising outlook. "WheelTug" already demonstrated a similar system in 2005 on a Boeing 767, as illustrated in Figure 5.7. Since then, more than 20 airlines have placed over 1000 orders at WheelTug, while still in its certification phase. This shows that this technology is of high demand within the aviation sector and also proved that it was a feasible option for this design.

[2] https://www.pwc.ca/en/products-and-services/products/auxiliary-power-units [Cited 21 June 2020]

The main driver for implementing this idea was to further decrease the greenhouse gas and noise emissions of HAMMER. Using an electric, green system, replaces the use of fossil fuel consumption in combination with inefficient jet engines with green energy powered, electrically driven motors. This decision was at the cost of a weight increase. An on-board system was preferred since it can not be said with certainty that all airports will have a fully operating electric tow truck system by 2035. Furthermore, the on-board system can reduce the turnaround time by allowing for its own push-back, by simply putting the electric system in reverse mode. The aircraft can now do the ground operations fully autonomous. A positive side effect of this is the reduction of total airport movements, thus working towards simpler airport operations.

Figure 5.7: WheelTug's electric taxiing system.

The system will be integrated with the main landing gear (MLG). This was to firstly done to overcome slip since only a small portion of the weight is on the nose landing gear (NLG). This could be problematic during bad weather conditions. Also, the eight MLG wheels allow for more redundant motors and thus a system with higher reliability. Another feature of electric taxiing is reduced wear of the brakes. The brakes are not used as heavily when comparing to conventional taxiing with the turbofans, thus increasing their lifetime and reducing maintenance.

For powering this system, eight MLG motors were used. To size the battery that will provide energy to this system, the required power and energy must be calculated. The requirements and assumptions used for the calculations are:

- The aircraft shall taxi at a speed of 30 [km/h].
- The aircraft shall be able to start, accelerate to 30 [km/h] and stop again in 60 [s], in order to quickly cross runways and not obstruct traffic flow.
- The aircraft shall be able to perform the start stop manoeuvre four times per taxi.
- The aircraft shall be able to taxi for 15 [min], so almost always, fully electric taxiing is possible.
- The rolling friction coefficient of the aircraft is 0.009 [29].
- The coefficient of friction for a tire is 0.8 [29].
- A gear ratio of 13 can be achieved [29].
- As the maximum speed is 30 [km/h], it can be assumed that drag plays no significant role [29].

With these assumptions and requirements, the resulting system shall be able to complete the taxi phase completely electrical in almost all situations. The 15 [min] 30 [km/h] drive gives the system an effective range of 7.5 [km]. Taxiing can take longer than the sized 15 [min], but most of the time the aircraft stands still for a significant portion of this time. If this is not the case, a slightly lower taxi speed can be adopted. If this is not wanted, the APU can assist with power provision. Also, significant extra energy is available due to the start-stop requirement. This can be used if the allocated energy for taxiing at constant speed is finished since the aircraft does not need to accelerate so often and fast under normal use. The complete list of computations is found in Appendix C. An overview of the resulting values is shown in Table 5.5.

Table 5.5: The power and energy required for the Electric taxiing system.

Variable	**Value**	**Variable**	**Value**
P_{avg} [kW]	89.47	$P_{avg_{tire}}$ [kW]	11.18
P_{max} [kW]	151.25	$P_{max_{tire}}$ [kW]	18.91
E_{req} [kWh]	29.93		

Nitrogen Generation System

The nitrogen-generation system filters air to a nitrogen-rich gas. With this nitrogen gas, the fuel tanks get refilled when the fuel is pumped out. This so-called "fuel inerting" is done to lower the likelihood of a fire occurring in the fuel tanks. Fuel inerting is the prevention of combustion by using a nonreactive gas. In this case, nitrogen is used. It must be noted that no nitrogen is generated, it is just filtered.

Battery

Due to the electric taxiing, a significantly larger battery is necessary. The determination of the required battery capacity consists of two parts, the capacity needed for the electric taxiing system plus the capacity needed to supply all other systems. For the electric taxiing system, the capacity mentioned in Table 5.5 was used, adjusted for an efficiency of 93% for the gearbox and 85% for the motor/inverter, as mentioned in Heinrich et al. [29]. A depth of discharge of 75% was used to increase battery life. For all other subsystems, it was hard to calculate the required battery capacity, since all reference aircraft have a pneumatic system, except for the Boeing 787. Therefore, it was chosen to simply add the battery capacity of this aircraft to the capacity needed for the ETS. To determine the weight of this battery, a linear relationship with Rolls-Royce's new aircraft battery was adopted[3]. Since the battery consists of closely packed cells, these can be down-scaled to meet the specific requirements. This battery was designed for fully electric planes and is thus assumed to be top of the line. Using this battery furthermore allows for meeting the 2035 EIS requirement. Also, the maximum power required as shown in Table 5.5 is met by this battery. All battery characteristics can be found in Table 5.6.

Table 5.6: HAMMER's battery characteristics.

Variable	Value	Variable	Value
E_{tot} $[kWh]$	52.9	W_{bat} $[kg]$	330.6
$E_{tot_{ETS}}$ $[kWh]$	50.49	Specific Energy $[Wh/kg]$	165
$E_{tot_{oth}}$ $[kWh]$	2.415		

Other Electrical Systems

Next to the systems described above, a lot of other systems are powered electrically on an aircraft. These consist of, for example, cabin lightning and television screens in large aircraft. Systems like these are grouped in the Aircraft's bus. Either in the Alternating Current (AC) or the Direct Current (DC) version, depending on the type of electricity they consume. Furthermore, the electrically powered systems that are essential for the safe operation of the aircraft are grouped in the aircraft's essential bus, also using alternating or direct current. Examples of these systems are flight instruments and warning lights in the cockpit. An overview of the flow between the bus systems and generators is shown in Figure 5.8. The red, dotted lines show the redundant flow options in case of failure of one or multiple components. For every essential path, at least three direct flows of energy are present and even more indirect flows. The Transformer Rectifiers can convert the alternating current to direct current. The Static Inverter does the opposite.

[3]https://spectrum.ieee.org/energywise/energy/batteries-storage/the-battery-innovations-behind-rolls-royces-ultrafast-electric-airplane [Cited 20 June 2020]

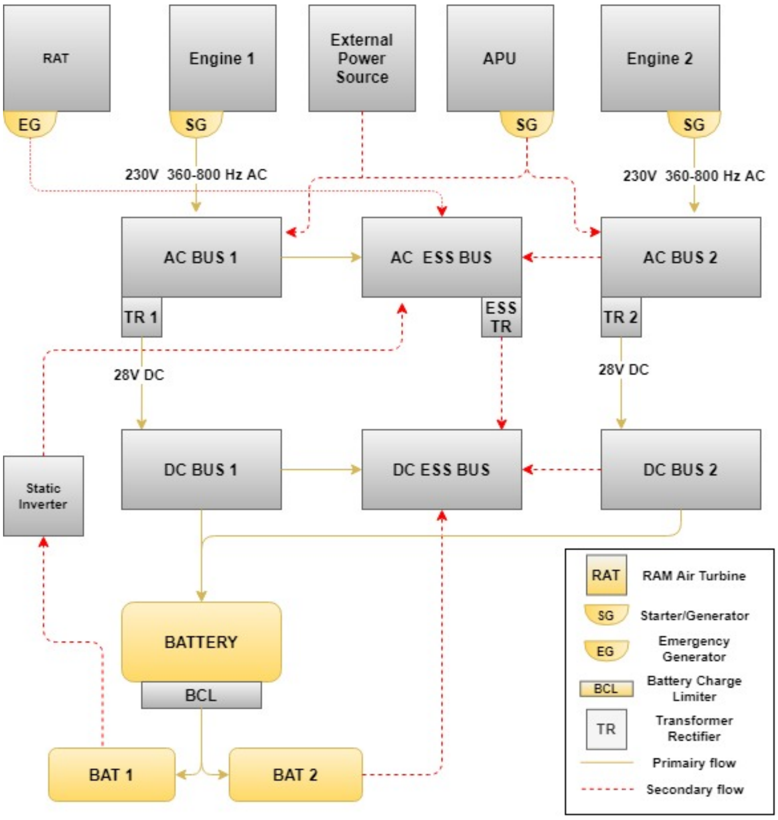

Figure 5.8: Electrical block diagram including optional flows in case of failure.

This diagram was based on the A320's electrical system. adjusted by that of the Boeing 787, to account for the extra electricity needed for the no-bleed system. The preferred order of power provision in case of failure is own engine's generator, external power source, APU, opposite engine generator, RAM Air Turbine. The RAM Air Turbine is thus the last emergency source of power provision.

The various hardware and software components present in the bus systems and their mutual relations are shown in Figure 5.9. Several characteristics typical for HAMMER can be found in this diagram. Examples are the control surfaces both on the aft and forward wing, as well as the jump strut.

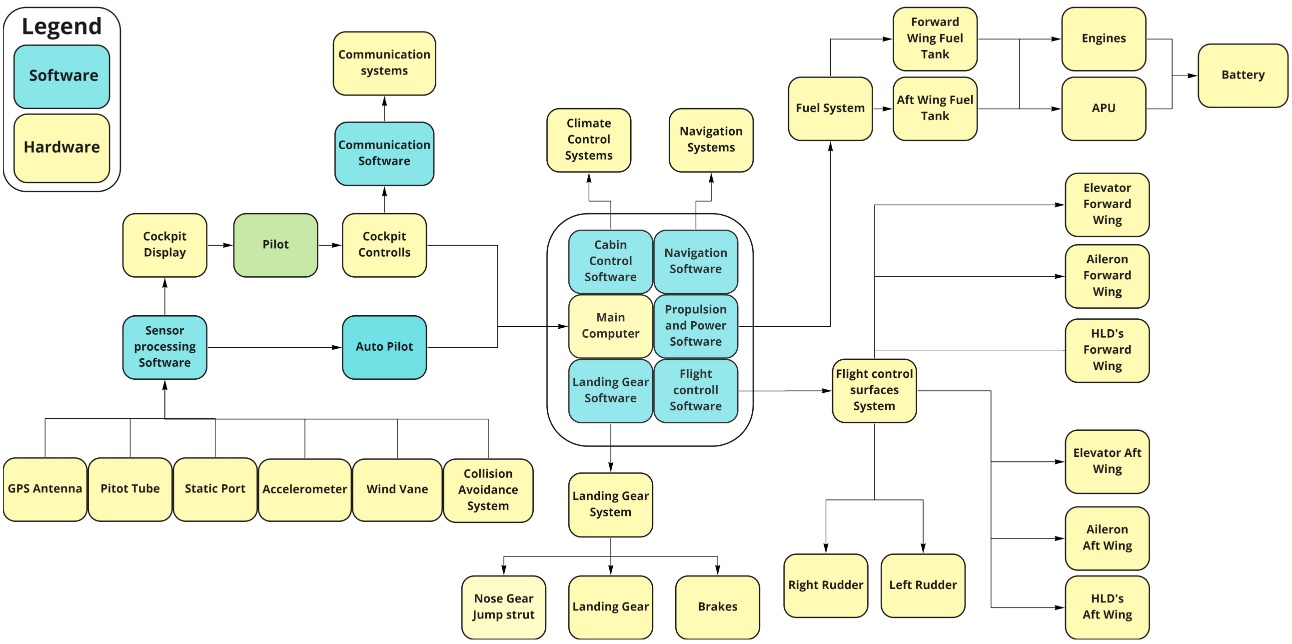

Figure 5.9: Block Diagram of the HAMMER hardware and software.

5.3. Verification and Validation

For verification of the propulsion system, a variety of tests were done. First of all, some pressure ratios and temperature ratios over specific components were checked by hand, for both the on-design cruise and off-design take-off. Also, the engine group and nacelle group weight estimation were verified by hand calculations. Unit tests in GSP were also performed as an additional check. It was assumed unlikely that the program itself contained mistakes due to its wide application in engine design. For the no-bleed architecture, the calculations for the ETS and battery sizing were verified by changing the numbers in the excel sheet by known values from other cases, this was done to check for the same results. This way, the correct implementation of the formulas was verified.

To validate the GSP model built, the GE90 engine data was also used as input in the model. With these inputs, the TSFC of the created model and similar, already validated, models could be compared. The model was compared with a Numerical Propulsion System Simulation by Georgia Tech [72]. This comparison could also help to determine the created model's accuracy. An overview of the inputs is found in Table 5.7. The resulting outputs of the model and the comparison can be found in Table 5.8.

Table 5.7: Used inputs for validation of the GSP model with GE90's values [72].

Variable	Value	Variable	Value	Variable	Value
$\pi_{fan}[-]$	1.58	$\eta_{fan}[-]$	0.9153	BPR [−]	8.7877
$\pi_{LPC}[-]$	1.26	$\eta_{LPC}[-]$	0.9037	OPR [−]	40
$\pi_{HPC}[-]$	20.033	$\eta_{HPC}[-]$	0.9247	Alititude $[m]$	10668
$\eta_{HPT}[-]$	0.9121	$\eta_{LPT}[-]$	0.9228	$M_{cr}[-]$	0.80
T_{t4} $[K]$	1500	$\eta_{comb}[-]$	0.997	T_{cr} $[kN]$	73

Table 5.8: Validation of used model vs. the NPSS by Georgia Tech [72].

Variable [*kg/N/h*]	GSP model	NPSS model	Percentage difference
TSFC	0.05707	0.05522	+3.35 %

The 3.35% discrepancy in TSFC was considered to be within allowable limits. This discrepancy can originate from various reasons, such as different gas properties assumed, the used component maps and other simplifications in the model.

To validate the no-bleed system, the block diagrams were compared with those of reference aircraft. This way it could be seen if important parts were missing and if the overall structure was the same.

5.4. Sustainability Analysis

As a significant part of the aircraft's pollution is caused by propulsion and power systems, sustainability was an important parameter in the design. Therefore, during the design, the main focus was on creating a sustainable system that remained within operational limits. A full quantitative analysis of the emissions of the aircraft is performed in Chapter 13. This section provides a more qualitative approach, only using a few numbers for comparison. Furthermore, it discusses sustainability factors that were or need to be taken into account in the design.

The fuel economy of the designed engine with respect to common engines operating in the 2000 time frame is an interesting statistic since it gives an insight into the increase in engine efficiency over the years. It also indicates how well sustainability issues are addressed in this design. TSFC does not follow a linear relationship with (carbon dioxides) CO_2 or nitrogen oxides (NO_x), but the three are somewhat related. To compare, the engine of the most used civil aircraft of 2000, the Boeing 737 Classic and Airbus 320, was related to the newly designed version.

Table 5.9: TSFC comparison between 2000 and newly designed engines [22] [32].

Mission phase *[kg/N/h]*	**CFM-56**	**Designed Engine**	**Percentage Reduction**
$TSFC_{cr}$	0.06799	0.05348	21.34%
$TSFC_{TO}$	0.04032	0.02825	29.94%

From Table 5.9, it can be concluded that a significant reduction in fuel consumption by the aircraft engines is present. This is achieved due to technological progress over the past decades, resulting in engine characteristics with increased BPR's, OPR's and component efficiencies. The new CFM International LEAP, introduced in 2016, is nowadays used by the 737 and A320. It is advertised to lower the TSFC by approximately 15%, with respect to the CFM-56 [4]. The newly designed engine for HAMMER can, therefore, conclude to also outperform the currently used engines.

Also, due to the implementation of the no-bleed system, the engines are to be operated much more efficiently and no excess energy needs to be dumped overboard on a large scale. This results in even less fuel consumption during cruise and other flight phases. HAMMER's no-bleed system will reduce the weight of the general system by making a large part of the valves and tubes redundant, decreasing the weight of the APU, de-icing system and many other parts. Boeing estimated the total fuel savings of a no-bleed system at 3% [66]. Furthermore, the electric taxiing system allows HAMMER to taxi to the runway completely autonomous and carbon neutral. This reduced turn around time and emissions during this phase for every flight.

Besides, a list with the upcoming, most relevant turbofan technological revolutions that must be considered for future design phases is listed and shown below. These recommendations for further design all contribute to a more sustainable engine.

- Carbon fibre fan blades with a titanium coating, instead of completely titanium fan blades. These carbon fibre resins have enhanced toughness. The coating is applied to maintain protection against foreign object ingestion, birds and corrosion. This advanced material could save HAMMER 700 [kg] and reduce fuel consumption more than 25%.[5]
- Better core components, to lower emissions by enhanced fuel burn efficiency
- Variable nozzle area and improved inlet geometry, for improved performance and reducing noise

5.5. Risk Assessment

For the propulsion system, most of the technology is already used on a large scale and tested before. Therefore, not many uncertainties and thus risk arise at first sight. Also concerning maintenance and production, due to the long use of turbofans, no risk was identified in this field. The no-bleed architecture for the power of on-board systems is also already fully operational. The Boeing 787 uses this system and it is assumed to be more reliable than its pneumatic version. Thus, also no risks arose from this part of the design.

The risk related to engine design originates from the expected component development. If these are not met, the engine performs worse. On the other hand, the probability of these developments not being realised is considered small. Turbojet manufacturers are continuously announcing new, innovative turbofans, pushing the technological limits and implementing sustainability regulations. This means that research is ongoing in this particular field and components optimisation is an unfinished task. Therefore, the risk associated with a stop in engine efficiency development is considered small.

The electric taxiing system that was introduced in the HAMMER design does have risks related to the 2035 EIS requirement. Since this system is still in development face and no airliners or large civil jets use this system on a consistent basis, it can not be said with 100% certainty that this technology will be usable on a large scale in 2035. The change of not being ready by then, and thus this risk occurring, was estimated very small. Multiple companies are researching the subject and a large number of orders have already been placed. Furthermore, successful demonstrations have been performed on several occasions.

[4] https://www.cfmaeroengines.com/engines/leap/ [cited 27 June 2020]
[5] https://www.rolls-royce.com/media/our-stories/innovation/2016/advance-and-ultrafan.aspx#overview [cited 19 June 2020]

5.6. Requirements Compliance

An overview of all the requirements of this part of the design is given in Table 5.10. It was shown that the design of the power and propulsion systems has been performed while continuously aiming at a low fuel economy, for example by lowering the combustor exit temperature or adopting the no-bleed architecture, so this requirement is met. This also results in minimal use of toxic substances. Besides, the engine protects against bird strikes and foreign object by using the conventional technologies of titanium fan blades and strong engine casing. This was accounted for by sizing the engine based on relations using these materials. It is recommended though, to look at other, lighter materials, for these parts, while still ensuring this protection for future design. An example of this is the discussed carbon fibre fan blades with the titanium coating. The necessary equipment for communication, prevention of collision, correction of course deviation and an autopilot were also implemented, an overview of how this is done is found in Figure 5.9. It can thus be concluded that all requirements presented in Table 5.10 are met.

Table 5.10: Compliance with the engine requirements.

	Requirement
✓	CMR-SR-SU-2 - The aircraft shall use engines prioritising low fuel economy.
✓	CMR-SR-SU-11 - The aircraft shall be able to manage bird strikes.
✓	CMR-SR-SA-AS-5 - The aircraft shall be able to contain damage due to foreign object ingestion.
✓	CMR-SR-SA-AS-1 - The aircraft shall be able to communicate with air traffic control.
✓	CMR-SR-SA-AS-4 - The aircraft shall be able to autonomously prevent collision with other aircraft.
✓	CMR-SR-SA-AS-6 - The aircraft shall be able to correct unwanted course deviation.
✓	CMR-SR-AO-AC-3 - The aircraft shall have an autopilot.
✓	CMR-SR-SA-GS-2 - The aircraft shall require minimal use of toxic substances to function.

5.7. Conclusion

In conclusion, a power and propulsion system was developed that meets all set requirements. The engines were tested to comply with the cruise and take-off requirements. The technological development, necessary to be able to design this engine, was based on past trends and does not include an unrealistic outlook. Sustainability issues were addressed and the engine was shown to be more fuel-efficient than its competitors. Besides, the no-bleed architecture will further reduce the fuel consumption of HAMMER. Using the new technologies of this system, in combination with the electric taxiing system, creates a revolutionary aircraft in this department on the fields of sustainability, maintenance and degree of hybridisation. For this no-bleed power system, only the parts that were most key and changed significantly with respect to conventional aircraft were discussed. This was decided to since the list of systems on-board is endless and most are self-explanatory. Also, for the not discussed systems, no significant improvements were found, thus they would be the same as for conventional aircraft. A recommendation for further research would be to find the exact power all the systems in the no-bleed architecture need, so the battery can be sized more accurately.

6 Fuselage and Payload Configuration

The configuration of the payload is presented in this chapter. First, the design process carried out to design the cabin layout is explained. Then, the layout of the cargo compartment, where some aircraft subsystems and most of the luggage are placed, is depicted.

6.1. Cabin Layout

In the midterm report [21] a double-bubble fuselage configuration with all-economy seating was chosen for HAMMER, with a full-density capacity of 320 passengers (pax), without exceeding the length requirement. This length requirement is given by the fuselage length of the longest aircraft that connects to gate type C, which is the A321 with a length of 45 [m]. Also, in order to meet aviation and safety requirements, a total of eight cabin crew members and two cockpit crew members per aircraft were chosen. An extensive explanation and justification of the choices can be found in [21].

The seating configuration will vary depending on the fuselage width at that location. A sketch of how the rows at the widest part of the fuselage will look like is depicted in Figure 6.1. For this cabin section, a 2-4-2 configuration was chosen, as it allows for more passengers carried in a shorter length but it does not hinder passengers' comfort when they want to reach the aisle, as they are always very close to it.

In Table 6.1, the different parameters that were either set or computed to design the fuselage cross-section can be found. The seat width and arm rest were taken from literature [71], where a range of values was given for each parameter. The minimum dimensions needed for short- and medium-range flights were taken for HAMMER, allowing for a compact aircraft design. The aisle width was taken to be double that what is usually used for aircraft of similar range so that two people could fit on the aisle at the same time, reducing the turnaround time during (de)boarding. In order to check that two people could fit in the aisle at the same time, a simulation of two people was placed on the cross-section. This can be seen in Figure 6.1. The height and width of each person were set to the US average for men and women, and they were then scaled to the cross-section dimensions. A wall is present in the middle of the cross-section to reinforce the airframe. It will have cut-outs to allow groups of more than two people to travel together and interact with each other. In order to place cut-outs, the thickness of the wall will vary throughout the cabin height. An interior view of the fuselage with the middle wall can be seen in Figure 6.2. Also, the dimensions of this wall are present in Figure 6.3. More details of the reinforcing wall can be found in Chapter 8. Finally, the other parameters depicted in Table 6.1 were measured from Figure 6.1.

Table 6.1: Fuselage cross-sectional dimensions.

Parameter	Unit	Value
Seat Width	[m]	0.432
Arm Rest Width	[m]	0.051
Aisle Width	[m]	0.914
Aisle Height	[m]	2.061
Row Width	[m]	5.842
Fuselage Inner Width	[m]	6.011
Fuselage Outer Width	[m]	6.111
Fuselage Height	[m]	4.316
Bubble Radius	[m]	2.108
Wall Thickness	[mm]	3.62 - 5.17
Wall Width	[m]	1.5
Floor Thickness	[m]	0.1

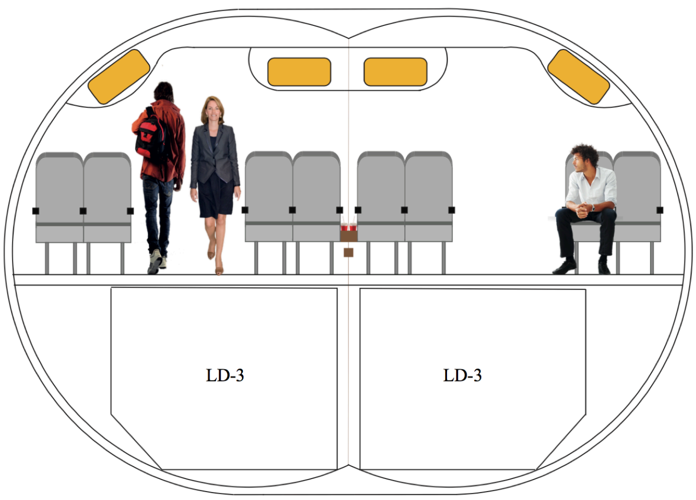

Figure 6.1: Fuselage cross-section of HAMMER.

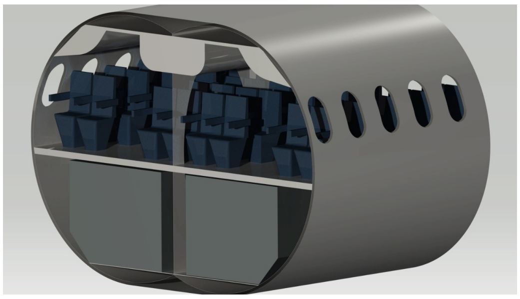

Figure 6.2: Fuselage view to show the middle wall.

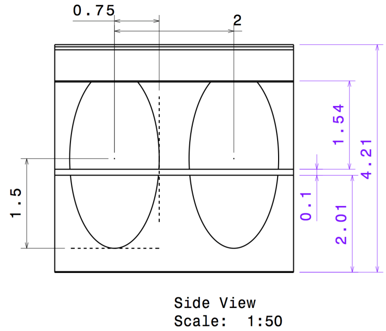

Figure 6.3: Dimensions of the middle wall.

Assuming that all passengers and the ten crew members have one carry-on suitcase of maximum dimensions (45x25x56 [cm]), the total carry-on volume will be 20.664 [m^3]. Adding a safety factor of 1.05 to account for suitcases not aligning perfectly next to each other led to a volume of 21.98 [m^3]. However, as it can be seen in Figure 6.1, suitcases can only fit in the overhead compartments by being placed in one specific orientation. By dividing the length of the cabin, excluding toilet and doors areas, by the maximum width of a suitcase, the number of pieces of luggage that fit in each of the compartments of the aircraft can be calculated. Multiplying this number by 4, the number of overhead storage compartments in the cabin, yields the total number of suitcases that fit in the cabin. Thus, the luggage volume that fits in the overhead cabins is 17.136 [m^3], meaning that 4.561 [m^3], a total of 46 carry-on suitcases, would need to be carried in the cargo compartment.

The cross-section design was performed by using an inside-out approach. In other words, first the seats, floor, cargo units and other design parameters were determined and drawn and later the double-bubble contour was placed. The main advantage of this approach is that the wanted seating configuration was achieved and the fuselage shape allowed for a maximised effective area. Moreover, a 115°guidance angle (Figure 6.4) was pursued for manufacturing purposes, as this allows for cargo hold and cabin structural layouts similar to the ones in a conventional fuselage [39]. The structural effects of this will be addressed in Chapter 8.

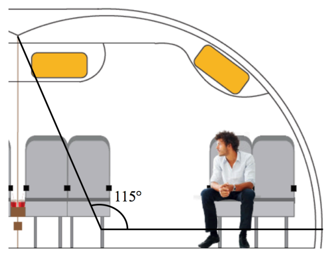

Figure 6.4: Detail view of the cross-section showing the guidance angle.

The parameters that were used to determine the fuselage length can be found in Table 6.2. The seat pitch in normal rows was taken from literature and was set to the minimum used in short-range flights [71]. The pitch of the emergency rows was based on the width of the emergency exits placed on those rows. Along the cabin section that does not interfere with the nose- or tail cone, six passengers were placed in each row. For the other sections in which the fuselage diameter is reduced, less passengers were placed per row to account for the reduced height on the sides of the fuselage. Moreover, the cabin crew will be sitting in folding seats next to the aircraft walls.

Table 6.2: Parameters used to determine the fuselage length.

Parameter	**Unit**	**Value**
Seat Pitch in Normal Rows	[m]	0.762
Seat Pitch in Emergency Rows	[m]	0.961
Number of Rows	[-]	42
Number of Passengers at Full Density	[-]	318
Cabin Section Length	[m]	35.85
Nose Cone Length	[m]	9.47
Nose Length	[m]	3.58
Tail Cone Length	[m]	6.72
Tail Length	[m]	5.6
Fuselage Length	[m]	44.97

Two different door types are used in the fuselage. In emergency exits that are also used as passenger doors for (de)boarding, type A doors were placed. These are the widest doors available, which would reduce the turnaround time as it would allow for a faster flow of passengers. For the other six doors, which are used either for catering or emergency purposes, type I doors were placed. These doors are smaller than type A but they are big enough to allow for a fast emergency evacuation. They are used in short-range aircraft such as A320's. According to CS specifications, the maximum number of passenger seats permitted is 110 per type A exit and 45 per type I exit[1]. Thus, the current configuration would be valid for up to 490 passengers and is thus valid for the HAMMER passenger capacity of 320. Also, a change in the number of passenger doors was performed compared to what was decided on the midterm report [21]. The reason of going from three to two passenger doors was that the turnaround time would not be affected significantly by having one extra door but both the operational costs and the structural weight to the fuselage would be significantly increased.

The length of the nose- and tail cones was determined by inspecting two graphs in [71]. A graph relating the Mach number at drag divergence, M_{dd}, and the nose fineness led to the value of the nose cone length. For M_{dd} = 0.84, the fineness ratio (l_{nc}/d_{fus}) is 1.55. Thus, with a fuselage diameter of 6.111 [m], the nose length was computed to be 9.47 [m]. The cockpit length was set to be 2.5 [m] to fit one pilot and one copilot, based on literature [71]. In order to determine the tail cone length, a graph relating the afterbody base drag and the afterbody fineness ratio was used. As an exact number for the afterbody base drag was not known, a fineness ratio was chosen to keep the drag as low as possible. The result for this was a tail cone fineness ratio (l_{tc}/d_{fus}) of 1.1, and thus a tail cone length of 6.72 [m]. The tail length was set based on the dimensions of the vertical tail and the engine location.

Finally the lengths of the cabin section and the fuselage were measured from the sketch in Figure 6.5. In the drawing, the number of toilets and galleys can also be seen. This number is based on the number of operational items as in an A320's and A330's. As HAMMER is slightly above average, it makes sense that the number of passengers is closer to the A330.

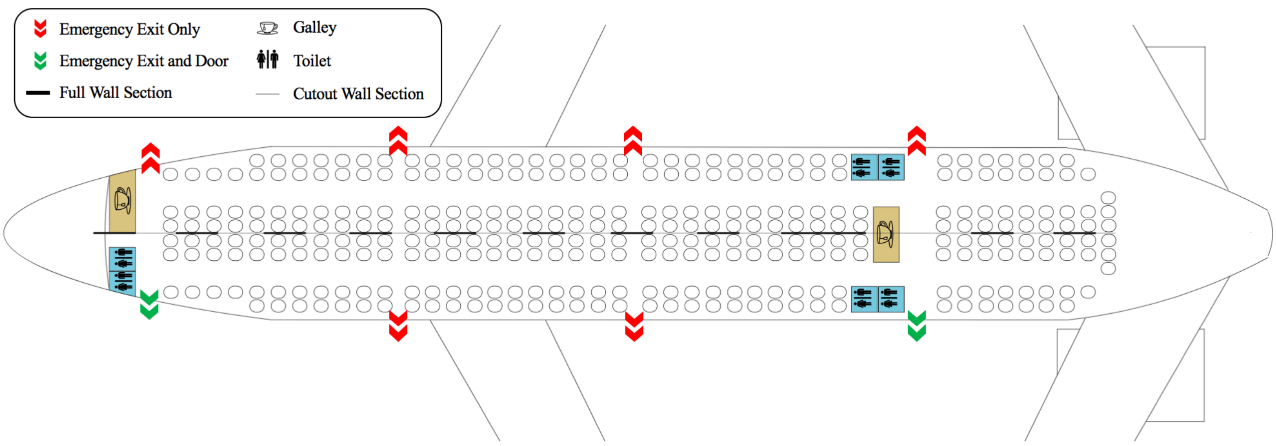

Figure 6.5: Cabin floor map showing seating configuration, emergency exits and location of toilets and galleys.

6.2. Cargo Compartment Layout

Dimensions as given by requirement CMR-SR-SU-7, the aircraft shall make use of standardised cargo units. For HAMMER, LD-3 (Loading Device-3) unit devices were chosen as they were the biggest ones that could fit in the cargo compartment. The dimensions can be found in Figure 6.6. In order to carry two checked-in pieces of luggage per passenger, a volume of 78.88 [m^3] is required. Moreover, by adding a safety factor of 1.25 to account for passengers purchasing extra luggage and for luggage not aligning perfectly next to each other, the volume needed for checked-in luggage is 98.61 [m^3] . Also, the excess 4.56 [m^3] of carry-on would need to be transported in the cargo compartment, leading to a total

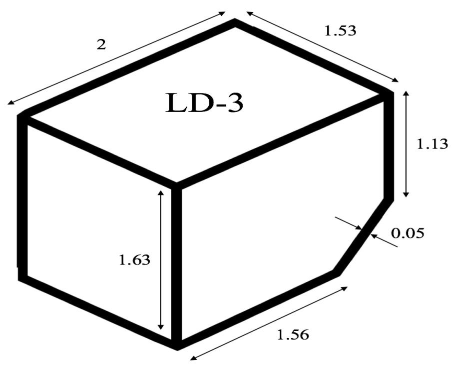

Figure 6.6: Dimensions in [m] of LD-3 cargo units.

[1]https://www.law.cornell.edu/cfr/text/14/25.807

cargo volume of 103.17 [m^3]. The volume that can fit in a LD-3 cargo unit is 4.474 [m^3], meaning that for the cargo volume that HAMMER would need to transport, 24 LD-3 cargo units would be needed.
The aircraft's cargo compartment will not only be used for the storage of the passengers' luggage but also for storing aircraft subsystems and the central wing box, as depicted in Figure 6.7 and 6.8. A long cargo hold is present with 24 LD3 devices in total and one cargo door on each side, as the middle wall does not allow for (un)loading from one side only. All the necessary cargo holds for the desired mission range are located aft of the main wing, so only the two aft doors will be used in normal flight conditions. However, if the airline chooses to transport more cargo or to increase the mission range, six LD3 cargo unit devices are present before the main wing to allow for this. The idea behind this is that the additional cargo units can be also used as extra fuel tanks. As (un)loading of the necessary cargo unit devices was aimed to be done from the aft doors only, all the general aircraft systems except the APU, are located forward in the aircraft to allow space for this.

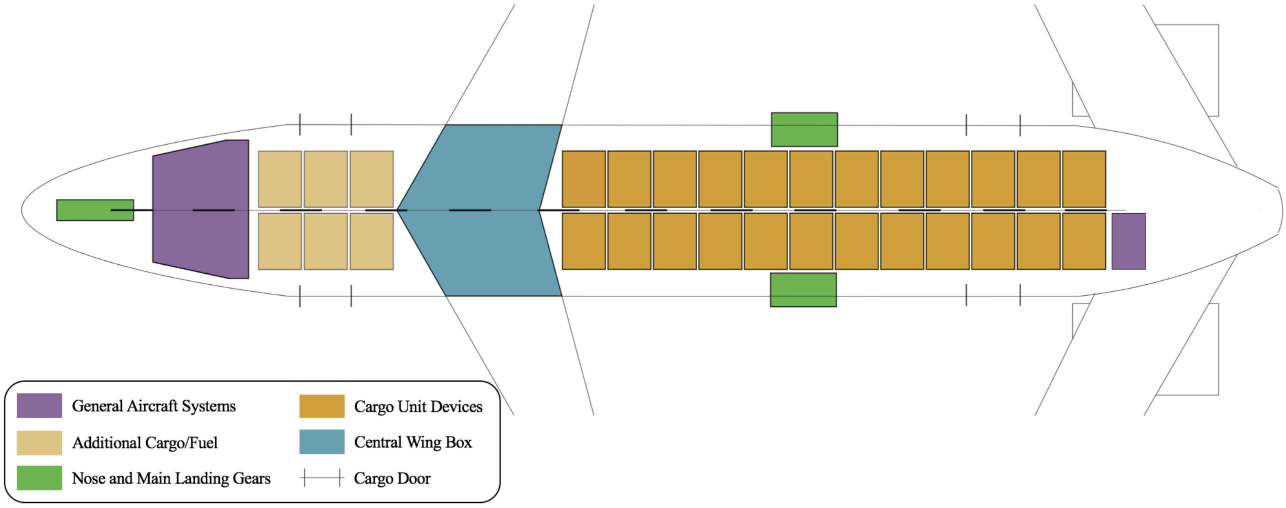

Figure 6.7: Top view of the cargo compartment configuration.

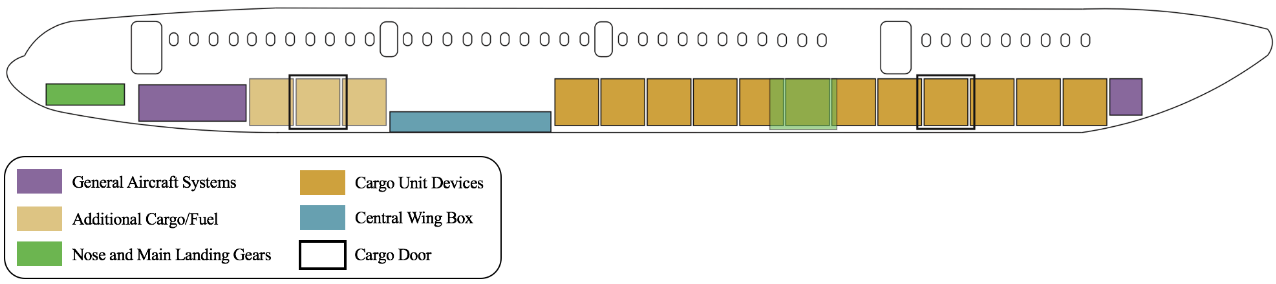

Figure 6.8: Side view of the cargo compartment configuration.

6.3. Verification and Validation

In order to ensure that each design step yielded correct values, some verification procedures were performed. One of them was to check the values for luggage volume by using another calculation method. Initially, the luggage volume was calculated by checking different airline volume specifications, calculating the average dimensions and then computing the maximum allowable volume carried on board. Another way of doing this was to calculate the maximum luggage weight allowed per person, and thus, by multiplying this value with the total number of passengers, the total luggage weight could be calculated. Then, with a luggage density of 170 [$\frac{kg}{m^3}$] [71], the total volume could be obtained and it could be compared with the volume calculated using the main method. An error of 6.79% was found, which was assumed to be negligible due to possible rounding errors and the fact of having a slightly different luggage density than the one mentioned in literature. The other verification procedure that was performed more than once in this chapter was to check if the volume calculated would fit into the aircraft. This was done by drawing sketches with accurate dimensions (Figure 6.1, Figure 6.5 and Figure 6.7) and placing all the operational items inside.

The next step would be to validate the design choices made. However, as it is still hard to do this at an early design phase, the validation procedure was not performed but it is instead given as a suggestion for future design phases. The idea would be to set up an environment with similar aisle dimensions to simulate what the passenger (de)boarding time would be with the current cabin configuration and to ensure that two people fit in the aisle. Moreover, a similar simulation could be done to see to ensure that the current cargo compartment configuration is more efficient than others.

6.4. Sustainability Analysis

The configuration of the fuselage and payload has been focusing on the three main aspects of sustainability during the design process. First of all, social sustainability was one of the main priorities to ensure that the product would please to the public. Although it's not the main reason, passengers' comfort has been taken into account when deciding for a wider aisle, to allow for more room and thus allow a faster and easier (de)boarding, making people less frustrated. Also, power sockets were placed on the walls to counteract the fact that half of the rows do not have a cutout in the middle and can thus lead to a more enclosed atmosphere. Secondly, environmental sustainability is a constant objective in aviation in order to reduce the environmental footprint of the sector. For this, a cross-section that would be as compact as possible but still with the features needed to reduce turnaround time such as wide aisles was aimed at, as it would then cause less drag and therefore reduce the fuel consumption, consequently reducing the emissions. This would also be beneficial for the economic sustainability of the airline, as fuel constitutes a big part of the operational costs of an airline. Finally, another option to make the project more economically sustainable is to recycle the interior parts of the aircraft, such as seats, toilets or overhead compartments.

6.5. Risk Assessment

With such a non-conventional fuselage shape, it can be assumed that some risks will be related to this design choice.

FU-1: Middle fuselage wall blocks passengers from moving to one side of the aircraft.

- Action: The wall will hinder the way to the people seating on a row that does not have a cutout. This can be remedied by improving evacuation plans in the aircraft

Furthermore, if one cargo door is blocked, the cargo units from that side will not be able to be taken out until the problem is solved. Finally, having too many families travelling in the same flight might lead to a lack of rows with a cutout, separating some of these families. However these are not critical risks and are therefore not taken into account.

6.6. Requirements Compliance

The requirements related to the fuselage and payload configuration are listed in Table 6.3. Only CMR-SR-AO-PA-6 is not met, as the new iteration aimed at a compact fuselage and thus, part of the cabin cargo compartment volume was left out. However, each passenger will be allowed to carry two pieces of 23 [kg] checked-in luggage.

Table 6.3: Compliance with the fuselage and payload requirements.

	Requirement
✓	CMR-SR-SA-AS-3 - The aircraft shall provide sufficient visibility for the pilot. An over nose angle between 11 and 20 [°], and an over side angle of 35 [°].
✓	CMR-SR-AO-PA-1 - The aircraft shall provide leg space for people up to 2 [*m*].
✓	CMR-SR-AO-PA-2 - The aircraft shall adhere to passenger safety certification.
✓	CMR-SR-AO-PA-4 - The aircraft shall provide reclining seats.
✓	CMR-SR-AO-PA-5 - The aircraft shall provide windows for passengers to look outside.
✖	CMR-SR-AO-PA-6 - The aircraft should accommodate 20 [*kg*] of carry-on luggage per passenger.
✓	CMR-SR-AO-PA-9 - The aircraft shall provide adequate space for a personal armrests at both sides of the seat.
✓	CMR-SR-AO-AS-3 - The aircraft shall make use of standardised unit loads for cargo.
✓	CMR-SR-AO-AC-1 - The aircraft shall have a cockpit for 2 pilots.
✓	CMR-SR-AO-AC-2 - The aircraft shall have a conventional cockpit layout.
✓	CMR-SR-AO-AL-6 - The aircraft shall have a system in place to isolate passengers for travel during pandemic circumstances.
✓	CMR-SR-SU-7 - The aircraft shall make use of standardised cargo units.
✓	HAMMER-FPC-01 - In a commercial airline, there shall be one cabin crew member per 50 pax.
✓	HAMMER-FPC-02 - One cabin crew member shall be assigned per floor-level exit as a means to mitigate the risk associated with unsupervised exits during emergency evacuations [46].

6.7. Conclusion

A fuselage iteration was performed during this design phase, which led to a more compact cross-section and fuselage length, thus meeting the length requirement for gate type C. However, in order to make the fuselage less than 45 [m] long, part of the carry-on luggage did not fit anymore in the cabin. An idea that was considered during this last iteration was to include shelves throughout the aircraft where passengers could store additional luggage and most specially, odd-shaped luggage such as musical instruments, skis or strollers. This idea was discarded at an early stage as the aircraft length requirement would then be exceeded. In the future, additional iterations could be performed to study how an increase in the aircraft's width would affect the aerodynamic performance of HAMMER. If this increase is assumed to be negligible compared to the benefits it brings with respect to payload capacity, then more seats would fit in each row and the shelves could be incorporated, leaving more space for luggage. Also, by implementing this, requirement CMR-SR-AO-PA-6 would be met. Moreover, the seats at the back that are close to the engine would not be there anymore and none of the passengers would complain about a noisy trip.

7 Stability and Controllability

This section performs a static and dynamic analysis of the stability and controllability of the aircraft. For this, the wing position is determined, the landing gear is positioned and sized, the vertical tail is sized and finally the dynamic analysis is provided.

7.1. Wing Positioning

The positioning of the wing is a vital step in ensuring the stability and controllability of the aircraft. In conventional aircraft, the tail generates the required moments to keep the aircraft stable and controllable. In a box wing configuration, this dynamic is different. Instead of a horizontal tail section, generating negative lift to counteract the forces and moments of the wing, there is now a second wing generating roughly half the lift. Adding to that, the aft wing also generates an aerodynamic moment, whereas conventional horizontal tails are usually symmetric airfoils and the moment generated can be neglected. This means that tools like a scissor plot can not be used as there are additional moments involved. To analyse the stability and controllability of the box wing, different tools have to be used [60].

Like the scissor plot, both stability and controllability were used to define limits to the wing placement. For the stability limit, the starting point was the position of the neutral point with respect to the centre of gravity (c.g.). To be stable, the neutral point always has to be behind the c.g such that any change in lift causes a pitch moment opposite to the direction of rotation to restore the equilibrium. This creates a limit, based on the position of the wing, for which the c.g. cannot go past.

For controllability, trimming was considered. As both wings generate roughly equal amounts of lift, the c.g. must not shift too much to the front wing, to prevent the moment generated by the aft wing becoming too large. While there is still the moment around the aerodynamic centres to counter act this moment, there has to be a limit restricting the c.g. nevertheless. This means that that controllability requirement imposes a lower limit to the c.g. location.

These limits are visualised in Figure 7.1. In this diagram, C_1 and C_2 are the mean aerodynamic chords of the front and aft wing respectively. h_0 is the distance fraction between the leading edge and the aerodynamic centre of the front wing, which is assumed to be 0.25. $h \cdot C_1$ is the distance between the leading edge and the c.g.. Lastly, l' is the distance between the aerodynamic centres of the front and aft wing.

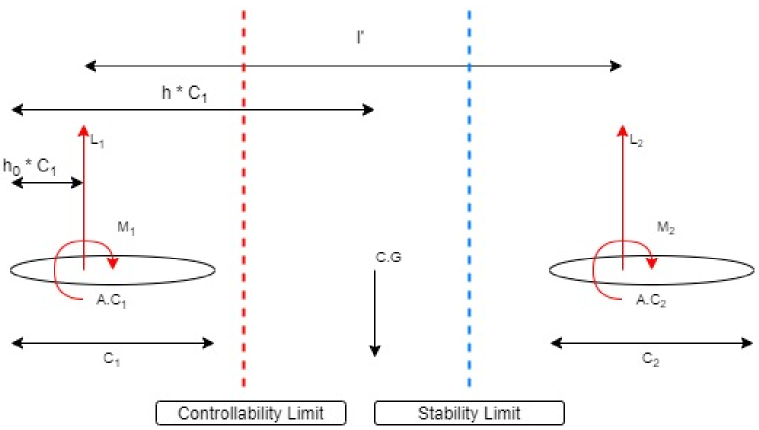

Figure 7.1: Schematic overview of the controllability and stability limits for the centre of gravity for a box wing configuration.

As longitudinal properties are evaluated, both wings are assumed to be placed at the same height, this has no influence on the generated moments. Using the distance definitions defined by Figure 7.1, the following relations for the distance factor, h, were defined: Equation 7.1 for the stability limit and Equation 7.2 for the controllability limit [60]. Here, $\bar{c}$ is given by $\bar{c} = S_1 \cdot C_1 + S_2 \cdot C_2$ with S_1 and S_2 being the surface areas of the front and aft wing. The terms $dC_{L,2}/dC_L$ and V' can be substituted with Equation 7.3 and 7.4, where V' is the adjusted tail volume for a box wing, a and a_2 are the lift curve slopes of the total wing and the aft wing, respectively, and $d\epsilon/d\alpha$ is the downwash gradient due to the front wing [60]. Upwash due to the aft wing is neglected in this analysis, however it is recommended that in future analysis this effect is properly incorporated. Lastly, the C_L's are the lift coefficients and the C_m's the moment coefficients of the total wing (without subscript), the front wing (subscript 1) and the aft wing (subscript 2). Furthermore, the aerodynamic data described in Section 4.1 was used.

$$h < h_0 + \frac{dC_{L,2}}{dC_L} V' \frac{\bar{c}}{C_1} \quad (7.1) \qquad h > h_0 + \frac{C_{L,2}}{C_L}\frac{V'}{C_1'} + \frac{C_{M,1}}{C_L} s_1 + \frac{C_{M,2}}{C_L} s_2 \frac{C_2}{C_1} \quad (7.2)$$

$$\frac{dC_{L,2}}{dC_L} = \frac{a_2}{a} * \left(1 - \frac{d\epsilon}{d\alpha}\right) \quad (7.3) \qquad V' = \frac{l' * S_2}{\bar{c} * S} \quad (7.4)$$

Both limits were plotted in combination with a loading diagram, shown in Figure 7.2, to show whether the aircraft remains stable and controllable during the duration of the mission. The weight distribution was based on the Class II weight estimation, performed in the conceptual design phase [21]. The exact placement and mass of the components taken into account for the loading diagram can be found in Table 7.2. An operating empty weight c.g. location at 26.4 [*m*] was computed and the wing dimensions are as described in Table 7.1. As can be seen in Figure 7.2, the stability criteria is the most limiting factor as the c.g. comes closest to it. The black horizontal lines indicate different weights: operative empty weight (OEW), maximum zero fuel weight (MZFW) and maximum take-off weight (MTOW).

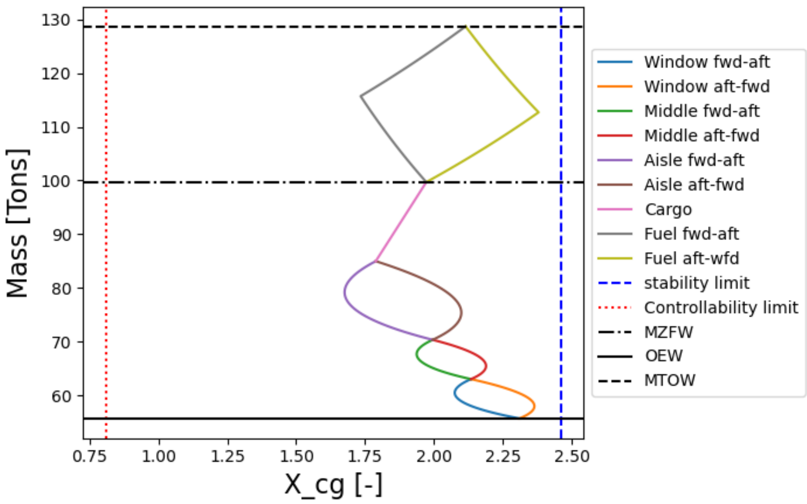

Figure 7.2: Loading Diagram of the HAMMER. The c.g. location is given as a fraction of the front mean aerodynamic chord. The c.g. excursion as indicated ranges from 24.1 to 26.6 [*m*] measured from the nose.

From Figure 7.2, a few things can be concluded. The stability margin could be improved by moving the front wing more aft, or the operative empty weight (OEW) more forward as this would give more options for future upgrades, e.g. heavier engines or adding equipment. However, this would interfere with the long cargo hold. The cargo hold could be broken up in different sections but this negates one of the advantages of HAMMER compared to a conventional aircraft. To accommodate this desire of a long cargo hold, the fuel tank capacity in the front wings were increased compared to the aft wing. The fuel division that results in the smallest c.g. excursion is a 55% - 45% split between the front and aft wing. Furthermore, it was decided to place a lot of the systems in the front of the aircraft such as avionics systems and potable water tanks. The operative empty weight is still relatively far aft. This has as downside that there is not a lot of room to shift subsystems around, as this would disturb the balance in the aircraft.

Table 7.1: Overview of the placement of the front and aft wing. The specified distance is measured from the nose, at the root chord.

	Leading edge [*m*]	Trailing edge [*m*]
Front wing	13.5	18.6
Aft wing	39.75	44.8

Table 7.2: Inputs for the Loading Diagram.

Parameter	Value	Parameter	Value
Operative Empty Aircraft			
Weight Front Wing [kg]	5692.3	Weight Aft Wing [kg]	5692.3
Weight Vertical Connection [kg]	1138.46	Weight Engines [kg]	12000
Weight Fuselage [kg]	15974.1	Miscellaneous Weight [kg]	5000
Weight Nose Landing Gear [kg]	1500	Weight Main Landing Gear [kg]	6000
Weight Vertical Tail [kg]	1898	Operative Empty Weight [kg]	55703.12
Front Wing c.g. [m]	18.9075	Aft Wing c.g. [m]	37.9725
Vertical Connection c.g. [m]	28.44	Engine c.g. [m]	40
Fuselage c.g. [m]	22	Miscellaneous c.g. [m]	6
Nose Landing Gear c.g. [m]	4	Main Landing Gear c.g. [m]	29
Vertical Tail c.g. [m]	38	Operative Empty Aircraft c.g. [m]	26.38
Loading the Aircraft			
Cargo Weight excl. LD3 empty weighty [kg]	14720	Weight of one Passenger [kg]	91.5
Front Wing Fuel Weight [kg]	16339	Aft Wing Fuel Weight [kg]	13398
Cargo c.g. [m]	29	Number of Passengers [-]	320
Seat Pitch [m]	0.762	Number of Rows [-]	42
Location First Row [m]	5.57	Location Last Row [m]	38.75
Front Wing Fuel c.g. [m]	18.9075	Aft Wing Fuel c.g. [m]	37.9725
Stability and Controllability Limits Calculation			
MAC Front Wing [m]	3.63	MAC Aft Wing [m]	3.63
Surface Area Front Wing [m^2]	119	Surface Area Aft Wing [m^2]	119
Moment Coefficient Front Wing [-]	-0.125	Moment Coefficient Aft Wing [-]	-0.125
Lift Curve Slope General Aircraft [-]	0.102	Lift Curve Slope Aft Wing [-]	0.109
Lift Coefficient General Aircraft [-]	2.0	Lift Coefficient Aft Wing [-]	1.9
Location of Front a.c. relative to MAC [-]	0.25	Downwash Gradient [-]	0.13

7.2. Landing Gear

For HAMMER to be stable on ground, the landing gear (LG) must be sized and placed in a correct manner. The landing gear from the conceptual design had 2 nose wheels and 4 main wheels. After further research on the retraction system, it was noted that almost all aircraft with a similar MTOW have 8 main wheels[1]. Thus, it was decided to also use 8 main wheels for HAMMER. The size of the wheels was then iterated with the new amount of wheels, the iterated MTOW (with a safety margin of 5%) and the correct load on the nose wheel, being 10% of the total load for the final position of the landing gear instead of the 8% used in the initial design. This resulted in a nose wheel outer diameter and width of 0.7366 [m] and 0.1956 [m], respectively, and for the main wheels a nose wheel outer diameter and width of 1.1176 [m] and 0.4064 [m] respectively.

The position from the conceptual design was also iterated. A more accurate c.g. position was found using the loading diagram, as explained above, and the cockpit was designed to be 3.1 [m], which means the nose landing gear (NLG) could be placed at 4 [m] instead of 5.07 [m]. The position of the main landing gear (MLG) was then iterated as well, and placed at 29 [m] to meet the different position requirements. These concern the pitch angle, scrape angle and load distribution, shown in Figure 7.3, the ground clearance, shown in Figure 7.4, and the turn over angle, shown in Figure 7.5.

The distance between the two main struts, or track width, was determined based on the integration of the landing gear in the fuselage. The main landing gear will be partly in the fuselage and partly podded, to make sure a long cargo hold was possible. The integration can be seen in Figure 7.7. This means the track width will be 5.6 [m] and the total width of the fuselage at the location of the pod will be 8.07 [m]. The track width was checked with the turn over angle and with the gate requirement, which state the track width

[1]https://en.wikipedia.org/wiki/List_of_airliners_by_maximum_takeoff_weight [cited 12 June 2020]

should be lower than 9 [m], both requirements were complied with. Furthermore, it will retract forward in the fuselage. This way it will benefit from the aerodynamic drag when extending [41]. The landing gear pod will then be 2.55 [m] long, it start at 26.45 [m] and end at 29 [m].

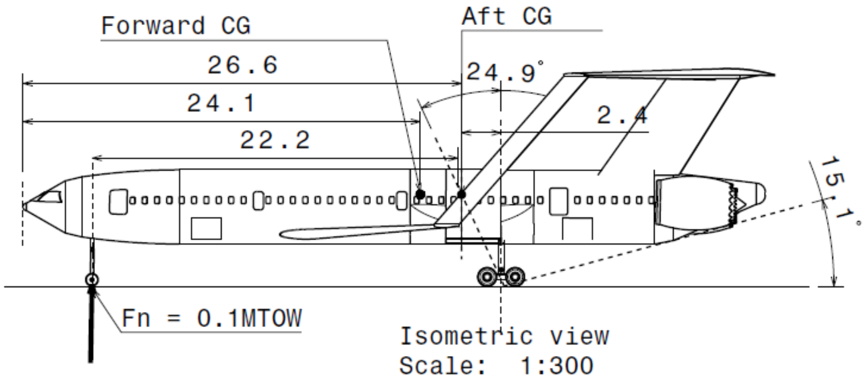

Figure 7.3: Illustration of the pitch angle, scrape angle and load distribution requirements.

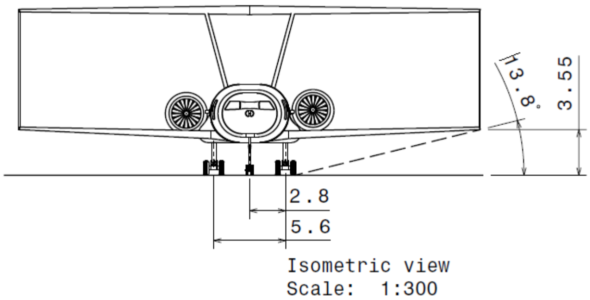

Figure 7.4: Illustration of the ground clearance requirement.

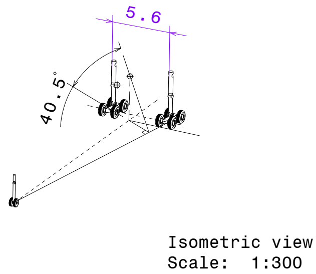

Figure 7.5: Illustration of the turn over angle requirement.

The nose gear will also retract forward in the fuselage, again to benefit from aerodynamic drag when extending. As the space underneath the cockpit is empty, it could easily fit. It is slightly obstructed by the centre wall that support the double bubble when the cabin is pressurised. However, this wall can be easily mounted on the nose gear hold instead of on the bottom of the fuselage, while keeping the same effect. In addition, the nose gear hold will be made as round as possible for structural advantages. A visual representation of this can be found in Figure 7.8.

The side view, in which one can see both retractions, is given in Figure 7.6. In this sketch the wheels and distances to the ground are on scale but the top of the figure, where the struts connect to the fuselage, are not representative. These connections can be seen in the two cross-sections.

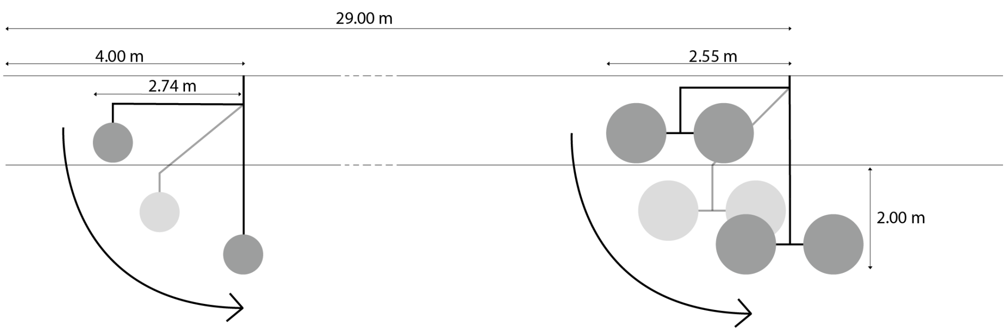

Figure 7.6: Side View of the Fuselage with integrated Landing Gear.

In addition to the conventional tricycle gear layout, a reverse tricycle was also investigated. The idea behind this concept was that the main gears could retract into the front wings such that no pods were required. The single aft wheel would retract into the fuselage the same way the nose gear does in the conventional tricycle configuration. This idea was not adapted due to several disadvantages. The first being that a reverse tricycle is inherently unstable, any course deviation would result into the aircraft veering off-track. Secondly, the aft wheel would occupy and block the long cargo hold which negates a lot of the advantages HAMMER has over other aircraft. In addition, putting the main gears in the wings limits the placement of the aft wheel. If the same weight ratio of 90%:10% is used to ensure enough ground steering force, the aft wheel should be place very far aft which makes rotating the aircraft on take-off very difficult. Although this could be resolved by partially retracting the aft wheel to create the necessary angle of attack. Lastly, storing the main landing gear in the wing would mean there is less volume for fuel. The front wing now carries the maximum amount of fuel in order for HAMMER to be stable, hence lowering this might cause stability problems. Still, if the structural and aerodynamic advantages of storing the main gear in the front wing outweigh these disadvantages, a reverse tricycle could be considered.

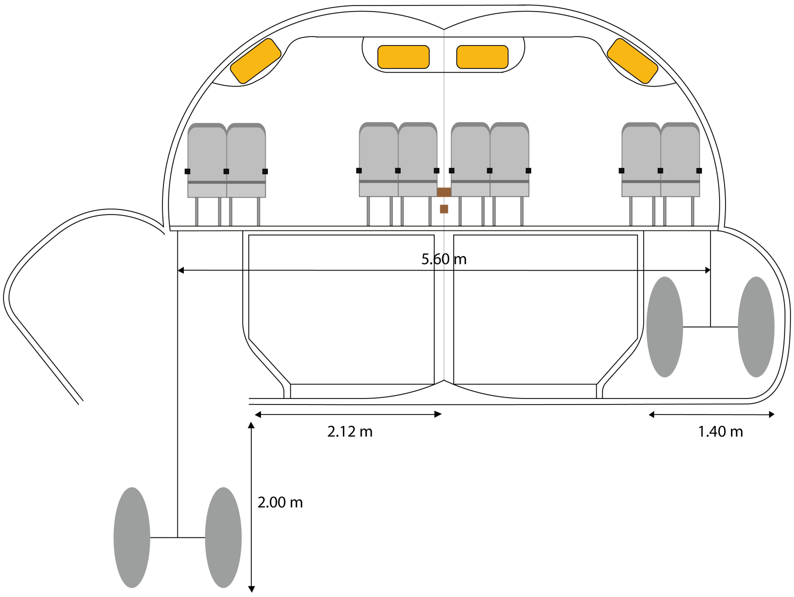

Figure 7.7: Integration of the Main Landing Gear in the Fuselage.

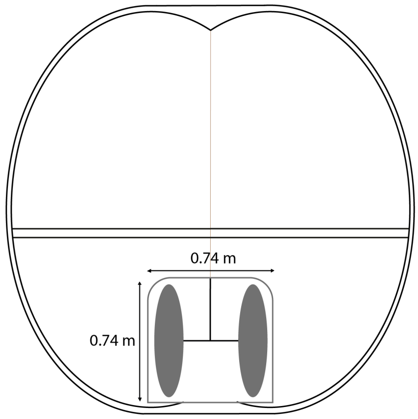

Figure 7.8: Integration of the Nose Landing Gear in the Fuselage.

The struts were initially sized using a method depicted by Roskam [51]. Here, the size and diameter are determined based on the load on the landing gear and how much of that load is already taken up by the wheels. The main strut size was calculated to be only 33 [*cm*], which is rather small considering that the wheels are 1.1 [*m*] high. However, as this was based on the load it must carry, it was assumed that this was a minimum value and the strut can be longer. First, the requirements for placing the landing gear were taken into account. For this, HAMMER could be placed rather low. If the fuselage would be mounted on top of the wheels it would still not be a problem. The strut was then made longer to be able to accommodate a passenger bridge, as explained in more detail in Chapter 10. For this, the bottom of the fuselage needed to be 2 [*m*] above the ground. The size was then determined to be 3.35 [*m*], also based on the integration in the fuselage. The main strut diameter was calculated to be 29 [*cm*] and this was kept the same.

The nose gear strut was sized in a similar way. It was calculated to be 20 [*cm*] but again made longer, as for the nose gear it is important the aircraft is levelled. The nose gear strut length was thus set to 2.43 [*m*] and the diameter was calculated to be 20 [*cm*]. It was found that using a jump strut in the nose gear has the advantage that a shorter take-off length is needed [23]. However, no sizing methods were found for this, hence, the strut was sized as a conventional oleo-pneumatic strut. But a jump strut can be considered in a further design phase.

All the dimensions concerning the landing gear are summarised in Table 7.3. Some (simplified) renders of the main landing gear and nose landing gear can be seen in Figure 7.9 and Figure 7.10, respectively.

Table 7.3: Overview of the landing gear dimensions.

	Parameter [m]	Value
MLG	Outer Diameter of a Wheel	1.12
(8 Wheels)	Width Wheel	0.41
	Longitudinal Position	29
	Track Width	5.6
	Strut Length	3.35
	Strut Diameter	0.29
LG Pod	Length	3.35
	Maximum Fuselage Width	8.07
NLG	Outer Diameter of a Wheel	0.74
(2 Wheels)	Width of a Wheel	0.19
	Longitudinal Position	4
	Strut Length	2.43
	Strut Diameter	0.20

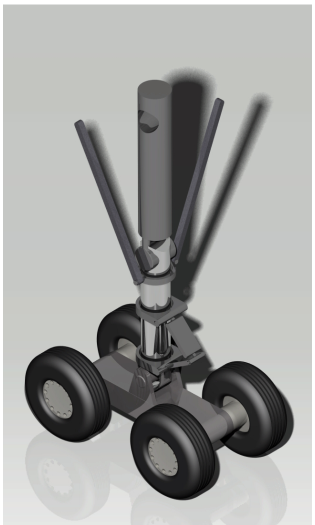

Figure 7.9: Render of one of the main landing gear tracks.

Figure 7.10: Render of the nose landing gear.

7.3. Vertical Tail

The design of the vertical tail, vt, depends a lot on the integration with the fuselage and the second wing. First the two vertical tails were placed with 3.6 [m] in between them and the root chords of the vertical tails denoted by $c_{r_{vt}}$ were placed at a longitudinal distance of 34.1 [m]. This was done by visually determining a good location on top of the tail cone. Then the surface area of the tail, already determined in the conceptual design phase, was iterated using the iterated wing surface and the new longitudinal distance. This resulted in a surface area, S_{vt}, of 28.42 [m^2] per vertical tail, which is almost double of what was determined in the midterm report but there the tail arm was greatly overestimated [21]. In addition, the inclination and taper ratio, λ were chosen to be 15°and 0.9 respectively. Then, using the initial height of the vertical tail, h_{vt}, and the aft wing dimensions, the tail tip chord, denoted by $c_{t_{vt}}$ was determined, as this should be the same as the chord of the wing at the place the tail is mounted.

With this tip chord and using Equation 7.5 and 7.6, the root chord and mean aerodynamic chord (MAC) of the vertical tail were calculated. Next, the height was calculated using the geometry of the tail planform, as described in Equation 7.7. This resulted in an iterative process where the tip chord was determined with this new height, until the two values for the height were the same. The height of the second wing was thus dependent on the vertical tail height. Lastly, knowing the position of the root and tip chord, the sweep, Λ, was calculated using Equation 7.8. However, the vertical tail sweep must be higher than the wing sweep, thus this results in an extra boundary. All these boundaries, calculations and iterations result in a tail height of 6.07 [m], a tip chord and root chord of 4.43 [m] and 4.92 [m], respectively, and a sweep angle of 38.3°, which is indeed higher than the wing sweep of 30.03°. This also means the second wing will be 5.86 [m] above the fuselage.

$$c_{r_{vt}} = \frac{c_{t_{vt}}}{\lambda} \tag{7.5}$$

$$MAC_{vt} = c_{r_{vt}} \frac{2}{3} \frac{1+\lambda+\lambda^2}{1+\lambda} \tag{7.6}$$

$$h_{vt} = \frac{S_{vt}}{MAC_{vt}} \tag{7.7}$$

$$\Lambda = \tan^{-1}\left(\frac{l_{c_t} - l_{c_r}}{h}\right) \tag{7.8}$$

Lastly,a NACA0012 airfoil was chosen for the vertical tail. This symmetric airfoil has a medium high thickness over chord ratio. Thickness is a structural advantage, which is important since the vertical tail transfers the loads from the wing to the fuselage, but it also can't get too thick or the drag will be too high.

A summary of the vertical tail dimensions calculated in this section, can be found in the table below. As one might note, the height is quite large. This is because the sizing and positioning was done to increase the height as much as possible. The main reason for this is that the location of the aft wing depends on the height of the tail and a large vertical distance between the two wings has aerodynamic advantages.

Table 7.4: An overview of the vertical tail dimensions.

	Parameter	Value
Planform	Surface Area of one part [m^2]	28.42
	Tip Chord [m]	4.43
	Root Chord [m]	4.92
	Mean Aerodynamic Chord [m]	4.68
	Height [m]	6.07
	Inclination [°]	15
	Taper Ratio [-]	0.9
	Sweep Angle [°]	38.3
Location	Longitudinal Position Root Chord [m]	34.1
	Longitudinal Position Tip Chord [m]	38.44
	Distance between the two parts [m]	3.6

7.4. Dynamic Stability Analysis

The eigenmotions of the aircraft were evaluated with AVL to check whether the aircraft was also stable in motion. First the equations of motion of conventional aircraft were studied to see if anything changes now that there are two wings. It was found that to set up the equations of motion, overall forces and moments, as well as overall deflections of control surfaces can be used. Therefore, the tool in AVL can be used without modification.

Symmetric Motion

Symmetric motion at cruise conditions was analysed at MTOW. First the equations of motion were rewritten to a state space matrix to calculate the time response to flap deflection input. A flap deflection of 10°was used as input for the system.

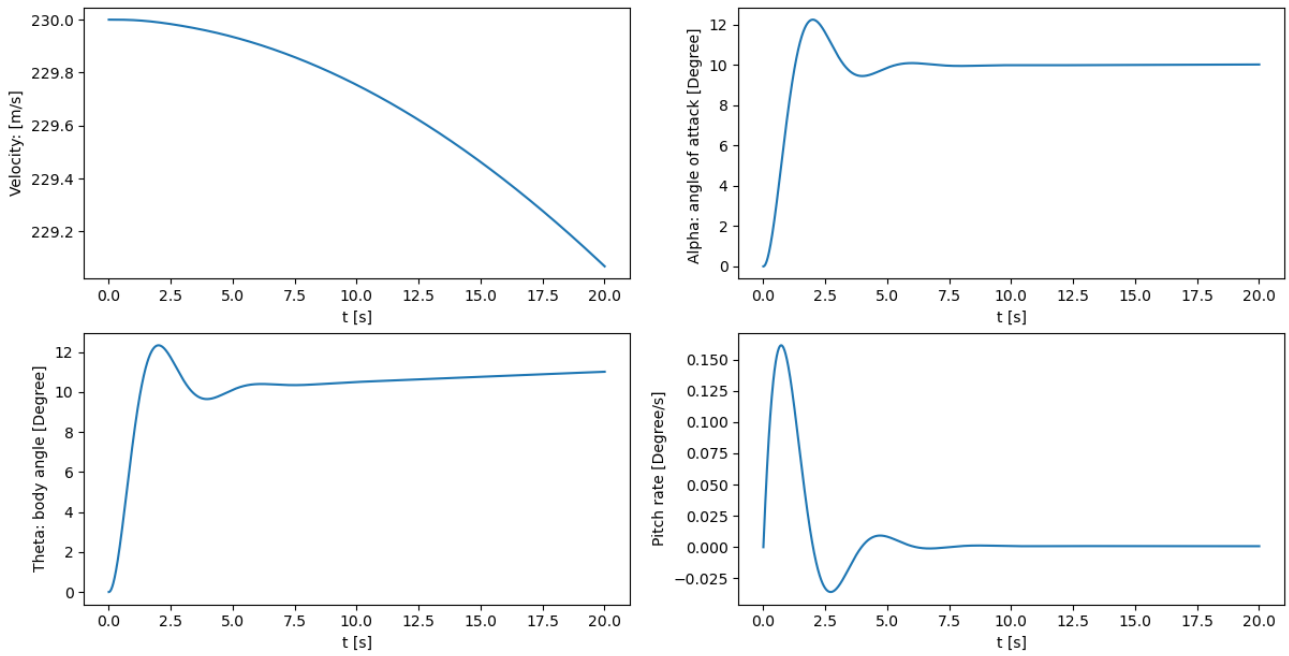

Figure 7.11: Short period response to elevator deflection input of 10 degrees at cruise conditions.

As can be seen in Figure 7.11, the aircraft responds very quickly to a flap deflection input, damping out the motion quickly. This can be attributed to the large aft wing working as a corrective force to hold the plane steady. This is especially visible in the pitch rate plot which shows a large initial spike followed by a flat line, meaning that after the initial change in angle the aircraft stabilises. Looking at the phugoid movement, the following plot can be generated:

Similar to the short period motion, the phugoid motion shows highly damped behaviour in the first few seconds of flight, followed by slow pitch motion. The aircraft does show diverging behaviour when looking at the airspeed, however the increase per wave cycle is very small.

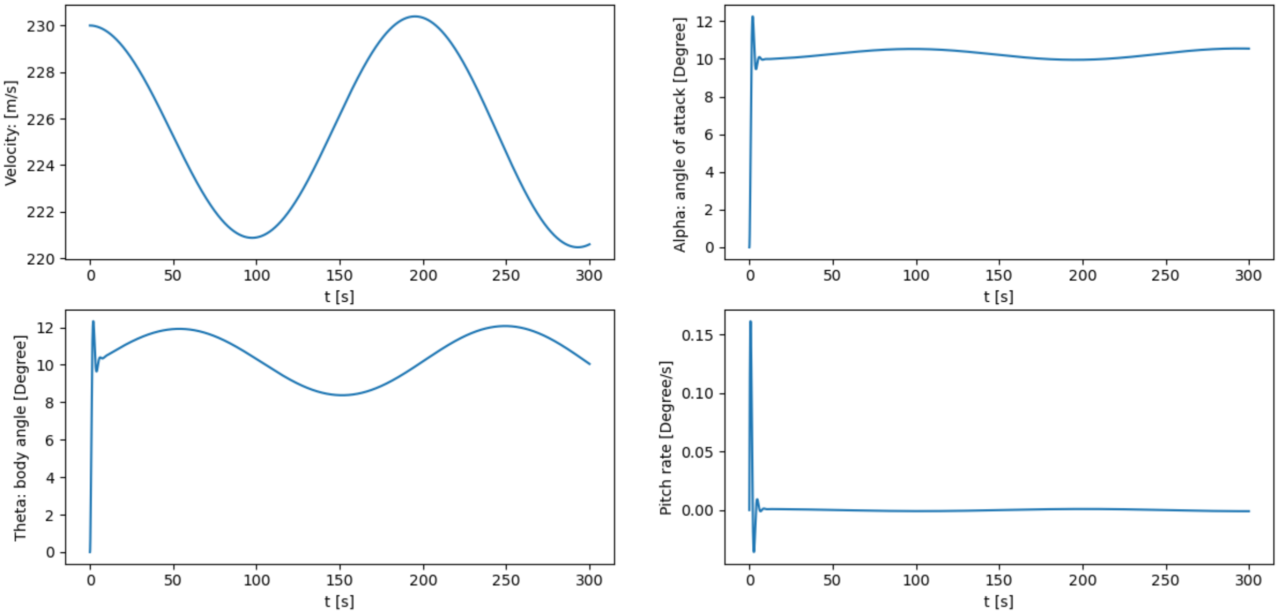

Figure 7.12: Phugoid motion response to elevator deflection input of 10 degrees at cruise conditions.

Asymmetric Motion and Model Deficiencies

For asymmetric motion, like symmetric motion a state space representation of the aircraft lateral motion was created. However, as the AVL model used for the stability derivatives is not complete, no analysis on the lateral motion could be performed. An alternative to AVL would be deriving the coefficients from literature, however this approach was deemed too imprecise to yield good results.

While a proper analysis using AVL cannot be performed, a qualitative analysis based on HAMMER's current configuration can be performed. Compared to a regular aircraft, HAMMER has quite large vertical stabilisers. This means that a large correcting moment can be generated to straighten the aircraft after yaw input. This advantage of a high surface area is slightly diminished, however, due to the fact that the c.g. is relatively far aft.

Concerning roll characteristics, there are now two wings to attach ailerons to, meaning that more force can be generated to improve roll performance. Furthermore, the lateral connector between the front and aft wing could also be used for manoeuvring. A split rudder or drag rudder system could be incorporated there to improve moment generation. A split rudder system works through the generation of a large drag force near the wing tip to generate a yawing moment. By angling the deployed flaps either a rolling or yawing moment could be generated. Further research should be conducted to investigate how such a system could be deployed and the feasibility of such a system.

7.5. Verification and Validation

Verification of the designs was mainly done by unit tests and making sketches. Unit testing includes checking subparts of a tool for bugs, for example checking for spelling mistakes or incorrect links, and checking whether the units in formulas are consistent or whether conversions are done correctly. Singularity checks were also performed, to confirm dividing by zero or the tangent of 90°gives an error. In addition, on all outcomes of the tools a sanity check was performed, to ensure they were within acceptable grounds. If an outcome was not correct or unexpected, hand calculations were performed as a second check.

To verify the wing positioning, not only sketches of the wing were made, but of the whole aircraft to make sure the values used in the loading diagram made sense. Special attention was given to the distance between certain parts, for example between the engine and the passenger windows. The engine was placed such that the aircraft is stable but it must also be compatible with the fuselage interior. The drawings of the final design can be found in Appendix D. In addition, the landing gear retraction and the vertical tail design were mainly based on making sketches to visually see how everything fits.

Verification of the program used for the eigenmotion response was done by means of unit tests and comparison to textbook references [40]. Eigenmotion responses to flap deflection input were compared using a Cessna Ce500 ‘Citation’. The generated plots were identical to the displayed plots in [40]. It can therefore be assumed that program is accurate and can be trusted for an initial analysis.

The design of the wing positioning and vertical tail is not easily validated, as it cannot be compared to reference aircraft due to its reliance on many other design decisions to make the aircraft stable. However, a dynamic stability analysis can be done to validate the response of the aircraft to its eigenmotions. Unfortunately the dynamic analysis was not complete, but this can be done in future phases.

The landing gear, on the contrary, could be easily validated using reference aircraft. The number of wheels was based on the aircraft in the same MTOW range, which all had 8 wheels, and the size of the wheels could be validated in the same way. The diameter of the wheels of an A330 are 1.5 [*m*], which is similar to the 1.1 [*m*] diameter of this aircraft’s wheels, considering the MTOW of the A330 is also slightly higher [58]. Finally, for the design of the retraction system, videos of many different retraction systems were viewed to determine which one could work for this design.

7.6. Sustainability Analysis

Since stability and controllability is more an analysis to make sure the aircraft can fly, than a design, it is hard to incorporate sustainability. However, there are some small elements that can be done to be sustainable. For example, a lot of research is being done about ’green tires’ for cars and it can be expected to enter the aircraft industry as well[2]. The landing gear will also be electrically powered, as previously explained in Section 5.2.

Furthermore, reducing drag can also be sustainable. The vertical tail was made as high as possible for aerodynamic advantages. The landing gear was made higher as well and was podded to benefit the use of passenger bridges and have a long cargo hold, which are advantages for ground operations. Thus, this combination of advantages was chosen above reducing a small amount of drag for sustainability. However, the height of the tail and the drag the tail induces need to be evaluated in a further design phase, to verify that this was indeed the right decision.

7.7. Risk Assessment

For stability and controllability the following technical risks were identified.

SC-1: Not enough stability margin was taken due to wrong aerodynamic coefficient modelling:
- Action: research can be done to improve the accuracy on the stability model used. Using more final values for certain aerodynamic parameters improves safety. The c.g. range can be adjusted accordingly. Subsystems might have to be removed.

SC-2: Wrong weight estimation leads to incorrect balancing of the aircraft:
- Action: Research can be performed to better investigate sizing methods and how these should be adopted for the boxwing.

As for all aircraft, the weight distribution is key. A lot of weight is located at the aft of the aircraft, making HAMMER extra sensitive to this due to the extra aft wing and the constraint from the front wing not interfering with the long cargo hold. This means extra care should be taken to check if the limits laid out in Figure 7.1 are safeguarded.

7.8. Requirements Compliance

Unfortunately, for stability and controllability a lot of requirements, namely HAMMER-SCL-02 until HAMMER-SCL-07.4, are not currently met. The reason for this is that it was not possible to research these requirements with the available resources, including time, software and expertise. The aircraft behaviour in these situations will thus need to be researched in the further design phases of the project. In addition, requirement HAMMER-SCL-08.3 was not applicable for this design, as the engines are not

[2]https://www.tirereview.com/technology-advances-in-green-tires/ [cited 17 June 2020]

wing-mounted and thus no ground clearance needs to be complied with. Instead, ground clearance with respect to the tip was met. An overview of all the requirements can be found in the table below.

Table 7.5: Compliance with the stability and controllability requirements.

	Requirement
✓	CMR-SR-AC-FP-1 - The aircraft shall be stable.
✓	CMR-SR-AC-FP-2 - The aircraft shall be controllable.
✓	CMR-SR-AO-PA-3 - The aircraft shall be designed for stability to increase comfort.
✓	HAMMER-SCL-01 The neutral point of the aircraft shall always be behind the aircraft centre of gravity i.e. $(x_{np}-x_{cg}) > 0$.
✖	HAMMER-SCL-02 - The aircraft shall be satisfactorily controllable with cross wind of 20 knots or 0.2 VSO (stall speed), whichever is greater, while operating on the ground.
✖	HAMMER-SCL-03 - The aircraft shall have a positive directional stability for any flap and landing gear configuration at speeds from 1.13 VSR1 (refers to each specific configurations stall speed), up to VFE (stall speed at maximum flap extension), VLE (maximum speed at which the landing gear is extended), or VFC/MFC (maximum speed for specific stability characteristics), whichever is appropriate.
✖	HAMMER-SCL-04 - The aircraft shall be able to positively damp any lateral-directional oscillations without exceptional pilot intervention.
✖	HAMMER-SCL-05 - The yaw moment induced by an inoperative off axis engine shall be able to be compensated for by the aircraft, without exceptional pilot intervention.
✖	HAMMER-SCL-06 - The aircraft shall be able to make sudden course correction up to 15° with an inoperative engine in the direction of that engine.
✖	**HAMMER-SCL-07** - The control surfaces responsible for pitch shall be adequate in size to generate the forces required to realise the required manoeuvres.
✖	HAMMER-SCL-07.1 - The aircraft shall be able to pitch as required by CS-25.
✖	HAMMER-SCL-07.2 - The aircraft trim drag shall be smaller than 10% of the total aircraft drag.
✖	HAMMER-SCL-07.3 - The aircraft shall be able to yaw as required by CS-25.
✖	HAMMER-SCL-07.4 - The aircraft shall have a roll-rate as required by CS-25.
✓	**HAMMER-SCL-08** - The landing gear shall be positioned such that every clearance angle is complied.
✓	HAMMER-SCL-08.1 - The turn over angle shall not be greater than 55°.
✓	HAMMER-SCL-08.2 - The pitch angle shall be bigger than 15°.
✓	HAMMER-SCL-08.3 - The aircraft shall have a lateral ground clearance of at least 8° for engines located close to the wing root and at least 5°for engines located near the wing tip.
✓	HAMMER-SCL-08.4 - The weight on the front landing gear shall be in between 8% and 15% of the total weight, as required by CS-25.
✓	HAMMER-SCL-08.5 - The landing gear shall be able to retract such that it does not interfere with structural components or control surfaces.

7.9. Conclusion

The aircraft is now designed to be statically stable. The wing positioning resulted in a c.g. range that is between the stability and controllability limits and makes a long cargo hold possible. The landing gear position complies with all the stability requirements and its integration in the fuselage takes into account aerodynamic and ground operation advantages. The vertical tail size was also iterated, based on the integration with the fuselage and wing planform. In addition, a dynamic stability analysis was performed for the symmetric motion. However, the asymmetric motion will have to be analysed in a further design phase. In addition, further aerodynamic research is needed to confirm the aerodynamic coefficients used in the loading diagram and to confirm the height of the vertical tail is indeed an advantage. Other recommendations for the stability and controllability of the aircraft is to study the sizing of a nose gear jump strut, as this can have significant take-off advantages, and to study the effect of a split rudder design.

8 Structures and Materials

In this chapter the structures and materials of HAMMER are described. First, a material selection is done based on the expected loads. This is followed by an analysis of the wing system. The fuselage skin optimisation and airframe architecture are covered and the fuel tank design is discussed.

8.1. Material Design

8.1.1. Wing Loads

The wing is mostly affected by the aerodynamic loads that occur during flight. These loads include torsion, bending, fatigue and shear loads. The connected wings cause large bending moments at the tip of each wing, resulting in a significant amount of bending and shear loading along the chord [26].

8.1.2. Fuselage Skin Loads

The fuselage skin is a supporting structural component. It provides an aerodynamic shape, helps with the dissipation of forces, protects all inboard subsystems for which fracture toughness is important and dissipates loads induced by the airframe.

Usually, either fatigue resistance due to cyclic pressurisation or fracture toughness are limiting factors for the fuselage skin design. However, an analysis on the fracture toughness is hard to perform and will most likely result in an out-of-order thickness for the fuselage skin. This is because the airframe would need to be taken into account as well, which was deemed to complicated for a preliminary anlysis.

8.1.3. Fuselage Airframe Loads

The fuselage airframe acts structurally as a main subsystem to which all other subsystems are attached to. It carries many different kind of loads and has to be able to deal with the loads associated with: in-flight manoeuvres, gust winds, (emergency) landings and handling loads at the airport like towing, taxiing and push-back [6]. The airframe will need to cope with all the different loads introduced into the structure and provide load paths for the stresses to dissipate.

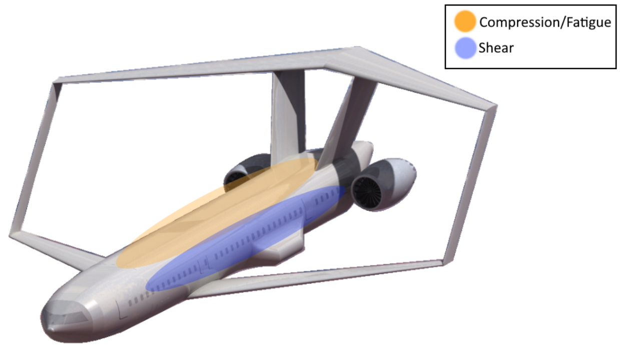

Figure 8.1: Dominant load cases in a box wing fuselage during cruise.

A result of the wing being connected to the fuselage in two locations is that the dominant load types in the inter-wing section are compressive stresses on the top skin and tensile stresses on the bottom skin. Both result from the dynamic torque induced by the wing system. This makes fatigue an issue and special attention should be given to this failure mode designing the longitudinal stiffening elements and fuselage skin, Figure 8.1.

The other major force that primarily needs to be resisted by the airframe is torsion. The torsional loads introduced by the wing system and vertical stabilisers, are translated into bending moments and have to be resisted by longitudinal stiffening elements. Box wing aircraft experience fewer shear stresses than conventional fixed wing aircraft due to the closed wing system.

8.1.4. Material Selection

Since a top-level analysis was performed on structures and materials, only a handful of materials were considered. These materials and their most important properties can be found in Table 8.1.

Table 8.1: Material properties of considered materials [1] [2] [3] [7] [27].

Parameter	Al 2024-T3	CFRP Fabric	CFRP UD	Glare 3 (3/2)	Glare 3 (2/1)
Ultimate Tensile Strength [MPa]	483	600	1500	666	627
Ultimate Compressive Strength [MPa]	483	570	1200	666	627
Tensile Yield Strength [MPa]	345	N/A	N/A	260	267
Compressive Yield Strength [MPa]	345	N/A	N/A	298	305
Shear Strength [MPa]	283	158	70	249	254
Young's Modulus [GPa]	73.1	49.64	135	56.2	59
Shear Modulus [GPa]	28	15	5	16.4	18.4
Density [g/cm^3]	2.78	1.6	1.6	2.67	2.69
Cost [Relative to aluminium]	1	1.2	1.2	1	1

For aircraft materials, properties such as stiffness, strength, fatigue resistance and fracture toughness are the most important. Aluminium (Al), Glass Laminate Aluminium Reinforced Epoxy (GLARE) and Carbon Fibre Reinforced Polymer (CFRP) were already mentioned in the midterm report [21]. The Aluminium alloys and different fibre orientations/configurations were added to this report based on their history of applications in aerospace structures. For CFRP, a lay-up was chosen to achieve quasi-isentropic conditions[4]. In addition, Uni-Directional (UD) CFRP was also considered for cases of uni-directional loading. The technology exists to produce carbon fiber stiffening elements, but the high manufacturing cost would need to be taken into consideration.

Material Manufacturability

Depending on the material, skin thicknesses are limited to ensure structural integrity, although these limits may change with more advanced knowledge of the loads in the structure.

- **Al 2024-T3** It would be optimal to provide the cross-section with the exact thickness necessary to cope with the local pressure forces. However expensive, a skin-section with variable thickness is possible to manufacture. Thicknesses are limited to a minimum of 0.4 [mm].
- **CFRP** Unlike metals, composite fabrics are more restricted by manufacturing processes and therefore it might not be possible to construct variable thickness fuselage sections. For the analysis, CFRP will be modelled by a constant thickness based on the maximum stress concentration. Additionally, one CFRP ply has a minimal thickness of 0.2 [mm] and thus a minimum skin thickness of 1 [mm] is required to ensure isotropic properties of the fabric [53].
- **Glare 3** Comprised of glass fibre reinforced epoxy and aluminium, Glare unifies the best of both materials. A Glare 3 (3/2) and (2/1) has a minimum thickness of 1.4 [mm] and 0.85 [mm], respectively. Lower manufactured thicknesses might be possible in the future.

Sustainability Review

As described in the midterm report, the recyclability of laminated materials is poor compared to metals [21]. Especially for GLARE, the extraction of the separate material components for recycling is complicated. Therefore, if a metal-composite material was not deemed significantly better, it was omitted from the design. Although, with effort, recycling CFRP is possible, it is not ideal and should also be taken into consideration when designing the aircraft structure. CFRP requires a lot more energy to produce compared to aluminium. Therefore, if no significant weight reductions can be made, the choice to use CFRP cannot be justified.

[1]Personal Communication Dr.ir. R.C. Alderliesten [cited 11 June 2020]
[2]http://www.performance-composites.com/carbonfibre/mechanicalproperties_2.asp [cited 8 June 2020]
[3]http://asm.matweb.com/search/SpecificMaterial.asp?bassnum=MA2024T3 [cited 8 June 2020]
[4]https://dragonplate.com/quasi-isotropic-carbon-fiber-sheets [cited 22 June 2020]

8.1.5. Fatigue Analysis

The fatigue properties of materials were analysed to determine the material of the fuselage skin. Fatigue performance of materials is commonly characterised by Wohler curves, also known as S-N curves, where the cyclic stress (S) is plotted against the cycles to failure (N). The S-N curves were estimated and plotted logarithmic, such that a linear relation exists, as seen in Equation 8.1. Here, both α_m and β_m were coefficients determined from material characteristics.

$$log(S) = \alpha_m * log(N) + \beta_m \tag{8.1}$$

To construct S-N curves three properties were defined for each material. The ultimate strength, S_u and the fatigue strength at 10^3 cycles and 10^6 cycles, defined as S_m and S_e respectively. For materials with unequal compressive and tensile ultimate strength, the lowest of the two was taken. S_m was approximated for metals as 0.9 S_u[1]. A reliable source was not found for S_m of composites and thus the same value was taken, but it should be noted that this could be inaccurate. The same cannot be said for S_e as the fatigue properties of materials widely differ. For aluminium 2024-T3 an S_e of 0.32 S_u was chosen[2].

The determination of S_e for carbon fibre and GLARE is not well defined as the fatigue behaviour of composites is extremely hard to predict. It is known that they perform better than metals, but it cannot be confidently quantified on how good they exactly perform. Metal fatigue is characterised by a single self-similar form of damage: cracks. However, composites have several non-self-similar forms of damage, including matrix cracks, fibre fractures, fibre-matrix de-bonding, fibre kinking, fibre pull-out or interlaminar delamination[3] [25].

Resources and experiments have indicated that for CFRP, S_e is equal to 0.8 S_m[4] [18][31]. This value was taken, but it should be noted that due to the fact that aerospace structures have extremely high safety and reliability standards, the fatigue lifetime of composite structures is generally over-designed to not take full advantage of composite's resistance to fatigue [25]. This is done by using higher knockdown factors such that fatigue cracking can never occur. These knockdown factors are discussed later on.

Less is known about the fatigue behaviour of GLARE. It is known that GLARE has better fatigue properties than aluminium, but literature and models that predict fatigue behaviour of GLARE are limited and too complicated to interpret correctly [9] [67]. The Metal Volume Fraction (MVF) method was used to determine the S_e of GLARE as this is commonly used to determine properties, such as S_u, of Fibre Metal Laminates (FMLs). Initially this method was deemed inaccurate as the glass fibre epoxy shows similar fatigue properties as aluminium with a S_e of roughly 0.4 S_m [10]. This is because the fatigue properties of GLARE are different from both of these materials due to the laminated composition of GLARE [8]. Due to no other available method, it was advised to use a S_e of 0.8 S_m for the fibre layer contribution of GLARE to account for this[5]. This resulted in a S_e of 0.49 and 0.46 S_m for GLARE 3 (3/2) and (2/1), respectively.

As previously mentioned, the pressurisation cycles are cyclic, meaning that they are roughly zero when HAMMER is grounded and maximum when HAMMER is at cruise altitude. Thus, the cyclic loading of the fuselage shell stresses does not have an average of zero and the mean stress is roughly equal to the stress amplitude of the cycle. A correction factor was applied for this condition. For all materials, S_m was divided by two. For aluminium, S_e was corrected by means of a linear intersection resulting in a reduction of 37%. While for CFRP and GLARE S_e was divided by two.

[1] http://www.engineeringarchives.com/les_machdes_endlimitandultstrength.html [cited 11 June 2020]
[2] Personal Communication with Dr.ir. R.C. Alderliesten [10 June 2020]
[3] https://www.quora.com/How-does-carbon-fiber-CFRP-behave-in-fatigue [cited 11 June 2020]
[4] https://www.quora.com/How-does-carbon-fiber-CFRP-behave-in-fatigue [cited 11 June 2020]
[5] Personal Communication Dr.ir. R.C. Alderliesten [6 June 2020]

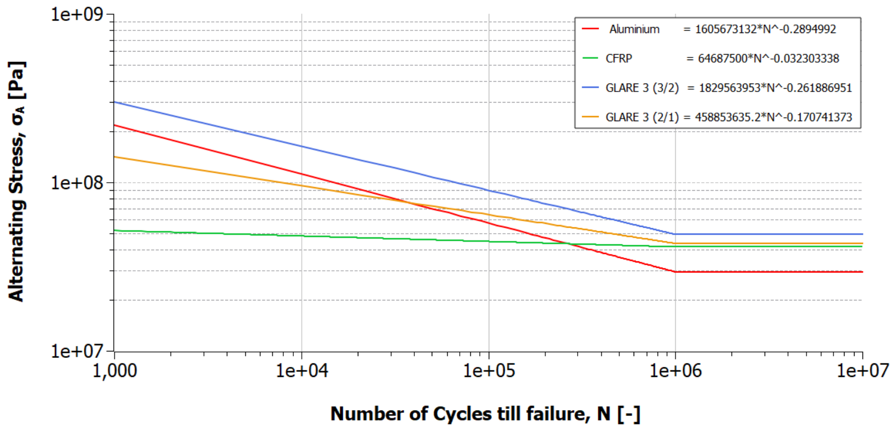

Figure 8.2: Maximum allowable alternating stress as a function of number of cycles for each material with $K_t = 3$ $[Pa]$.

Additionally, since the fuselage contains cut-outs, stress concentration factors K_t were taken into account. For the fuselage shell of an aircraft a K_t of 2, 2.5 and 3 were considered for the upper, side and bottom part of the fuselage, respectively[6]. For its influence on the S-N curves, the notch sensitivity of the material was used as a measure. CFRP is the most notch sensitive, followed by GLARE and lastly aluminium [6] [7] [35]. For aluminium, S_e was divided by K_t and for CFRP both S_e and S_m were divided by K_t [7]. The effect of K_t for GLARE was estimated as the average of aluminium and CFRP.

The resulting S - N curve for $K_t = 3$ can be seen in Figure 8.2. Only CFRP fabric was plotted, as CFRP UD was discarded early on. It can be seen that GLARE (3/2) has the largest allowable alternating stress for all cycles and CFRP has the best resistance against fatigue, as the maximum allowable stress decreases the least per cycle. However, it also has the least amount of allowable stress for 10^3 cycles.

Lastly, as previously mentioned, knockdown factors must be applied. The aircraft is designed for 30,000 flight cycles, but it must be ensured that materials will not fail due to fatigue prior to 30,000 cycles. Therefore, a knockdown factor of 8 was applied to aluminium and a knockdown factor of 16 was applied to CFRP and GLARE[8]. Meaning that for aluminium, HAMMER is designed for 240,000 cycles and for CFRP and GLARE HAMMER is designed for 480,000 cycles. Subsequently, the maximum allowable stresses for each material for different K_t were computed and can be found in Table 8.2. These will be used to determine the required thickness and thus weight for the fuselage skin and centre cabin wall. It can be seen that Glare 3 (3/2) has the highest allowable stress, but as Table 8.1 shows it has a considerably higher density than CFRP.

Table 8.2: Maximum allowable stress for each material depending on stress concentration factor $[MPa]$.

Condition	Al 2024-T3	CFRP fabric	Glare 3 (3/2)	Glare 3 (2/1)
K_t = 1	106.3	127.2	158.8	141.3
K_t = 2	61.3	63.6	82.9	73.7
K_t = 2.5	51.4	50.9	67.1	59.7
K_t = 3	44.5	42.4	55.3	49.2

8.1.6. Conclusion

The most promising materials to consider further are Al 2024-T3 and CFRP fabric. However, while CFRP fabric has better overall strength properties, aluminium is a less energy intensive option to produce and has favourable recyclability characteristics. Therefore aluminium is advised to be used in the general airframe like the floor and stringers.

CFRP is proposed for the skin material as it is high in strength compared to its weight. The skin makes up a significant part of the fuselage and weight savings can most likely be justified. Additionally, it is more difficult to produce complicated elements. These manufacturing difficulties raise the cost. However, as it is a cutting edge technology, it shall be considered for special cases where a critical weight reduction is required.

[6]Personal Communication Dr.ir. R.C. Alderliesten [11 June 2020]
[7]Personal Communication Dr.ir. R.C. Alderliesten [11 June 2020]
[8]Personal communication Dr.ir. R.C. Alderliesten [15 June 2020]

8.2. Wing Design

In order to assess the structural feasibility of the box wing design, a preliminary design for the wing structure was created. However, due to the over-constrained nature of the structure it was hard to make a correct assessment in this stage of the project. Therefore, this section aims at creating a first-order conservative estimation of the internal loads, together with the structural properties. Due to the use of geometrical and aerodynamic parameters, this estimation will have a higher accuracy than the statistical methods used for the class II sizing and can therefore be used as an input for a finite element model in a later design stage.

8.2.1. Wing Modelling

The wing was modelled as two beams, connected by a rigid connection. The first beam was clamped to the fuselage and the second one to the vertical tail. The ends of both beams were connected by a rigid lateral connector, as can be seen in Figure 8.3. Since all forces of the aft wing flowed through the vertical tail, the wing section between the two vertical tails was ignored. This section would normally relief the bending moment of the tail by providing an opposite bending moment with respect to the wing section outwards from the vertical tail. Therefore, this method was conservative by overestimating the bending moment. On top of that, since the vertical tail had limited stiffness, it was known that this support would not be fully clamped, but the loads could be partly relieved by rotation of the tail. A preliminary study of this effect will be done in Section 8.6.

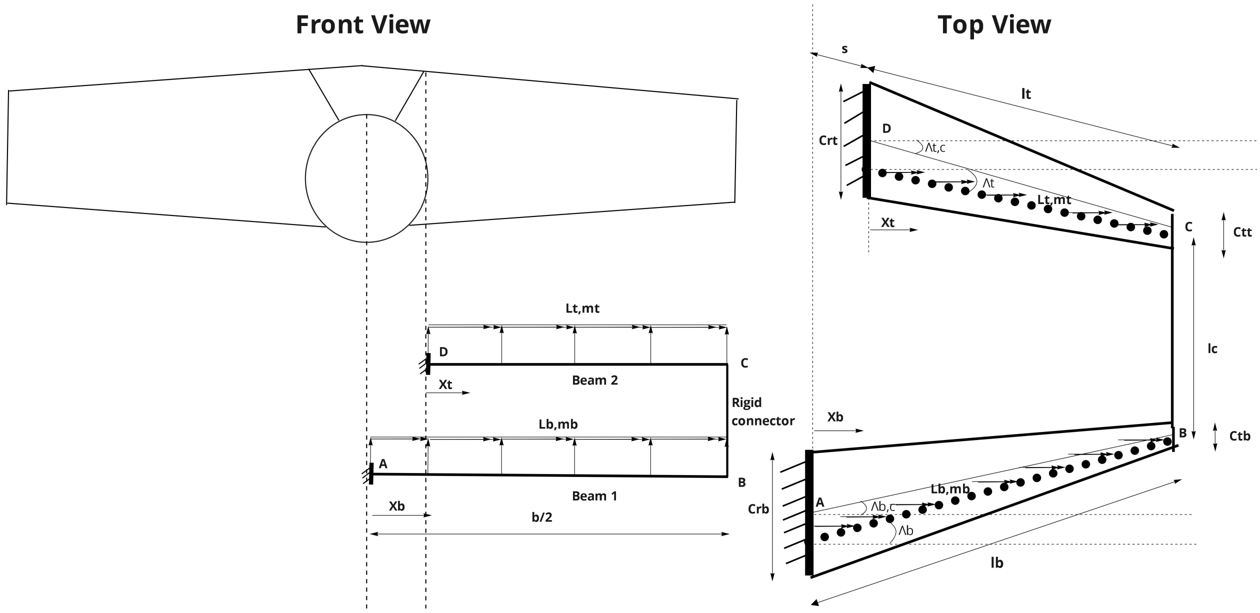

Figure 8.3: Structural model of the wing and its geometric definitions.

8.2.2. External Load Modelling

It was known from aerodynamics that the lift distribution could be represented by the sum of an elliptical and a uniform distribution, but as not enough aerodynamic data was available at this stage of the design it was assumed to be completely uniform. Since the elliptical distribution decreased along the span this again led to an overestimation of the bending moment. Also, the weight forces of the structure were neglected. It should be noted however that the fuel weight could provide a considerable relief in bending moment as it lowered the distributed load due to the aerodynamic forces by providing a counter force downwards. This assumption was justified as it was conservative. On top of that, the fuel was spread over two wings. In this stage of the design it was not known which tank would be drained first, or if both would be drained simultaneously. Therefore it was hard to model fuel weight relief correctly. However, once a fuel draining strategy would be developed, the model could be updated to account for it and obtain higher structural optimisation.

It was assumed that the lateral connector created zero lift. In the ideal case the connector creates a horizontal lift force in order to obtain a minimal induced drag, but since the connector chord was small with respect to the MAC, this was ignored. On top of that, the small dihedral angles were neglected, resulting in the Lift pointing straight up. As a result, there were no axial loads in the structure.

Drag was also neglected, as it was at least an order of magnitude lower than the Lift force. This, in turn, eliminated all forces in the direction along the fuselage length. Neglecting these forces is an obvious underestimation, but is was justified by considering that the bending moment, which largely contributed to the tensile and compressive stresses, was overestimated considerably.

In order to assess torsion, the location of application of the lift distribution was considered. From aerodynamics it was known that the lift applied along the quarterchord line of the airfoil, together with the aerodynamic pitching moment. Here, the aerodynamic pitching moment was modelled as a distributed moment, as given by Equation 8.2. In this equation, the subscripts b and t refer to the bottom and top beam, or equivalently the front and aft wing, respectively. Additionally, m(x) is the distributed moment as a function of span location x, C_m the moment coefficient of the airfoil, ρ the air density, V the air velocity and c(x) the chord length as a function of span position x. As the centre of pressure was not constant, C_m changed for different Mach numbers. For cruising Mach, a value of -0.14 was used, as obtained in Table 4.4.

$$m_b(x_b) = C_{m_b} * \frac{1}{2}\rho V^2 c(x_b)^2, m_t(x_t) = C_{m_t} * \frac{1}{2}\rho V^2 c(x_t)^2 \tag{8.2}$$

8.2.3. Reaction Force and Wing Internal Loading Determination

With the external forces known, the reaction forces could be calculated. However, since the structure was statically indeterminate, boundary conditions with respect to the rotation and deformation of the two separate beams needed to be established.

To obtain these relations three free body diagrams were used: one of the complete structure, one of the front wing (beam 1) and one of the aft wing (beam 2), as presented in Figure 8.4. Here, the clamped supports were replaced by a vertical reaction force and a torsion and bending moment. For the separate beams, the vertical force, torsional moment and bending moment in point B and C needed to be considered as well, since these would not go to zero due to the rigid connector. From these three body diagrams nine equilibrium equations were obtained, with twelve unknowns.

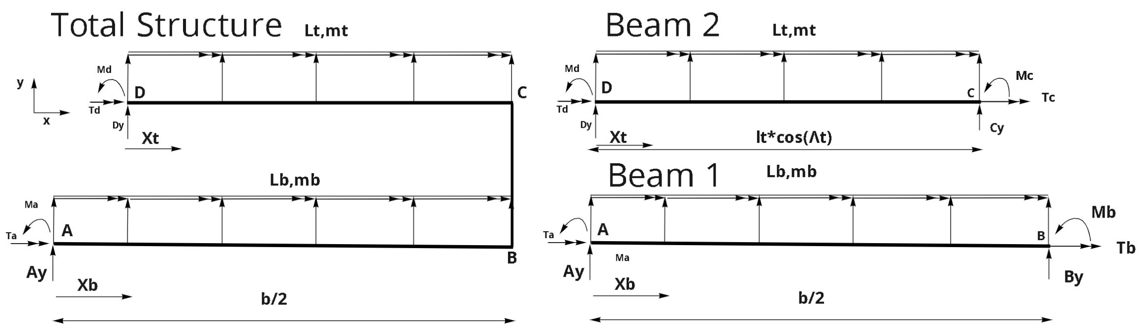

Figure 8.4: The free body diagrams of the total wing structure and separate beams.

The remaining equations followed from compatibility. First, the internal shear and moment distribution in beam 1 and beam 2 were obtained, as given in Equation 8.3 and Equation 8.4. In these equations the subscripts b and t again refer to the beam considered. A_y and D_y refer to the vertical reaction forces at the roots of the beams, L is the distributed lift force and Λ the quarter-chord sweep angle. V and M refer to internal shear force and bending moment respectively. A graphical representation of this nomenclature is shown in Figure 8.3 and Figure 8.4. As a next step, the rotation and deformation of beam 1 and 2, both scaled with the factor EI of structural integrity, could be found by integrating Equation 8.4 once and twice respectively. For this integration, the cross-section of the beam was considered to be constant along the span, hence EI is constant. Here, E refers to the Young'smodulus of the used material and I to the moment of inertia of the cross-section.

$$V_1(x_b) = A_y + \frac{L_b x_b}{cos(\Lambda_b)}, V_2(x_t) = D_y + \frac{L_t x_t}{cos(\Lambda_t)} \tag{8.3}$$

$$M_1(x_b) = -M_a + A_y x_b + \frac{L_b x_b^2}{2cos(\Lambda_b)}, M_2(x_t) = -M_d + D_y x_t + \frac{L_t x_t^2}{2cos(\Lambda_t)} \tag{8.4}$$

By integrating twice for both beam 1 and 2, four additional unknowns were introduced. These unknowns could easily be solved by imposing the structural constraints of the clamps, namely no deformation and rotation. Then, two more equations could be found by imposing a condition on the end rotation and deformation of both beams. Since the lateral connector was modelled as a rigid part, both beams had to rotate and deform an equal amount at the end points. The impact of this simplification will be further analysed in Section 8.6.

The last equation came from torsional compatibility. The internal torque distribution was given by Equation 8.5 and Equation 8.6, where T refers to the torsional loading and is used to calculate the twist of both beams. $\Lambda_{b,c}$ and $\Lambda_{t,c}$ represent the sweep at the chord line through the centroid of the wing box and Δc is the distance along the chord between the quarterchord point (where the lift applies) and the centroid, as a fraction of the chord length. Then, C_{slope} is the reduction in chord length per unit span. The term GJ is the torsional equivalent of EI, it determines the structural integrity for torsion, for calculation purposes it is assumed constant along the span. G then represents the shear modulus of the material, while J denotes the torsional constant of the cross-section. Since the aft wing torqued the front wing counterclockwise, while the front wing torqued the aft wing clockwise, the twist values were not equal. It was assumed that the twist was the same in magnitude, but opposite in sign. The validity of this assumption is tested in Section 8.6.

$$T_1(x_b) = -T_a + A_y tan(\Lambda_{b,c}) x_b - \int_0^{x_b} m_b dx_b + \frac{L_b x_b}{cos(\Lambda_b)}(\Delta c\left(C_{rb} - C_{slope_b}\frac{x_b}{2}\right) + 0.5 x_b tan(\Lambda_{b,c})) \tag{8.5}$$

$$T_2(x_t) = -T_d - D_y tan(\Lambda_{t,c}) x_t - \int_0^{x_t} m_t dx_t - \frac{L_t x_t}{cos(\Lambda_t)}(\frac{x_t}{2} tan(\Lambda_{t,c}) - \Delta c(C_{rt} - C_{slope_t}\frac{x_t}{2})) \tag{8.6}$$

The resulting equations can be found in Appendix A Equation A.1-Equation A.16. In this appendix the constants C1-4 represent the integration constants of the deformation equations. It can be seen that the rotations and deformations at the clamps are not set to 0, but have been left as variable, $\frac{d\nu}{dx}$ for bending rotation, ν for bending deformation and θ for angle of twist. This will later be used in Section 8.6 to analyse the sensitivity of the results. The same was done for the last three compatibility equations, where a difference in deformation was added for analysis purposes. Here, the Δ symbol represents difference. The system of equations was put into matrix form and solved for the reaction forces and moments, as well as the constants of integration.

With the reaction forces known, the internal loading as a function of x_b and x_t along beam 1 and beam 2 respectively were easily obtained by Equation 8.3, Equation 8.4, Equation 8.5 and Equation 8.6. The resulting loadings can be seen in Figure 8.5 and Figure 8.6. These loadings were obtained from a load case with a load factor of 2.75 at 230 $\frac{m}{s}$. This case was found to be the limit load, as can be seen in the V-n diagram, which is presented in Figure 3.3. Furthermore it was assumed that 60% of the lift was applied to the front wing and 40% to the aft wing, as was obtained in Subsection 4.1.4. Since the internal loading distribution depended on the stiffness configuration, it changed with changes in the structure. These graphs are given for the latest design iteration.

8.2.4. Wing Box Modelling

In order to cope with all the forces, a wing box was needed. The front spar of the wing box was placed at 15% chord and the aft spar at 65%. These values were chosen such that the high lift devices and control surfaces could fit into the wing. The wing box was then formed by the front spar, aft spar and two parts of load carrying skin, which followed the shape of the airfoil. It was assumed that the wing box structure carried all internal loads calculated in Subsection 8.2.3, while the remaining part of the wing structure was designed to carry additional loads introduced by the high lift devices and control surfaces.

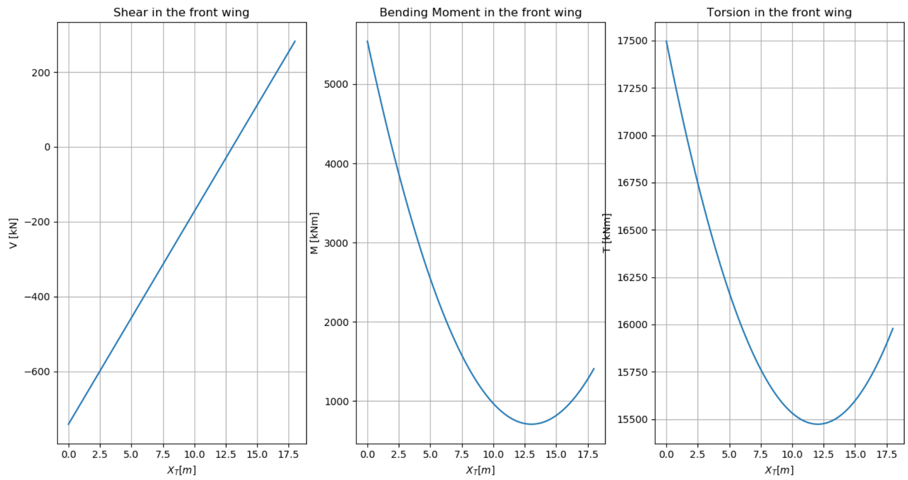

Figure 8.5: Internal loading in the front wing.

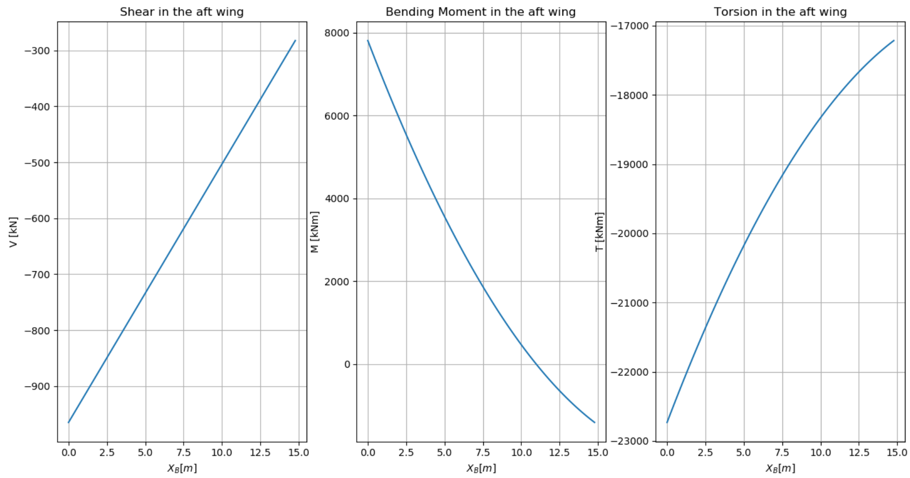

Figure 8.6: Internal loading in the aft wing.

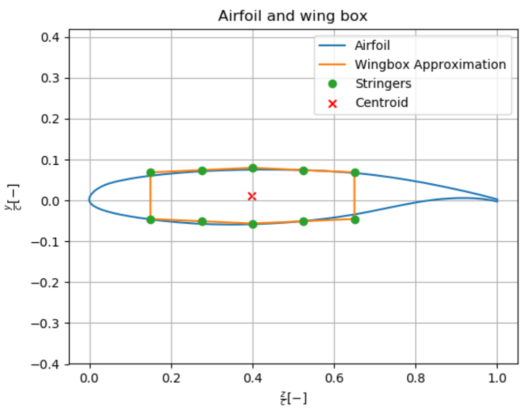

Figure 8.7: The airfoil and its central wing box.

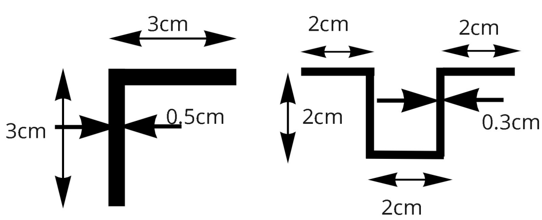

Figure 8.8: The stringer geometry.

The wing box was modelled as a set of 6 thin, flat plates, which gives a reasonable approximation of the shape of the airfoil, as can be seen in Figure 8.7. The size and angle of each plate was chosen such that it would form a symmetrical cross-section, while still being a good approximation of the overall shape.

To create a more realistic structure, 10 stringers were added onto the wing box, as be seen in Figure 8.7. Four of them were placed in the corners to connect the spars to skin panels. These stringers were L-shaped. The remaining six stringers were then evenly spaced along the skin panels and were taken as hat stringers. This was done since torsional loads were expected to be rather high in some parts of the wing box. Hat stringers form a closed section which would be better capable of resisting this torsion. The geometry of the stringers can be seen in Figure 8.8. For now, a cross-sectional area of 3 [cm^2], constant along the span, was chosen. It should be noted however that this is only a first design value and can be changed in later iterations to further optimise the design.

As the wing box was modelled as a symmetric section, the centroid was in the middle. Next to that it was known that the shear centre laid on the plane of symmetry, if it existed, and was therefore coincident with the centroid. The Moment of inertia could now be calculated using Equation 8.7. Here l_i represents the length of the thin plates. Additionally β_i is the angle between the horizontal axis and the line along the direction of the plate, t_i is the thickness of the plate, A_i the area and $\bar{y}$ and $\bar{y_i}$ the y location of the centroid of the cross-section and the thin plates, respectively. The thin plates were uniform, therefore their centroid was in the middle. The stringers were modelled as booms and therefore only the second term of the equation was taken into account for contribution of these stringers.

$$I_{zz} = \sum \frac{t_i l_i^3 sin^2(\beta_i)}{12} + \sum A_i(\bar{y} - \bar{y_i})^2 \tag{8.7}$$

Next to the moment of inertia, the torsional resistance was also calculated. This was done by Equation 8.8, which was valid as long as the thickness was constant along a plate. Here A_m is the enclosed area, which is easily calculated by dividing the section into two triangles and a trapezoid. The effects of the stringers were neglected for this analysis, as they would carry a very low torsional load.

$$J = 4A_m^2 * \sum \frac{t_i}{l_i} \tag{8.8}$$

8.2.5. Stress Analysis

In order to obtain an estimate for the required skin thickness, the wing box was sized for bending and shear. As the torsion loads of the current model turned out to be inaccurate, which will be explained in Section 8.6, torsion was left out.

The considered load case was the limit load, as was used for the determination of internal loading. This load case showed a load factor of 2.75 at a velocity of 230 [$\frac{m}{s}$], as can be seen in Figure 3.3. As stated by the CS25 a safety factor of 1.5 was taken to translate from limit load to ultimate load [1]. A quasi-isentropic CFRP was chosen as wing material. Using Table 8.1, and taking into account the safety factor, led to a maximum allowable stress of 400 [MPa] in tension, 380 [MPa] in compression and 105.3 [MPa] in shear.

Bending

The bending loads were calculated using Equation 8.9. Here, M refers to the internal bending moment, y to the vertical distance to the centroid and I to the moment of inertia. As the bending loads were not constant along the span, the wing was divided in 100 sections and the bending stress was calculated for every section. The calculation was repeated for a wing division of 1000 sections as well, showing no difference in results. This showed that 100 sections was sufficient to accurately describe the stress distribution along the span.

$$\sigma = \frac{My}{I} \tag{8.9}$$

The internal moment was simply obtained from the internal moment distribution, which was established in Subsection 8.2.3. The moment of inertia could be calculated using Equation 8.7, where all terms had to be scaled by the chord length at that section. The chord length was obtained by Equation 8.10, where $\frac{dc}{dx} = \frac{c_r - c_t}{\frac{b}{2}}$ for the front wing and $\frac{dc}{dx} = \frac{c_r - c_t}{l_t cos(\Lambda_t)}$ for the aft wing. Half the height of the cross-section was chosen for y, as this was the location of maximum bending stress.

$$c(x) = c_r - \frac{dc}{dx}x \tag{8.10}$$

As the cross-section is symmetric, the maximum stress occurred in the highest point as compression and in the lowest point as tension, for a positive shear. Since the compressive strength was lower, this was the critical value. The stress was then calculated along the span and the thickness was iterated until all stresses were below the maximum allowable. It was found that a thickness of 2.5 [cm] for the skin and 3.5 [cm] for the spar was needed for both the front and aft wing. For these thicknesses the results are displayed in Figure 8.9. For comparison, the cross-section was also sized in the case stringers would not be included. It was found that then a thickness of 2.6 [cm] and 4.0 [cm] were required for the skin and spar respectively. The stress distribution however was almost identical.

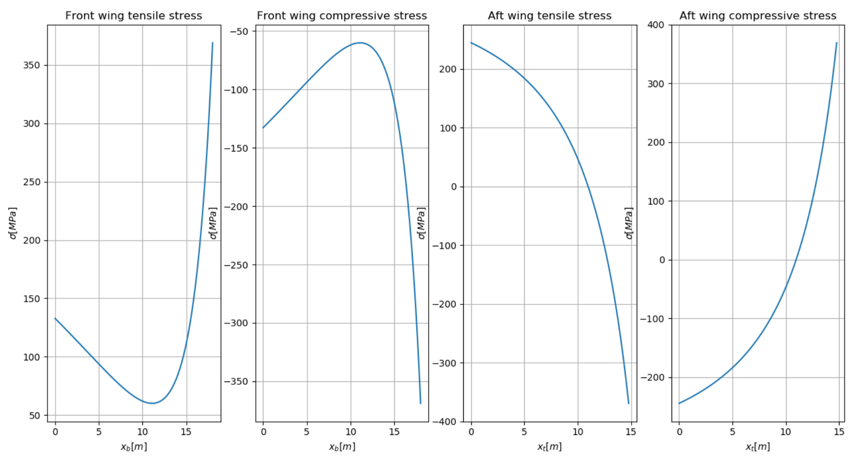

Figure 8.9: Normal stress distribution along the span.

It was seen that for the bottom wing the stresses near the tip were significantly higher than near the root. This was explained by the significant decrease in moment of inertia, which outweighed the decrease in bending moment. The same trend was seen in the top wing. However, since the stress changed sign, the difference was smaller. It was desired to have this stress distribution along the span as constant as possible, at a value near the maximum allowable stress, in order to have the highest structural efficiency. It was observed that the addition of stringers helped achieving smaller stress differences between root and tip. However, it was clearly seen that the stress at the root is significantly lower. Therefore, it was proposed that next iterations should incorporate a thickness distribution along the span. Of course, manufacturing constraints should be taken into account for these thickness gradients. Also, care should be taken as sudden changes in thickness can cause undesired stress concentrations.

Shear

The shear flows were calculated using Equation 8.11. Here s represents the location along each thin plate and ranges from 0 until its length. The sum of $\frac{A}{I_{zz}}$ represents the contribution of the stringers, which are modelled as booms for this equation. It means that the contribution of the boom should be added for all coordinates of s larger or equal to the s-coordinate of the stringer. The term $q_{i-1}(l_i)$ represents the shear flow at the end of the previous plate, as integration is started over again for every plate. For the first plate considered, this term will be equal to the redundant shear flow q_{s_0}. Integration was started at the bottom of the cross-section and done in a counterclockwise manner. Since the cross-section is symmetric and since only a vertical shear was applied, it was known that $q_{s_0} = 0$. The values for y(s) were obtained analytically using Equation 8.12.

$$q(s)_i = \frac{V_y}{I_{zz}} \oint_0^s tyds + \sum_{s<=s_0} \frac{A}{I_{zz}} + q_{i-1}(l_i) \tag{8.11}$$

$$y(s) = y_{start} + sin(\beta_i) * s \tag{8.12}$$

The shear flow was then computed for every location along the cross-section. The shear stress then simply followed from $\tau = \frac{q}{t}$. The maximum shear stress was then saved for every location along the span. The result is shown in Figure 8.10. The same thickness of 2.5 $[cm]$ for the skin and 3.5 $[cm]$ for the spars, as used for the bending stresses, were used. It can be seen that the shear stress for these thicknesses was significantly below the maximum allowable stress. When the no-stringer thicknesses of 2.6 $[cm]$ and 4.0 $[cm]$ were used instead, the tip stresses were found to be similar, while stresses at the root were even lower. As the tip loads were expected to be critical for the design, it was still expected that the incorporation of stringers would lead to a more efficient structure.

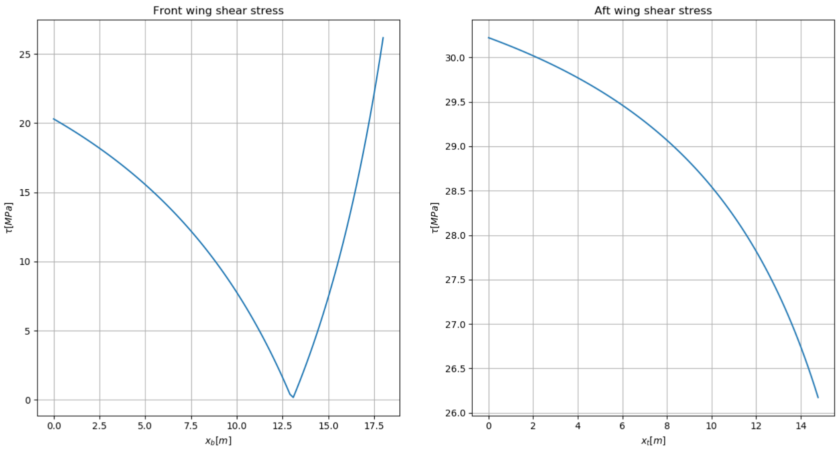

Figure 8.10: Maximum shear stress along the span.

It should be taken into account however that torsion also induced shear stresses into the structure. It will be of extreme importance that torsion gets evaluated more accurately in the next stage of the design in order to confirm that the structure is able to withstand all the loading.

8.2.6. Wing Box Preliminary Weight Estimation

With the thickness distribution known, a preliminary estimation of wing box weight was made. First the area as a function of the span was obtained by multiplying the length of every thin plate with the appropriate thickness for either the skin or the spar. Then these areas were integrated numerically along the span. The material contribution of the stringers was then simply added, as their cross-sectional area is constant along the span. It was then found that a volume of 2.04 $[m^3]$ and 1.51 $[m^3]$ of layered CFRP was needed for the front wing and aft wing, respectively. As the wings were modelled as half wings, these values were multiplied by 2 to obtain values for the complete wing system. Using a CFRP density of 1.6 $[\frac{g}{cm^3}]$ a weight of 11,367 $[kg]$ was found. For comparison, the weight was also calculated for structural thicknesses of 2.6 $[cm]$ and 4.0 $[cm]$, where no stringers are added. This weight was found to be 11,653 $[kg]$. It was seen that the addition of stringers saved almost 300 $[kg]$, and this number is expected to increase even further as stringer location and size gets optimised in later iterations. On top of that all computations of the stress analysis were repeated for a material choice of aluminium. With a estimated weight of 22,600 $[kg]$ it was clearly not beneficial to use aluminium. However, in regions with high shear stresses, aluminium could be considered to be used as reinforcement.

It should be noted that the calculated weights were an overestimation, since the thickness is expected to drop in further iterations, when the internal loadings are more accurately defined and a thickness distribution is applied. As the wing box was sized to carry all the loads, it was expected that the weight estimation presented in this section would give an acceptable prediction on the structural weight of the wing. On the other hand, extra weight due to systems like the high lift devices and control surfaces was not taken into account. As soon as an estimation for these weights is available they can be summed to the structural weight to give a more accurate representation of the total weight of the wing system. This weight could then be used instead of the values estimated by the Class II for further design iterations.

8.3. Fuselage Skin Design

The double-bubble design was chosen in the midterm report [21]. In this section the material, the thickness and the weight of the double-bubble structure are determined. This is done by only analysing the pressurisation forces. Shear is not analysed as this is often not a limiting factor the fuselage skin as stated Subsection 8.1.2.

8.3.1. Cabin Pressure Analysis

For the pressurisation of the fuselage, both the cargo and passenger compartment are pressurised such that the pressure is best distributed. The pressure force for the cross-section of the fuselage is then expressed by Equation 8.13.

$$F_{pressure} = \Delta p \int_0^{2\pi} R(\phi) \cdot sin(\phi) d\phi \tag{8.13}$$

It was seen that the outward force of the internal pressure was dependent on the difference between the internal and external pressure, Δp, distance to centroid, R, and angle ϕ [6].

As discussed in Chapter 4, cruise altitude will be at 36,000 [*ft*]. However, due to service ceilings being higher than that, it was designed for the proof load n_2 such that the cabin pressure is designed for cruise at 45,000 [*ft*] where there is an ambient pressure of 14,748 [*Pa*]. The internal pressure followed from Chapter 6 where an internal cabin pressure of 75,626 [*Pa*] was specified.

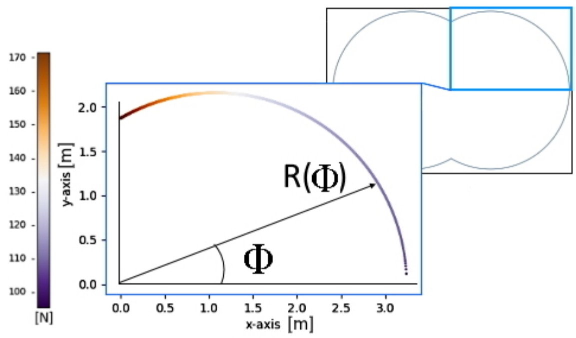

Figure 8.11: Stress distribution on double bubble section.

The double-bubble has a varying R for each ϕ. Therefore the integral was evaluated numerically such that the pressure force can be found on each differential element of the geometry. Force concentrations could subsequently be mapped onto the geometry as depicted in Figure 8.11 which helps to visualise the pressure's effect on the double bubble geometry.

Skin thickness determination

As the geometry was built up out of discrete elements, Equation 8.14 was used to determine the thickness. However, to obtain a useful thickness, the domain should be divided in smaller segments. The differential thicknesses summed together resulted in the average thickness for that particular segment. In the analysis, the maximum pressure force in a segment was used to compute the local skin segment's thickness.

$$2\sigma t(\phi) = \Delta p R(\phi) sin(\phi) d\phi \tag{8.14}$$

8.3.2. Cabin Support Structure

The pressure forces in the double-bubble cross-section are not uniform. A force concentration is present at the junction of the bubbles where the skin will be pushed outwards. Figure 8.12 shows where the resultant force F_r will act. To prevent this, a support structure had to be added to aid in maintaining the double-bubble shape. All multi-bubble configurations have this problem. For example, the A380's vertical double-bubble uses a floor as a support structure to prevent the double bubble from bulging outwards.

Consequently, a vertical wall has been added to the design. A wall is more efficient than support columns. Occasionally placing a support column would cause locations without support to bulge outwards introducing unwanted stress concentrations. Additionally, a support wall can double as a structural support to help the fuselage cope with the bending moments introduced by the wing system.

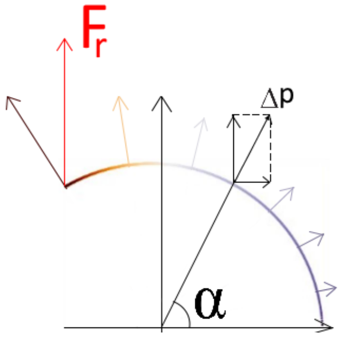

Figure 8.12: Determination resultant force.

To determine the resultant force F_r, it had to be noted that pressure always acts perpendicular to a surface, for this purpose angle α was introduced. The pressure force cancelled out in the horizontal axis but for vertical axis, $sin(\alpha)$, a resultant force F_r was found. This implied that the resultant force differed for every double-bubble layout. The effect of the vertical support wall on the overall weight was taken into account when finding an optimum double-bubble configuration.

Resultant Force over Cabin Length
To analyse the thickness of the cabin support structure, Equation 8.13 was extended to integrate over the length of the fuselage s as seen in Equation 8.15. The vertical wall was only sized to resist the tension force from the resultant. Influences from bending were neglected as the compressive strength of CFRP fabric was superior over Al2024-T3 Table 8.1. Therefore, the resultant force was assumed constant along the length of the fuselage.

$$F_p = \int_0^s \int_0^{2\pi} [\Delta p R(\phi) sin(\phi) d\phi] \cdot sin(\alpha) ds \tag{8.15}$$

From here, the wall cross-sectional area could be computed from which a wall thickness and weight could be derived.

Design for Cutouts
For an initial analysis, the wall was not optimised. However, as the wall thickness was important for the interior design, an estimation was given for the maximum thickness of a given cutout size and pitch. To find the maximum thickness it was assumed that the wall thickness t increased proportionally to the decreasing distance between cutouts s as shown in Figure 8.13. The consequence of this assumptions was that the presence of cutouts would not influence the mass of the wall, the material only shifts such that the same stress density was kept throughout the support wall. Furthermore a continuous wall was assumed such that extra cutouts for subsystems like the nose landing gear, were not considered.

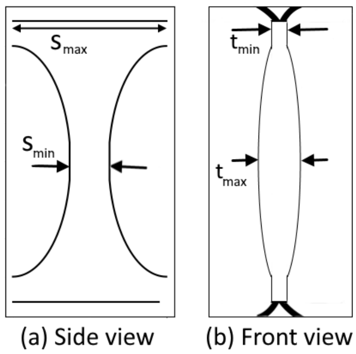

Figure 8.13: Cabin cutout wall thickness assumptions.

8.3.3. Double-Bubble Optimisation and Weight Estimation
Each double-bubble configuration can be described by a singular angle θ as depicted in Figure 8.14(a). By ranging θ from 90° to 180° all possible double bubble configurations of interest were analysed.
To ensure a fair comparison, each tested configuration had the same width, Figure 8.14(b). The purpose was to find a double bubble configuration that optimised volume while also minimising weight. An analysis was performed to determine an optimal range of θ as the weight of the structure was highly dependent on several components.

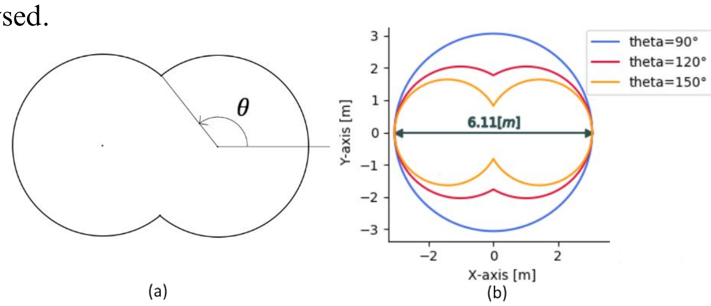

Figure 8.14: Effect of theta on the double bubble layout.

For this analysis, four components were taken into account:

1. Material selection and manufacturability limits.

2. Varying the material K_t factor which was dependent on the location α in the fuselage.
3. The pressure force on the fuselage skin depending on its shape θ that determines the skin thickness to design for fatigue.
4. The cabin support wall weight based on the resultant pressure force F_r and the height of the wall $2rsin(\theta)$.

For this analysis, a range of θ was presented for which a design could be considered structurally efficient. The approach to find an optimal θ range was by minimising the double-bubble weight per enclosed area. As determined in Chapter 6, $\theta = 115°$ was used for the analysis which can then be checked if it is structurally sensible and estimate possible weight savings for later iterations.

Alpha Determination

The different stress concentrations K_t affects the maximum allowable stress in various parts of the fuselage. To include the influence of these stress concentrations, the fuselage was divided in three sections: top, middle and bottom section. The fuselage sections are represented by the angle α. The top and bottom skin are symmetric around the x axis such that both sections can be described by only a single angle α, as shown in Figure 8.15(a). It was observed that α has an optimal value as shown in Figure 8.15(b). However, this optimal angle α most likely underestimates the stress concentration range that would be observed in the top and bottom sections. Consequently it has been chosen to limit α to $rsin(\alpha) = rsin(\theta)$ to better approximate reality. For a $\theta = 115°$, this corresponds to $\alpha = 65°$.

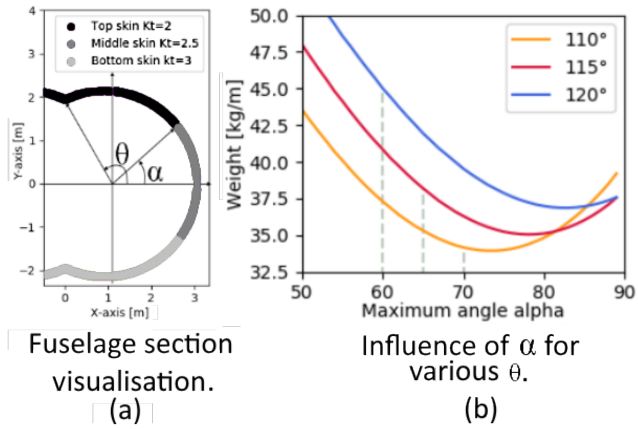

Figure 8.15: Effect of α in the double bubble layout.

Weight Comparison

The results are shown in Figure 8.16. The goal of this analysis was to find a range θ for which a double-bubble layout could be considered efficient. From Figure 8.16(a) it can be seen that there is an optimum at $\theta = 101°$. This optimised the enclosed volume for the least amount of structural material, although it has a very large cross-section and is not aerodynamically efficient. From Figure 8.16(b) it can be seen that there is a second optimum at $\theta = 130°$. This coincides with the geometric optimum and could therefore enclose the maximum amount of volume for the minimal amount of weight. This was structurally and aerodynamically the most ideal but due to the constricted shape, the volume was more difficult to utilise efficiently for the cabin design. As discussed in Chapter 6, the fuselage has to be comfortable for passengers and consequently an angle of $\theta = 115°$ has been chosen. It can be concluded that it lies within the optimal range of $101° < \theta < 130°$ but for later iterations, larger angles of θ would be advised as the structural weight will decrease with larger θ.

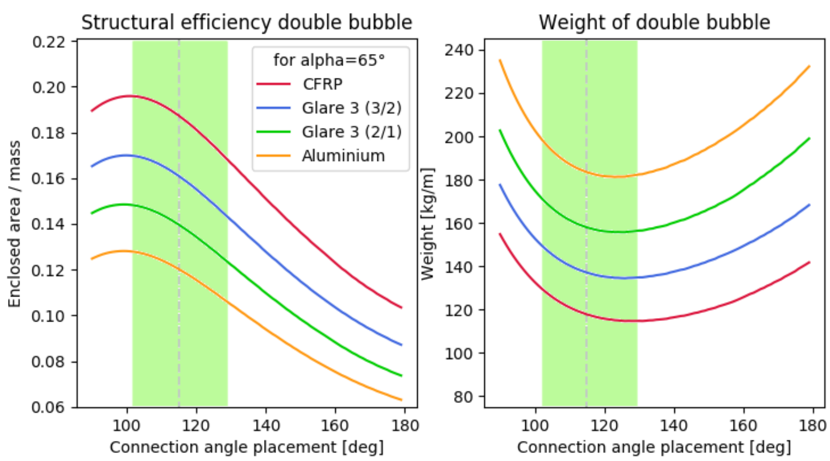

Figure 8.16: Optimum weight determination for double bubble configuration.

The CFRP design was favourable with a layout as depicted in Figure 8.15 where the minimum cross-section thicknesses as well as the locations for the different skin sections are illustrated. With a fuselage of length 45 [*m*] weighing roughly 117.7 [*kg/m*], the fuselage skin structure with cabin support wall weighed 5297 [*kg*].

For the design of the vertical support wall the same fatigue analysis was used as for the fuselage skin. However, stress concentration factors were not considered as the wall thickness increased proportionally to the amount of distance between cutouts. Additionally, CFRP fabric was selected as a material due to the wall being predominantly subjected to tension. A maximum allowable stress of 127.2 [*MPa*] was used, Table 8.2. This resulted in wall width of 3.64 - 5.17 [*mm*] with a weight of 963 [*kg*].

Table 8.3: Summary overview of fuselage thicknesses.

Section	**Thickness [*mm*]**
Top skin	4.1
Middle skin	2.0
Bottom skin	6.2
Cabin wall	3.64 - 5.17

Skin Weight

Taking into account the manufacturability of the materials, the geometric shape θ and the different stress concentration factors, K_t, the thicknesses are shown in Table 8.3 and a total fuselage skin weight of 4334 [*kg*] was found. For these thicknesses, no manufacturability concerns were found.

8.4. Fuselage Airframe Architecture Design

The fuselage is comprised mainly out of the longitudinal stiffening elements, fuselage frames and a floor structure. In this section only the longitudinal stiffening elements and floor are sized as they were expected to carry most of the stresses.

8.4.1. Airframe Architecture

Floor sizing

The floor is a significant factor in the fuselage weight. Restrictions on the thickness required a solution that was unconventional. The floor sizing was based on the data shown in Table 8.4[9][10]. A load factor n_3 was chosen to ensure safety. As the cabin is relatively wide, a floor beam spanning the width of the cabin would not weight efficient, a solution therefore needed to be found to support the floor in the middle.

Table 8.4: Reference weights.

Component	**Weight [*kg*]**
Passenger	75
Seat	34
Loaded Service trolley	115

A proposed solution was to install a support structure adjacent to the cabin wall to which the cabin floor is suspended, as shown in Figure 8.17. The advantage of suspending the floor from the ceiling is that it helps to maintain the double bubble shape and decrease the weight and fatigue load amplitude for the cabin wall. By suspending the floor in contrast to supporting it, the cabin wall structure was found to be 10.5% lighter. For this design, in Table 8.5, a weight estimate is presented for a floor beam with a width of 5 [*cm*] and a height which was 0.5 [*cm*] below the maximum allowable height of 10 [*cm*]. This was to allow some extra space such that floor deflections under loading would not damage the LD3 containers.

Table 8.5: Floor design breakdown.

	Quantity	**Weight**	**Total weight [*kg*]**
Floor beam	59 [#]	81.9	4830
Floor support	118 [#]	0.57	67
Floor panel	265 [m^2]	2.5	663
			5560

Each beam supports a row of seats spaced in accordance to the seat pitch. A maximum bending moment of 1850 [*Nm*] and a reaction force of 6654 [*N*] was found. Using aluminium 2024-T3, this resulted in a structure weighing 5560 [*kg*] including the floor panels[11] and the floor support Table 8.5. Due to the floor mainly comprising of support beams, it was not taken into consideration for resisting bending moment.

[9] https://www.aviationbusinessnews.com/cabin/catering-trolleys-aircraft-regulations/ [cited 16 June 2020]
[10] cited Nuori5048: https://www.airliners.net/forum/viewtopic.php?t=755723 [cited 16 June 2020]
[11] https://www.thegillcorp.com/home.php?cPath=38_23 [cited 26 June 2020]

This was a conservative estimate. When increasing allowable floor space to 13 [*cm*], the total weight reduced by 40% with the same cutout pitch. A trade-off can be made between floor beam thickness and floor support pitch for less visual obstruction in the cabin. This will remain a recommendation as changing the fuselage cross-section layout at this stage would affect a lot of subsystems.

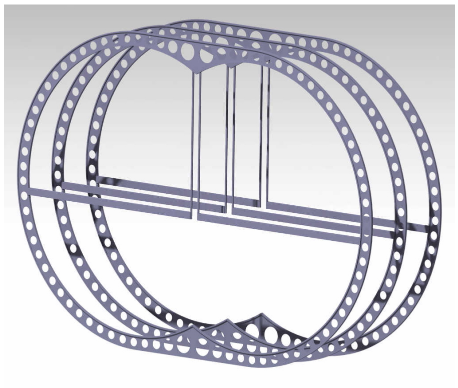

Figure 8.17: Illustration of the proposed floor structure at seat pitch.

Optimal Number of Stringers

For the longitudinal stiffening of an aircraft, elements such as stringers and longerons are used. Usually longerons have greater cross-section than stringers and consist out of 4-8 elements. Stiffeners are much smaller and can have 50-100 elements in the airframe cross-section for a conventional fuselage [12]. For the longitudinal stiffening elements, only stringers were considered.
For the the box wing configuration, it was assumed that the CG is in the geometric centre of the double-bubble fuselage. A generic analysis is performed where the moment of inertia is divided by the total weight of the structure to find the optimum number of stiffening elements. It was concluded that 70 stringers is optimum with a layout as seen in Figure 8.18.

Stringer Sizing

For the stringer sizing, the most critical flight phase was taken as a baseline for this structural analysis, take-off at MTOW. To determine the total cross-sectional area of the stringers, the maximum bending moment was identified. This was done by constructing a bending moment diagram from all the subsystems modelled as a distributed load and wing bending moment as a torque, shown in Figure 8.19. The torque ratios were taken from Section 8.2 and were used in balancing out the moment equilibrium resulting into T_1 and T_2. From here, the moment diagram was derived from which a maximum bending moment was found of -20.6 $\cdot 10^6$ [*Nm*].

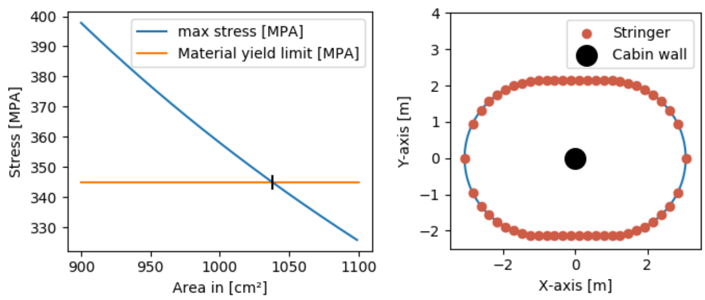

Figure 8.18: Stringer lay out for 70 stringers.

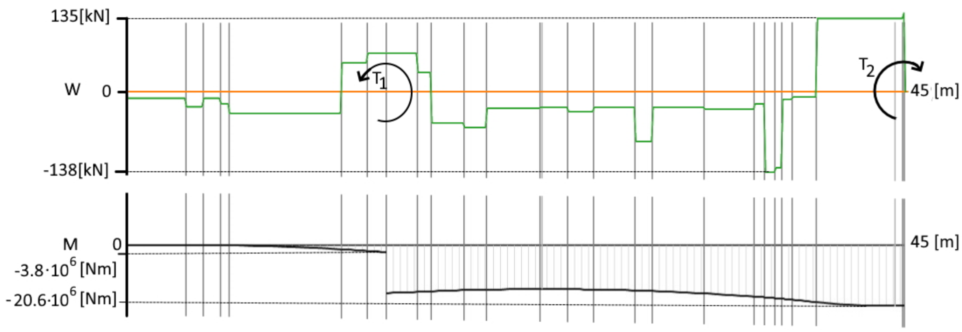

Figure 8.19: Load diagram with corresponding bending moment diagram along the length of the fuselage.

To analyse the stresses in each individual stringer, an idealised boom analysis method was set up. This took into consideration the average skin thicknesses in Subsection 8.3.1 and the cabin wall. With 70 elements to resist this bending moment, the maximum bending moment was determined using Equation 8.16, where σ_{boom} is the stress found in the boom, n_3 is the ultimate load, M is the maximum bending moment, I the moment of inertia and y the distance to the centroid [37]. Aluminium 2024-T3 was used which has a σ_{yield}=345 [*MPa*].

[12]https://www.slideshare.net/subhan90/skin-stringersinanaircraft-56785765 [cited 16 June 2020]

$$\sigma_{boom} = n_3 \frac{M}{I} \tilde{y} \tag{8.16}$$

It was found that a total of 1037 [*cm²*] stiffening area was necessary such that none of the stingers would exceed the maximum bending moment of σ_{yield}.

This was then associated with a stringer area of 14.81 [*cm²*] which is rather large for a stiffener element. Therefore, an analysis was done to study the effect of reducing stringer size while increasing the stringer number. The results can be seen in Table 8.6. These suggested a better weight estimate would be the airframe stiffener weight for 150 stiffening elements. It was therefore concluded that the airframe would weigh roughly 3511 [*kg*].

8.4.2. Stringer Profile Design

Both the bending moment and torsion induced by flight are translated into the airframe as bending stresses. The stringers are principal structural elements bearing the load induced by flight. Therefore a cross-section with a high moment of inertia was desired. A second consideration was made by installing the stringers inside the fuselage. An I-beam is inconvenient to attach the airframe to the fuselage skin and was not considered for this reason. C-beams are interesting as the shear centre isn't coinciding with the centroid. Therefore the profile of the stringer geometry was designed such that the shear centre lies outside of the profile such that it can more efficiently resist stresses which act through the shear centre. This would be beneficial for dissipating torsional loads.

Table 8.6: Asymptotic stiffener behaviour for increased number of stiffeners

# Stringers	Stringer Area [*cm²*]	Weight [*kg*]
20	51.85	3282.9
50	20.74	3452.7
70	14.81	3479.3
150	6.91	3511.2
250	4.15	3520.2

8.5. Technical Design: Fuel Tank

With the geometry of the wing box known, a better estimation on fuel tank volume could be made. The fuel tank was modelled as a pyramid shape and its volume was calculated using Equation 8.17 [42]. Here S_1 and S_2 are the areas of the trapezoids formed by connecting the front and aft spar at the wing root and fuel tank end respectively. l_{tank} is the spanwise length of the fuel tank. The fuel tank end is normally located at 85% span to take into account the possibility of lightning strikes. This is however not applicable for a box wing. Instead, the end was taken at 97.5% span in order to leave some room for structural reinforcement of the lateral connector. This resulted in a wing tank volume of 22.36 [m^3] for the front wing. After taking a 4% margin for integration, as recommended by [42] and another 5% for expansion of the fuel, this resulted in a fuel mass of 16340 [kg] for the front wing. The fuel tank for the aft wing can in theory be the same size, but stability analysis showed that only 13398 [kg] could be placed in the aft wing without violating stability requirements.

$$V_{tank} = \frac{l_{tank}}{3} \left(S_1 + S_2 + \sqrt{S_1 S_2} \right) \tag{8.17}$$

This resulted in a total fuel mass of 29738 [kg], which is enough for the harmonic mission. On top of that the aircraft will have the possibility to install an extra tank of 9 [m^3] in the front cargo bay instead of 2 LD3 containers. This will add another 6866 [kg] of fuel which can be used when the aircraft is operated in a lower payload configuration. This will be elaborated further in Section 9.1.

8.6. Verification and Validation

8.6.1. Wing Design

Internal Loading Verification

The internal loading and reaction forces where verified in several ways. First the model was checked for a logic correspondence to a change in input. As expected it can be seen that increasing the lift force increases all internal loadings as well. Next to that a reduction in span corresponds with a reduction in bending moment and lowering the horizontal spacing between the wing reduces the torsion induced. As a final qualitative check the vertical tail connection is placed on the center line of the fuselage. As a result the front and aft wing become beams of equal length and it is observed that the internal shear and bending loads are then equal for both wings. The torsional loading is not exactly symmetric, but the reaction forces are close to each others negatives. This makes sense considering that the front and aft wing torque each other in opposite direction. The small difference in magnitude can be explained by the load application at quarter chord, which gives a clockwise moment around the centerline of both wings. This slightly breaks the symmetry of the problem, thereby changing the values a bit.

As a next step the internal loading diagrams were checked for consistency. As the bending moment is the integral of the shear force it was checked that a positive shear force resulted into a positive slope in bending moment. On top of that it was checked that a shear force of zero corresponded to a minimum or maximum in the bending moment, this is also clearly visible in Figure 8.5, where the moment diagram goes through a minimum as the shear changes sign. Also the internal loadings at the end points of the beam have been checked. As required by equilibrium all forces and moments should go to zero for any section of the beams. Now the internal loadings of the end beam have been found in two ways, by using Equation 8.3-Equation 8.6 and by obtaining them as output from the systems of equations defined in Appendix A. As expected both methods give the same result.

The reaction forces are obtained by solving the system of equations in Appendix A. As it is a complicated set of calculations it is prone to errors. Therefore all functions have been unit tested thoroughly in Python and after computation the obtained values are placed into the equations the other way around in order to check for compliance.

Internal Loading Validity

The validity of the obtained forces is now tested by use of a simple sensitivity analysis. All loadings are calculated based on a set of assumed compatibility equations. As the fuselage is very stiff it is standard to model it as a clamped support, this will not be investigated further. However, it is expected that when loaded the tail will deform and rotate, changing the internal load paths. Next to that the lateral connector is assumed to be fully rigid, while in reality it will deform to cope with a difference in bending rotation and deformation at the tips of both wings.

In the system of equations in Appendix A all compatibility equations have included either the rotation or deformation at the support, or a difference of them at the tip. These values are all taken as zero for the determination of the reaction forces. Now one of them will be changed at the time, in order to assess the impact on the internal loadings. The results can be seen in Table 8.7.

Table 8.7: Sensitivity of the loading to a change in compatibility conditions.

Compatibility condition	Imposed Value	A_y $[kN]$	M_a $[kNm]$	T_a $[kNm]$	D_y $[kNm]$	M_d $[kNm]$	T_d $[kNm]$
Original Model	-	-741.6	-5541	23335	-964.9	-7810	-18100
Clamped tail rotation	$(\frac{d\nu_t}{dx_t})_{x_t=0} = 5^\circ$	-741.8	-5543	23320	-964.8	-7808	-18089
Clamped tail deformation	$(\nu_t)_{x_t=0} = 0.1$	-741.7	-5541	23332	-964.9	-7809	-18099
Wing tips rotate together	$\Delta\frac{d\nu}{dx} = 5^\circ$	-741.5	-5540	23354	-965.1	-7810	-18115
Wing tips deform together	$\Delta\nu = 0.1$	-741.7	-5541	23332	-964.9	-7809	-18099
Wing tips twist same value, opposite direction	$\Delta\theta = 5^\circ$	-741.6	-5541	32202	-964.9	-7810	-26967
Wing tips twist same value, opposite direction	$\Delta\theta = -5^\circ$	-741.6	-5541	14468	-964.9	-7810	-9233

It can be observed that the loading is very constant for changes in compatibility equations in bending. However there is a large deviation when the twist gets changed. As it was difficult to establish a correct compatibility equation for twist it can not be guaranteed that the twist will be equal in magnitude for both wings. On the other hand, due to differences in loading it is rather unlikely. Therefore the distribution of twist between reaction forces at point A and D is concluded to be invalid. It should be noted however that the sum of T_a and T_d still provides equilibrium and is therefore assumed correct. But since the compatibility of the structure is not known it is impossible to establish a relation between T_a and T_d.

Wing Box Model
The moment of intertia is verified by inputting a geometry of 4 thin plates forming a rectangle of width w, height h and constant thickness t and comparing the results to the analytical solution, given by Equation 8.18. Also to check that symmetry is incorporated correctly, the moment of inertia around the zy axis, given by Equation 8.19, was calculated, which as expected comes out to be 0, verifying the use of symmetrical formulas.

$$I = \frac{1}{12}wh^3 - \frac{1}{12}(w-2t)(h-2t)^3 \tag{8.18}$$

$$I_{zy} = \sum \frac{t_i l_i^3 sin(\beta_i)cos(\beta_i)}{12} + \sum A_i(\bar{y}-\bar{y}_i)(\bar{z}-\bar{z}_i) \tag{8.19}$$

8.6.2. Stresses

In order to verify the bending stresses the developed Python functions have been unit tested thoroughly. Next to that a calculation by hand was made for the bending stresses at the root and tip chord, to check for the correct order of magnitude. For this calculation the wing box was approximated as a rectangle of 0.5cx0.12c with a thickness of 3 $[cm]$. As this is an overestimation of the moment of inertia the resulting bending stress will be slightly underestimated.

The hand calculation gave a result of 122.7 $[MPa]$ at the root and 359.9 $[MPa]$ at the tip, while the program output 130.4 $[MPa]$ and 380 $[MPa]$ respectively. Not only can it be seen that the order of magnitude is correct, but also the ratio between stress by hand assumption and stress by program is the same for the wing root and tip. This suggests that the scaling of the cross-section by appropriate chord lengths is implemented correctly into the program.

For verification of the shear flows the shear flows have been integrated along every plate and their additions to the vertical and horizontal force respectively summed together. The integration has been done numerically by dividing each plate in 100 nodes and then multiplying the shear flow with the spacing between each node and the cosine and sine of the plate, to obtain horizontal and vertical force respectively. These contributions are then summed together to obtain the resultant force. As expected all horizontal shear flows cancel out to machine error. Meanwhile the sum of all vertical shear flows added to 1.009 times the original shear. This value can be explained by the moment of inertia, as the calculation of moment of inertia uses a thin walled assumption, it is underestimated slightly. Because of that the shear flow, which scales with the inverse of the moment of inertia is overestimated. For this stage of the design this difference of less than 1% is deemed acceptable, especially since it is a conservative estimate.

8.6.3. Fuselage Verification & Validation

Fuselage Cabin Thickness Verification To verify the program used to calculate the pressure of a double bubble, the program was tested on a circle. As depicted in Figure 8.20, there is a constant pressure distribution. The total pressure force can be validated with the analytical formula and comparing it with the numerical solution, the program's results for thicknesses were 99.84% of the analytical value.

A second check was done by inspecting Figure 8.16 where the weights of $\theta = 90°$ and $\theta = 180°$ are roughly the same. Both θs have the same circumference so this can be expected. The deviation in weight is the the exclusion of the cabin wall for $\theta = 180°$ as at that angle the wall height is 0.

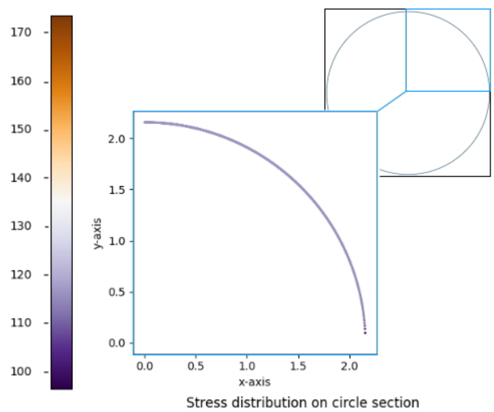

Figure 8.20: Visual validation of circle section where a constant force distribution can be seen.

Fuselage thickness validation To validate the fuselage thickness, it was compared to current aircraft to determine if its order of magnitude was reasonable. No comparable information was found regarding the thickness of CFRP fuselages. But, it was found that aluminium commercial aircraft have a skin thickness of roughly 1-2 [*mm*]. The analysis tool overestimates the results 1.5-2 times compared to reference aircraft. The design specification about commercial aircraft, could not be found. The deviation between HAMMER and other aircraft is most likely due to the approach that was taken for determining the maximum allowable stress of the fuselage skin.

Weight comparison verification To verify the weight comparison of Subsection 8.3.1, a study has been done to find the geometric optimum. This assumed no material properties nor cabin wall. This analysis provided the most efficient double bubble lay-out theoretically possible, this was found to be 130° Figure 8.21. In Figure 8.16, the minimal weight configuration lay-out can be found at $\theta = 130°$.

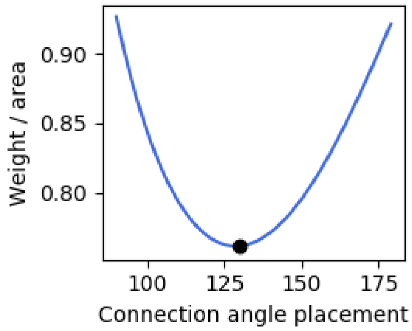

Figure 8.21: Mathematical optimum without material properties.

Airframe Stringer Verification The analysis tool was verified by checking trivial cases and with a manual calculation of a 6 element model. To ensure performance, the Python program was checked if the tool worked as expected when increasing the stiffening elements in the model. Maximum stress concentrations were also verified to see if the maximum allowable stress didn't surpass the σ_{yield}. However, comparing with a second model for verification purposes, the weight doubled. The verification model placed all stiffening elements at a distance y=1.91 from the centroid, which is where the double bubbles intersect. The cabin support wall and skin area were deducted from the total amount of area needed to achieve the area necessary to resist the bending load. An increase in weight was expected, however, it is questionable whether it would be by this margin.

8.6.4. Weight verification with Class II estimation

In this chapter a significant part of the OEW weight was found to be 26,021 [*kg*], a break down of the weight is shown in Table 8.8. CFRP was used only when significant weight savings could be made with respect to Al2024-T3. Comparing to the Class II estimation, for only the fuselage and wing system, a weight was found of 28,496 [*kg*]. It was expected to find a weight exceeding the class II estimation as its based on conventional aircraft statistics. However, the weight is expected to increase for the fuselage section in later iterations. The fuselage frames, interior furnishings, landing gear and electronics still need to be added.

Table 8.8: Summary overview of component weights.

Component	**Material**	**Weight [*kg*]**	**Savings**
Wing system	CFRP	11653	48%
Fuselage skin	CFRP	4334	36%
Cabin support wall	CFRP	963	54%
Stringers	Al 2024-T3	3511	-
Floor	Al 2024-T3	5560	-
Total		**26021**	**34%**

8.7. Sustainability Analysis

For this report, the main criteria was to make the aircraft structures as light as possible. However, as discussed in Subsection 8.1.4 other parameters were also taken into account. Additionally, the cost, toxicity and the hazards of certain materials and maintenance of materials were considered as well. Nevertheless, the large difference in weight was the deciding factor of the material choice.

8.8. Risk Assessment

SM-01 Fracture Toughness of Fuselage Skin A rupture would cause a loss of pressure within the cabin to which the pilot would need to perform emergency manoeuvres to reach lower altitudes to maintain a safe environment for passengers.

SM-02 Support Wall Cutouts

- SM-02-WO: The wall was designed as continuous structure. The different subsystems that also lie on the longitudinal axis have not been taken into account (landing gear, central wing box, central fuel tank).
- SM-02-CO: The bending stiffness is calculated with average thickness of the wall but in reality they are wall columns which have locally worse bending characteristics. This can cause the central wall to break under the bending moment if the wall isn't designed properly.

SM-03 Airframe Due to the bending moment being four times higher in the inter-wing part. The extra material there causes the CG further aft negatively influencing the longitudinal stability during flight.

8.9. Requirements Compliance

In Table 8.9 the requirements concerning the structures of the design can be found. Two out of four are met, the other two, CMR-SR-AC-MA-3 and CMR-SR-SU-3, were not researched. However, no unusual design choices were made that would result this requirement not being complied with.

Table 8.9: Compliance with the structural requirements.

	Requirement
✓	CMR-SR-AC-MA-1 - The aircraft shall use complex and non standard manufacturing processes only if no other option is possible.
~	CMR-SR-AC-MA-3 - The aircraft shall be easily serviceable for maintenance checks.
~	CMR-SR-SU-3 - The aircraft shall have a design which is easily accessible for repairs.
✓	CMR-SR-SU-5 - The aircraft shall be designed with components based on existing production methods.

8.10. Conclusion

The wing box, double bubble and stiffeners have been determined for the HAMMER, both in size, mass and material. For the wing box it is chosen to use CFRP. Using preliminary modelling techniques a skin thickness of 2.5 [cm] was found, with a spar thickness of 3.5 [cm]. Ten stringers are added along the wing box structure, four are L stringers which have as a side function to fasten the spar to the skin. The remaining six stringers are hit stringers which are equally spaced along the top and bottom skin panel. With this a first estimation of wing box weight was found to be 11367 [kg].

The double bubble thickness is comparable to that of other aircraft and the total weight of the fuselage is in line with the class II weight estimations. The fuselage skin and cabin wall will be made out of CFRP, while the fuselage frames, floor and stringers are made out of aluminium.

Recommendations

The structural design can be further optimised and improved in accuracy. Recommendations are given below to achieve this.

- No buckling analysis was performed, this might be critical for the wing structure sizing.
- More accurate data on torsional loads should be obtained in order to verify the structures ability to cope with shear stresses.
- The vibrational loads both wings induce on each other should be studied to make sure no resonance and flutter occurs.
- The fuselage should be resistant to dynamic (oscillatory loads) induced by the wing. Natural frequencies of fuselage should be outside the range of potential frequencies which are anticipated.
- Compression loads in the bottom of the fuselage can be limiting, this must be further researched.
- Investigate the impact of flight altitude to structural weight and efficiency of the aircraft.
- The increasing thickness of the wall may not be enough to efficiently distribute the stresses to achieve no stress concentrations, this must be analysed in more detail.
- Determine cut-outs in the vertical support wall that optimise uniform thickness and minimise K_t factors.
- Angle $\theta = 115°$ is not an optimum which means there is a θ for which the same volume can be enclosed by less material. This lies at 130°, it must be further researched if this angle can reduce the weight for the same effective cross-sectional area.
- The airframe can be more optimised by modelling the cross-section with longerons& stiffeners with an updated CG location. Also if values for torque due to manoeuvres are provided, fuselage frames to resist torque can be added in the analysis.

9 Flight Performance

In this chapter the flight performance characteristics of HAMMER are described. First, the payload range diagram is discussed, followed by the specific range and payload range efficiency. Furthermore the chapter describes the airfield and climb performance of HAMMER.

9.1. Payload Range Diagram

A Payload Range Diagram (PRD) was constructed for two flight configurations and is shown in Figure 9.1. The first configuration, denoted by the blue line, fuel tanks are only in the wings. In the second configuration an additional tank is placed in the fuselage as shown in Figure 6.7, with a size of 9 [m^3]. It should be noted that this additional fuel tank is placed in the front cargo hold and therefore two less LD-3 containers can be placed in the front cargo hold while this fuel tank is installed.

In the diagram four points are present. Point A, denotes the combination of zero-fuel mass with maximum payload mass of HAMMER. Fuel was added till the MTOW is reached which is denoted by point B which also denotes the harmonic range of HAMMER, equal to 2200 [*NM*]. Beyond point B, payload was exchanged for fuel until the fuel tank capacity is reached. Here, the two lines split due to the total available fuel storage. Beyond point C, the range of is increased by simply removing payload. Therefore, a range far beyond point C is not of interest, as its not economically viable to fly at low payload masses.

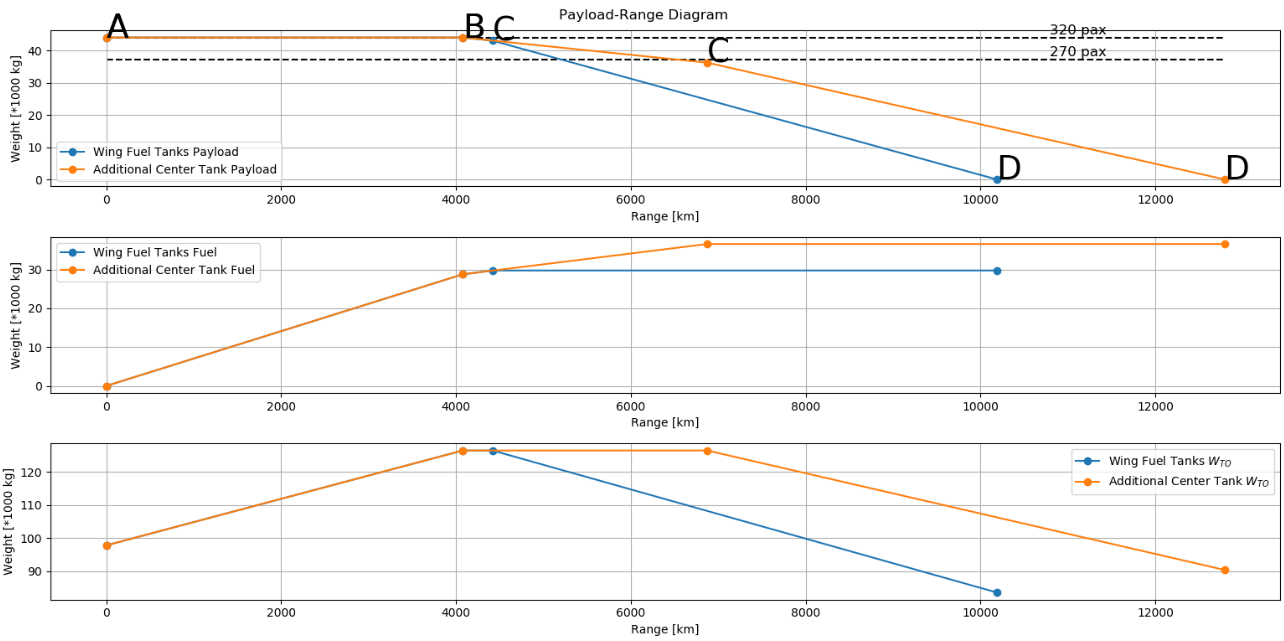

Figure 9.1: The Payload Range Diagram of HAMMER.

9.2. Flight Performance Characteristics

This section will go into detail about two important flight performance characteristics for measuring efficiency: the Specific Range (SR) and the Payload Range Efficiency (PRE).

9.2.1. Specific Range

The specific range is defined as the amount of distance an aircraft can fly with a certain amount of fuel, given a reference weight. Its value can be calculated using Equation 9.1. Here C_t is the thrust specific fuel consumption taken from the midterm report [21]. The specific range was calculated for the design cruise altitude of 36000 [*ft*] at a velocity of 0.78 Mach. As a reference weight the average weight of start of cruise and end of cruise was used, considering a take-off at MTOW, which results in 1.131 [*MN*]. The resulting SR is 305 [$\frac{m}{kg}$]. For reference, the optimum value for HAMMER, as obtained by using the optimum lift and drag coefficient value as given by Equation 9.2 [54], was found to be 313 [$\frac{m}{kg}$].

$$SR = \frac{v}{C_t \frac{C_D}{C_L} W} \quad (9.1)$$

$$C_{L_{opt}} = \sqrt{\frac{C_{D_0} \pi A e}{3}}, \quad C_{D_{opt}} = \frac{4}{3} C_{D_0} \quad (9.2)$$

For an A320 an SR of 297 [$\frac{m}{kg}$] was found, for a cruising altitude of 35000 ft at mach 0.78 and 96.2% MTOW [63]. It should be noted that this value is for an A320ceo, which is an older aircraft with 15-20% more fuel use than the A320neo. For a fair comparison the SR of HAMMER was calculated for the same inputs of cruising altitude, cruising speed and relative MTOW, resulting in a specific range of 288 [$\frac{m}{kg}$].

When a 20% fuel reduction of the A320neo with respect to the A320ceo is taken into account, it can be concluded that the specific range of HAMMER is only 20% smaller than that of the A320neo. At the same time HAMMER has a significantly higher payload mass, resulting in an overall more efficient design than the a320.

9.2.2. Payload Range Efficiency

The Payload Range Efficiency (PRE) is a metric that quantifies the performance of an aircraft for a combination of payload mass, required fuel and obtained range. It is defined in Equation 9.3 and one of the primary design objectives of HAMMER. In Equation 9.3 $W_{payload}$ and W_{Fuel} refer to the payload and fuel weight respectively, while R indicates the obtained range for this combination of payload and fuel. Their values can be obtained for different reference cases from the PRD presented in Section 9.1.

$$PRE = \frac{W_{Payload} \cdot R}{W_{Fuel}} \quad (9.3)$$

The PRE was calculated for two reference cases, the harmonic mission and a maximum range flight for a payload capacity of 270 passengers. For the latter it was assumed that the additional fuselage tank is installed in order to load enough fuel into the aircraft to obtain MTOW. The resulting PREs are 6237 and 6813 [$\frac{kg \cdot km}{kg}$] respectively. In comparison, the harmonic mission of the A321neo has a PRE of 7611 [$\frac{kg \cdot km}{kg}$]. The difference is most likely due to the combination of the relative high amount of reserve fuel HAMMER carries of corresponding to its low range, with roughly 30% of the total fuel mass being reserve fuel. Although unrealistic, if no reserve fuel was assumed HAMMER would have a Payload range efficiency of 9500 [$\frac{kg \cdot km}{kg}$] which is considerably higher than the values previously stated.

9.3. Airfield Performance

In this chapter the airfield performance of HAMMER is described. First the take-off performance is computed, followed by the landing performance

9.3.1. Take-Off performance

The take-off performance is measured by its required field length. The required field length is preferably smaller than 1800 [*m*], such that HAMMER is categorised by ICAO Aerodrome reference code 3. The take-off performance was determined for International Standard Atmosphere (ISA) sea-level conditions, as this is takes as the standard reference case for comparing take-off performance of different aircraft. Additionally, no slope, wind or other non-ideal weather conditions were assumed to be present.

The required length was split into ground run, transition and airborne phase. Only a normal take-off is analysed, an aborted take-off and one-engine operative take-off are not covered. The ground phase is ended by HAMMER reaching the lift-off velocity, v_{LOF}, which was set equal to 1.2 v_{stall}. The ground run distance, x_{ground} is given by Equation 9.4 [54]. The stall velocity, v_{stall}, is given by Equation 9.5. For the take-off a $C_{\text{L, max}}$ of 2.8 was taken from Table 3.6.

$$x_{\text{ground,TO}} = \frac{(v_{\text{LOF}}^2)(W/g)}{2\left\{T - [D + \mu_r(W-L)]_{\text{av}}\right\}} \quad (9.4)$$

$$v_{\text{stall}} = \sqrt{\frac{2W}{\rho S C_{L,\max}}} \quad (9.5)$$

Here, μ_r is rolling friction coefficient and was set equal to 0.02 [11]. The weight was assumed constant and equal to the MTOW. Average value were taken for the lift and drag, computed at 0.7 v_{LOF} [54]. For the drag calculation, ground effect was taken into account by means of a ground effect factor, ϕ [11]. It was only taken into account for the forward wing and it was assumed that 60% of the lift force is generated by this wing, as mentioned in Subsection 4.1.4. The ground effect is defined by Equation 9.6.

$$\phi = \frac{(16h_W/b)^2}{1+(16h_W/b)^2} \tag{9.6}$$

Where h_w is the height of the forward wing measured from the ground and b is the span width.

After the plane has achieved lift-off, it will need to transition and climb to reach the screen height, h_{scr}. The horizontal distance required for rotation and climb are given by Equation 9.7 and Equation 9.8 respectively [50] [34].

$$x_{\text{trans, TO}} = \frac{v_{\text{LOF}}^2}{0.15g}\sin(\gamma_{\text{TO}}) \tag{9.7}$$

$$x_{\text{climb, TO}} = \frac{h_{\text{scr}} - (1-\cos\gamma_{TO})\frac{v_{\text{LOF}}^2}{0.15g}}{\tan\gamma_{TO}} \tag{9.8}$$

In these equations γ_{TO} is the flight path angle during take-off, which was assumed to be equal to 3°[1].

Summing these three different phases result in a total take-off distance of 1266 [*m*]. This is significantly lower than the take-off length of the A320-200 that is equal to 2090 [*m*] under ISA conditions [2]. This is likely due to the fact that the analysis does not consider any failure, aborted take-off or less than ideal conditions as well as the fact that that HAMMER has a significantly higher available thrust at take-off and low lift-off speed due to its high lift coefficient.

9.3.2. Landing Performance

Similar to the take-off performance, the landing performance is also described by its required field length and is preferably smaller than 1800 [*m*]. It is again determined for sea-level conditions and no slope, wind or other non-ideal weather conditions were assumed to be present.

Again the required field length was split into three parts, airborne, transition and brake phase. The airborne distance for approach, x_{airborne}, is given by Equation 9.9. The approach velocity, v_a, was set equal to 1.3 v_{stall} [11].

$$x_{\text{airborne}} = \sin(\gamma_a)\frac{v_a}{\Delta n \cdot g} + \frac{h_{scr} - (1-\cos(\gamma_a))\frac{v_a}{\Delta n \cdot g}}{\tan(\gamma_a)} \tag{9.9}$$

γ_a and Δn denote the flight path angle during approach and change in load factor respectively. These were set equal to 3°and 0.10 [50].
Next the transition phase and the break phase that is required after touchdown were considered. The required transition time was assumed to be 2 [*s*] [50]. This results in a transition distance, x_{trans}, of approximately 2.6 v_{stall}.

The braking distance is similar to the breaking distance for take-off and is given by Equation 9.10. However, instead of thrust, thrust reversal expressed by T_{rev} is present. A conservative approach was taken and therefore no thrust reversal was assumed. Additionally the braking coefficient, μ_{br} is used instead of the rolling coefficient. This was assumed equal to 0.4 [34] [11].

$$x_{\text{brake}} = \frac{W \cdot v_a^2}{2\left\{\bar{T}_{\text{rev}} + [D + \mu_{br}(W-L)]_{\text{av}}\right\}} \tag{9.10}$$

Regulations require that the calculated landing distance is factored by $\frac{10}{6}$ for safety reasons [50] [56]. This results in a landing field distance of 1437 [*m*]. For comparison, the A320-200 has a required landing field length of 1982 [*m*] at sea level conditions, although it was unclear to what other conditions regarding weather and slope were considered [56]. The difference can be further explained by the same type of reasoning given in Subsection 9.3.1.

[1]Personal Communication P.C. Roling [22-6-2020]
[2]https://www.skytamer.com/Airbus_A320.html [Cited 24-6-2020]

9.4. Climb Performance

A significant part of the mission profile consists of climbing to the desired cruise altitude. The climb performance of HAMMER was defined by its vertical speed, the Rate of Climb (RoC). The RoC was derived from equations of motions of an aircraft as seen in Figure 9.2.

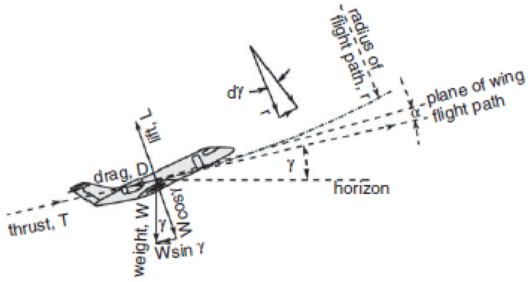

Figure 9.2: Simplified forces on an Aircraft [34].

This results in a RoC described by Equation 9.11. Here $\frac{dv}{dH}$ denotes the change in velocity over a change in altitude. Since HAMMER is a commercial aircraft, it is unlikely that it will have significant acceleration during climb. Thus, this was assumed to be equal to zero and results in Equation 9.12.

$$RoC = \frac{v[(T-D)/W]}{1+(v/g)(dv/dH)} \tag{9.11}$$

$$ROC = \frac{v(T-D)}{W} \tag{9.12}$$

It should be noted that drag changes with velocity and altitude and it was assumed that HAMMER climbs in a clean configuration with corresponding lift and drag coefficient taken from Table 3.6 and Table 4.6 respectively. The thrust of a turbofan engine is dependent on the velocity as well as the altitude. The relation can be seen in Equation 9.13 [54].

$$T = T_{\text{stat}}\left(1 - k_T \cdot v^{\frac{1}{2}}\right) \cdot \left(\frac{\rho}{\rho_0}\right) \tag{9.13}$$

Here ρ_0 is the density at zero altitude. The static thrust, T_{stat}, was assumed to be equal to T_{TO}. The thrust correction factor, k_T was determined using the relation between the thrust and velocity for given bypass ratios and was determined to be equal to 0.03. The higher the bypass ratio, the more a turbofan behaves as a turboprop and therefore the greater the decrease in thrust for increasing velocity.

As seen in Equation 9.13, the thrust decreases with altitude due to the lower mass flow rate caused by the lower density. The thrust slightly increases with altitude due to the lower ambient temperature, but this effect is minimal and was therefore neglected [54]. The effect of humidity on turbofan performance is minimal and was also neglected. Additionally, since the RoC is computed for different altitudes, the true velocity (airspeed) commonly denoted by V_{tas} was used.

The RoC was plotted as a function of true velocity, for different altitude, this can be seen in Figure 9.3. The RoC decreases for increasing altitude and the RoC shows a parabolic relation with velocity. This is due to the fact that the thrust increases almost linearly with velocity, while the drag increases cubically.

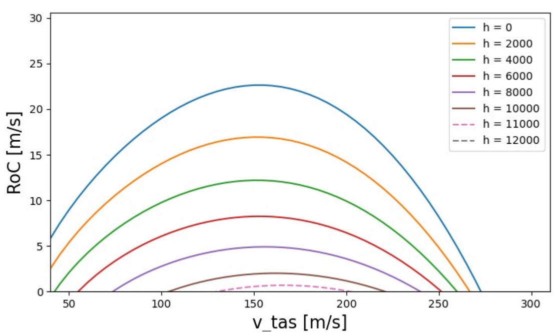

Figure 9.3: RoC as a function of true velocity, for different altitude.

As seen in Figure 9.3, the service ceiling, defined by a maximum rate of climb of 0.5 $[\frac{m}{s}]$ is roughly equal to 11000 $[m]$. In comparison, the A330-200ceo has a maximum service ceiling of 13000 $[m]$. The A330-200ceo has comparable thrust to weight ratio and similar cruise speed. In addition, HAMMER shows an adequate climb performance with a maximum RoC of 22.5 $[\frac{m}{s}]$. Moreover, the RoC and the service ceiling is likely underestimated, as lift was assumed equal to weight which is not the case during climb. Additionally the MTOW was used throughout the computation. Other factors could possibly be overestimated that nullify this effect.

9.5. Wake Turbulence

During operation the aircraft disturbs the air it passes through, causing it to become turbulent. This wake turbulence can be dangerous for other planes as it can lead to unwanted course deviations, unwanted rolling patterns and worst case even engine failure. This section briefly covers how wake is classified and which requirements need to be met. This section was previously described in the midterm report.

Table 9.1: ICAO Wake Categories.

ICAO Category	Identifier	Explanation
Light	L	MTOW $\leq$ 7000 [kg]
Medium	M	7000 [kg] <MTOW <136000 [kg]
Heavy	H	MTOW >136000 [kg]
Super Heavy	J	Airbus A380-800

Current ICAO wake categories only depend on the maximum take-off weight, as can be seen in Table 9.1 [3]. The aircraft wake class influences the separation distance between two aircraft and is dependent on the class of both the leading and the following aircraft. On top of that it also influences the separation time between take-offs and landings on a runway. Optimising wake performance can therefore increase the capacity of an airport and increased efficiency of airspace occupation.

Since HAMMER was designed to operate on small, regional airports it is desirable to keep the wake category as low as possible. This way the aircraft does not disturb airport runway traffic. Therefore it is important for the design to stay within category M.

It should be noted that the current wake categorisation is old and subject to change in the near future. It has been shown that the ICAO categorisation is not efficient and many separation margins between classes can safely be reduced. This is attractive for airports since it allows them to increase their runway throughput.

Thus, ICAO has been working in a joint study with Airbus, the Federal Aviation Administration (FAA), European Organisation for the Safety of Air Navigation (EUROCONTROL) and European Union Aviation Safety Agency (EASA) on the new Wake Turbulence Re-categorisation (RECAT) system. This project consists of three phases. In the first phase, the current wake categories are replaced by a new system consisting of six different wake categories [24]. Every aircraft will be placed in one of these six categories, with strict separation rules, both distance- and time-wise. In the second phase the classification will be done based on 115 different categories, requiring a much more elaborate analysis on wake generation. In the third phase of the project the phase two model will be extended to incorporate meteorological data in order to reduce separations even further.

The RECAT-EU system is currently being used at Paris-CDG and Paris-Le Bourget, showing an increased runway capacity between two and four aircraft per hour during peaks [4]. The system is also being used in London-Heathrow [5] and several airports in the United States [19]. The system is easy to implement at relatively low cost [24]. Therefore, it can be assumed that the RECAT system will become the standard before the EIS of 2035. The categories are defined by aircraft span and MTOW. For this system, HAMMER would fall in category C.

9.6. Verification and Validation

The PRD was checked for consistency with the class I estimations. Where the class 1 estimation uses fuel fractions and a target range to calculate the fuel mass, the PRD is generated by taking those fuel fractions and defining a fuel mass, for which a range is calculated. It was observed that the the harmonic range calculated for the PRD was equal to the design range, which confirms a correct implementation of the formulas.

Other than that all calculations done in this chapter were unit tested. Apart from that it is complicated to verify the defined parameters due to the nature of their computation. However as mentioned in the sections, the parameters were validated by comparing their values to similar aircraft.

[3]https://www.skybrary.aero/index.php/ICAO_Wake_Turbulence_Category [cited 22 June 2020]
[4]https://www.ecologique-solidaire.gouv.fr/sites/default/files/RECAT_EU.pdf [Cited 22 June 2020]
[5]https://www.internationalairportreview.com/news/68031/enhanced-time-based-heathrow/ [Cited 22 June 2020]

9.7. Sustainability Analysis

In this chapter only parameters were defined, no design choices were made. Therefore, a sustainability analysis is not present in this chapter.

9.8. Risk Assessment

The same reasoning as above applies. There are no inherent risks as no design choices were made. The only risks associated to flight performance is that the computed parameters are inaccurate.

9.9. Requirements Compliance

The requirements that are met concerning the flight performance are given in Table 9.2. No extensive research was performed on the cruise performance of HAMMER, but it is able to meet the required cruising altitude and speed. Additionally, HAMMER is considered to have adequate cruise performance, considering that the specific range per kilogram payload is significantly higher with respect to the A321neo. Moreover, the payload range efficiency was considered for the design of HAMMER. However, to meet the requirements for turn-around time significant cuts on PRE had to be made. Of course, within the given possibilities the PRE has been optimised as much as possible. Therefore it was given an approximate sign.

Table 9.2: Compliance of the flight performance requirements.

	Requirement
✓	CMR-SR-AC-CL - The aircraft shall have a adequate climb performance, as specified in the CS-25.
✓	CMR-SR-AC-CR - The aircraft shall have an adequate cruise performance.
✓	CMR-SR-AC-FP-3 - The aircraft shall be able to fly a holding pattern in case the runway at the arriving airport is occupied.
✓	CMR-SR-AC-FP-4 - The specific range of the aircraft during cruise condition should be within 5% of its optimum value.
~	CMR-SR-AC-FP-7 - The aircraft shall have a design priority to maximise the payload range efficiency.

9.10. Conclusion

HAMMER has a harmonic range of 2200 [*NM*] and this range can be further expanded by replacing payload for additional fuel. The specific range and payload range efficiency of HAMMER is comparatively low, but it has a significantly higher payload mass and a relatively high amount of reserve fuel. Its take-off and landing performance, makes it fall under ICAO Aerodrome reference code 3C at ISA sea level conditions. The computed lengths are shorter than the A320-200, but this is likely due to the fact that only the most ideal conditions were considered. In addition, HAMMER shows adequate climb performance with a maximum RoC of 22.5 and a service ceiling of roughly 11000 [*m*]. Lastly, HAMMER will fall in ICAO wake category M and RECAT-EU category C.

Recommendations

The flight performance computations can be improved in terms of accuracy. Recommendations are given below to achieve this.

- For take-off as well as landing, more critical conditions such as heavy crosswinds and rain need to be considered for worse case scenario field length requirements
- For the airfield performance, constant thrust, drag, velocity was used through phases. Additionally, a large number of assumptions were made. A more detailed analysis would lead to more accurate results.
- The climb performance was performed for simplified equations of motion. Once more information is known regarding HAMMER, a more accurate climb performance can be computed.
- More research can be done into the wake category and how it will specifically change in the future, such that HAMMER can be optimised for this.
- In the future the wake categorisation will be performed more specifically. Due to the large reduction of the vortices generated by the wings, HAMMER will likely perform well better than aircraft with the same ICAO/RECAT-EU wake category, but this must be researched in more detail.

10 Ground Operations

This chapter presents the ground operations aspect of the HAMMER. First the selection of an electric taxiing system is explained, after which turnaround procedures are discussed.

10.1. Electric Green Taxiing System

Fuel costs account for up to 50% of the airline direct operating costs and the CO_2 emissions caused during the taxiing phase of one aircraft are equivalent to the CO_2 emissions produced by 400 cars on European roads[1]. Research was performed to find a way of reducing this large amount of fuel spent when the aircraft has not taken-off yet. Electric Green Taxiing Systems (EGTS) have been developed by different companies. Some systems are placed on the nose landing gear but these were discarded for this project due to traction, agility and performance constraints. Thus, an EGTS on the main landing gear, particularly the one developed by Honeywell and Safran, was chosen instead. This system uses power from the Auxiliary Power Unit (APU) generator to electrically power motors fitted to the main landing gear wheels. This allows the aircraft to pushback and taxi towards the runway without assistance and with the main engines turned off.

The implementation of an EGTS offers many advantages with regards to the environment, the operational costs and the safety of the ground operational procedures. Implementing such a system would reduce the fuel costs per flight per aircraft by 4%, which is approximately equivalent to $650[2]. This could lead to airlines saving up to $500,000 per aircraft per year, as well as a reduction of their environmental footprint. The emissions in ground operations would be greatly decreased, with reductions of 51% in NO_x, 61% in CO_2 (reducing the yearly CO_2 emissions for short-haul flights from 13 to 5.07 million tons), 62% in HC and 73% in CO[3]. This would be a great step in the decarbonisation of air transport.

Moreover, noise would be greatly reduced in airport environments and residential areas nearby. From an operational point of view, ground equipment is no longer needed for pushback or towing operations. The autonomy of the aircraft on the ground would reduce the turnaround time of the aircraft, contributing to the decongestion of airports. By having the engines turned off when the aircraft arrives at the gate, the unloading of bags and the disembarkation would be much faster. Also, the ground-handling staff would have a faster and safer access to the aircraft as there would be no risk of damage from foreign objects being sucked into the engine. Finally, line maintenance time would be lowered due to a reduction in brake wear and an extension in engine life.

This system supposes two main drawbacks. First of all, this seems would add additional mass to the Operational Empty Weight (OEW), which will increase the fuel consumption during the flight. Secondly, this system has currently only been designed for single-aisle aircraft. However, with an Entry Into Service (EIS) of HAMMER in 15 years from now, it is expected that a similar system will exist for twin-aisle aircraft. As no research has been published yet about a twin-aisle EGTS, a linear relation between the MTOW and the weight of the motors was assumed for HAMMER. Airbus is currently implementing a 400 [kg] EGTS designed by Safran and Honeywell on the A320 family, which have an average MTOW of 79875 [kg][4]. Thus, for a MTOW of 126528 [kg], the motor weight will be 633.63 [kg].

Another option that was considered was having electric ground equipment to help with pushback. However, the HAMMER project strives for a minimised environmental footprint, as well as better health and safety of the ground-handling staff. For this reason, a full electric taxiing system was chosen.

10.2. Turnaround

A low turnaround time is a key aircraft feature from the perspective of a customer. It is therefore important to make an accurate estimation of the time it takes to prepare HAMMER for a new flight. In this

[1] https://tec.ieee.org/newsletter/march-april-2014/electric-green-taxiing-system-egts-for-aircraft [cited 22 June 2020]
[2] https://www.aviationtoday.com/2019/05/01/electric-taxiing-systems-past-present-possible-future/ [cited 22 June 2020]
[3] https://www.safran-landing-systems.com/systems-equipment/electric-taxiing-0 [cited 22 June 2020]
[4] https://www.airbus.com/aircraft/passenger-aircraft/a320-family.html [cited 22 June 2020]

section first a basis box wing aircraft turnaround time is estimated where no special features of HAMMER and ground equipment normally available to an A320 were assumed. Secondly, the effect of HAMMER's characteristics and the implementation of turnaround options is calculated to arrive at a final turnaround time. Turnaround data of reference single aisle and double aisle [2][3][4][5][56][57][58][59] aircraft are used. Numbers are selected conservatively to avoid a turn around time that is too optimistic.

10.2.1. Basis Turnaround Time

Passenger Handling

To determine the time taken for the deplaning and boarding of a box wing aircraft, the deplaning and boarding rates of the A330 were taken, these equal 25 [$\frac{pax}{min}$] and 15 [$\frac{pax}{min}$] respectively. The data of a wide body aircraft was used, as the amount of aisles has significant impact on the speed of passenger movement. It was assumed that the 320 passenger exchange is 100% and that no passengers with reduced mobility are present. In addition, last passenger seating allowance and head counting was assumed to add another 4 [min]. Positioning of the the bridges or stairs was taken equal to 2 [min], while removing the equipment was determined to take 1.5 [min]. Positioning can be initiated once the aircraft has come to a full stop. As the box wing aircraft is required to use the same airport facilities of an aerodrome reference code C aircraft, the bridge/stair positioning time of an A321 was selected. Lastly, it was assumed that passenger deplaning and boarding takes place via one passenger boarding bridge or via one or two boarding stairs. In the latter case, it is assumed that the passenger movement is divided equally over the two doors and that the deplaning and boarding happens at the same rate as via passenger boarding bridges [57].

Cargo Handling

For cargo handling no bulk loading was assumed. As stated in Chapter 6, in normal operations 24 LD3 containers will be used for unloading and loading the cargo. Again the time required for equipment positioning and removal of the A321 was used which equals 2 [min] and 1.5 [min] respectively. The same reference aircraft provided the rate for cargo loading and unloading: 1.5 [min] per container. As explained in Chapter 7, efforts were made to place the forward wing such that a relatively long aft cargo hold can be achieved. To clearly show the effects of this long cargo hold in Subsection 10.2.2, the assumptions in this section are aimed at a "normal" forward wing placement. For the basis turnaround time, it was assumed that the box wing has one cargo hold in front of the forward wing and one cargo hold after this wing. For the wide-body reference aircraft, the Unit Loading Device (ULD) number ratio between the aft and forward cargo hold is between 4:3 or 5:4 respectively. As the forward wing of a box wing is positioned more forward than a conventional wing, for the the box wing it was assumed that this ratio equalled 2:1. This results in 16 ULD3s in the aft cargo hold and 8 ULDs in the forward cargo hold. Each cargo hold will be serviced by one container loader. As for passengers exchange, a 100% cargo exchange was assumed. 24 LD3's are used in normal operations. The volume available for 6 extra LD3's was assumed not to be loaded in normal operations.

Refuelling

For the time required for refuelling first Equation 10.1 was defined [30].

$$\dot{v} = \dot{v}_0 * e^{\alpha_f t_f} \quad (10.1)$$

Where $\dot{v}$ is the fuel volume flow [$\frac{L}{min}$], $\dot{v}_0$ is the initial fuel volume flow [$\frac{L}{min}$], t_f is the refuelling time in minutes and α_f [min^{-1}] is the alpha factor. The latter is an indicator of how the volume flow decreases over time, due to increased static pressure and the closing of fuel pipes as the fuel tanks fill up. Then, Equation 10.1 was translated to an equation for total refuelling time, using V_f, the volume of fuel that is to be added in the tanks [55].

$$V_f = \int_{t=0}^{t_f} \dot{v} dt = \frac{\dot{v}_0}{\alpha_f}\left(e^{\alpha_f t_f} - 1\right) \quad (10.2) \qquad t_f = \frac{1}{\alpha_f} \cdot Ln\left(1 + \frac{V_f \cdot \alpha_f}{\dot{v}_0}\right) \quad (10.3)$$

Class II estimations provided that for a typical flight the aircraft needs to refuel 23896 [L]. The alpha factor was assumed using and a conservative value of -0.031 [min^{-1}] was taken [30][55]. From the same sources a $\dot{V}_0$ of 1575 [$\frac{L}{min}$] was taken. Furthermore it was assumed that refuelling takes place only when no passengers are on board. Similar to the A321, only one fuel truck was assumed available for fuel services to the box wing. The A321 accounts 2.5 [*min*] for connecting the fuel truck to the aircraft and the same time for disconnecting from the aircraft, for the basis turnaround time the same values were used.

Catering

The duration of catering services depends on the amount of Full Size Trolley Equivalents (FSTEs) that need to be swapped. With a small margin taken into account and correcting for the amount of passengers and range, from the Airbus reference aircraft it was assumed that 14 FTSEs were needed. The same swapping rate as for an A330 was assumed, 1.5 [$\frac{min}{FSTE}$]. Servicing was assumed to be done by one catering truck that sequentially services the forward right door and the aft right door, similarly to an A321. From the same source it was found that positioning the truck takes 2 [*min*] while removal takes 1.5 [*min*][57]. Driving from door 1R to door 2R takes another 2 [*min*][57]. Furthermore it was assumed that catering takes place without passengers on board.

Cleaning

It was assumed that the cleaning of the aircraft takes place when passengers are present in the aircraft. Cleaning will thus happen while the aircraft is either being refuelled, catered or both.

Other Ground Operations

Once the aircraft has come to a complete stop, it will be connected to a ground power unit. Also, the servicing of potable water can be started. From wide-body reference aircraft this takes 16 [*min*]. For hygienic reasons, only after potable water servicing, waste water servicing can be commenced. Derived once again from wide-body reference aircraft, this takes approximately 15 [*min*]. Optionally, air conditioning hoses can be connected to the aircraft.

The procedures described above resulted in a Gantt chart of the basis turnaround time, presented in Figure 10.1. The deplaning, catering and boarding of the aircraft together formed the turnaround critical path. Reducing the time of these operations results in a reduced turnaround time. Once one manages a sufficiently large time reduction, further reductions can also be achieved by reducing the time for cargo loading and unloading or the refuelling time.

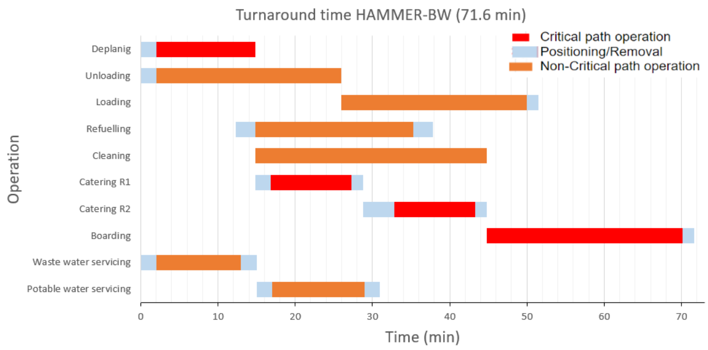

Figure 10.1: Gantt chart of the basis turnaround time of the HAMMER.

10.2.2. Optimised Turnaround Time

In the field of ground operations, the HAMMER allowed for some attractive characteristics. The first of those being the extra large aisles discussed in Chapter 6. The wide aisles allow passengers to pass each other in the aisle and thus allows for a reduction in boarding time. With respect to an A330 aisle the HAMMER aisle is 16 [*inch*] larger. According to [62] a single aisle aircraft increases its deplaning and boarding rate by 5-7% by an aisle widening of 8 [*inch*]. Two assumptions were made: this effect is similar for a double aisle aircraft. The widening of 16 [*inch*] instead of 8 [*inch*] has a marginal effect. From these two assumptions, conservatively an increase of 7% in deplaning and boarding rate was assumed. This results in rates of 26.75 [$\frac{pax}{min}$] and 16.05 [$\frac{pax}{min}$] respectively.

Secondly a method was considered to reduce the time taken for catering. A separation curtain was introduced at the forward right door, allowing the exchange of full size trolley equivalents (FSTE's) without disturbing the passengers. The 'kitchen counter' of the galley will be made liftable to allow FSTE movement under the counter without interfering with the passenger's path to or away from their seat. This can be seen in Figure 10.2.

Servicing the forward galley could thus begin when HAMMER is at full stop instead of after the deplaning. It was assumed that servicing speed for the forward galley was thereby reduced by 10% to 1.65 [$\frac{min}{FTSE}$]. The aft galley would still be serviced without passengers on board. Using a second catering truck to service the aft galley, reduced the turnaround time by several extra minutes, as the moving and re-positioning time of the truck was reduced. Instead of loading 7 FSTE's forward and 7 aft, 8 FSTE's were loaded forward and 6 aft, leading to a additional time reduction.

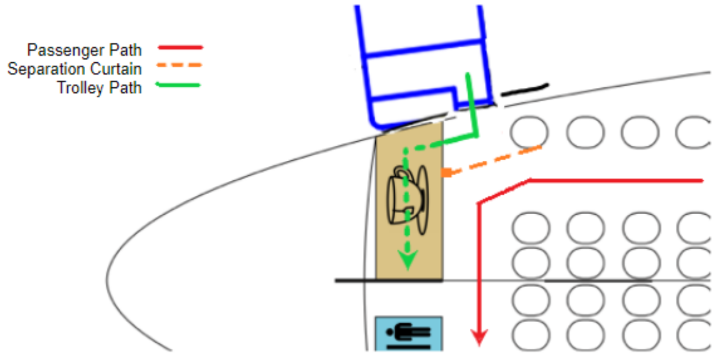

Figure 10.2: FSTE path behind the separation curtain.

With this adjustments the process of refuelling had become part of the critical path. The option for fuelling with passengers on board was studied for this purpose. However, due to safety regulations this was an option that could not be a featured. It is only within the power of an airport to (easily) allow fuelling with passengers on board. It is thus advised to double the amount of fuel trucks from one to two to increase the fuel flow. It was assumed that the initial volume flow doubles from 1575 [$\frac{L}{min}$] to 3150 [$\frac{L}{min}$]. For the occasional airport where refuelling is allowed with passengers on board, one fuel truck would still be sufficed. An design iteration involved the placement of fuel partly in the rear wing. As this increased the fuel piping complexity, the value of α_f was assumed to decrease to -0.041 [min^{-1}]. The latter assumption did not affect the total turnaround time.

With the time required for passenger handling, catering and refuelling reduced, it became interesting to reduce the time taken for cargo handling. Initially, an unique characteristic of the box wing was its allowance for a continuous cargo hold. Cargo could then be unloaded from one cargo door, while loading was done in parallel at another cargo door. However, it became apparent that lengthwise the hold had to be split into two parts by a wall. As in normal operations the forward cargo hold is unused, the box wing thus ended up with the usual two cargo holds. Still an advantage was found, unlike often the industry standard, the two used cargo holds are equal in size. For two cargo holds this resulted in an optimal (un)loading time.

To evaluate the increased loading time due to discarding the continuous cargo hold, the time for handling a continuous hold was calculated and compared to split hold handling. A 10% increased was assumed in ULD (un)rate, caused by congestion in a continuous unloading and loading flow. Moreover, it was found that additional time was required to let the unloading process create open volume for the loading process. A continuous hold resulted in a cargo handling time of 44.75 [*min*], while the handling time for a split cargo hold was computed as 43 [*min*]. Both cargo holds utilised two doors and two cargo loaders.

All of the improvements mentioned above lead to a new Gantt chart of the turnaround time, as presented in Figure 10.3. This resulted in a total turnaround time of 48.5 minutes, which, with respect to the basis turnaround time, is an improvement of 23.1 [*min*]. The turnaround of and A320 was found to be 44 [*min*], the turnaround time of HAMMER with respect to the A320 is thus a 10% increase in turnaround time

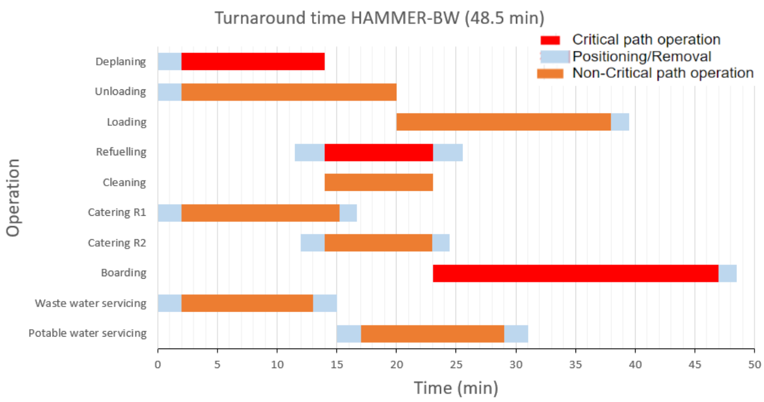

Figure 10.3: Gantt chart of the optimised turnaround time of the HAMMER.

for 113% more passengers and comparable range [56]. The turnaround of and A330 was found to take 59 [*min*], the decrease in turnaround time of HAMMER with respect to the A320 is thus a 18% decrease in turnaround time for a comparable payload and 65% smaller range. A factor to take into account was that when two stairs are used for passenger movement, the left side of the aircraft becomes inaccessible during deplaning and boarding. The passengers path to the rear stair cannot be crossed by ground handling units. This mainly affected cargo loaders operating from the left side of HAMMER. Resulting in a significantly larger turnaround time of 76.9 [*min*]. For operations it is thus always advised to solely make use of the first left door.

Compared to a single aisle aircraft, HAMMER makes use of an additional fuel truck and an additional catering truck. However, for the airport and the operator the discomfort (cost/limited resources) of using these extra trucks is marginal[5]. E.g. two trucks servicing for 9 minutes is not worse than one truck servicing for 18 minutes.

Additionally, to validate the proposed way of servicing HAMMER on the ground, a layout of the apron was drawn in Figure 10.4.

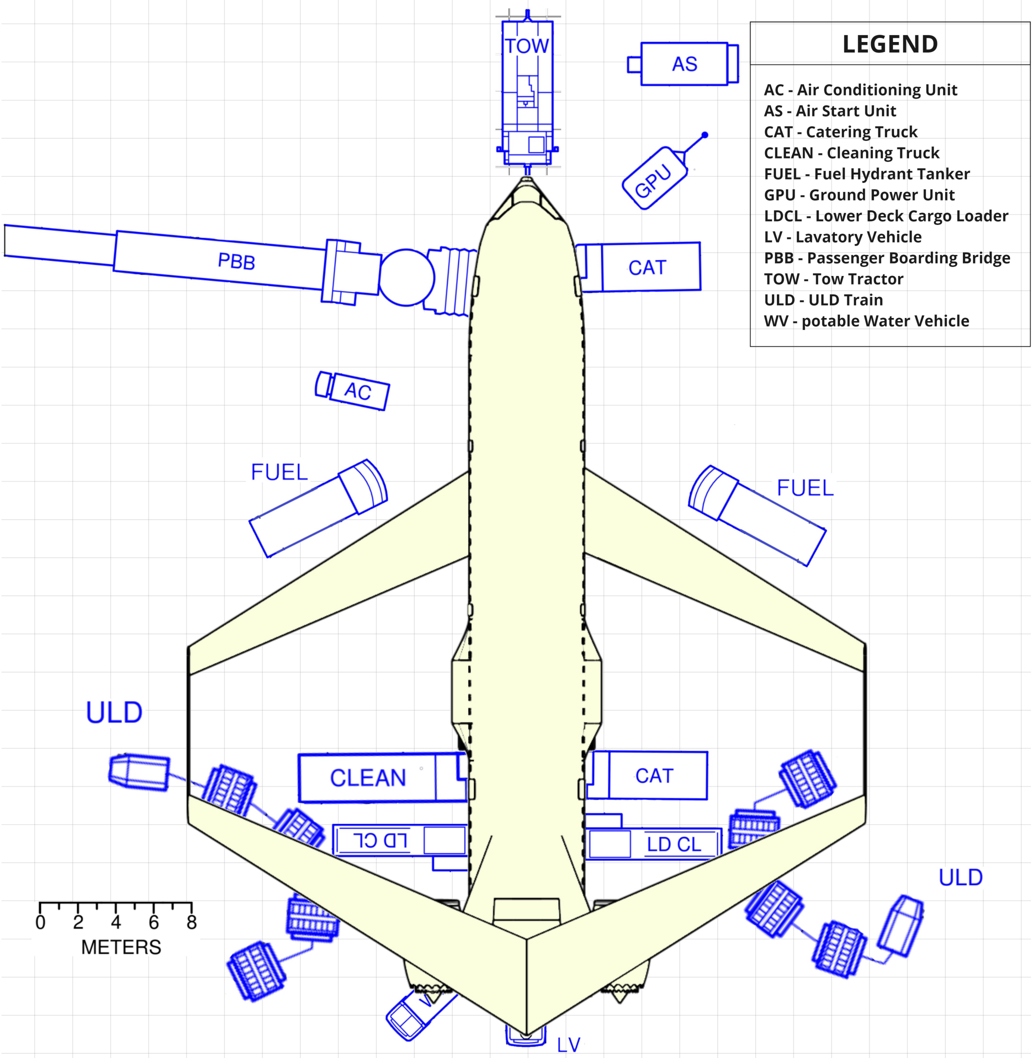

Figure 10.4: HAMMER apron layout.

Whenever no passenger bridge is available, deplaning and boarding can take place via an air stair. The figure shows that two vehicles are parked partly under the HAMMER fuselage or engine. Figure 10.5 shows that these vehicles do indeed fit in their desired positions.

[5]Personal Communication P.C. Roling [9 June 2020]

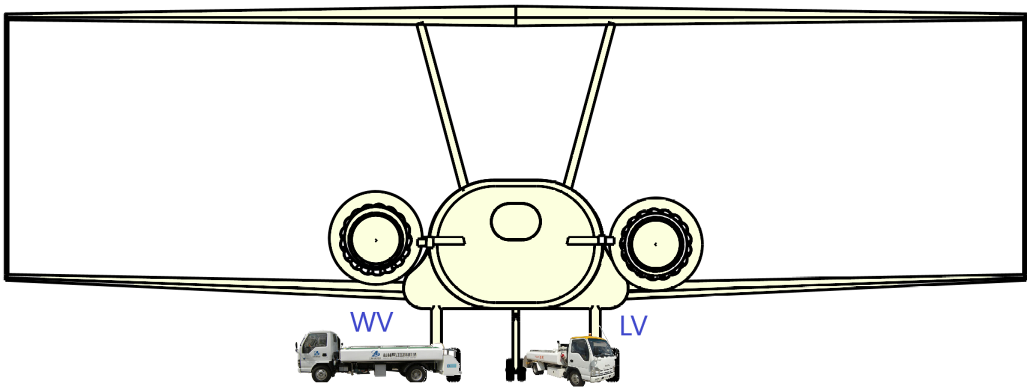

Figure 10.5: Fitting of potable water and lavatory vehicle under the fuselage.

Other improvements besides those mentioned in this chapter were considered, but were judged unfeasible or not ready by 2035. Still, they are worth mentioning for future studies for box wing aircraft. Firstly, an aircraft carried air stair was studied as an option for passenger (dis)embarking. However, systems for this stair are heavy and require relatively much maintenance[6]. A second consideration was a tail cargo door, allowing the two aft cargo holds to be loaded by the existing cargo doors, whilst being unloaded from the rear door. This was discarded as the idea involves a large extra cutout in the fuselage. In addition, the positioning of two container loaders at the rear was difficult, if not impossible. One loader positioned sideways at the tail also was not an option, as it resulted in long (un)loading processes.

Other recommendations can be made from the perspective of ground operations. In earlier stages of the design it was found that the HAMMER landing gear should be sized longer than required, to allow for comfortable usage of the passenger bridge. In a late stage of the project this extra length was discovered to be unnecessary. As the effect of an extra long landing gear is a weight and volume penalty, it is highly recommended that the strut length is reduced to its minimum in further phases. Ground servicing vehicles, such as the WV, that will interfere with the lowered fuselage can be re-positioned without losing their current way of operating. Their hose lengths are sufficiently long [56].

Furthermore it is strongly advised to look into the way cargo holds and their doors are used. Currently the HAMMER is equipped with four doors instead of the usual two. This results in a heavy weight penalty which is currently not accounted for. In addition, the rarely used forward cargo hold volume is not flown for free. Several directions are proposed as possible approaches:
- The forward cargo hold volume can be used in a more permanent way that does not require any cargo doors. One can think of a permanent fuel tank or more batteries.
- Openings in the middle wall (also at a weight penalty) could be created to unite the split cargo holds. Together with the previous suggestion a single door could even be sufficient. For an acceptable turnaround time, however, a minimum of two doors is suggested.

A final important note: normally driving vehicles under the fuselage or wing (besides fuelling and water service trucks) is not allowed. This rule applies differently for HAMMER: as usual, the area under the HAMMER fuselage and forward wing is not to be accessed by the usually prohibited vehicles. However, the area under the aft wing and the connectors is available for parking or under-passing, as these are sufficiently high, or not situated in places where elevated ground operations take place. This will have to be approved by air traffic authorities such as ICAO.

10.3. Verification and Validation

For verification, a variety of tests was done. Numerous calculations were executed of time taken for certain ground operations. It was checked if the outcome of these calculations had time as unit. In addition, the used equations were tested on the entry of '0'. For example the refuelling of the HAMMER with 0 $[L]$ of kerosene resulted in a refuelling time of 0 $[min]$. Sanity of all numbers was evaluated and they were

[6]Personal Communication Dr. Ir. G. La Rocca [8 June 2020]

recalculated by hand if suspicion rose. If deemed necessary, this resulted in a reconsidered equation or input value. In general, equations that were self-derived from sources were re-derived from other sources and adjusted whenever necessary.

Validation of ground operations was done in various ways. A first means was the generation of apron layouts. This validates that the position of ground operation units that operate in parallel are not interfering. It was validated that the space for passengers, catering trolleys or ULD's was available for loading, by checking if the aforementioned of the previous flight were unloaded first. The time taken by each individual ground operation was validated by comparison with four to eight reference aircraft. A similar check was performed for the total turnaround time of HAMMER. Lastly the angles, height and positions of ground operation units serving HAMMER were compared to those servicing the reference aircraft. When significant differences were found, the feasibility of the intended way of operating was checked. This, for example, resulted in a slight lading gear extension to avoid a steep slope for the passenger boarding bridge.

10.4. Sustainability Analysis

Sustainability is not a commonly prominent aspect of ground operations. However, it can certainly be assessed. HAMMER allows for a lower number of flights for the same amount of passengers, and thus a lower amount of turnarounds. As each turnaround is accompanied by a high number of ground vehicle movements, a reduction of turnarounds will reduce the harmful emissions of these vehicles. Secondly, a small turnaround time has its sustainable benefits. It reduces the need of airport expansion at the cost of nature or human populated grounds. Last but not least the introduction of electric taxiing allows a significant reduction of noise and emissions of gasses like carbon dioxide in the ground phase of a flight.

10.5. Risk Assessment

For ground operations several technical risks can be identified.

GO-1: Not enough ground operation units available for desired turnaround plan:
- Action: formulate multiple backup turnaround plans accounting for variations in available equipment.

GO-2: Airport specific ground operations requirements that are not accounted for:
- Action: research the requirements of all important (hub) airports for the HAMMER and multiple spoke destinations. Make adjustments accordingly.

10.6. Requirements Compliance

HAMMER's ground operations do not differ significantly from the operations of common aircraft like the A320 or A330. Therefore it was pronounced that the requirements concerning ground operations are all met after this analysis. They can be found in the table below.

Table 10.1: Compliance with the ground operations requirements.

	Requirement
✓	CMR-SR-SA-GS-1 - The aircraft shall be safe to operate by ground crew.
✓	CMR-SR-AO-AS-1 - The aircraft shall provide easy accessibility to prepare it for the next flight.
✓	CMR-SR-AO-AS-2 - The aircraft shall provide a safe way to load and unload cargo.
✓	CMR-SC-AC-3 - The aircraft shall be able to interface with existing airport infrastructure.

10.7. Conclusion

The ground phase of the HAMMER operations can be summarised as follows: the aircraft will taxi over the airport, making use of electric power. This adds weight, but reduced the amount of fuel used, among other benefits. The time for turnaround was reduced from 71.6 [*min*] basis turnaround time to 48.5 [*min*] for an optimised turnaround time. This was achieved by HAMMER's wide aisles, an increase of equipment used and by making more parallel operations possible.

11 Sensitivity Analysis

In this chapter a sensitivity analysis on the top-level requirements of HAMMER is performed. Meaning, it is inspected how sensitive the design would be to a change in the top-level requirements. In this sensitivity analysis both a stricter and looser requirement change is considered.

Payload Requirement
The payload requirement of 320 passengers and corresponding luggage fulfilled. If a larger payload capacity is required, a fuselage or possible aircraft re-design is necessary as the length of HAMMER is already at its limit for aircraft reference code C. If the length restriction is discarded, a change in payload capacity can be achieved by simply increasing the fuselage length. This will require a re-design of a lot of subsystems such as structures, stability and control and ground operations. However, these changes will most likely be relatively small. If a large increase in payload capacity is required, other fuselage configurations are most likely more efficient which would result in a greater amount of changes to design.

The design of HAMMER was built around maximising the allowable lengths for type C gate compatibility while also minimising turnaround time. Then, it was aimed to meet the payload capacity requirements, which ultimately were met. Therefore, a smaller payload requirement would likely not influence the design. Only if the extra payload capacity is deemed significantly inefficient. For instance if the aircraft is rarely fully booked. Similar re-designs as described above could be performed depending on the severity of the inefficiency.

Harmonic range
The aircraft was designed for a harmonic range of 2200 $[NM]$ based on the Class I weight estimations. The Class I and II weight estimations are a first order estimation based on other aircraft. The eventual aircraft weight could differ significantly from this. The weight distribution and therefore the harmonic range could largely differ from the initial estimation that was made. What can be said, is that the fuel tanks are not completely filled for the harmonic range and an additional fuel tank is possible in the front compartment of the fuselage. Thus, with the current design a larger range is definitely possible, if weight can be saved on other systems.

Moreover, a smaller required is unlikely, as the harmonic range requirement is already relatively small. Additionally a smaller harmonic range would make the aircraft less attractive to customers. Therefore, even if the requirement is set lower, the design harmonic range will likely not change.

Minimum operative Mach
A higher Mach speed requirement is possible and would not be an immediate issue, but it would hurt the performance of the aircraft. Additional thrust is available for higher speeds, but it will cause HAMMER to be less fuel efficient. Additionally, a small increase in Mach requirement would not require an airfoil change, as transonic conditions were already considered. But significantly higher Mach requirements will result in a different airfoil, because super critical airfoil will most likely be preferred due to the different design considerations.

A lower minimum operative Mach number would not result in any changes. The propulsion system is not limited by the cruise condition. Flying at a lower speed would not be more efficient due to the increase in cruise time.

ICAO Aerodrome Ref. Code = 3/4C
The field length requirements are met by a large margin, thus a lower field length requirement can be achieved. Moreover, further implementations such as the jump strut could decrease the required field length for take-off. The probability of this requirement changing is low, as this would require a large airport infrastructure change. HAMMER was not designed for its field length requirement, therefore a larger field length requirement would not influence the design. However this could be the case if a field requirement distances are not met. The most effective way to decrease the require field length would either be by an increase in thrust or aerodynamic properties.

As for the span width, the design is highly sensitive to a change in the span requirements. A smaller wingspan would result in a considerable amount of changes for almost every subsystem. These changes are expected to be so large that it could result in a complete design change. For example, if a smaller span requirement is set a box wing aircraft might not be possible if the payload and range requirements still need to be adhered.

As for a larger span constraint, a box wing aircraft could possibly be less efficient than a conventional fixed wing or other configurations. It is possible that a smaller span is still preferred due to other reasons, but similar to the mid-term report, a standalone report could be written regarding the exact effect of this change. A larger span would most likely be benifical with regards to aerodynamics, as a larger aspect ratio can be obtained, reducing induced drag.

Wake Turbulence Category = M
HAMMER can increase by 9482 [kg] and still meet the category M ICAO wake requirements, according to the current weight estimation. This is reasonably flexible, but as this is based on a first order estimation the eventual weight of HAMMER can differ significantly from this. If the weight needs to be lowered, it must be looked at where this could be saved. Logically, the larger the required weight change, the larger the resulting design change be. Moreover, it is unfeasible to meet stricter wake requirement for this system as this would require HAMMER to be approximately 19 times lighter with the current wake category classification.

However, as mentioned in the midterm report, the wake category system is likely to be changed to the RECAT-EU system which depends on two parameters, weight and span. Unfortunately most likely a large change in this system would be required for HAMMER to belong to a different wake turbulence category than it is currently in. A change in these parameters would also require a large amount of re-design, as was previously explained.

Expected EIS 2035
An earlier entry into service would be hard to realise depending on the considerations. If a full development of HAMMER from this moment of time is assumed, then it would already be challenging to have an EIS of 2035 for aircraft manufacturers Boeing and Airbus. The Airbus A380 had a development time of approximately 15 years and while it is considerably larger, it was not as groundbreaking compared to current aircraft as HAMMER [65]. For other companies it would be an even harder task considering the infrastructure and costs that are associated with a project of this size.

If only the design is considered, an earlier EIS would be reasonable to fulfil. Existing materials and technology is used, except for propulsion system. Thus only the propulsion system would require a redesign, due to the expected lesser performance of earlier engines. This re-design would most likely not significantly influence other subsystems. Even if the required thrust conditions cannot be met by two engines, an additional engine could be added between the vertical stabilisers.

A later EIS could occur causing HAMMER to possibly suffer from outdated technology. For instance, hybrid aircraft with improved materials could enter the market at that point. It is possible that HAMMER is already outdated for an EIS of 2035, although this is unlikely. Nevertheless, a earlier EIS is of course preferred, but competition and new technologies must be studied regardless to ensure that HAMMER will not be a failure.

12 Budget Breakdown and Contingency Management

In this chapter the current budget breakdown of the HAMMER is discussed. First, the change in contingency management with respect to the baseline report is explained [20]. Then the chapter is concluded with a budget breakdown of the mass, turnaround time and power.

12.1. Contingency Management

The resource allocation and budget breakdown of the HAMMER is based on calculations before the aircraft enters the future design phases. This induces a number of uncertainties in the budget breakdown process. This section explains how these uncertainties are dealt with and what kind of effect this has on the future development of the aircraft.

The resource allocation and budget breakdown of the concept aircraft was based on class II estimations and several models. However, the unconventional HAMMER aircraft will not fit entirely in these partly empirical methods. This means that some derived parameters are not accurate. One can therefore state with certainty that values have to be iterated upon throughout future design processes. To account for this contingency, a certain contingency margin was determined into the different budget breakdowns and resource allocations.

The values as calculated at this stage of the project is called the current value. This current value is then converted into a worst-case value by correcting for the contingency margin using Equation 12.1.

$$\text{Worst-case} = \text{Current} \cdot 1 + M_{contingency} \tag{12.1}$$

At this stage of the design, a new contingency strategy was started: design up to this stage mainly used the calculated current value. In further design processes it is strongly advised to perform calculations with the worst-case value. Subsystems are not to overshoot the worst-case value and in case they do, the margin on other subsystems will have to be decreased by an equal mass. When this measure does not solve the mismatch to the MTOW worst-case value, the impact of the overshooting should be studied and mitigated. The contingency margin should regularly be adjusted downwards according to the stage in which the design is.

12.2. Budget

In this section, the power, mass and turnaround time budget are discussed. These can be used for detailed design phases. The budgets are compared to the baseline budgets and a new margin for contingency is defined.

12.2.1. Power Budget

The power budget of the HAMMER at this stage of the design has not been researched thoroughly. A preliminary budget was based on [15] and calculations in Chapter 13. The budget provided in in [15] holds for an A320-like aircraft. As the HAMMER fuel consumption per passenger is reduced by 44% compared to the A320, for the power budget the power of an A320 was doubled and then reduced by 44%. As stated in Chapter 5, the usually pneumatic power consumption is taken up by electric systems. The roughness of the calculation implies a large contingency margin. This was therefore set to 25%. The power budget is shown in Table 12.1.

Table 12.1: Power budget.

	Current Value [kW]	Worst Case Value [kW]	Margin [kW]
Propulsive	44800	56000	11200
Hydraulic	269	336	67
Electric	13664	17080	3416
Mechanical	112	140	28
Total	58845	73556	14711

12.2.2. Mass Budget

The mass budget is based on class II estimations and department-wise calculations and is shown in Table 12.2 below. In the baseline report a contingency margin of 15% was applied, slightly more than half, 8%, was defined for this more developed design stage. As expressed in Figure 8.6.3, the weight of the fuselage knows a bigger uncertainty, therefore a margin of 21% was chosen for the fuselage weight.

Table 12.2: Mass budget breakdown.

Subsystem	Current mass [*kg*]	Worst-Case mass [*kg*]	Margin [*kg*]
Forward wing	5692	6147	455
Aft wing	5692	6147	455
Connectors	1138	1229	91
Fuselage	16493	19956	3463
Vertical tail	1898	2050	152
Engines	11962	12918	956
Landing Gear	7500	8100	600
Battery	331	357	26
Miscellaneous	5000	5400	400
OEW	55706	62304	6598
Payload	44000	47520	3520
Fuel	29738	32117	2379
MTOW	123871	141941	18070

12.2.3. Turnaround Time Budget

The turnaround time budget is based on calculations from the ground operations department and presented in Table 12.3. The data based on reference aircraft is judged to be reliable for the HAMMER. Therefore the baseline margin of 10% is lowered to 5%. Recommendations in the loading and unloading of the cargo lead to increased uncertainty for this operation, accordingly a margin of 30% is applied for cargo handling. The contingency margin for the total turnaround time was therefore set to 15%. The worst case value for the (un)loading process was assumed to be 6 minutes.

Table 12.3: Turnaround time budget.

Operation	Current Value [*min*]	Worst-Case Value [*min*]	Margin [*min*]
Total	48.5	55.8	7.3
Deplane passengers	13.9	14.6	0.7
Board passengers	25.3	26.6	1.3
Available cleaning time	9.1	9.6	0.5
Unload aft cargo holds	20	26	6
Load aft cargo holds	19.5	25.4	5.9
Unload fwd cargo holds	0	6	6
Load fwd holds	0	6	6
Refuelling	14.1	14.8	0.7
Potable water servicing	16	16.8	0.8
Waste water servicing	15	15.8	0.8
Catering R1	16.7	17.5	0.8
Catering R2	12.5	13.1	0.6

13 Sustainability Analysis and Development Strategy

The chapter discusses the project development strategy with regards to sustainability, and the future development plan of the HAMMER. A lifecycle analysis is performed of the project. Furthermore, a noise analysis is performed to compare the noise levels of the HAMMER aircraft. Finally, the requirements are verified in to see if the HAMMER complies with the sustainability requirements, and the chapter concludes with a short summary.

13.1. Project Development Strategy

The following development strategy as discussed in previous reports is followed, as seen in Table 13.1. Thus, the 4 main actions will be performed in this report as shown.

In this report, each department was responsible for ensuring that sustainability was taken into account in the design choices, which is shown in each chapter. This helped with ensuring that every aspect of the HAMMER project is to be as sustainable as possible. In this chapter each contribution from every department is taken into account to calculate the lifecycle emissions of the aircraft.

Table 13.1: The steps necessary to integrate sustainable manufacturing and assess sustainability.

Phase	Content	Sustainability Actions
A	Project Organisation	- Defining aircraft contribution to sustainability. - Identifying sustainability regulations, laws, and industry goals.
B	Project Familiarisation & Concept Generation	- Defining sustainability trade-off and weights. - Defining sustainability requirements. - Analysing & identifying sustainable technologies.
C	Concept Selection	- Incorporating sustainable technologies & features. - Gather info on materials used in design. - Perform preliminary lifecycle analysis. - Preliminary end-of-life design.
D	**Final Design**	**- Perform final lifecycle analysis.** **- Perform final end-of-life design.** **- Quantify sustainability with key indicators.** **- Verify that sustainability requirements are met.**

13.2. Future Development Strategy

With regards to the future development of the HAMMER, a number of sustainable principles should be applied.

First off, the production of the HAMMER should occur with the use of only green energy, reducing environmental costs. For production, a lean manufacturing method should be adopted. Lean manufacturing focuses on cutting out processes and parts that do not add value to a product, thereby also reducing waste. This is an excellent way to investigate the aircraft for future production phases to see what can be cut. A promising area is the field of topological optimization, where certain programs can determine areas of a part that can be cut without compromising the structural integrity, thereby saving weight and material use.

Secondly, as will be discussed later, it is proposed that the HAMMER will use biofuels instead of regular jet fuel. The HAMMER development team will also try to involve producers of biofuels, trying to make a good bridge between the aviation industry and fuel developers. The HAMMER should be at the forefront of sustainable development and ensuring that it will fly on 100% biofuels should be a goal of the project. The HAMMER can lead the aviation industry by example in dramatically reducing emissions associated with fuel use, which as shown in Section 13.3 is the most important factor in emissions of HAMMER's lifecycle.

Thirdly, the HAMMER should be designed such that as much of the parts as possible should be able to be reused or recycled. The HAMMER should not pollute the environment after it's lifespan is over. Currently, companies such as AELS[1] already disassemble aircraft piece by piece and sell the useful parts to secondhand buyers[2]. This not only shows that it is possible to fully disassemble an aircraft into useful components, but also that it is financially profitable for a company to do so. While there are many components that may have exceeded their design life or have suffered due to fatigue loading, these can be reused in other industries. Reduction in end-of-life waste improves sustainability and improves the profit that can be made from the aircraft by selling used parts.

End of life designing is also an important aspect to consider during design. Factors such as safe disassembly of the aircraft and possible options for recyclability must be taken into account, such that many systems can possibly be reused. Structural panels can be reused in less demanding applications such as in the automotive industry. Interior components such as seats, toilets and the like can be refurbished for further use. The main structural elements are all made out of recyclable materials, ensuring sustainable end of life solutions.

Another operational aspect that can be considered is maintenance, where predictive maintenance can help with reducing the time that an aircraft spends on the ground unused[3]. Predictive maintenance can be performed by using more advanced models and better measurements of the conditions of aircraft, where maintenance is only performed on when it is actually needed, instead of the current mandated checks that occur at a predetermined time, even if the aircraft is still good to go. This increases economic sustainability by reducing operating costs and potentially increasing the lifespan of the aircraft.

An additional factor is garbage produced during regular flight operations. Currently single-use items are generally given out during flight, which are absolutely wasteful and have an adverse effect on environmental sustainability. It is therefore important that potential HAMMER airline customers ensure that their on-board services are as sustainable as possible[4].

13.3. Lifecycle Analysis

In order to quantify HAMMER's total environmental impact in terms of greenhouse gasses emitted, a lifecycle analysis is performed. A lifecycle analysis takes into account the production of the materials and parts, and also the emissions during aircraft operation. The end of life aspect of the lifecycle analysis is somewhat difficult to perform as fewer details are available regarding that. However, it can be looked which materials and parts can be reused or recycled when the aircraft is at the end of its lifetime. The most important emissions to consider for aircraft are as follows: carbon dioxide (CO_2), sulfur oxides (SO_x), nitrogen oxides (NO_x), particulate matter, unburnt hydrocarbons (HC), carbon monoxide (CO), and soot. The most important ones out of these are CO_2 and NO_x. These are mostly related to fuel type and engine performance, although of course the overall aircraft performance (aerodynamics, weight) is also correlated, as a lower weight implies less need for fuel, thereby saving both greenhouse gas emissions and money.

13.3.1. Production Analysis

In order to quantify the production aspect of the lifecycle, it is looked at which materials are used for the main weight factors of the aircraft, only ignoring the miscellaneous weights. The energy used can be quantified using the average emissions produced by electricity generation. It is found that the average emissions per kilowatt hour is equal to $CO_2/kWh = 0.475$, where CO_2 is given in [kg] [5]. The main materials are CFRP, aluminium and steel. CFRP has been found to be very energy intensive to produce, especially when compared to more conventional materials such as steel.

[1] Aircraft End of Life Solutions

[2] https://aels.nl/we-love-to-sell-aircraft-parts/aircraft-nacelles [cited 22 June 2020]

[3] https://www.lufthansa-industry-solutions.com/de-en/solutions-products/aviation/advancing-the-future-of-predictive-maintenance/

[4] https://www.abc.net.au/news/2018-08-21/plastic-waste-created-in-plane-cabin-no-easy-solution/10117576

[5] https://www.co2emissiefactoren.nl/lijst-emissiefactoren/ [cited 22 June 2020]

The main advantage of carbon fibres is a significant weight reduction. This decreases the fuel use, which can offset the increased production costs of CFRP during the aircraft's lifetime. The LIBRE project is currently a large scale undertaking to develop more sustainable composites, by making the epoxy out of lignin waste from the paper industry and lowering the production energy needs by implementing heating by the use of microwave technology. Recycling options for CFRP have also been looked into. CFRP can be recycled using a variety of methods, with pyrolysis, chemical and fluid bed recycling being the most favourable [38].

Table 13.2: Energy and CO_2 emissions associated with the production of the main structural materials.

Parameter	Primary Production Energy $[\frac{MJ}{kg}]$	CO_2 Production $[\frac{kg}{kg}]$
Aluminium 2024 T-3	206	13.7
CFRP	723	50.5
Low Carbon Steel	32.3	2.44
Titanium	652	37.6
Styrene Butadiene Rubber	124	6.95

These materials are what the preliminary design of the aircraft will consist of. A number of assumptions are made regarding material use in some subsystems. It is now looked at what the total emissions are for each subsystem. The only significant weight item which is left out is the miscellaneous section, which is difficult to quantify or would not be an accurate quantification anyway. It is expected that the miscellaneous items would not contribute significantly to the overall emissions of the aircraft. The data was obtained from the use of CES, a database program with material statistics. The engine was decided to have an equal distribution of titanium, aluminium, and steel, to account for the many types of materials used, with the titanium and aluminium accounting for the main engine components and steel for any other components and the pylon attachment. The results can be seen in Table 13.3 and Figure 13.1.

Table 13.3: The material composition of the different subsystems.

Structure	Material Composition	Weight $[kg]$	CO_2 Emissions $[kg]$	Share [%]
Fuselage	14 % CFRP, 86%Aluminium	16,493	310,926	26.3
Wing System	100% CFRP	12,505	631,503	53.4
Engine	33% Titanium, 33% Aluminium, 33% Steel	11,962	212,137	17.9
Empennage	100% Steel	1,898	4,631	0.4
Landing Gear	15% Rubber, 85% Steel	7,500	23,374	2
Total	-	50358	1,182,569	100

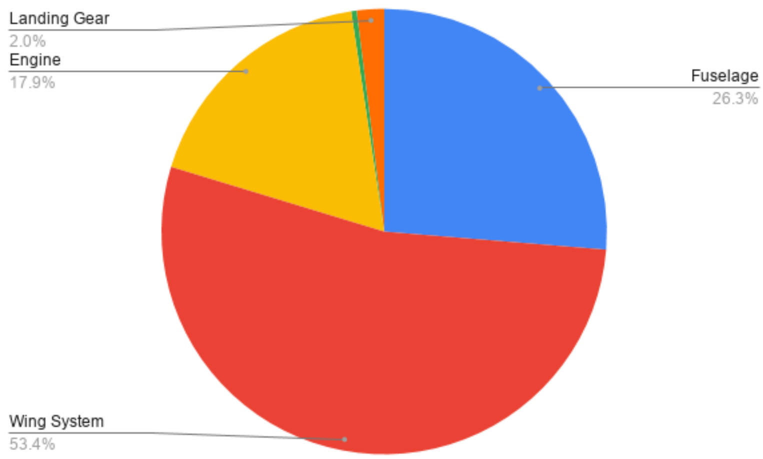

Figure 13.1: The share that each component has in the production of carbon dioxide emissions.

13.3.2. Operational Analysis

As the fuel performance is one of the most important things to look at for the operational part of the aircraft's lifecycle, an analysis is performed here. A comparison is made to the A320, one the main reference aircraft for this project.

A promising new direction for reduction of greenhouse gas emissions is biofuels. Biofuels can be made in a more sustainable way. Biofuels can also be burnt more efficiently than standard Jet A-1 fuel. Currently, second generation biofuels are available. The requirements for a second generation biofuel is that they should have the same performance characteristics as regular jet fuel, and that they do not take up land that would be used for agriculture or other foodstocks, or land that is taken up by high carbon stock land (primeval forests etc.) [14] . First generation biofuels did not have this requirement and were thus somewhat unattractive to use. However, as the entry into service date of 2035 offers new possibilities for perhaps a new generation of biofuels it is of interest to look into their potential benefits with regards to environmental sustainability.

It was found that biofuels based on a Fischer-Tropsch process were most efficient, with project reductions in CO_2 emissions reaching almost 95% from well-to-wake. Well-to-wake takes into account production as well. However, a major factor that has to be considered is cost. Large scale production of biofuels based on the Fischer-Tropsch (FT) process still produces biofuel that is about 3x as expensive (with the current COVID-19 crisis this is even 10x as expensive due to plummeting oil prices), which is a large hurdle to overcome for the low cost airlines that the HAMMER is marketed for. This is shown in Figure 13.2.

However, it is hoped that with more efficient production and government subsidies for sustainable aviation fuel this issue can be reduced. To provide a comparison, biofuels derived from Hydroprocessed Esters and Fatty Acids (HEFA) and Direct Sugars to Hydrocarbons (DSHC) methods are also shown in Figure 13.2 and Figure 13.3 to reflect the different performances of biofuel types. As can be seen the DSHC method is worse in practically all aspects, costing more and being less friendly to the environment. The HEFA method is a bit better, being cheaper than the FT process but still only reducing the CO_2 emissions by around 46%. With regards to fuel consumption, the HAMMER aircraft reduces fuel use per passenger by around 44% based on preliminary estimates. This can mostly be attributed to having around the same fuel mass as the A320, but carrying almost twice as many passengers. This is possible due to having a slightly shorter harmonic range, more efficient engines, and a more efficient aerodynamic design. The fuel use and emissions can be quantified over the course of the aircraft's lifespan by multiplying these numbers with the expected amount of flights. This can then be added to the production emissions and energy use to get a total picture.

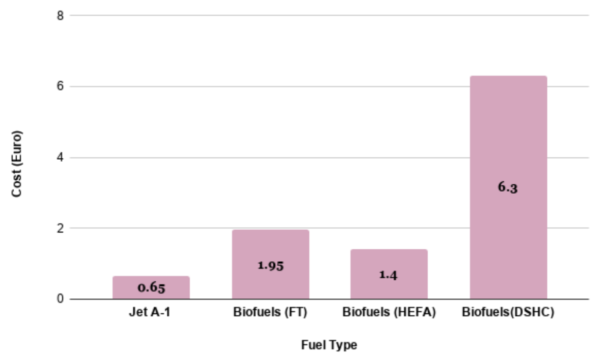

Figure 13.2: Fuel costs for conventional jet fuel and three selected biofuels.

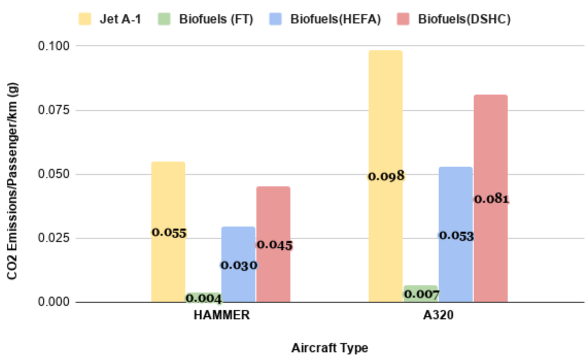

Figure 13.3: The calculated fuel emissions for the HAMMER and A320, with the use of 3 different biofuels included.

We can now extend these numbers to quantify the fuel use over the course of the aircraft's lifetime. This is set at 30,000 flights. An estimate is made for calculation that all these flights are at harmonic range and max capacity.

Table 13.4: The total emissions generated by the aircraft during operation.

Fuel Types	Lifetime CO_2 Emissions $[kg]$
Jet A-1	$2.14 \cdot 10^9$
Biofuels (FT)	$1.28 \cdot 10^7$

With regards to operational improvements in terms of sustainability, the adoption of an electric green taxiing system and a no-bleed air system is another solid improvement with regards to operational performance. The adoption of this system reduces the CO_2 output by almost 61% during ground operations, a substantial improvement. The no-bleed air system reduces the fuel flow during cruise during 3%, which can add up over time as well. The box wing design is also very beneficial with regards to drag reduction as previously mentioned and helps with increasing fuel efficiency.

13.3.3. End-of-Life Analysis

It is also of interest to see how much of the aircraft can be recycled in the end. To that end the recyclability fractions of each material can be researched. It is also of interest to investigate the emissions that recycling causes. It is assumed that all materials used in the aircraft can be recycled. Already, recycling exists for the metals used (Aluminium, Steel, Titanium). Recycling options for CFRP have also been looked into. CFRP can be recycled using a variety of methods, with pyrolysis, chemical and fluid bed recycling being the most favourable [38]. A recyclability fraction of 0.9 is assumed, to account for any inefficiencies in the recycling process. The results can be seen in Table 13.5 and Figure 13.4.

Table 13.5: The recycling emissions associated with the end of life solutions.

Structure	Recycling CO_2 Emissions $[kg]$	Share [%]
Fuselage	310,926	58.8
Wing System	631,503	11.9
Engine	212,137	23.8
Empennage	4,631	7.5
Landing Gear	23,374	4.7
Total	168,039	100

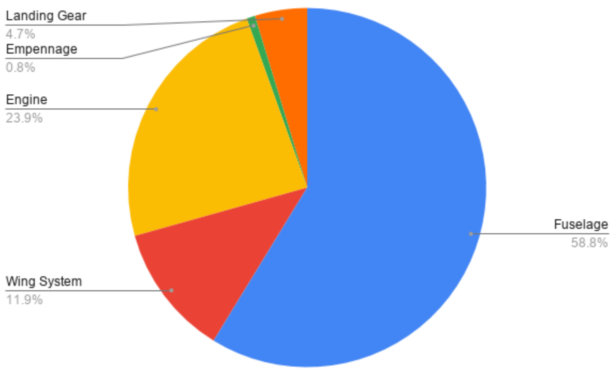

Figure 13.4: The share that each component has in the production of carbon dioxide emissions for recycling.

13.3.4. Complete Lifecycle Analysis

As can be gathered from the previous chapters, a rather complete lifecycle analysis was performed, as seen in Table 13.6. It can be seen that the use of biofuels decreases the lifecycle emissions by almost 95%, as previously stated. It is also of interest to see in Table 13.7 that the operational part of the lifecycle is by far the most important one, contributing the most to overall emissions. It is thus of vital importance to be able to reduce this part of the lifecycle as much as possible.

Table 13.6: The total carbon emissions for the two main fuel types of interest.

Total Lifecycle (Fuel Type)	CO_2 Emissions $[kg]$
Total (Jet A-1)	$2,139,660,000$
Total (Biofuels (FT))	$108,265,000$

Table 13.7: The share of each lifecycle aspect for the use of different fuels over the course of the aircraft's lifespan.

Lifecycle Aspect	Jet A-1 used	Biofuels (FT) used
Production Share (%)	0.055	1.09
Operational Share (%)	99.93	98.75
End-of-Life Share (%)	0.008	0.16

13.4. Noise Analysis

Aircraft noise is an important factor to consider for social and environmental sustainability. Ensuring that aircraft noise output is diminished helps with improving the quality of life of those living around airports. Some airports are also positioned nearby residential areas, which means that aircraft noise has a great impact on those living nearby. An important factor to consider is if one flight of a HAMMER-type aircraft causes less noise pollution than two A320 flights, for example. Due to the nature of the decibel scale, a reduction of 3 [*dB*] in noise halves the perceived noise level. Thus, if the hammer is 3 [*dB*] louder than the A320, one flight of the HAMMER is equal to two A320 flights. Obviously, it is beneficial to reduce this number. The threshold however for noise is then stated as the lowest value of either the noise certification limits or the noise levels of the A320 with 3 [*dB*] added.

Within aerospace regulations, it is common to represent the annoyance of the noise as [*EPNdB*], which stands for Effective Perceived Noise levels in dB. It combines the peak intensity of the noise with its duration and frequency, according to Equation 13.1. This metric represents the severity and annoyance of the noise, as perceived by humans. [6].

$$EPNdB = PNL_{max} + 10log(\frac{t_{10}}{20}) + F(dB) \tag{13.1}$$

Where PNL_{max} is the maximum Perceived Noise Level, t_{10} is the is the duration (in seconds) of the noise level within 10 dB of the peak PNL, and F is the correction factor for pure tones, which are usually found more annoying than regular ones. This number is usually equal to approximately 3. The intensity of the noise decreases with distance, therefore three separate reference points that have been identified by ICAO [45]:

- Lateral full power-reference: The point with maximum noise level, at a line 450 [m] away from the centre line of the runway and parallel to the runway.
- Flyover reference: A point 6500 [m] away from the start of roll of the aircraft, on the extended centre line of that runway.
- Approach reference: A point on the extended runway centre line, 2000 [m] before the start of the runway.

In Table 13.8 it can be seen that the noise limitation with regards to the A320 was the most important, as it has a large cumulative margin and thus very good noise performance. A cumulative margin of at least 26.85 is needed to ensure adequate noise performance with respect to the A320. This is however only a baseline requirement, and any additional noise savings are of course welcome.

However, for HAMMER no simulation is unfortunately possible to measure the [*EPnDB*] levels. This is still mostly done using either very advanced modelling software or using actual measurement data.

Table 13.8: The max noise levels for two reference aircraft, the A320 and the 767-300. The 767-300 is chosen as an additional reference due to the similarity in MTOW between it and the HAMMER.

Noise Parameter	**HAMMER**	**A320**	**B767-300**
Lateral full power level max [*EPNdB*]	98.76	97.02	98.67
Lateral full power level actual [*EPNdB*]	-	84.62	94.79
Max HAMMER w.r.t. A320	87.62	-	-
Approach noise level max [*EPNdB*]	102.32	100.74	102.25
Approach noise level actual[*EPNdB*]	-	92.43	95.35
Max HAMMER w.r.t. A320	95.43	-	-
Flyover noise levels max [*EPNdB*]	94.59	91.87	94.48
Flyover noise levels actual [*EPNdB*]	-	82.77	88.17
Max HAMMER w.r.t. A320	85.77	-	-
Cumulative margin [*EPNdB*]	**26.85 (Projected Minimum)**	29.8	17.1

[6]https://www.sfu.ca/sonic-studio-webdav/handbook/Effective_Perceived_Noise_.html [cited 22 June 2020]

<table>
<tr><td colspan="2">M = Maximum take-off mass in 1 000 kg</td><td>0</td><td>20.2</td><td>28.6</td><td>35</td><td>48.1   HAMMER 120 150</td><td>280</td><td>385</td><td>400</td></tr>
<tr><td colspan="2">Lateral full-power noise level (EPNdB) All aeroplanes</td><td colspan="4">94</td><td colspan="3">80.87 + 8.51 log M</td><td>103</td></tr>
<tr><td colspan="2">Approach noise level (EPNdB) All aeroplanes</td><td colspan="4">98</td><td colspan="2">86.03 + 7.75 log M</td><td colspan="2">105</td></tr>
<tr><td rowspan="3">Flyover noise levels (EPNdB)</td><td>2 engines or less</td><td colspan="5">89</td><td colspan="2">66.65 + 13.29 log M</td><td>101</td></tr>
<tr><td>3 engines</td><td colspan="3">89</td><td colspan="4">69.65 + 13.29 log M</td><td>104</td></tr>
<tr><td>4 engines or more</td><td colspan="2">89</td><td colspan="5">71.65 + 13.29 log M</td><td>106</td></tr>
</table>

Figure 13.5: The weight class regulation area in which the HAMMER falls.

With regards to noise, the main contributors are as follows:
- Engine noise
- Wing noise
- HLD noise
- Landing gear noise

The HLD and landing gear noise play a role, exacerbating the issue, as these only come into play during take-off and landing, when the aircraft is closest to the ground. However, as the HAMMER has slightly less use of flaps than conventional aircraft, and has a short takeoff runway distance, it is expected that the noise levels can be comparatively lower, as the HAMMER requires less time spent taking off, which is when the largest noise levels are produced. Wing noise is generally a small contributor to noise [64], so it is expected that the fact the HAMMER has an extra wing will not contribute as much to noise levels.

For the noise analysis it was considered too difficult to implement a full noise model. Instead, empirical data from other aircraft will be used to come up with noise levels for the aircraft. Several promising noise reducing technologies will be implemented in the design, for which some preliminary noise reduction levels have been determined.

In Figure 13.6a and Figure 13.6b the noise contours for the A320 have been plotted using the Dutch Calculation Model [64]. It was determined that the critical situation is mostly the take-off, where the engines have to produce the most power and thus also produce the most noise. For HAMMER aircraft this might be even more pronounced, due to the fact that the engines are far larger but the take-off distance is still quite short, and thus the engines need to provide even more thrust.

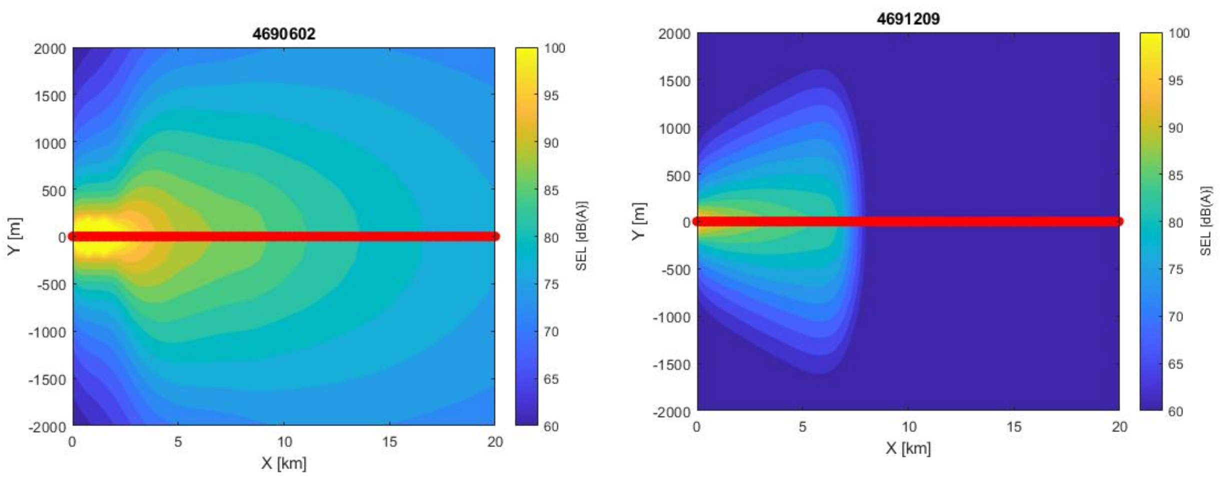

(a) The A320 noise contours for a straight flight takeoff.

(b) The A320 noise contours for a straight flight constant descending landing.

Figure 13.6: The A320 noise contours.

13.4.1. Airframe Noise

In order to quantify airframe the noise, NASA's Aircraft Noise Prediction Program is used (ANOPP) [64]. Here, the four main components of airframe noise are quantified based on their geometry. This can then be converted to sound pressure levels and decibels, from which the highest decibel number can be used for the noise annoyance factor, to calculate the [*EPnDB*], which is a value with which aviation authorities measure noise annoyance due to aircraft. The calculations in the ANOPP method are as follows.

The noise components are modelled according to Equation 13.2. P is the power function and $F(S)$ is a spectral function depending on the dimensionless Strouhal number. p_e^2 is the effective pressure in $[Pa^2]$ (or $[\frac{N}{m^2}]$), ρ_∞ is the upstream air density, c is the speed of sound, r is the observer distance in meters, M is the Mach number, and θ and ϕ are polar and azimuthal directivity angles, respectively. These angles can be viewed in Figure 13.7. These are accounted for in the dimensionless directivity function $D(\theta, \phi)$. This differs for each noise component. In the Strouhal number equation, the noise frequency is the most important input variable, as by varying the frequency in a certain range a noise spectrum can be analysed. In his case, the frequency range is in between 0-20 $\cdot$ 10^4 [*Hz*], as this is the general limit of human hearing. Each component is modelled using equations from Table 13.9, Table 13.11, and Table 13.10.

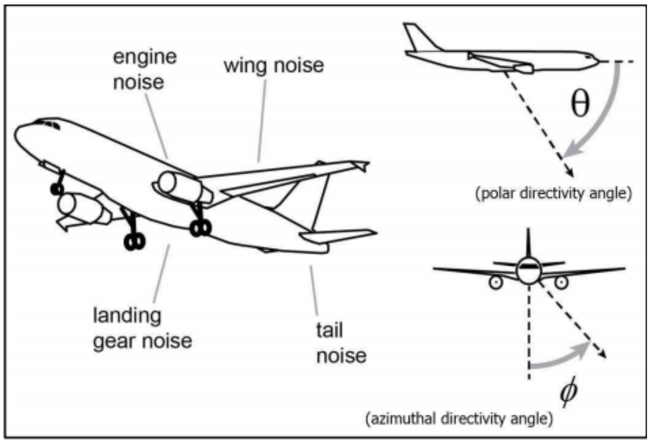

Figure 13.7: The definition of θ and ϕ in the ANOPP method.

$$p_e^2(f, \theta, \phi) = \frac{\rho_\infty c P D(\theta, \phi) F(S)}{4\pi r^2 (1 - M cos(\theta))} \quad (13.2)$$

$$P = K M^a G(\rho_\infty c^3 b_w^2) \quad (13.3)$$

$$S = \frac{f L (1 - M cos(\theta))}{M c} \quad (13.4)$$

$$SPL = 10 \cdot log_{10}(\frac{p_e^2}{p_{e0}^2}) \quad (13.5)$$

Table 13.9: Different noise parameters used to calculate the airframe noise levels.

Noise Source	G	L	K	a
Wing	$0.37\frac{a_w}{b_w^2}(\frac{\rho_\infty M c A_w}{\mu_\infty b_w})$	$G b_w$	$4.464 \cdot 10^{-5}$	5
Slats	$0.37\frac{a_w}{b_w^2}(\frac{\rho_\infty M c A_w}{\mu_\infty b_w})$	$G b_w$	$4.464 \cdot 10^{-5}$	5
Flaps	$\frac{A_f}{b_w^2} sin(\delta_f)^2$	$\frac{A_f}{b_f}$	$2.787 \cdot 10^{-4}$	6
Landing Gear	$n(\frac{d}{b_w})^2$	d	$3.414 \cdot 10^{-4}$	6

Table 13.10: Directivity functions for each component.

Noise Source	Directivity Function
Wing	$D(\theta, \phi) = 4cos^2(\phi)cos^2(\theta/2)$
Slats	$D(\theta, \phi) = 4cos^2(\phi)cos^2(\theta/2)$
Flaps	$D(\theta, \phi) = 3(sin(\delta_f)cos(\theta)$ $+cos(\delta_f)sin(\theta)cos(\phi))^2$
Landing Gear	$D(\theta, \phi) = \frac{3}{2}sin^2(\theta)$

Table 13.11: Spectral functions for each component.

Noise Source	Spectral Function
Wing	$F(S) = 0.613(10S)^4[(10S)^1.5 + 0.5]^{-4}$
Slats	$F(S) = 0.613(10S)^4[(10S)^{1.5} + 0.5]^{-4} +$ $0.613(2.19S)^4[(2.19S)^{1.5} + 0.5]^{-4}$
Flaps	$F(S) = 0.0480S$ for $S < 2$ $F(S) = 0.1406S^{-0.55}$ for $2 < S < 20$ $F(S) = 216.49S^{-3}$ for $S > 20$
Landing Gear	$F(S) = 0.0577S^2(0.25S^2 + 1)^{-1.5}$

Table 13.12: Inputs for each reference point.

Measurement Reference Point	$r[m]$	$\theta[°]$	$\phi[°]$
Lateral	450	0	90
Approach	72	90	0
Flyover	705	90	0

The values for the previously identified three measurement points are as follows for the HAMMER, as seen in Table 13.12. In the end the lateral point is not relevant for airframe noise, as engine noise is by far the most important component at startup, and airframe noise is only mostly heard when the aircraft flies overhead. It is however included for completeness.

It is found that the wing noise is generally the weakest noise contributor, as seen in Figure 13.8a and Figure 13.8b. It is therefore expected that the box wing will not have more noise due to the fact it has two wings instead of one. Instead, the main noise sources are thought to be the landing gear and high lift devices, especially the flaps. The landing gear can also cause more noise due to it being in a fairing, but this is to be left as a future research recommendation.

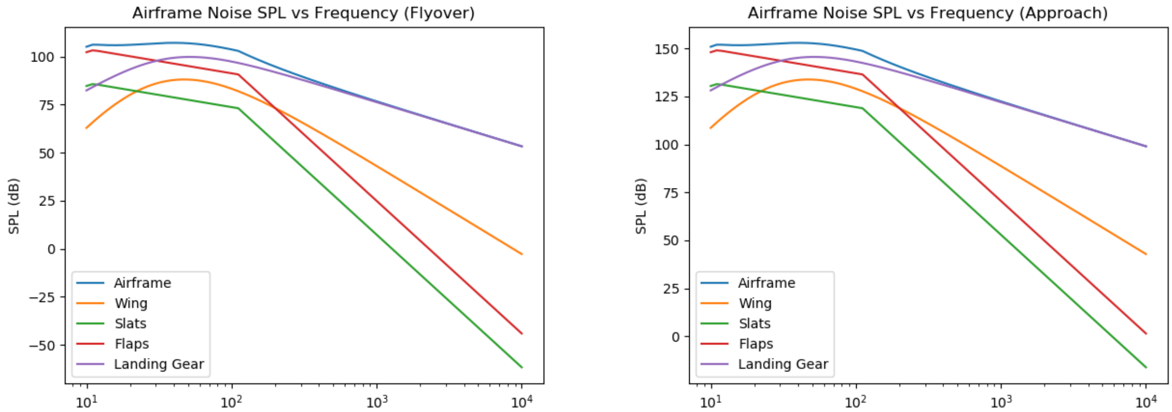

(a) The noise levels for the HAMMER aircraft due to the airframe at flyover.

(b) The noise levels due to the airframe for HAMMER at landing.

Figure 13.8: The noise levels for HAMMER.

13.4.2. Engine Noise

In order to quantify engine noise, another relation was used. According to Equation 13.6 [64], the acoustic power of the engine noise source is related to its jet flow velocity V, and diameter D, with the upstream density ρ_∞ and speed of sound c being flow variables. It is possible to relate engines using this number with similar thrust levels. It shows that a reduction in either jet flow velocity or diameter can reduce the noise levels. By increasing the diameter, the jet flow velocity can increase by a far greater factor due to it being to the power 8. Comparing this with engines from the B767-200 and B757-200, both aircraft with similar engine thrust levels, it was found that a significant reduction in noise was achieved. Because of the way the dB scale works, a -3 [dB] reduction is half of the original noise level. It can be seen that the noise reduction is thus almost half in comparison with the B767-200, and slightly less in comparison with the B757-200, which can be seen in Table 13.13.

$$W \sim \frac{\rho_\infty V^8 D^2}{c^5} \tag{13.6}$$

Engine type	HAMMER engine noise reduction w.r.t. aircraft	% Reduction
B767-200 - Rolls Royce RB211-535	-2.40 [dB]	-40%
B757-200 - Pratt & Whitney PW2000	-1.83 [dB]	-30.5%

Table 13.13: The engine noise levels of the HAMMER related to noise levels of current aircraft engines.

13.4.3. Noise Reduction Technologies

The aerospace industry is busy with developing new noise reduction technologies. In a workshop at the TU Delft a number possible technologies to implement for noise reduction were identified [12]. The following technologies were identified as appropriate to incorporate, as seen in Table 13.14. One noise reducing element that unfortunately could not be implemented due to size constraints was placing the engines in between the vertical tails due to the rather large size of the engines that were needed. This would have been a considerable reduction, estimated at 10 [*dB*] or more. It is a recommendation for future research to look into this possibility, as it offers quite some advantages with regards to noise shielding. However, the engine noise is still partially shielded by the aft wing, which somewhat compensates for this. Engine chevrons are already integrated into the engine design as shown in Figure 13.9.

Table 13.14: Noise reduction technologies [12].

Noise Reduction Technology	Estimated Reduction [*EPndB*]	Design Implications
Landing gear mesh fairings	3-5	Landing gear design, maintenance, weight
Flap porous edge device	5	Maintenance
Slat setting optimisation	3-5	Additional slat complexity
Engine chevrons	1-2	Slight weight increase

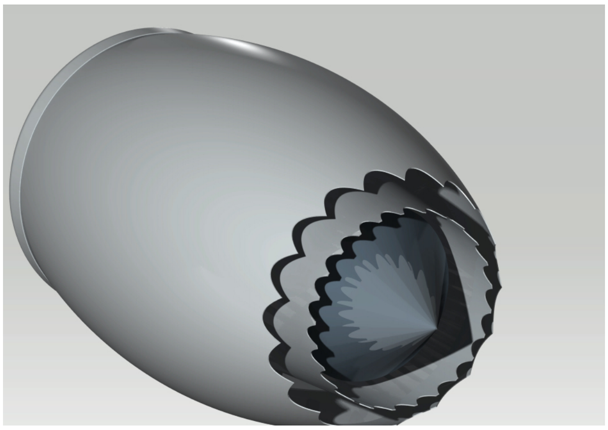

Figure 13.9: The engine chevrons integrated into the nacelle

13.4.4. Noise Conclusion

In the end, although it is difficult to get a full quantification, it is thought that with the aforementioned noise reduction technologies, the quieter engine, and the possible reduction in engine noise due to the box wing configuration, that the HAMMER will meet the requirement of a reduction of -26.85 [$EPNdB$], especially looking at current trends regarding aircraft noise, as seen in Figure 13.10, which shows that over time the noise characteristics of all aircraft have improved, and that in 2030 a reduction in -30 [$EPNdB$] is predicted as a minimum. Another thing to consider is that due to the HAMMER's short takeoff and runway length, the aircraft can be less noisy as it can climb away faster and spends less time on the runway, which is when the loudest noise emissions are emitted generally.

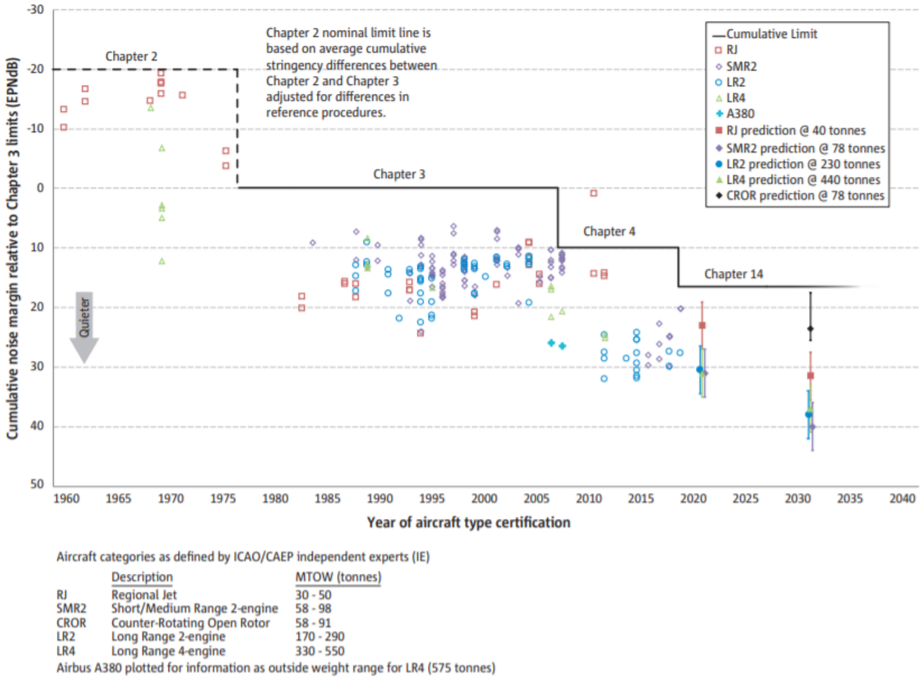

Figure 13.10: The current trend in noise performance with regards to the new ICAO chapters.

13.5. Requirements Compliance

In order to make sure that HAMMER is compliant with the requirements set out previously, the compliance matrix for sustainability is discussed here. In the end, the nitrous oxide requirement is left for future research, as it depends on a variety of complicated factors, which relate to high levels of detail of engine design and flight path settings.

Table 13.15: Compliance with the sustainability requirements.

	Requirement
✓	CMR-SR-SU-1 - Materials used in the aircraft shall be reusable wherever possible
✓	CMR-SR-SU-4 - The aircraft shall not exceed current operating cost for medium range aircraft
✓	CMR-SR-SU-9 - The aircraft shall emit 50% less CO2 emissions than medium range aircraft from 2005.
~	CMR-SR-SU-10 - The aircraft shall emit 90% less NOx than medium range aircraft from 2000.

13.6. Conclusion

To conclude, it is found that the HAMMER is 44% more efficient in terms of CO_2 emissions than the A320, which is the main reference aircraft. This due to its low fuel use and more efficient aerodynamic design, as well as being able to carry almost double the passengers. With biofuels a further savings percentage can be achieved of up to 95%. A number of recommendations were made to improve sustainability in the long term view, and a lifecycle analysis was performed. Biofuels were identified as promising with regards to sustainability. A noise analysis was performed, and it was found that the HAMMER engine noise is comparatively quieter than current aircraft in the same thrust and weight category in absolute terms. It was also identified that the HAMMER would need to meet a reduction in noise of -26.85 [$EPNdB$]. It is thought that this requirement can be met with promising noise reduction technologies, but this is to be quantified in future research. The HAMMER is also less noisy due to its comparatively lower use of flap systems.

Thus, the HAMMER contributes to a sustainable aviation future with not only a more efficient aircraft in terms of fuel use, but also being quieter, and being more sustainable for operators in terms of economic aspects as well. The major components of the HAMMER can also be recycled, further contributing to sustainability.

14 Risk Assessment and RAMS

To evaluate the performance of an aircraft, especially related to aircraft safety, risk analysis plays a big role. For every design there are inherent risks connected to it which must be reduced as much as possible. This chapter deals with analysing the non subsystem specific risk and safety of the design. First a risk assessment is performed followed by a risk mitigation plan. Then a RAMS (Reliability, Availability, Maintainability, Safety) analysis is done to further analyse the safety of the aircraft. Lastly, an overview of the challenges regarding certification is given.

14.1. Risk Assessment

Besides subsystem specific risk, there are also risk that threaten the project in a different way. To sort and classify these risks, three phases in the life cycle were established for which different risks could be identified. These are the development phase, production phase, and the operational phase. For each risk there is a certain probability of occurrence and an associated impact. The probability of occurrence ranges from very low to very high, while the impact ranges from negligible to catastrophic, each with three steps in between. The impact of each risk is based on the economic impact on development costs or operating costs for airlines.

Depending on each risk, steps can be taken to mitigate the impact and to reduce the likelihood of occurrence. These steps are:

1. **Neglect:** No mitigation action can be taken or needs to be taken as the combination of the probability of occurrence and impact is not high enough to warrant attention
2. **Observe:** The parameter is not of critical importance but also can't be neglected or not enough information is know yet. It will be observed for the time being and possible actions may be required later.
3. **Research:** Additional research is done of said risk to get a better understanding and to decrease its probability of occurrence and/or impact
4. **Take action:** Direct action is performed either before or when the event occurs to decrease its probability of occurrence and/or impact.

14.1.1. Risk Phases

The first phase, development, deals with any risk to the target entry into service of 2035. Risk concerning technical faults are not incorporated here as they are covered in their respective chapters.

D-1: Technology used not yet mature enough before the entry into service of 2035

- Observe: Utilised technology development should be closely monitored to anticipate and adapt to any changes in performance. However no action can be directly taken to ensure that there are no changes.

D-2: Delays in certification due to novel concept delaying the entry into service.

- Research: More research should be done into certification. This includes designing flight systems from the ground up with safety margins baked into the design.

D-3: Due to the novel concept, standard tools might be inaccurate requiring redesign of subsystems

- Action: Standard sizing tools based on empirical relations should undergo extensive verification and validation procedures to check if the methods are still applicable

break

The second phase, production, deals with regarding production and preparation of the aircraft. **P-1:** Production delays due to new tools being required for box wing specific parts.

- Action: during prototyping and development, development partners should be consulted as much as possible to build experience with constructing a box wing aircraft.

P-2: Extended retraining time required for ground crew and air crew.

- Research: additional research should be performed to streamline the process of transitioning crew to the new concept. This includes researching flight characteristics to implement into a flight simulator, as well as refining ground operation procedures.

P-3: Heavy use of advanced composites might result in a shortage of specialised required equipment.

- Observe: by keeping an eye on the project schedule, enough time can be allocated for sourcing equipment and setting up an assembly line.

The third phase deals with risks that could be encountered when actually operating the aircraft.
OP-1: The box wing requires more airport adaption than anticipated
- Research: more research studying aircraft servicing routines should be performed and redesign of certain areas should be done if it is impractical with current equipment.

OP-2: Maintenance tools required differ too much from existing aircraft, limiting home ports for airlines.
- Research: similar to the retraining of crew, additional research into maintenance tools and designing parts to be compatible with standard tools.

OP-3 Inaccurate modelling of aircraft performance leads to increased fuel costs
- Observe: No preventative action can be taken to mitigate this risk as real life performance is difficult to predict. However performance should be closely monitored to intervene in a timely manner if the actual aircraft performance is less than predicted. Operational conditions should be monitored to detect any performance changes

OP-4: General hesitance to adopt the HAMMER aircraft by airlines
- Action: airline companies should be adequately made aware of the advantages of a box wing aircraft. Extra effort should be taken to prove that the aircraft is safe to fly to remove any doubts about the new concept.

OP-5: Aircraft fatigue properties improperly modelled requiring earlier retirement
- Observe: this risk will only become apparent after a significant operational use. Extra measurements can be taken to compare the theoretical service life compared to the actual service life.

14.1.2. Risk map
For the established risks, the following risk map and mitigated risk map can be created:

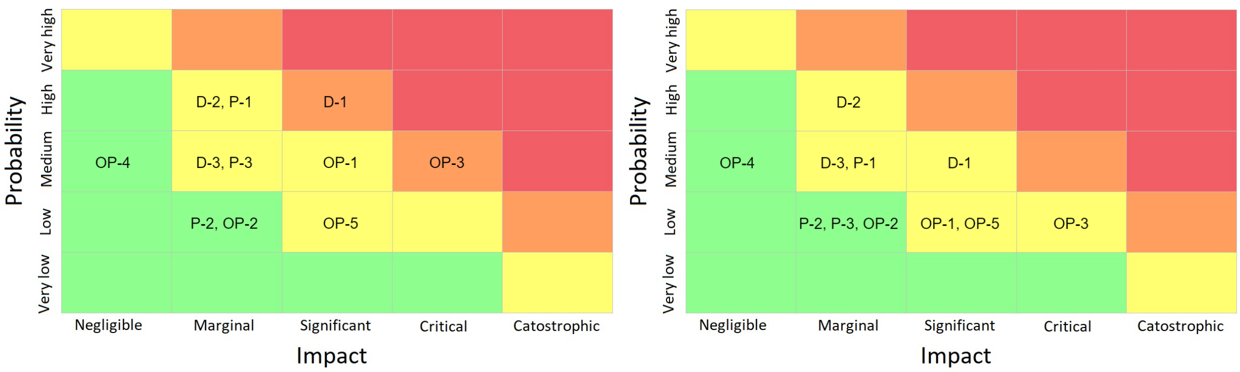

(a) Risk map of each phase in the HAMMER project.

(b) Mitigated risk map of each phase .

When looking at Figure 14.1a and Figure 14.1b, it can be seen that there are no high probability-high impact risk. There are two medium probability-medium to critical impact risks. The first risk, D-1, concerns technology readiness. As this risk mainly depends on future research, the best way to mitigate this as stated in Subsection 14.1.1 is to monitor development. Performance margins can be used to lower the probability of a disappointing performance however the impact, having to redesign certain aspect, remains.

The second medium probability, medium/critical impact risk, OP-3, concerns operational performance. By closely observing the first batch of aircraft, useful performance metrics can be extracted to further optimise the aircraft to make sure the aircraft performs as required and is profitable enough to encourage future orders. Additionally, in the design phase extra validation and verification actions can be taken to prevent this problem from occurring.

14.2. RAMS
With the major project risks known, this chapter deals with explaining how the aircraft will mitigate risks in more detail.

14.2.1. Reliability
Aircraft reliability is key to successful operation. It is defined as the probability of a system to perform in a satisfactory manner. When looking at the aircraft as a system, it can be seen that there are many subsystems that make up a grand system. To improve the reliability, every subsystem must be made as reliable as possible. To do this several actions can be undertaken, these actions can be divided into analysis tools and design tools.

Starting with analysis tools, the first tool is Failure Mode, Effect, and Criticality Analysis (FMECA) [43]. FMECA analysis start by defining the system and making functional block diagrams. Next, all failure modes and causes are thoroughly analysed to account for every possible scenario and the probability of occurrence. The most severe or highest probable risks failure modes are then further analysed and improvements are implemented.

The second analysis tool is the Fault Tree Analysis [43] [28]. Starting at top level events, usually flight critical failures, possible failure mode paths are analysed. This analysis prevents individual subsystem failure to cascade into multiple subsystem failure. Like FMECA analysis this gives greater insight in how a system works and what the risks are.

Besides these analysis tools, attempts to improve reliability can also be made during the design phase. Examples of these attempts in the HAMMER project are less complicated servicing systems aboard such as the no-bleed system. This reduces the amount of plumbing needed in the aircraft which decreases the possible points of failure in a system which increases the reliability.

Looking at unit-level of a system, a lot of effort can be made to increase reliability. Starting with the use of redundant systems, this ensures that there is a back up such that no single point of failure can cause system failure. Furthermore improving the quality of a single unit decreases the chance of that part breaking when used

14.2.2. Availability

Availability is the probability of a system ro be ready and available. Availability is largely dependent on a systems maintainability, which will be discussed in the next section. Two types of availability exist, inherent and achieved availability[21], which can be calculated using Equation 14.1 and Equation 14.2:

$$A_i = \frac{MTBF}{MTBF + MTTR} \qquad (14.1) \qquad\qquad A_a = \frac{MTBM}{MTBM + MTTM} \qquad (14.2)$$

where MTBF is the Mean Time Between Failures, MTTR is the Mean Time To Repair, MTBM is the Mean Time Between Maintenance and MTTM is the Mean Time To Maintain. Inherent availability is the probability that the system will operate satisfactory at any point in time, excluding scheduled and preemptive maintenance, as well as logistics. Achieved availability includes scheduled and preemptive maintenance, however logistics are excluded. As maintenance is always planned and random repairs are not common, achievable maintenance is the leading factor. Looking at Equation 14.2, availability is increased if the mean time to maintain is decreased or if the mean time between maintenance is increased. This can be achieved in various ways.

The first way is to increase monitoring in fatigue sensitive areas, More targeted repairs can be carried out making the repair more efficient, thereby decreasing maintenance. This point heavily ties in with reliability as an increase in reliability also means an increase in availability. The second way is to increase the mean time between maintenance by using more durable materials and systems. Again this point is dependent on an other factor, namely maintainability.

14.2.3. Maintainability

Maintainability deals with how well maintenance is able to be performed on the aircraft regarding safety, ease, accuracy, and economic impact. According to [28], maintenance time schedule can be defined as:

- Mean Time To Repair (MTTR): The time needed to restore a system to its full operational status, also known as the Mean Corrective Maintenance Time.
- Mean Preventive Maintenance Time (MPMT): The time required for preventive maintenance operations.
- Mean Time To Maintain (MTTM): The time required for both corrective and preventive maintenance.
- Mean Down Time (MDT): The total time the aircraft can not be used. This included the MTTM, but also the logistical delays.

Diving deeper into reducing repair times, several things come to light. The first deals with ease of repair. By placing frequently changed subsystems in an accessible place, less time has to be spent removing other parts to reach that system. As the HAMMER aircraft is a wide body aircraft, more space can be allocated for maintenance room. The box wing configuration does bring its downsides in this area, as a large part of the wing is in a less accessible place than a conventional wing.

Secondly, availability and commonality of parts also influence repair time. The use of industry standard parts and tools allows the aircraft to be easier maintained and at more airports compared to a few airports that have specialised parts.

Furthermore the type of bonds present influences how easily an aircraft is to maintain. By designing an aircraft such that adhesive bonding or welded joints are kept to a minimum and replaced by bolt joints, maintenance becomes easier as damaged parts can be quickly removed.

14.2.4. Safety

Lastly, safety is how the aircraft interacts and prevents harm to the environment. Safety is a key part of aerospace applications and therefore also for the HAMMER project.

Starting with design principles, the design principles of fail-safe and safe-life were applied. The former is done by sizing aircraft components with the idea that it could compensate for the failure of another component. By having redundant systems in place, there is no risk of danger to payload even if there is a subsystem failure. This principle of redundancy can be expanded by designing the aircraft such that even if there is a system failure, the aircraft is still able to fly. An example of this is the avionics system. As described in Chapter 7, a box wing aircraft is naturally stable due to the position of the aft wing. This means that even in case of failure of the avionics system the aircraft would not become unstable.

Regarding safe-life, this is principle is mainly applied in areas deemed too important to fail. An example of this is the landing gear. The struts should be able to hold their entire service life without showing signs of fatigue because a single propagating crack or tear could prove devastating for the entire aircraft. This design philosophy however is not sustainable in the whole aircraft as this would mean that every part, even non critical parts would be over designed. Therefore mainly the design philosophy of fail-safe was applied.

Furthermore, safety regulations play a big role in the design of the aircraft. Initial sizing has been done based on airworthiness regulations as specified by EASA in CS-25 [1].

One foreseen challenge is in the flight control design verification and validation. Conventional aircraft can rely on tried and tested flight systems. However, the flight dynamics for a box wing differs greatly from a conventional aircraft as there is no traditional main wing-tail interaction. That being said, there are also advantages to the box wing regarding safety. As the box wing is able to directly adjust the generated lift, instead of requiring the tail to rotate the aircraft causing a change in angle of attack meaning more direct control. Furthermore the box wing can generate a pure couple moment which increases manoeuvrability. Combined with the fact that there are more control surfaces compared to conventional aircraft, which automatically incorporates redundancy into the aircraft, the box wing does have all the characteristics to be an aircraft with a very high operational safety score.

Another challenge is in the structure certification. As the applied forces and how they are introduced in the fuselage is different from conventional aircraft, different ways have to be found to make sure that the HAMMER aircraft is up to the same standards as other aircraft.

Another important thing to note is that safety is also determined by the reliability of the aircraft. As one of the key requirements for this project was that the aircraft has a quick around time, it is important that every system is reliable. Multiple flight cycles must be able to be performed without worsening performance of components as thorough inspection is not possible.

15 Compliance Matrix

In the previous chapters the design of the aircraft has been laid out. This chapter describes whether the design satisfies all the requirements. In Table 15.1, the user requirements are given with a check mark if the design meets the requirement or a tilde if it is expected to be met but it cannot be proven. This is the case for requirement CMR-SR-SU-8 as the parameter was not calculated with enough accuracy but there is also no reason for now to say it would not meet the requirement. It is highly recommended that these requirements are checked when the design is in a later stage.

Table 15.1: Compliance matrix with the user requirements.

	Requirement
✓	**CMR-SR-AC-CR-1** - The aircraft shall have minimum cruise Mach number of 0.78.
✓	**CMR-SR-AC-FP-5** - The aircraft shall have a harmonic range of 2200 [*NM*].
✓	**CMR-SR-AC-FP-6** - The aircraft shall have a capacity of 250-320 passengers with cargo.
✓	CMR-SR-AC-FP-6.1 - The aircraft shall be able to transport 320 passengers in a 1 class configuration.
✓	CMR-SR-AC-FP-6.2 - The aircraft shall be able to transport a minimum of 250 passengers in a 2 class configuration.
✓	**CMR-SR-AC-FP-8** - The aircraft shall have a turnaround time that does not exceed the turnaround time of a Boeing 737 and Airbus A320 by more than 50%.
✓	**CMR-SR-AO-PA-8** - The aircraft shall have efficient embarking and disembarking procedures.
~	**CMR-SR-SU-8** - The aircraft shall comply with ICAO Stage 5 noise certification.
~	**CMR-SR-SU-9** - The aircraft shall emit 50% less CO2 emissions than medium range aircraft from 2005.
✓	**CMR-SC-DC-2** - The aircraft shall use current technology so it can enter in service in the year 2035.
✓	**CMR-SC-DC-4** - The aircraft shall be of the category ”wing lifting” design.
✓	**CMR-SC-AC-1** - The aircraft design shall comply with the ICAO Aerodrome ref code= 3/4C.
✓	CMR-SC-AC-1.1 - The aircraft has a wingspan between 24 [*m*] and 36 [*m*], according to the C designation.
✓	CMR-SC-AC-1.2 - The outer main wheel gear span is smaller than 9 [*m*], according to the C designation.
✓	CMR-SC-AC-1.3 - The aircraft balanced field length shall be ICAO Category 3, between 1200 [*m*] and 1800 [*m*], for any configuration not in high density.
✓	CMR-SC-AC-1.4 - The aircraft balanced field length shall be a maximum ICAO Category 4, 1800 [*m*] and above, for a high density configuration, if ICAO Category 3 can not be fulfilled in high density configuration.
✓	**CMR-SC-AC-2** - The aircraft shall fall in the wake turbulence category C ’Lower Heavy’ of the RECAT EU system.

After all the subsystem requirements and user requirements were analysed, some miscellaneous requirements were left. These are presented in Table 15.2. The first requirement, CMR-SR-AO-AL-1, is again not researched in enough detail to know if it is met. However, except for the special design of the wing, which might lead to higher maintenance costs but this is not certain, the maintenance costs can be assumed to be the same as a conventional aircraft. Concerning CMR-SR-SA-AS-10, the EASA CS-25 requirements were incorporated as much as possible, but as there are many requirements specified, it can not be guaranteed that all of them have been met with this design at this stage of the design phase. Hence, both these requirement were given an approximate sign.

Table 15.2: Compliance matrix with miscellaneous requirements.

	Requirement
~	CMR-SR-AO-AL-1 - The aircraft shall equal or reduce maintenance cost of current mid range aircraft.
✓	CMR-SR-AO-AL-3 - The aircraft shall not require extensive training to operate.
✓	CMR-SR-AO-AL-4 - The aircraft shall be reliable for up to 30000 flights.
~	CMR-SR-SA-AS-10 - The aircraft shall comply with the EASA CS-25 requirements [1].
✓	CMR-SR-AC-MA-2 - The aircraft shall utilise off-the-shelf components wherever possible.
✓	CMR-SR-SA-AS-7 - The aircraft shall provide protection against on board calamities.
✓	CMR-SR-SA-AS-8 - The aircraft shall provide a safe environment for passengers and crew.

16 Future Phases

After this initial design phase, many more activities need to be described before HAMMER goes into service and when HAMMER is in service. These activities are are described as future phases in this chapter.

16.1. Project Design and Development Logic

The initial design of the HAMMER concept is now finished. However, before the HAMMER concept is ready to entry into service, it has to go through a lot more phases. These phases include further research and development, manufacturing and testing and certifying. Figure 16.2 shows these phases, including some more detailed tasks. For example, in further research, a client will have to be found first and the recommendations presented in this report will have to be incorporated. They are included in the diagram in general technical departments, but the specific recommendations can be found in the separate chapters in this report. Then, the aircraft will need to be manufactured to produce a 'number zero' aircraft, used for testing. This phase is not presented in detail here but will be presented in Section 16.2. When the aircraft is fully tested, the aircraft can be certified and more aircraft can be build. Lastly, the diagram shows a general timeline of the different phases. This timeline is given in more detail in Section 16.3.

16.2. Manufacturing, Assembly and Integration Plan

The Manufacturing, Assembly and Integration (MAI) plan gives a time ordered outline of the activities required to construct the product from its constituent parts [49]. It is a detailed version of the manufacturing phase of the project design and development logic diagram that appears in Figure 16.2. The green boxes are common in both diagrams and the white boxes are the intermediate steps that are taken to go from one top level activity to the other. There are several AND and OR loops to illustrate the activities that can be performed simultaneously and the activities that exclude each other.

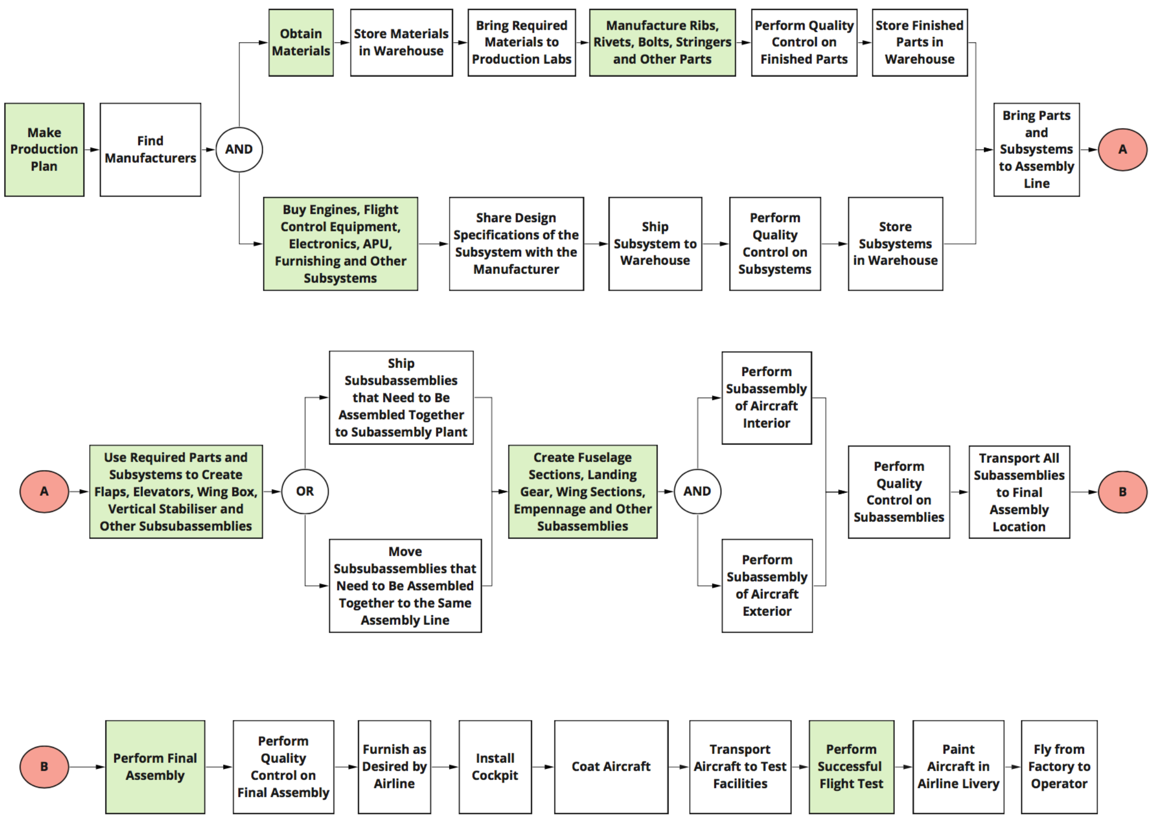

Figure 16.1: Manufacturing, Assembly and Integration (MAI) plan.

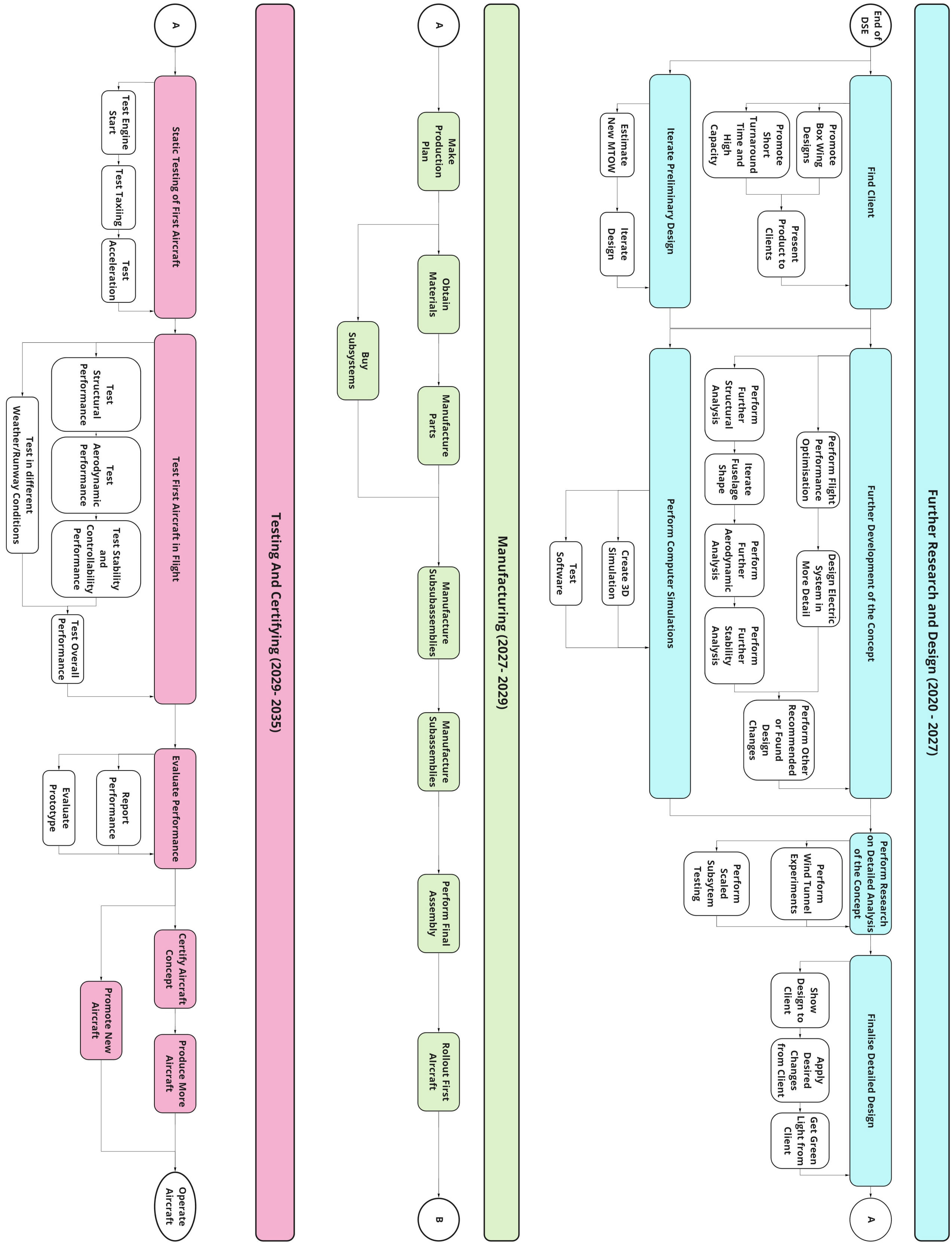

Figure 16.2: The future phases of the project.

16.3. Project Gantt Chart

In Figure 16.3 the Gantt chart of the future phases of the HAMMER is shown. It is aligned with the project design and development logic diagram in Figure 16.2 and adds a time indication to is facets. As required the HAMMER will be ready to fly in 2035. Since the amount of flights was estimated to comparable to that of an A320, a lifetime of 25 years was assumed[1], after which the aircraft is partly recycled and partly disposed.

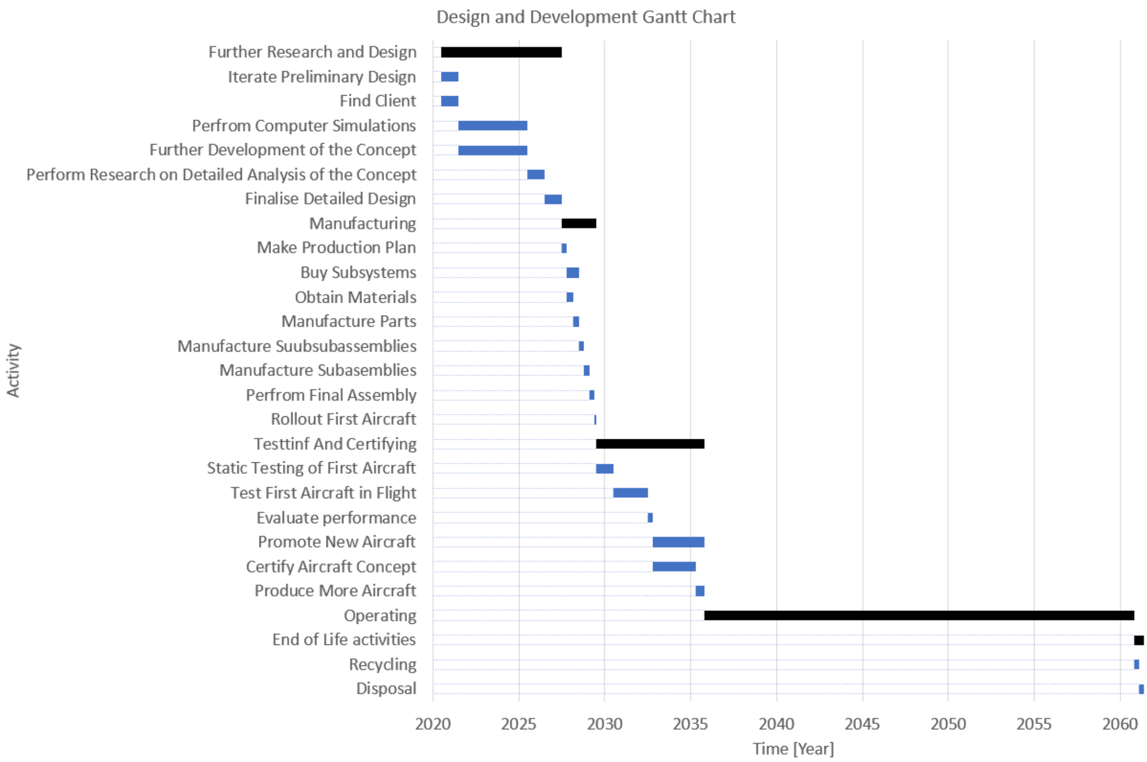

Figure 16.3: Gantt chart of the future phases for HAMMER.

16.4. Operations and Logistic Concept Description

After manufacturing HAMMER is distributed from the factory to the new base of the aircraft with a ferry flight. Operators need to hire a ferry pilot for this flight. Once the aircraft has arrived at its base operations can start. During operation, HAMMER is supported by several systems and aviation parties. These elements either ensure the physical fly-ability or contribute to the planning of flights or exact routes. Regular civil operations are describe in four facets below. The facets are visualised by support pyramids of three levels. Generally the top-level has direct verbal or physical contact with HAMMER. The second level provides the first level. Lastly, the third level formulates general restrictions, regulations or flight specific wishes for the facet in question.

Crew

An aircraft crew provides HAMMER with piloting and guidance and service for passengers. Operators provide their aircraft with a crew and determines services like how often the crew is to offer beverages to the passengers. Being part of the HAMMER crew requires knowledge of the HAMMER systems. Flight (attendant) academies and operators will thus have to educate crews about the relevant ins and outs of HAMMER. This also requires flight simulator companies to provided proper box wing simulations. The aircraft manufacturer will provide the specifications of the HAMMER to both simulation companies and training instances for the crew. The crew support pyramid is show in Figure 16.4. Crew has to be accommodated by HAMMER as well as the equipment they use for their services. One should think of seats for cabin crew and pilots, galleys for catering trolleys and the controls and displays in the cockpit.

Airport

A crucial role in operations is played by the airport. The aircraft is serviced directly serviced by several vehicles and ground operation agents. Passenger related services are the catering of the aircraft, potable and waste water servicing, cleaning and the handling of the passengers up until entering the aircraft en from the moment they leave it. More technical airport services include the refuelling of the box wing and proving ground power by a ground power

[1]https://sim-on-a320.com/blog/2018/01/07/airplane-lifespan-maintenance-disassembly-and-dismantle/[Cited 29 June 2020]

unit. Besides the aforementioned the airport has to provide the aircraft with a place to park, a strip to land on and a strip for take-off. Without saying this also comes routes for taxiing form and to the runway. One could say the above are in direct contact with the HAMMER, however, they need to be managed and/or maintained. Both the airport and several airport situated companies provide the trucks and personnel that service the aircraft. An apron coordinator is needed for safe ground handling procedures. Operators, airports and airport situated companies will have to contract and schedule their co-operations. Guidelines for the airport related operations are provided by air traffic authorities and the aircraft manufacturer. Specific wishes are communicated by the operator. The airport support pyramid is shown in Figure 16.5. The HAMMER thus requires interfaces to allow the services to the aircraft. This amounts to the necessary presence of interfaces like fuelling ducts and doors for catering. This pyramid formed a large basis for the operations described in Chapter 10.

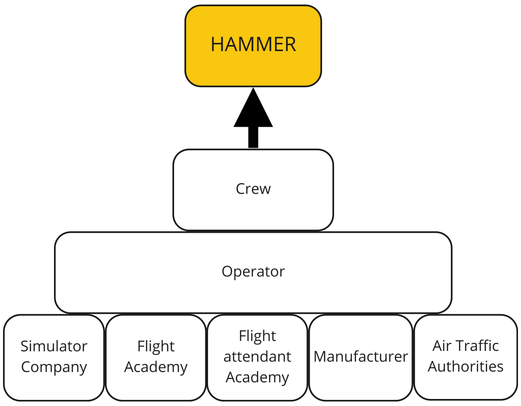

Figure 16.4: Operational support by the crew pyramid.

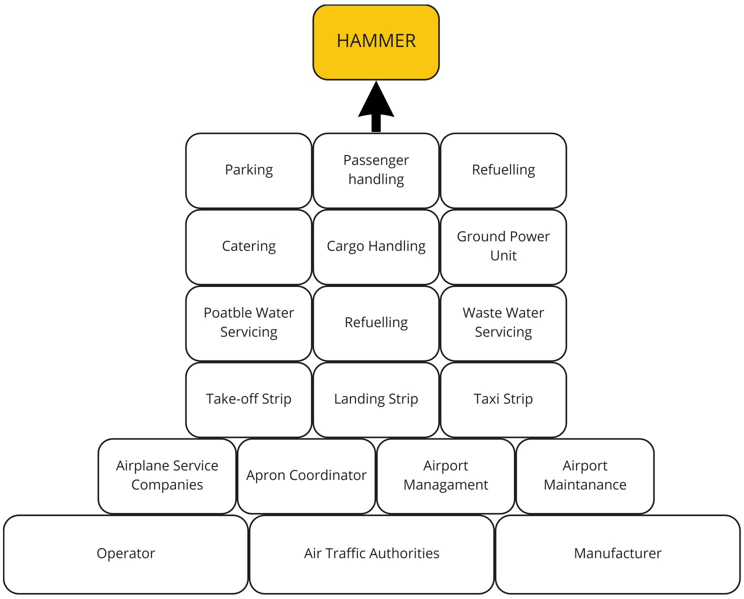

Figure 16.5: Operational support by the airport pyramid

Maintenance
The aircraft needs to be maintained. This can either be planned maintenance or maintenance because of recorded damage during checks if unplanned maintenance is needed. Directly involved with this are the mechanics that execute this maintenance. These are provided by maintenance companies. When and how maintenance or checks are done is determined by a mix of manufacturer guidelines, air traffic authority restrictions, the aircraft operator and how mechanics are trained. Also the plane and ground crew are expected to pay attention to possibly present damage and report this. The maintenance support pyramid is show in Figure 16.6. Crew is also found int the second level, as they do have the responsibility of checking if maintenance is needed. Maintenance requires the aircraft to be accessible for maintenance and inspection by doors, hatches, instruments and removable plates. Parts should be replaceable is necessary.

Flight planning
The routes that HAMMER will fly have to be determined both at macro and micro level. Planning the when and where of a flight is done by the operator and scheduled after contact with the involved airports. The precise timing, airport routes, headings and altitudes are determined by air traffic control: Tower Control, Approach Control, Area Control, Ground Control and Delivery / Startup. Air traffic control is partly provided by airports, partly by non-departmental agencies and partly government regulated. Again, guidelines and restrictions are formulated by air traffic authorities and national and international policies. The flight planning support pyramid is show in Figure 16.7. The HAMMER requires systems like the transponder and radio's to be supported by the organs described above.

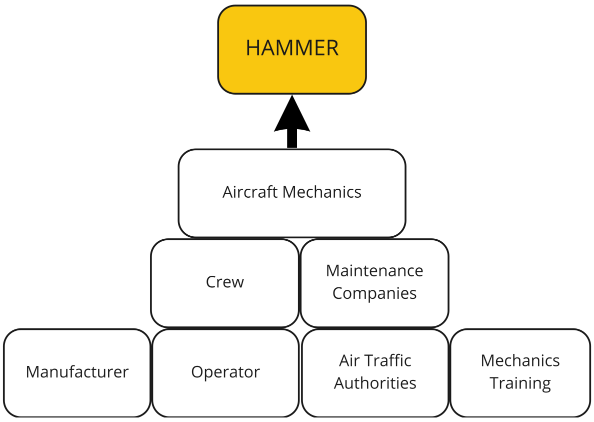

Figure 16.6: Operational support by the maintenance pyramid.

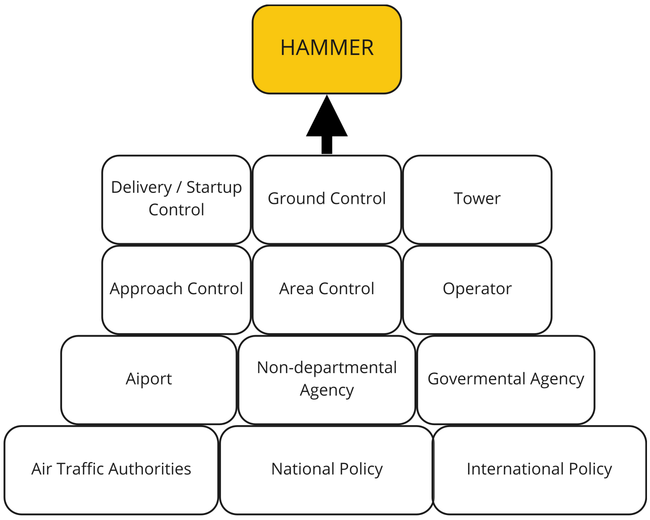

Figure 16.7: Operational support by the flight planning pyramid

17 Conclusion and Recommendations

17.1. Conclusion

This DSE started of with a handed objective: evaluate the design feasibility and socio-economically accessibility of a compact, high-capacity, mid-range aircraft that has a short ground turnaround time, with 10 students for 10 weeks. Fulfilling this objective meant to fill a gap in the civil aviation market that asks for the transport of an A330 payload, while matching the airport characteristics of the A320.

A box wing configuration was selected for what would become the HAMMER aircraft, as this configuration proved to be an efficient way to keep the wingspan of the aircraft below 36 [m] whilst generating sufficient lift for 320 passengers in a single class configuration. The general layout is further completed by a double vertical tail, the horizontal double bubble shaped wide-body fuselage, two fuselage mounted turbofan engines and a tricycle landing gear. The layout can be viewed in the CAD drawings in Figure 17.1 and Figure 17.2. An overview of the HAMMER characteristics can be found in Table 17.1.

The chosen configuration is innovative and unconventional, which brings its challenges in every aspect of the design. Landing gear pods on the side of the fuselage enabled integration of the landing gear, without interfering with the cargo holds. Large and highly efficient turbofan engines were installed, in combination with the possibility of installing a jump strut, to achieve a low take-off distance. A wall within the aircraft cabin allowed for the pressurisation of the double bubble, while providing new marketing possibilities for solo travellers who would like more privacy during the flight.

A length requirement on the aircraft challenged the design a lot, however in the end the design goal of transporting 320 passengers was exactly met. HAMMER is able to reach the cruise speed of 0.78 Mach, noise levels are kept within acceptable limits and HAMMER can be operated at airfields suitable for ICAO reference code 3C aircraft. The complete HAMMER aircraft was successfully designed to be operational by 2035.

To conclude, it was found that indeed the aircraft can perform the design mission with excellence, using an astonishing 44% less fuel than the A320 per passenger per kilometre. However, the maximised payload range efficiency of 6237 [$\frac{kg \cdot km}{kg}$] for HAMMER was not found to be higher than the PRE of the airbus A321. The turnaround time is within limits, being only 10% larger than the A320's. Compared to the A330 the turnaround time was decreased by 18%.

From an economical perspective, the HAMMER aircraft provides business opportunities for all major stakeholders. Airports can see their revenue increase due to the decongestion and increase in annual passenger movements. Manufacturers of HAMMER can capitalise on the fastest growing market segment with 33,000 forecasted aircraft deliveries worth an estimated $4.5 trillion. Operators of HAMMER can expect their operational profits to increase by 112% compared to current narrow body commercial jets in operation. All in all, for all stakeholders, the HAMMER aircraft is predicted to economically outperform current commercial jets.

Figure 17.1: View of HAMMER parked at an airport.

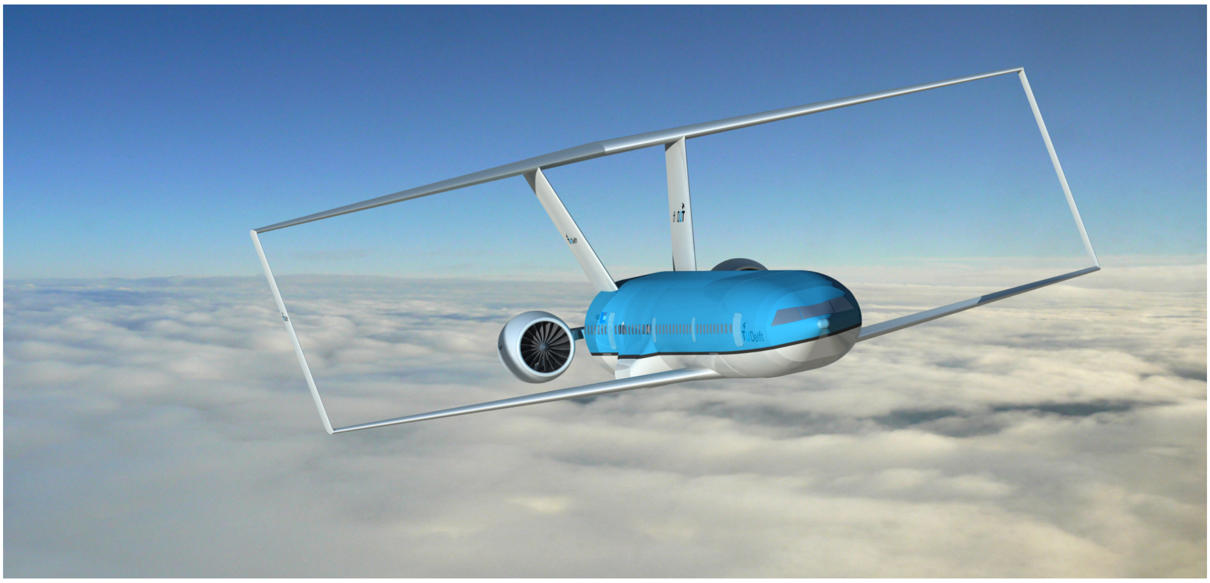

Figure 17.2: View of HAMMER in flight.

Figure 17.3: View of HAMMER at Schiphol airport.

17.2. Recommendations

Several aspects of the HAMMER were not, or not sufficiently, studied during this project due to constraints in resources. Multiple unsolved problems, preliminary estimations and unexplored but interesting options are still left to be explored in greater detail. Therefore, for the future of this project, several recommendations were made:

- Improving the aerodynamics and flight dynamics model: One problem area of this project is the aerodynamic model used for analysis. Improving the accuracy of the gathered values has a lot of consequences for the aircraft. Many gains can be made for the departments of stability and controllability, structural and materials, and aerodynamics. This is mainly due to the uncertainty of the distributed forces of the wing. In a conventional wing configuration the lift is introduced in a single point. While lift distribution is still important, a change in distribution wont shift the application point much. In a box wing however the lift application points are separated by a large distance which greatly affect the stability and structural design. Improving the used tools will therefore greatly assist to advance the project. Especially a more accurate AVL model and a model that is standard for a box wing aircraft instead of a conventional aircraft.
- Improving the weight estimate: Due to the unconventional design, the weight distribution is different from conventional aircraft. For example, the vertical supports required for the double bubble design add weight that is not present in most aircraft. Furthermore, the initial weight estimation that was done uses a statistical relation based on reference aircraft that have a conventional configuration. This does not include the contribution of the extra central wing box required for the aft wing or the existence of the lateral connectors and vertical tail structural reinforcements. Lastly, a large number of LD-3 containers were added but these also

greatly increase weight. Improving the weight estimation will yield a better estimate of the aircraft balance which improves the stability and controllability aspects. Additionally, a better estimate of the overall weight increases the accuracy of the flight performance analyses.

- Improving the structural model: Many structural components are sized using preliminary, conservative sizing estimates. The accuracy of these models is rather low, leading to a high uncertainty in structural parameters. On top of that, several failure modes of the structures are not covered. These include but are not limited to torsional loads, vibrational loads like flutter, as well as buckling. Including these failure modes into the analysis and adopting more complete (finite element) models will allow for a more efficient structural design, with a higher accuracy, leading to an overall safer and lighter structure.
- Further optimising the double bubble configuration: As stated in Chapter 8, the aircraft could benefit from optimising the double bubble configuration to minimise the cross section. This would not only reduce the structural weight, but it would also contribute to lower drag, which results in improvements such as lower fuel consumption.
- Further research in the double bubble cabin: The double bubble fuselage is a way of creating a wide fuselage without this fuselage being unnecessary high. However, a middle wall (closed or with holes) is needed for pressurisation, which limits freedom in the use of HAMMER volume. It is thus recommended to research efficient ways to deal with the pressurised double-bubble and the efficiency of other configurations that allow for a wide body.
- Further development of the electric taxi system and APU: The electric taxi system proved to be a promising system for the HAMMER project. However, such a system does increase the power consumption and requires extra batteries. To add to that, an off the shelf APU is used. To improve the sustainability, and improve future expandability, new types of APU system should be researched.

Table 17.1: An overview of the preliminary characteristics of the box wing concept.

Parameter	**Value**	**Parameter**	**Value**
MTOW [*kg*]	126518	Take off distance [*m*]	1266
OEW [*kg*]	53773	Landing field distance [*m*]	1437
Fuel mass [*kg*]	28744	Taper ratio [-]	0.295
Payload mass [*kg*]	44000	Root chord [*m*]	5.10
Wing loading [N/m^2]	5218	Tip chord [*m*]	1.51
Thrust to weight ratio [-]	0.33	Aspect ratio (total) [-]	5.45
Passengers [-]	320	Sweep angle [°]	30.0
Wing surface area [m^2]	237.9	Payload-range efficiency [$\frac{kg \cdot km}{kg}$]	6237
Wingspan [*m*]	36.0	CO_2/km/passenger [$g/km/pax$]	55.0
Cruise speed [m/s]	230	Fuel savings w.r.t. to A320/per pax [%]	-44.1
Oswald efficiency [-]	1.27	Fuselage length [*m*]	44.97
Zero-lift drag coefficient [-]	0.0181	Fuselage diameter [*m*]	6.1
Project cost [$]	23.5 Billion	Unit cost [$]	220Million
Takeoff thrust [kN]	402.18	Cruise thrust [kN]	173.1
Turn around time [min]	48.5	Turn around time w.r.t. A320 [-]	+10%

Bibliography

[1] European Aviation Safety Agency. *Certification Specifications and Acceptable Means of Compliance for Large Aeroplanes CS-25*. 2016.
[2] Boeing Commercial Airplanes. 767 airplane characteristics for airport planning, September 2005.
[3] Boeing Commercial Airplanes. Preparing ramp operations for the 787-8, July 2008.
[4] Boeing Commercial Airplanes. 777 airplane characteristics for airport planning, May 2015.
[5] Boeing Commercial Airplanes. 737 max airplane characteristics for airport planning, July 2019.
[6] R. Alderliesten. Introduction to aerospace engineering - structures and materials, October 2011.
[7] R. Alderliesten. *Fatigue and Fracture of Fibre Metal Laminates*. Springer, 2017.
[8] R.C. Alderliesten and A. Vlot. Modelling fatigue crack growth characteristics of glare. 2001.
[9] R.C. Alderliesten, M. Hagenbeek, J.J. Homan, P.A. Hooijmeijer, T.J. de Vries, and C.A.J.R. Vermeeren. Fatigue and damage tolerance of glare. *Applied Composite Materials*, pages 223–242, 2003.
[10] R.C. Alderliesten, M. Hagenbeek, J.J. Homan, P.A. Hooijmeijer, T.J. de Vries, and C.A.J.R. Vermeeren. An empirical model for fatigue behavior prediction of glass fibre-reinforced plastic composites for various stress ratios and test frequencies. *Composites Part A: Applied Science and Manufacturing*, pages 313–326, 2003.
[11] J. D. Anderson. *Introduction to Flight*. McGraw-Hill Education, 2016.
[12] L. Bertsch, D. G. Simons, and M. Snellen. Aircraft noise: The major sources, modelling capabilities, and reduction possibilities.
[13] Boeing. Boeing commercial market outlook 2019 - 2038, September 2019.
[14] J. Bosch, S. de Jong, R. Hoefnagels, and R. Slade. Aviation biofuels: strategically important, technically achievable, tough to deliver, 2017.
[15] S. Bozhko, C. Hill, and T. Yang. *More Electric Aircraft: Systems and Modeling*. 06 2018. doi: 10.1002/047134608x.w8367.
[16] M. K. Bradley and C. K. Droney. Subsonic ultra green aircraft research: Phase i final report. Technical Report NASA/CR–2011-216847, Boeing Research & Technology, NASA, April 2011.
[17] M. K. Bradley, C. K. Droney, and T. J. Allen. Subsonic ultra green aircraft research: Phase ii - volume i - truss braced wing design exploration. *NASA/CR-2015-2178704*, I:18–19, 2015.
[18] A.A.R. Broer. Fatigue life prediction of carbon fibre-reinforced epoxy laminates using a single s-n curve, 2018.
[19] J. Charytonowicz. Advance in human factors, sustainable urban planning and infrastructure, 2018.
[20] F. Collot d'Escury, G. Frehe, I. Janssen, W. Kruin, G. Maré, P. Meseguer Berroy, J. Phillips, J. de Ridder, S. Vanleeuwen, and S. Verweij. Baseline report - new generation high capacity compact mid ranger, 2020.
[21] F. Collot d'Escury, G. Frehe, I. Janssen, W. Kruin, G. Maré, P. Meseguer Berroy, J. Phillips, J. de Ridder, S. Vanleeuwen, and S. Verweij. Midterm report - new generation high capacity compact mid ranger, 2020.
[22] EASA. Easa type-certificate data sheet cfm56, 2008.
[23] J.C. Eppel, G. Hardy, and J.L. Martin. *Flight Investigation of the Use of a Nose Gear Jump Strut to Reduce Takeoff Ground Roll Distance of STOL Aircraft*. Ames Research Center, 1994.
[24] EUROCONTROL. European wake turbulence categorisation and separation minima on approach and arrival, 2015.
[25] V. Giurgiutiu. *STRUCTURAL HEALTH MONITORING OF AEROSPACE COMPOSITES*. Elsevier, 2016.
[26] R. Groot. Stability & control derivatives prediction for box wing aircraft configurations, 2019.
[27] M. Hagenbeek, C. Hengel., O. J. Bosker, and C. A. J. R. Vermeeren. *Static Properties of Fibre Metal Laminates*. Springer, 2013.
[28] R.J. Hamann and M.J.L. van Tooren. Systems engineering and technical management techniques lecture notes, 2006.
[29] M. T. E. Heinrich, F. Kelch, P. Magne, and A. Emadi. Investigation of regenerative braking on the energy consumption of an electric taxiing system for a single aisle midsize aircraft. *IECON 2014 - 40th Annual Conference of the IEEE Industrial Electronics Society*, pages 3023–3029, 2014. doi: 10.1109/IECON.2014.7048940.
[30] T. Horstmeier and F. de Haan. Influence of ground handling on turn round time of new large aircraft. *Aircraft Engineering and Aerospace Technology*, pages 266–270, 2001.
[31] T. Horstmeier and F. de Haan. Fatigue strength of carbon fibre composites up to the gigacycle regime (gigacycle-composites). *International Journal of Fatigue*, pages 261–270, 2006.
[32] L. Jenkinson, P. Simpkin, and D. Rhodes. *Civil Jet Aircraft Design*. American Institute of Aeronautics and Astronautics, Inc., 1999.
[33] H. Korner and G. Redeker. Recent developments at dfvlr, 1924.
[34] A. K. Kundu, M. A. Price, and D. Riordan. *Conceptual Aircraft Design: An industrial approach*. John Wiley & Co, 2019.
[35] K.Y. Maalawi. *Optimum Composite Structures*. IntechOpen, 2019.
[36] J. D. Mattingly, W. H. Heiser, and D. T. Pratt. *Aircraft Engine Design*. American Institute of Aeronautics and

Astronautics, Inc., 2002.
[37] T. Megson. *Aircraft structures for engineering students*. Elsevier, 2013.
[38] F. meng, S. J. Pickering, and J. McKechnie. An environmental comparison of carbon fibre composite waste end-of-life options, 2018.
[39] V. Mukhopadhyay and M. R. Sorokach. Composite structure modeling and analysis of advanced aircraft fuselage concepts, 2016.
[40] J.A. Mulder, W.H.J.J. van Staveren, J.C. van der Vaart, E. de Weerdt, C.C. de Visser, A.C. in 't Veld, and E. Mooij. Flight dynamics, October 2013.
[41] A. Nutia, F. Bertinia, V. Cipolla, and G. Di Ritoa. Design of a fuselage-mounted main landing gear of a medium-size civil transport aircraft. *The Journal of Aerospace Science, Technology and Systems*, 2018.
[42] Dr. F. Oliviero. Aerospace design and systems engineering elements ii ae2111-ii aircraft part - aircraft aerodynamic analysis – mobile surfaces of the wing, 2018.
[43] Dr. F. Oliviero. *Systems Engineering and Aerospace Design: Overview and Recap, Aircraft Balance*. Delft University of Technology, 2020.
[44] F. Oliviero, V. Cipolla, and D. Zanetti. Flight dynamics model for preliminary design of prandtlplane wing configuration with sizing of the control surfaces. *The Journal of Aerospace Science, Technology and Systems*, 95: 201–210, 2016.
[45] International Civil Aviation Organisation. Noise certification workshop, 2006.
[46] International Civil Aviation Organisation. Manual on the establishment of minimum cabin crew requirements, 2017.
[47] L. Prandtl. Induced drag of multiplanes, 1924.
[48] P. Proesmans. Preliminary propulsion system design and integration for a box-wing aircraft configuration, 2019.
[49] G. La Rocca. Project guide design synthesis exercise:new generation high-capacity compact mid ranger. TU Delft, 4 2020.
[50] P.C. Roling and M. Voskuijl. Airfield performance - flight and orbital mechanics, 2018.
[51] J. Roskam. *Airplane Design Part 1 to 4*. Roskam Aviation and Engineering Corporation, 1985.
[52] J. Roskam. *Airplane Design VIII: Airplane Cost Estimation: Design, Development, Manufacturing and Operating*. DARcorporation, 1990.
[53] M. A. Rossi. Design and analysis of a composite fuselage. *Brazilian Symposium on Aerospace Eng. & Applications*, 2009.
[54] G. J. J. Ruijgrok. *Elements of airplane performance*. Delft Academic Press, 2013.
[55] D. R. Sanchez. Analysis of ground handling characteristics of innovative aircraft configurations, September 2009.
[56] AIRBUS S.A.S. A320 aircraft characteristics airport and maintenance planning, April 2020.
[57] AIRBUS S.A.S. A321 aircraft characteristics airport and maintenance planning, April 2020.
[58] AIRBUS S.A.S. A330 aircraft characteristics airport and maintenance planning, April 2020.
[59] AIRBUS S.A.S. A350 aircraft characteristics airport and maintenance planning, May 2020.
[60] D. Schiktanz and D. Scholz. Box wing fundamentals - an aircraft design perspective. *Deutscher Luft- und Raumfahrtkongress*, pages 606 – 607, 2011.
[61] D. Schiktanz and D. Scholz. Box wing fundamentals – an aircraft design perspective. *Journal of Aircraft*, pages 601–615, 2011.
[62] M. Schmidt. A review of aircraft turnaround operations and simulations. *Progress in Aerospace Sciences*, pages 25–38, 2017.
[63] AIRBUS Customer Services. aircraft performance monitoring, December 2002.
[64] D. G. Simons. *Introduction to Aircraft Noise*. TU Delft, 2019.
[65] G. M. Simons. *The Airbus A380: A History*. Pen and Sword Aviation, 2014.
[66] M. Sinnett. 787 no-bleed systems: Saving fuel and enhancing operational efficiencies. *Aero Quarterly*, QTR 4, 2007.
[67] S.W.F. Spronk, I.Sen, and R.C. Alderliesten. Predicting fatigue crack initiation in fibre metal laminates based on metal fatigue test data. *International Journal of Fatigue*, pages 428–439, 2015.
[68] T. Stalnaker, G. Alport, A. Buchanan, and A. Taylor. Airline economic analysis 2018-2019 edition, 2019.
[69] C. Varriale, A. Raju Kulkarni, G. La Rocca, and M. Voskuijl. A hybrid, configuration-agnostic approach to aircraft control surface sizing, 2019.
[70] R. Vos and J.A. Melkert. *Aerospace Design and Systems Engineering Elements I*. Delft University of Technology, 2017.
[71] R. Vos and J.A. Melkert. *Aerospace Design and Systems Engineering Elements I: The Design of the Fuselage*. Delft University of Technology, 2017.
[72] M. A. York, W. W. Hoburg, and M. Drela. Turbofan engine sizing and tradeoff analysis via signomial programming. *Journal of Aircraft*, 55:988–1003, 2018. doi: 10.2514/1.C034463.

A Wing Loading System of Equations

In order to estimate the reaction forces of the wing a system of sixteen equations has to be solved. These equations are presented in this appendix. The first three equations follow from equilibrium of the total structure, the next six from equilibrium of the bottom and top beam respectively. Then four equations are obtained by applying the clamped support boundary conditions and two from the bending compatibility of both beams. The last equation is found by considering the twisting compatibility of the beams. The nomenclature is in line with Chapter 8. Graphical representations of the terms can be found in Figure 8.3 and Figure 8.4.

Total structure:

$$\sum F_y : A_y + D_y + L_t l_t + L_b l_b = 0 \tag{A.1}$$

$$\sum M_D : -A_y scos(\Lambda_t) + M_a + M_d + L_b l_b(0.5cos(\Lambda_b)l_b - scos(\Lambda_t)) + 0.5L_t l_t^2 cos(\Lambda_t) = 0 \tag{A.2}$$

$$\begin{aligned}\sum T_D : T_a + T_d - A_y(l_c + \frac{b}{2} * tan(\Lambda_{b,c}) + l_t * cos(\Lambda_t) * tan(\Lambda_{t,c})) + \int_0^{\frac{b}{2}} m_b dx_b \\ + \int_0^{l_t cos(\Lambda_t)} m_t dx_t - L_b l_b \left(\frac{l_b sin(\Lambda_b}{2} + l_c + l_t sin(\Lambda_t) + \Delta cc_{rt}\right) - L_t l_t \left(\frac{l_t sin(\Lambda_t}{2} + \Delta cc_{rt}\right) = 0\end{aligned} \tag{A.3}$$

Beam 1:

$$\sum F_y : A_y + B_y + L_b l_b = 0 \tag{A.4}$$

$$\sum M_B : M_a + M_b - A_y l_b * cos(\Lambda_b) - 0.5L_b l_b^2 cos(\Lambda_b) = 0 \tag{A.5}$$

$$\sum T_B : T_a + T_b - A_y \frac{b}{2} tan(\Lambda_{b,c}) + \int_0^{\frac{b}{2}} m_b dx_b - L_b l_b(\Delta c(c_{rb} + c_{tb})0.5 + 0.5\frac{b}{2}tan(\Lambda_{b,c})) = 0 \tag{A.6}$$

Beam 2:

$$\sum F_y : D_y + C_y + L_t l_t = 0 \tag{A.7}$$

$$\sum M_C : M_c + M_d - D_y l_t cos(\Lambda_t) - 0.5L_t l_t^2 cos(\Lambda_t) = 0 \tag{A.8}$$

$$\sum T_C : T_c + T_d + D_y l_t cos(\Lambda_t) tan(\Lambda_{t,c}) + (0.5 l_t cos(\Lambda_t) tan(\Lambda_{t,c}) - \Delta c 0.5(c_{rt} + c_{tt})) + \int_0^{l_t cos(\Lambda_t} m_t dx_t = 0 \tag{A.9}$$

Bending compatibility:

$$C_1 = (EI)_b \left(\frac{d\nu_b}{dx_b}\right)_{x_b=0} \tag{A.10}$$

$$C_2 = (EI)_b(\nu_b)_{x_b=0} \tag{A.11}$$

$$C_3 = (EI)_t \left(\frac{d\nu_t}{dx_t}\right)_{x_t=0} \tag{A.12}$$

$$C_4 = (EI)_t(\nu_t)_{x_t=0} \tag{A.13}$$

$$\begin{aligned}\left(\frac{1}{EI}\right)_b \left(-M_a\frac{b}{2} + \frac{A_y \frac{b}{2}^2}{2} + \frac{L_b \frac{b}{2}^3}{6cos(\Lambda_b)} + C_1\right) = \\ \left(\frac{1}{EI}\right)_t \left(-M_d l_t cos(\Lambda_t) + \frac{D_y(l_t c0s(\Lambda_t))^2}{2} + \frac{L_t(l_t cos(\Lambda_t))^3}{6cos(\Lambda_t} + C_3\right) + \Delta\frac{d\nu}{dx}\end{aligned} \tag{A.14}$$

$$\left(\frac{1}{EI}\right)_b\left(\frac{-M_a\frac{b}{2}^2}{2}+A_y\frac{\frac{b}{2}^3}{6}+L_b\frac{\frac{b}{2}^4}{24cos(\Lambda_b)}+C_1\frac{b}{2}+C2\right)=$$
$$\left(\frac{1}{EI}\right)_t\left(\frac{-M_d(l_tcos(\Lambda_t))^2}{2}+\frac{D_y(l_tcos(\Lambda_t))^3}{6}+\frac{L_t(l_tcos(\Lambda_t))^4}{24cos(\Lambda_t)}+C_3(l_tcos(\Lambda_t)+C_4\right)+\Delta\nu \tag{A.15}$$

Torsion compatibility:

$$\left(\frac{1}{GJ}\right)_b\int_0^{\frac{b}{2}}T_1dx_b+\left(\frac{1}{GJ}\right)_t\int_0^{l_tcos(\Lambda_t)}T_2dx_t=\Delta\theta \tag{A.16}$$

B Engine Nacelle

Maximum nacelle diameter:

$$\varnothing_{nac_{max}}=1.21\cdot\varnothing_{fan} \tag{B.1}$$

Total nacelle length:

$$L_{nac_{tot}}=L_{cowl}+L_{afterbody} \tag{B.2}$$

$$L_{cowl}=2.36\cdot\varnothing_{fan}-0.01\cdot\left(\varnothing_{fan}M_{M0}\right)^2 \tag{B.3}$$

$$L_{afterbody}=\left((0.000475\cdot BPR\cdot\dot{m}+4.5)^2-\sqrt{\left(18-55\cdot\left(ln\left(\frac{\dot{M}}{(BPR+1)OPR}\right)\right)^{2.2}\right)}\right)\cdot 0.23 \tag{B.4}$$

C Electric Taxiing System

These are the formula's used for calculating the properties of the ETS, based on the predefined requirements. The formula's are partly retrieved from [29] and adjusted for this specific case.
Total rolling resistance force. The rolling friction coefficient is μ_r.

$$F_{tot_r}=F_w\cdot\mu_r \tag{C.1}$$

Total traction force on the MLG. WD is the fraction of the total weight that the MLG carries. COF is the coefficient of friction.

$$F_{tr_{MLG,max}}=COF\cdot F_W\cdot WD \tag{C.2}$$

Total traction force per tire in the MLG.

$$F_{tr_{MLG,S.T.}}=\frac{F_{tr_{MLG,max}}}{n_t} \tag{C.3}$$

Total traction force on the NLG

$$F_{tr_{NLG,max}}=COF\cdot F_W\cdot(1-WD) \tag{C.4}$$

Total traction force per tire in the NLG.

$$F_{tr_{NLG,S.T.}}=\frac{F_{tr_{MLG,max}}}{n_t} \tag{C.5}$$

Maximum traction force at maximum acceleration.

$$F_{tr}=m_{tot}\cdot a_{max} \tag{C.6}$$

Using the set requirements, one can calculate the total required work by summing the different taxi phases:

$$W_{req}=\int_0^s F_{tr}(s)ds \tag{C.7}$$

Required power, also to calculate max power:

$$P_{req}=\frac{W_{req}}{t} \tag{C.8}$$

Torque of a tire:

$$T_{tire} = \frac{F_{tr} \cdot r_{tire}}{n_t} \tag{C.9}$$

Torque of the motor, using the Gear Ratio (GR):

$$T_{tire} = GR \cdot T_{tire} \tag{C.10}$$

D A3 Diagrams

In this appendix the A3 diagrams are presented. First the functional breakdown structure and functional flow diagram are presented. Then, some technical drawings of the full aircraft, the engine and the landing gear are shown. These drawings of the full aircraft could be used to verify and validate how the different subsystems are integrated.

Functional Breakdown Structure

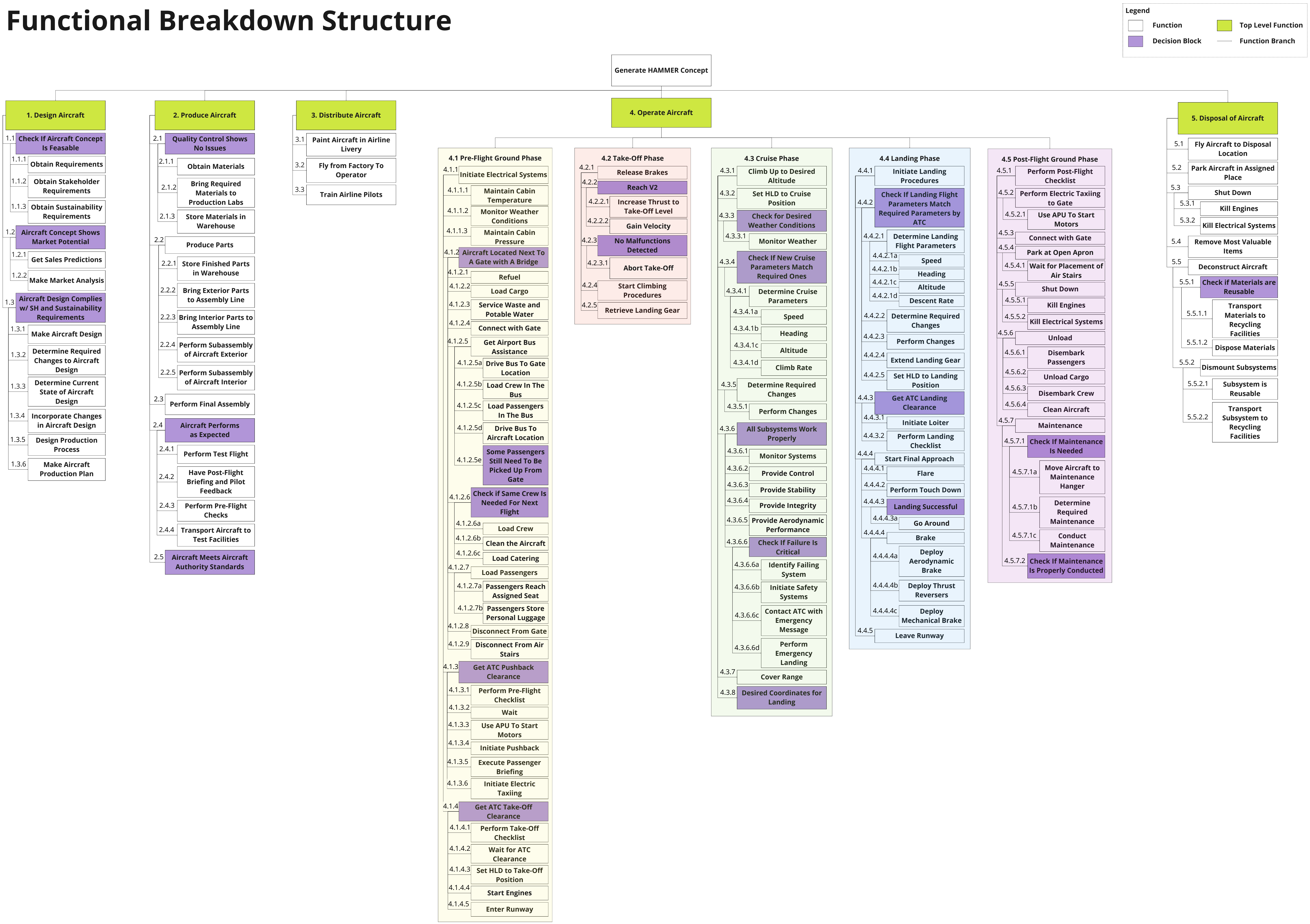

Functional Flow Diagram

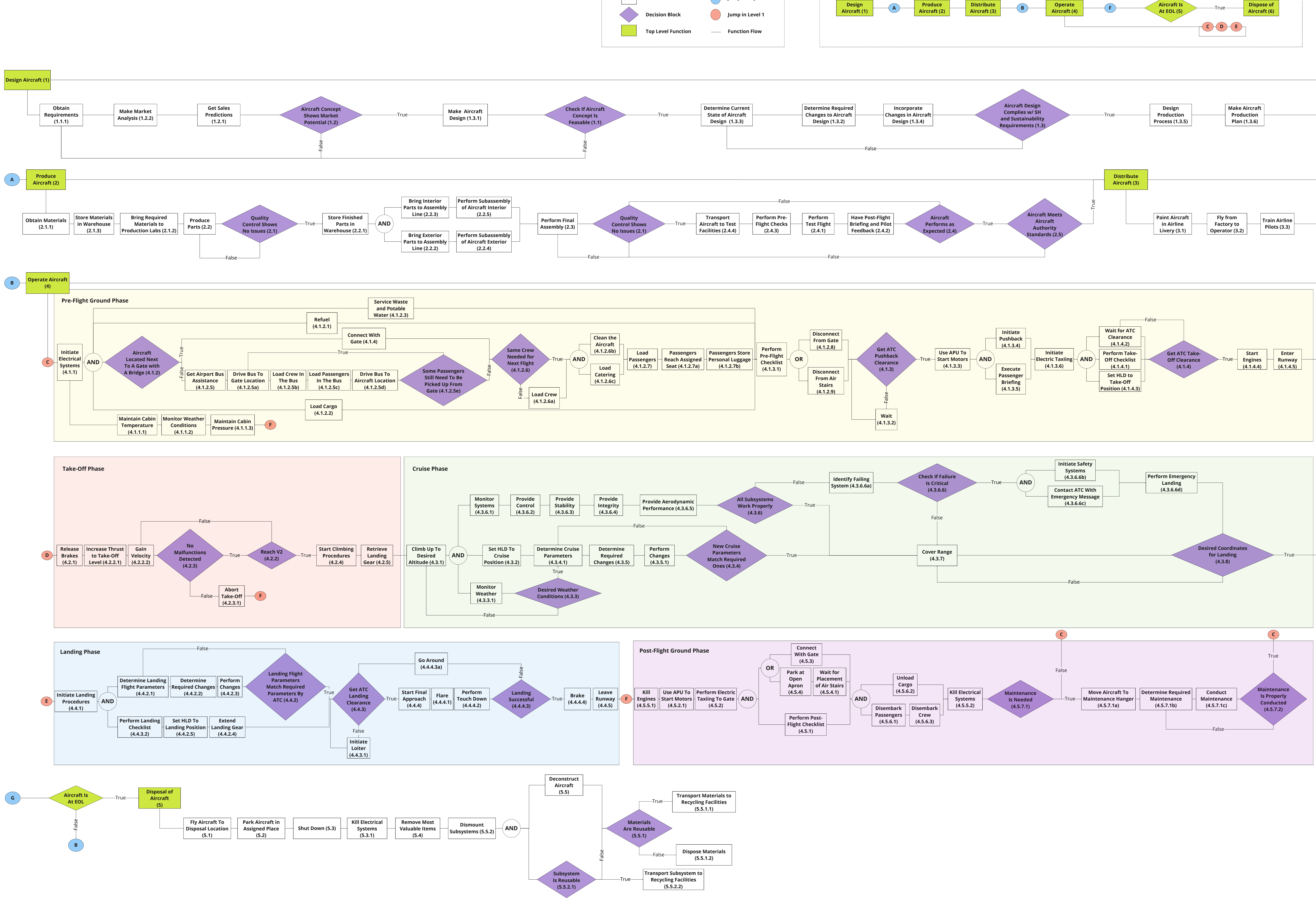

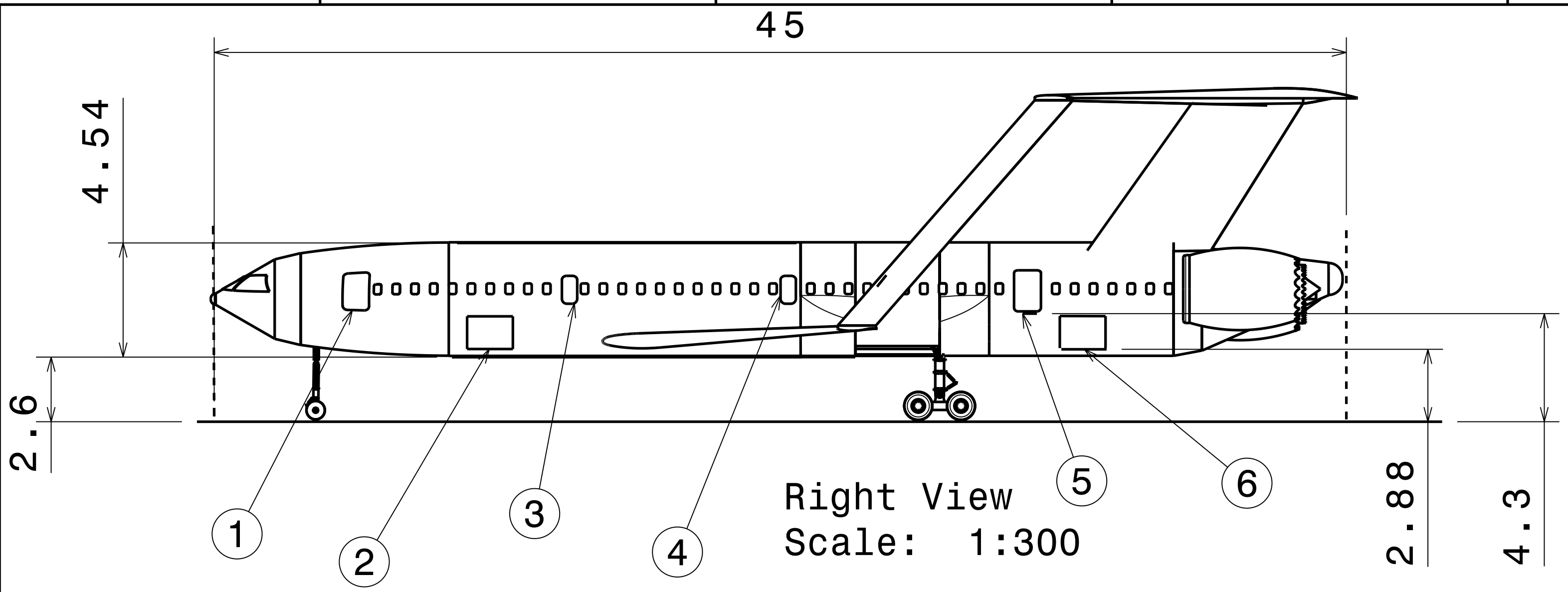

Right View
Scale: 1:300

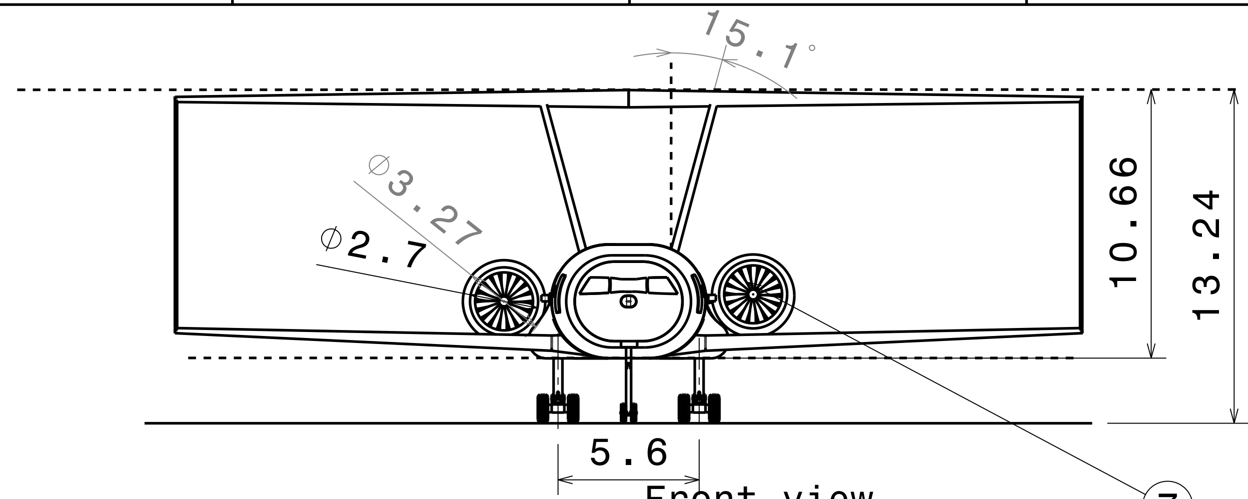

Front view
Scale: 1:300

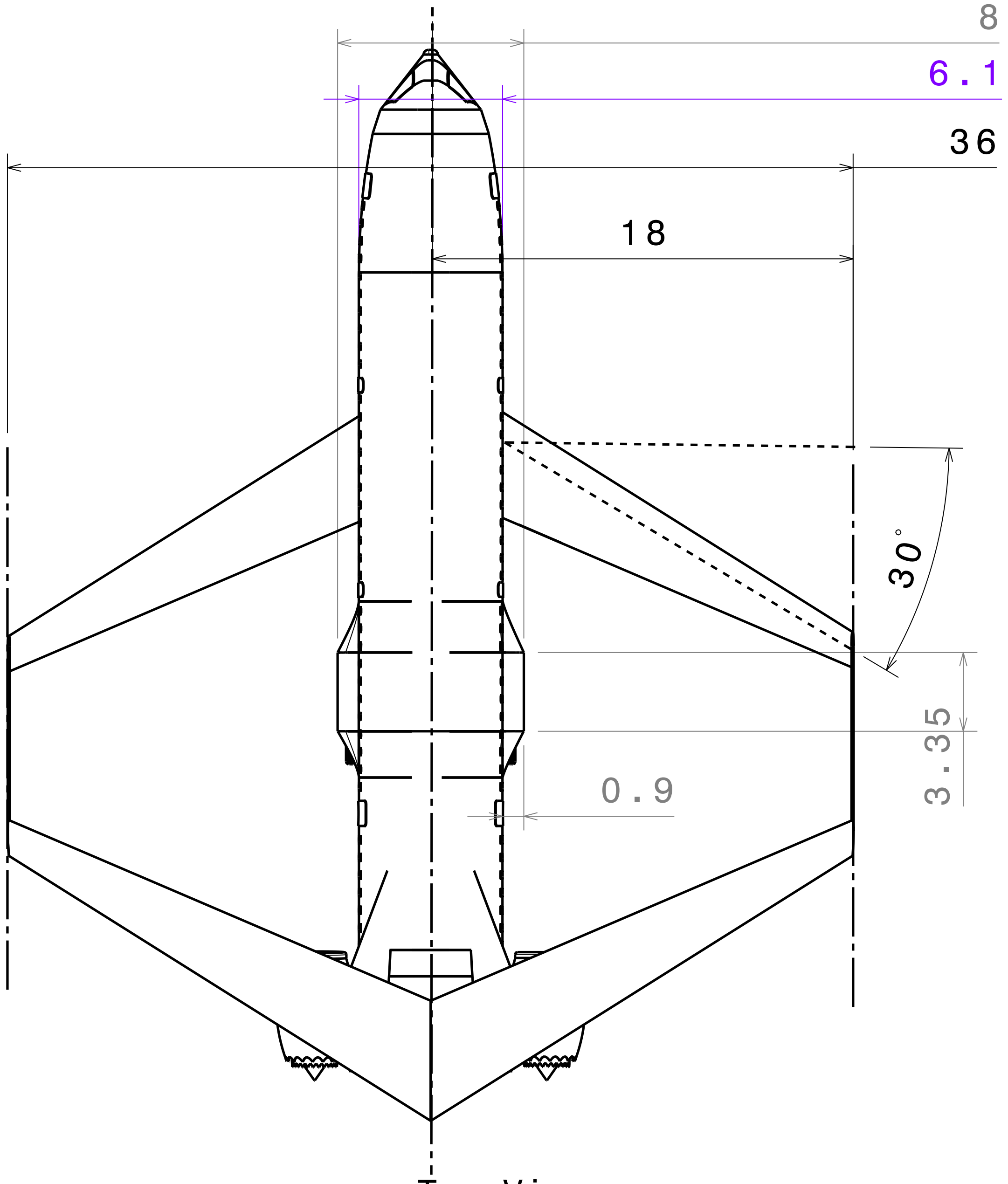

Top View
Scale: 1:300

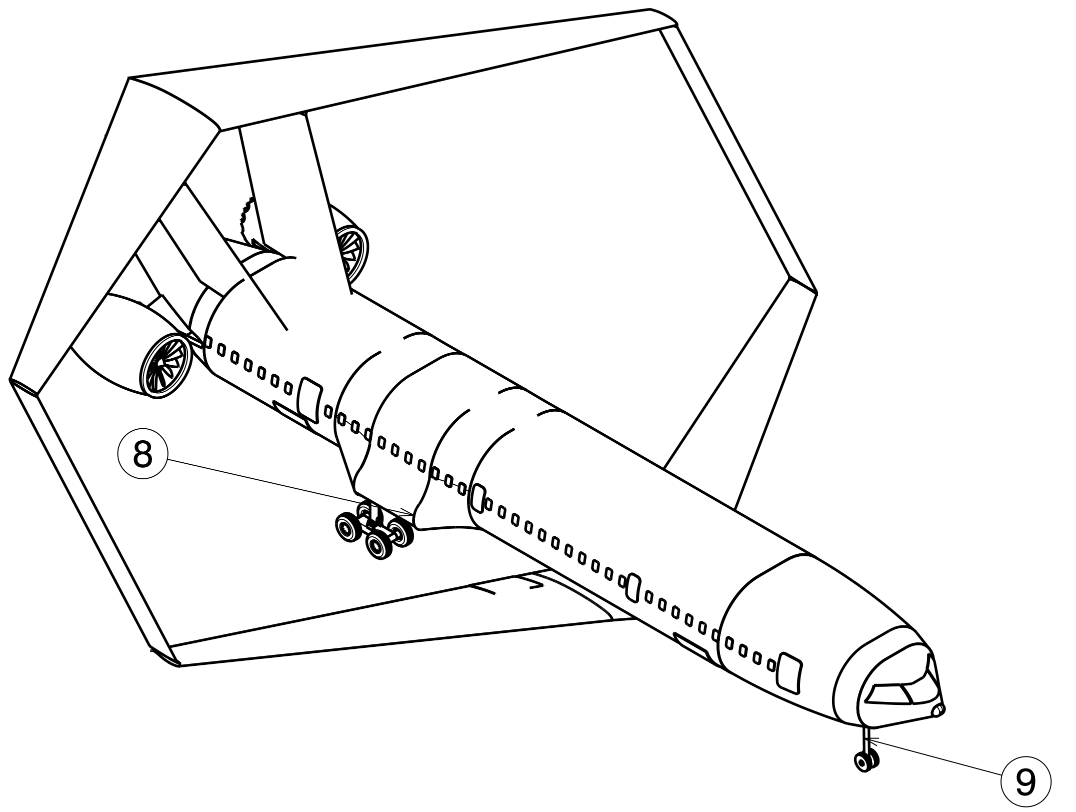

Isometric view
Scale: 1:300

1	Type A Door
2	Front Cargo Door
3	Type I Door
4	Type I Door
5	Type A Door
6	Aft Cargo Door
7	HBR Turbofan
8	Main Landing Gear Pod
9	Nose Landing Gear

DSE Group 18

DRAWN BY Gijs Frehe	DATE 28-6-2020	DRAWING TITLE HAMMER		
CHECKED BY XXX	DATE XXX	SIZE A3	DRAWING NUMBER 2	REV X
DESIGNED BY XXX	DATE XXX	SCALE 1:300	- -	SHEET 1/1

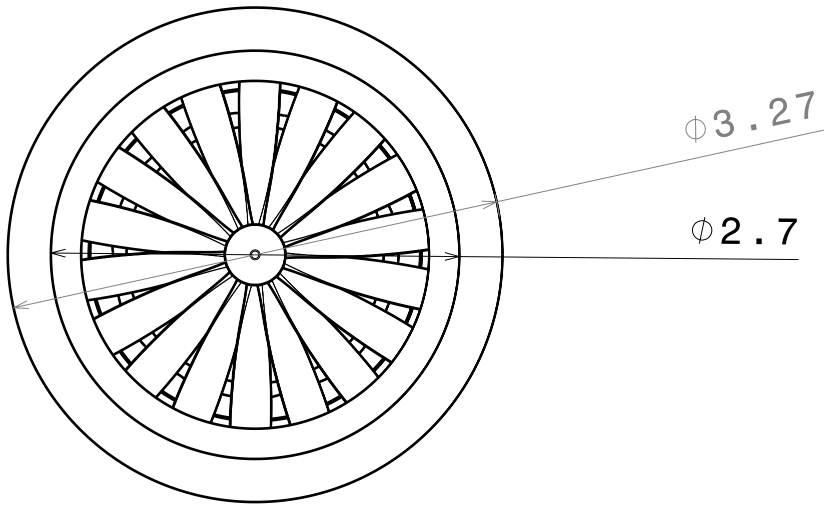

Front view
Scale: 1:50

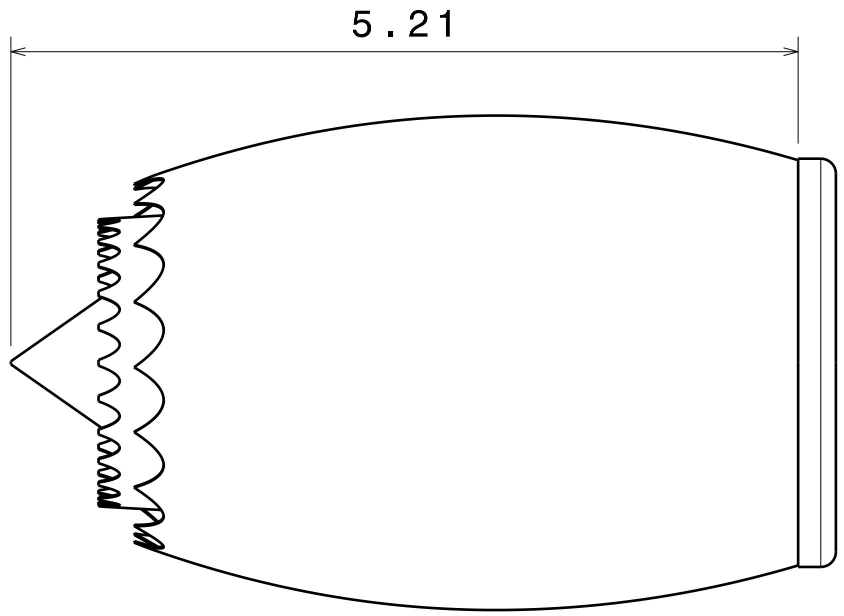

Left view
Scale: 1:50

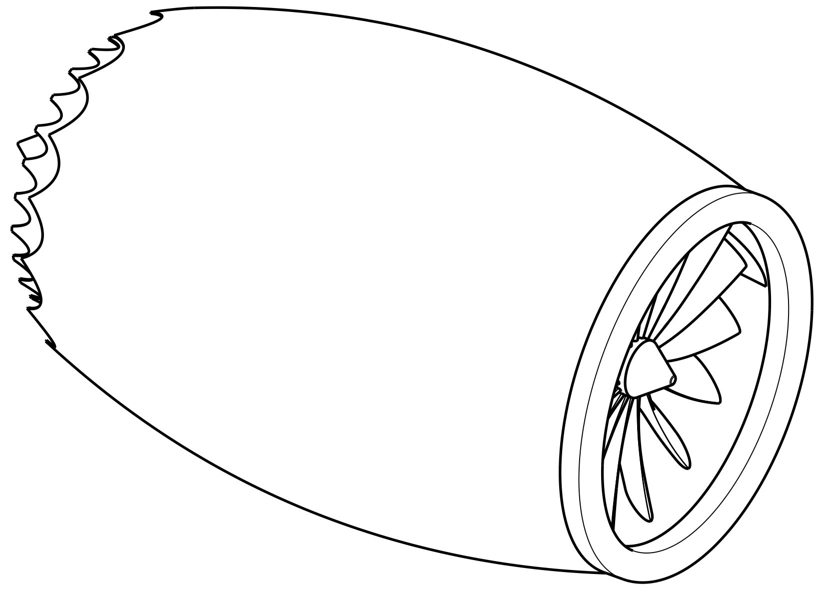

Isometric view
Scale: 1:50

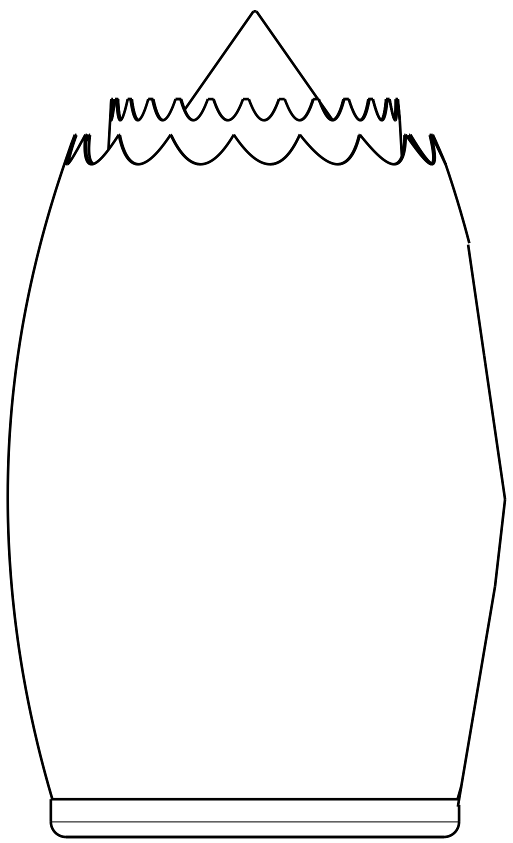

Top view
Scale: 1:50

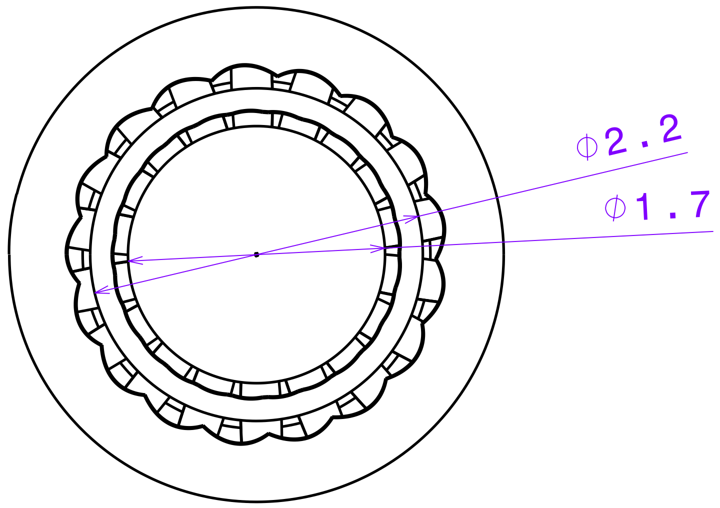

Rear View
Scale: 1:50

DRAWN BY gijsg	DATE 29-6-2020	DASSAULT SYSTEMES				
CHECKED BY XXX	DATE XXX	DRAWING TITLE				
DESIGNED BY XXX	DATE XXX	SIZE A3	DRAWING NUMBER Product1.3			REV X
		SCALE 1:50	WEIGHT(kg) 19.061,45		SHEET 1/1	

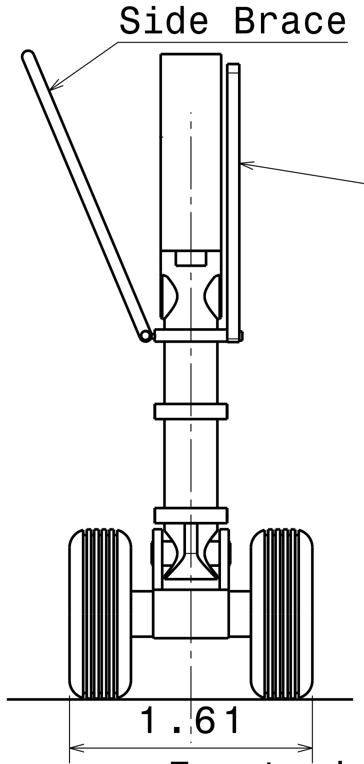

Front view
Scale: 1:50

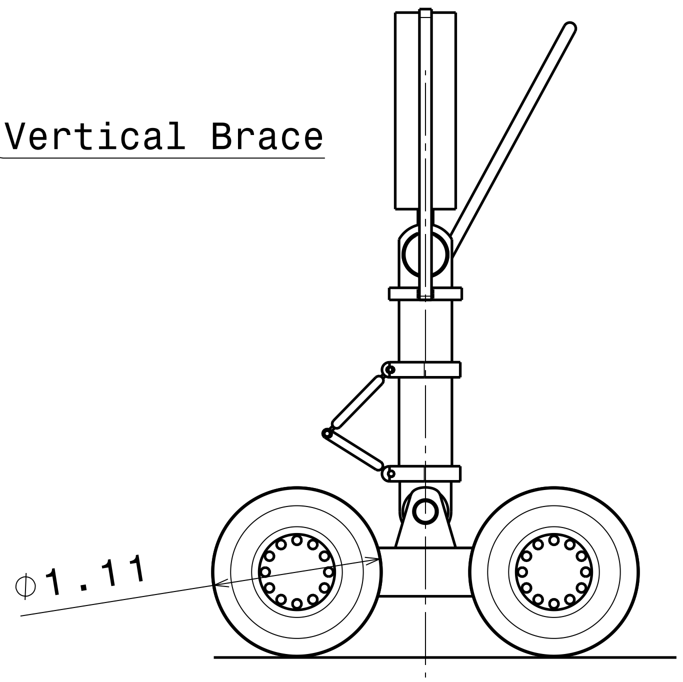

Left view
Scale: 1:50

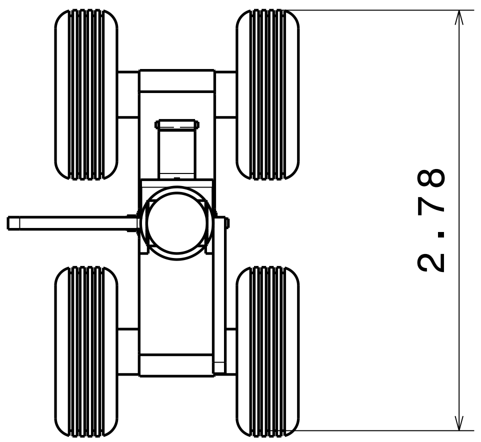

Top view
Scale: 1:50

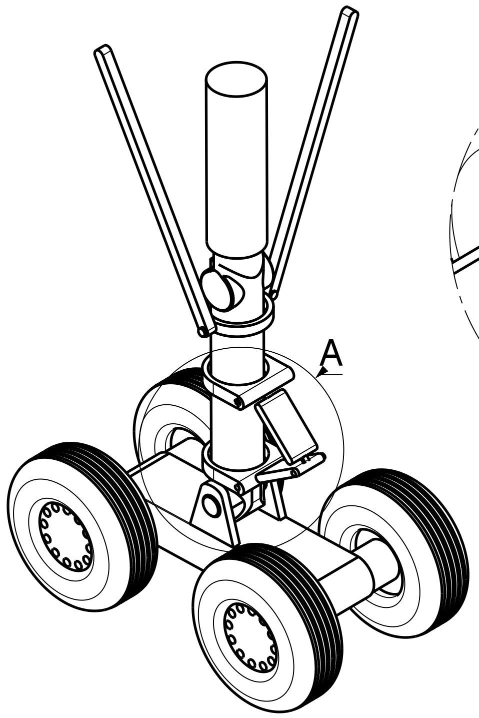

Isometric view
Scale: 1:50

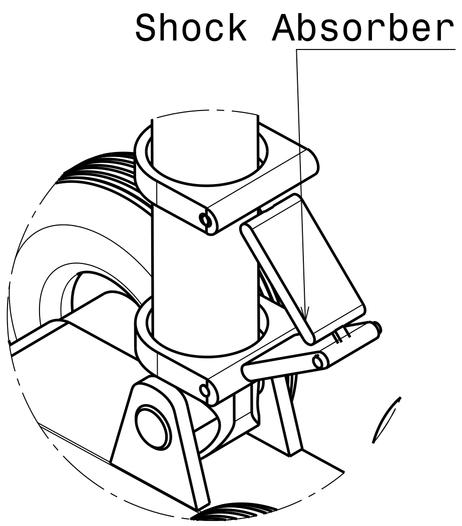

Detail A
Scale: 1:25

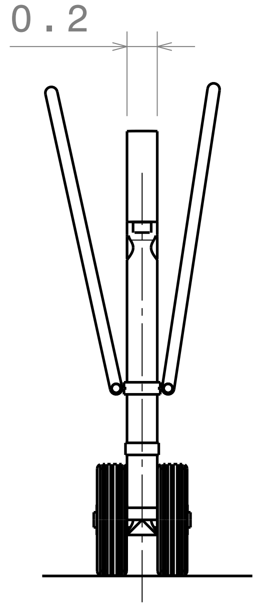

Front view
Scale: 1:50

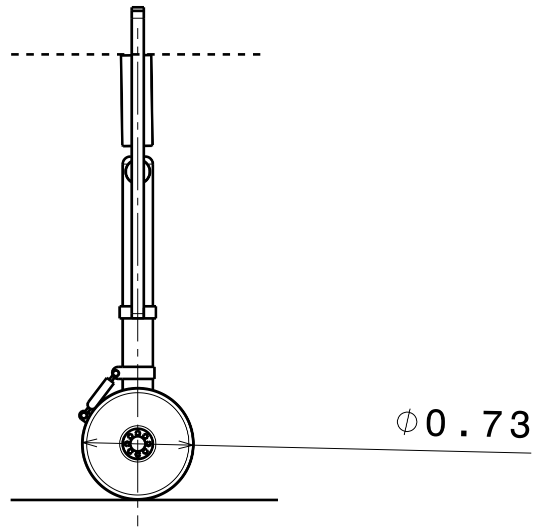

Left view
Scale: 1:50

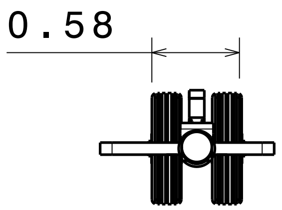

Top view
Scale: 1:50

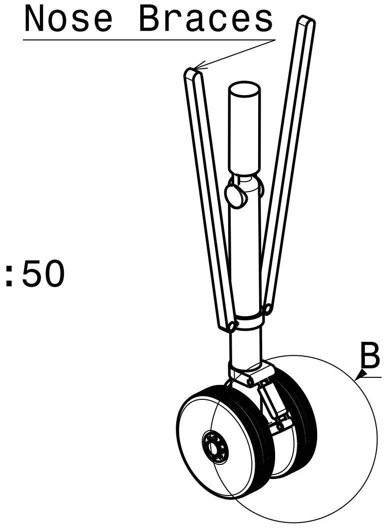

Isometric view
Scale: 1:50

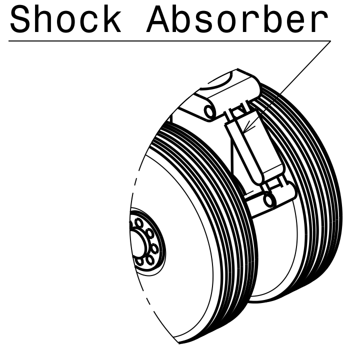

Detail B
Scale: 1:25

DASSAULT SYSTEMES

DRAWN BY: Gijs Frehe	DATE: 29-6-2020	DRAWING TITLE: Main & Nose Landing Gear	
CHECKED BY: XXX	DATE: XXX	SIZE: A3	DRAWING NUMBER: 2 — REV: X
DESIGNED BY: XXX	DATE: XXX	SCALE: 1:50	WEIGHT(kg): - — SHEET: 1/1